FINAL REPORT

U.S. Department of Energy

Microbially Promoted Solubilization of Steel Corrosion Products and Fate of Associated Actinides

Principal Investigator: Yuri A. Gorby
Pacific Northwest National Laboratory
P.O. Box 999, MSIN P7-50
Richland, WA 99352
Email: yuri.gorby@pnl.gov

Collaborator: Gill G. Geesey
Montana State University
Center for Biofilm Engineering
409 Cobleigh Hall
Bozeman, MT 59717
406-994-4770 (phone)
gill_g@erc.montana.edu

Collaborator: Frank Caccavo, Jr.
Whitworth College
Department of Biology
Mail Stop 3902
300 W. Hawthorne Road
Spokane, WA 99251
509-777-4576 (phone)
fcaccavo@whitworth.edu

Collaborator: James K. Fredrickson
Pacific Northwest National Laboratory
P.O. Box 999, MSIN P7-50
Richland, WA 99352
509-373-6177 (phone)
509-376-1321 (fax)
jim.fredrickson@pnl.gov

Project 64931
October 1, 1998 to September 30, 2001

CONTENTS

Executive Summary 3
1.0 RESEARCH OBJECTIVES 5
2.0 METHODS AND results 6
2.1 Microbial Reduction of Pu(IV). 7
2.2 Bacterial Attachment 8
2.3 Bacterial Detachment 8
2.4 Description of Bead-Based Treatment 10
3.0 RELEVANCE, IMPACT, AND TECHNOLOGY TRANSFER 11
4.0 PROJECT PRODUCTIVITY 12
5.0 PERSONNEL SUPPORTED 12
6.0 PUBLICATIONS 13
7.0 INTERACTIONS 13
8.0 TRANSITIONS 14
9.0 PATENTS 14
10.0 FUTURE WORK 14
11.0 LITERATURE CITED 14
12.0 FEEDBACK 17
13.0 APPENDICES 17

EXECUTIVE SUMMARY

Radionuclides and heavy metals contaminate metal surfaces used in the production, processing, and storage of radioactive material at many DOE sites. Much of the contamination of is associated with surface metal oxides formed during the corrosion of the steel surfaces. Dissimilatory iron reducing bacteria (DIRB) can potentially remove contaminated surface corrosion through an enzymatic process known as reductive dissolution, where iron oxide solids present on the corroding are reduced to soluble forms that are either released into solution or accumulate on the surface bacterial surface. The contaminants, particularly plutonium and technetium, are also amenable to enzymatic reduction by metal reducing bacteria. The reduced forms of Pu(III) are more soluble

The ultimate goal of this project was to demonstrate that metal-reducing bacteria could be used to remove heavy metal and radionuclide contaminants from the surfaces of corroding steel surfaces. Toward this end, fundamental scientific issues regarding (1) factors influencing the adhesion and colonization of DIRB on mineral surfaces, (2) the enzymatic activity of cells once they have adhered to mineral surfaces, (3) and (4) methods for recovering bacteria and attendant radionuclides following release from mineral surfaces were addressed. The fate of radionuclides (plutonium) contaminants following reduction by DIRB,

Research results demonstrate that dissimilatory iron reducing bacteria attach to mineral surfaces primarily, but not exclusively, by means of their flagella. Once initial attachment is complete, the bacteria more firmly adhere to the mineral surface apparently through the use of hydrophobic proteins on the bacterial cell surface. Attached bacteria enzymatically reduce ferric iron, Fe(III), to ferrous iron, Fe(II), by terminal metal reductases (proteins) located on their external surface. The bacteria remain firmly attached to the mineral surface, withstanding physical and chemical treatments designed to remove them. Although DIRB strongly adsorb trivalent cations, such as Pu(III), our results suggest that recovery of firmly attached DIRB and associated radionuclides would be impractical as a means for decontaminating corroding stainless steel . Hence, we investigated the ability of soluble, reduced metabolic products to transform radionuclides into forms that could be recovered. We demonstrated that Fe(II) and reduced quinone-like compounds, which are both products of anaerobic respiration and can be generated by DIRB not attached to mineral surfaces, can rapidly reduce solid Pu(IV) to soluble Pu(III)

to chemically reduce solid Pu(IV) to soluble Pu(III). Given these results, we conceptualized and partially tested a microbial bead-based method in which bacteria are encased in porous alginate beads. The beads, which prevent attachment of bacteria to mineral surfaces, can be easily manipulated and recovered as part of a treatment for removing corrosion scale from contaminated metal surfaces.

The fundamental research embodied by this project supports the objectives of the DOE EMSP by investigating the potential utility of an environmentally benign approach for removing heavy metals and radionuclides from corroded steel. Although the research apparently has no immediate impact on the decontamination and decommissioning of DOE facilities, it serves to advance our understanding of the biogeochemical processes related to bacterial-mineral interactions; processes that control not only the release of contaminants from corroding surfaces, but also fate and transport of metal contaminants from oxide minerals typically found in subsurface sediments.

1.0 RESEARCH OBJECTIVES

Processing and disposal of radionuclides has contaminated metallic surfaces throughout the DOE complex. Currently, the DOE Decontamination and Decommissioning Program (D&D) estimates that nearly 180,000 metric tons of contaminated stainless and mild steel structures and piping will be disposed of as radioactive solid waste, since current technologies for dealing with these wastes, are inadequate and costly. DOE is faced with meeting D&D obligations at many of its facilities by the year 2019. If decontamination to levels required for free release could be achieved, some of this material could be released as scrap into the commercial sector for reuse or recycling. The estimated value of scrap metal across the DOE complex was estimated to be greater than $1 billion dollars in 1993. Thus, if effective and economic approaches for decontaminating metal surfaces were developed they could result in considerable savings by reducing the volume of radioactive waste requiring disposal and by rendering the metals as a potentially valuable commodity. Microbial enzymatic dissolution of post-corrosional oxide scales has considerable potential for environmentally benign and economic treatment of contaminated metallic surfaces. However, fundamental scientific information is lacking in key areas that prevent the development of such approaches. These areas include the mechanisms involved in the attachment, colonization, and detachment of iron-reducing bacteria from corrosion scales, the quantitative reductive dissolution of mineralogically, morphologically, and compositionally diverse metal oxides that comprise the scales, and the post-reduction solubility and distribution of the scale-associated contaminants.

This research project investigated processes related to the microbial reductive dissolution of mild and stainless steel corrosion products and the fate of associated radionuclide and metal contaminants. The general goals were to:

- develop an improved understanding of microbial reductive dissolution of iron oxide scales that form on corroding steel and act as highly efficient scavengers of radionuclides, as a function of oxide form and composition
- evaluate approaches for promoting the attachment to and colonization of surfaces by iron-reducing bacteria and the biological and chemical factors that promote the formation of iron-reducing biofilms.
- identify the potential for actinide binding to cells as a function of solution chemistry.

To this effect, the proposed research addressed fundamental scientific questions regarding the attachment and colonization of iron reducing bacteria to corrosion products and the fate of associated radionuclide and metal contaminants. These questions include:

- How do the mineralogy, morphology, and contaminant composition of oxide minerals formed on corroded steel influence the attachment and colonization by iron-reducing bacteria and the subsequent reductive dissolution reactions?
- How does aqueous chemical composition influence the rate and extent of microbial reductive dissolution of corrosion products and the subsequent solubility of associated contaminants?
- What is the fate of radionuclides associated with corrosion products that are dissolved via microbial reductive dissolution? Are the contaminants selectively accumulated or biosorbed by the cells or biofilms, released into solution, or repartitioned to the surface of the metal or into secondary mineral phases?
- Can soluble quinones, such as anthraquinone disulfonate (AQDS), facilitate dissolution of oxides and oxide films, including surface features and pores inaccessible by the bacteria, via electron ‘shuttling’ from cell to oxide surfaces with subsequent bonded electron transfer, and thereby enhance removal of contaminants from the surface?

This research contributes to our understanding for developing a safe and effective biological approach for decontaminating mild and stainless steels that were used in the production, transport, and storage of radioactive materials. The research complements a variety of fundamental and applied research programs within the DOE Office of Science. Those projects include, but are not limited to:

The Natural and Accelerated Bioremediation Research Program (NABIR) Office of Biological and Environmental Research (BER).

Effect of Microbial Exopolymers on the Spatial Distributions and Transformations of Cr and U at the Bacteria-Geosurface Interface
PRINCIPAL INVESTIGATOR: Dr. Ken Kemner

Fe(II)-Induced Inhibition of Dissimilatory Bacterial Reduction of Metals and Radionuclides: The Role and Reactivity of Cell-Surface Precipitates
PRINCIPAL INVESTIGATOR: Yuri A. Gorby

Microbial Stabilization of Plutonium in the Subsurface Environment
PRINCIPAL INVESTIGATOR: Bruce Honeyman

Biogeochemical Processes Controlling Microbial Reductive Precipitation of Radionuclides
PRINCIPAL INVESTIGATOR: Jim K. Fredrickson

Impacts of Mineralogy and Competing Microbial Respiration Pathways on the Fate of Uranium in Contaminated Groundwater
PRINCIPAL INVESTIGATOR: Joel E. Kostka

2.0 METHODS AND RESULTS

The project has resulted in 6 peer-reviewed publications. An additional 2 publications are in preparation for submission. Published articles appear in Appendix A and should be referenced for details of materials and methods.

Results from our work definitively demonstrate that *metal reducing bacteria can remove Pu from Fe(III) oxides through enzymatic reduction and dissolution*. Consistent with our hypotheses, biogenic Pu(III), formed from the reduction of insoluble Pu(IV), accumulated on the bacterial cells. However, we incorrectly hypothesized that cells could be easily removed and recovered from the metal oxide surfaces. Results are summarized below and clearly show that:

- Metal reducing bacteria enzymatically reduce Pu(IV) solids to soluble Pu(III), which subsequently sorbed to bacterial cells.
- Bacterial cells attach to oxide surfaces, but attached biomass cannot be easily removed or recovered
- Microbially-reduced AQDS can reduce Pu(IV) to Pu(III) and can serve as an electron shuttle between bacterial cells and Pu(IV).
- Cells embedded in alginate beads can facilitate the removal of Pu(IV) from Fe(III) oxides (corrosion products). Pu(III) generated by this process accumulates in the beads and can be easily separated from the bulk aqueous phase.
- Flagella are involved in, but not required for, the attachment of DIRB to mineral surfaces.
- Bacteria sorb and accumulate trivalent cations, such as Pu(III).
- Bacteria attached to oxide surfaces are very difficult to remove and, hence, recovery of bacteria with sorbed Pu(III) is impractical.
- Fe(II) and reduced quinone-like compounds, which are both products of anaerobic respiration, can chemically reduce solid Pu(IV) to dissolved Pu(III).
- Channel-flow flat plate reactor and reporter genes can be used to quantify the accumulation rate and detachment rate of iron reducing bacteria growing on mineral surfaces that serve as the sole electron acceptor for energy production and growth.
- Accumulation rate, growth rate, maximum surface-associated cell densities, and detachment rate of the dissimilatory iron reducing bacterium Shewanella oneidensis MR1 during anaerobic respiration can be

quantified on different solid phase iron oxides. The bacteria colonize hematite surfaces and accumulate to greater cell densities on hematite compared to magnetite (111) and (100) surfaces

- Iron site density alone in iron oxide minerals does not control bacterial cell accumulation rates and maximum surface-associated cell densities during anaerobic iron oxide reduction by Shewanella oneidensis MR1.
- Iron sulfide pyrrhotite precipitated during biofilm formation by the dissimilatory sulfate reducing bacterium Desulfovibrio desulfuricans G20 on the surface of the iron oxide hematite.
- Desulfovibrio desulfuricans G20 biofilms growing on iron oxide surfaces reduce soluble uranyl ion to insoluble uraninite
- The complete base sequence of the ferA gene encoding a c-type cytochrome involved in dissimilatory iron reduction by the dissimilatory iron reducing bacterium Geobacter sulfurreducens was determined. The sequence information provides the opportunity to develop assays to follow the expression of this iron reduction gene during growth on iron oxides.
- In-situ reverse transcriptase polymerase chain reaction (RT-PCR) can be used to detect expression of genes encoding functions of metal reduction, sulfate reduction and hydrogen reduction in individual cells attached to iron oxide surfaces.

2.1 MICROBIAL REDUCTION OF PU(IV)

Plutonium on iron oxide surfaces and corrosion products is expected to be present primarily in the tetravalent state. Pu(IV) readily forms very insoluble hydrous oxide. The solubility product of hydrous oxide ($PuO_2(am) + 2\ H_2O = Pu^{4+} + 4\ OH^-$) is very low (log K^0 = -56.85, Rai 1984), and thus shows that Pu(IV) would be soluble in appreciable quantities only under very acidic conditions. Microbial activity can cause reducing conditions that can transform Pu(IV) to Pu(III). With the exception of phosphate compounds, most Pu(III) compounds are highly soluble in acidic to near-neutral conditions. Therefore, we previously hypothesized that metal reducing bacteria could enzymatically reduce insoluble Pu(VI) to soluble Pu(III) and that the Pu(III) would sorb to the surface of the bacteria. *As part of our initial EMSP project, we confirmed that cells of S. putrefaciens strain BrY reduced Pu(IV) to Pu(III) with H_2 as the electron donor* (Figure 1).

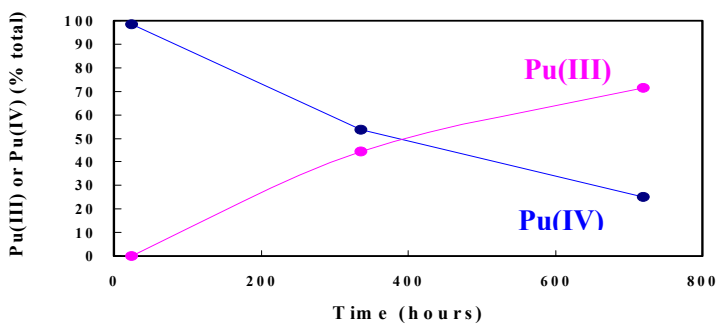

Figure 1. Enzymatic reduction of Pu(IV) to Pu(III) by S. putrefaciens strain BrY in an anaerobic medium with H_2 as the electron donor. Oxidation states of Pu were determined by scintillation counting using a modified extraction method (Schramke et al. 1989).

Virtually all of the Pu(III) generated through the direct enzymatic of Pu(IV) solids was associated with a phase (presumably bacterial surfaces) that could be removed from the suspension by passing the solution through 0.2 um filters. The sorptive capacity of cells of S putrefaciens strain BrYwas examined using neodymium, Nd(III), as a non-radioactive analogue for Pu(III). A solution of 3 uM NdCl3 received washed cells of strain BrY ranging from 106 to 1010 cells ml-1. Figure 2 demonstrates that aqueous equilibrium concentration and the amount of sorbed Nd(III) per cell increased with decreasing cell concentration. The data suggest that Nd began to precipitate on cell surfaces when the aqueous equilibrium concentration reached about 2.6 uM. The results support our hypothesis that sorption/precipitation is an important process for removing trivalent cations, such as Pu(III), from solution. These results underscore the importance of investigating the factors that influence attachment and detachment of

metal reducing bacteria to for developing the approaches for recovering cells and cell-associated actinides as part of a remediation strategy.

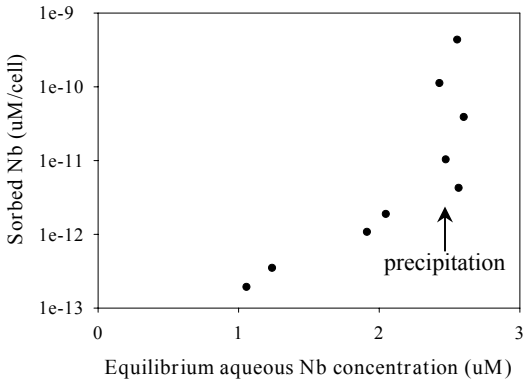

Figure 2. Sorption of Nd(III) onto cells of S. alga strain BrY. Initial concentration of dissolved Nd(III) was 3 uM at pH 6.5. Cell concentration ranged from 10^6 to 10^{10} cell ml^{-1}.

2.2 BACTERIAL ATTACHMENT

Adhesion of the iron reducing bacterium *Shewanella alga* strain BrY to hydrous ferric oxide, goethite, and hematite was examined. The results demonstrated that:

- The bacteria readily adhere to both crystalline and amorphous Fe(III) oxide surfaces.
- Adhesion of S. alga strain BrY to hydrous ferric oxide (HFO) was correlated with ionic strength, and thus was accurately described by the DLVO theory.
- Rate of solid phase iron reduction was directly correlated with adhesion of cells with surfaces and, hence, with ionic strength of the medium.
-

The distribution of attached cells on synthetic hematite crystals was examined to determine if cells preferentially attached to sites on the oxide surface. To facilitate direct observation of cells on oxide surfaces without using fluorescent stains that would compromise cell viability, genes encoding for green fluorescence protein (GFP) were inserted into strain BrY. Hence, cells were imaged by confocal laser microscopy as they entered an anaerobic flow chamber and attached to the surfaces of specular hematite. The results, some of which are illustrated in Figure 3, revealed that:

- Primary cells adhesion occurred through flagellar attachment.
- Cells were heterogeneously distributed on hematite surfaces, with preferential attachment observed at cracks, steps, and crystal defects.
- Luminescence was greater with cells attached at the cracks, steps and defects, suggesting that cells were metabolically active at these sites.

2.3 BACTERIAL DETACHMENT

Considering the ability for metal reducing bacteria to reduce and accumulate plutonium, approaches for removing or detaching cells from oxide surfaces were investigated. Cells attached to hematite surfaces were starved for electron donor and other nutrients required for growth. As shown in Figure 4:

- Cells treated in this manner formed small (100 nm) vesicles on the cells surface.
- Cells began to detach from the mineral surface.
- Vesicles remained attached to the mineral surface

- Vesicles could not be removed by benign changes in aqueous chemistry (ionic strength, lowering the pH) or by enzymatic digestion with trypsin.

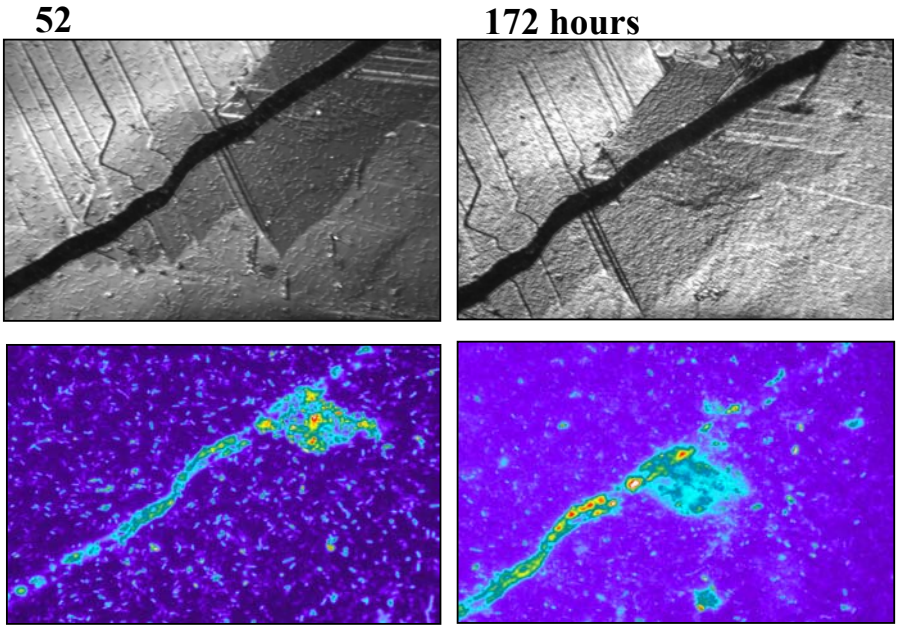

Figure 3. Confocal images of S. alga strain BrY taken on a (001) hematite surface after 52 and 172 hours. The top panels were taken using the reflectance channels of the confocal microscope. The bottom panels were obtained using the fluorescence channel. Fluorescence results from excitation of a green fluorescence protein (GFP) that was inserted into the bacterial genome and expressed. Bright cells are particularly associated with the step edge, suggesting that these cells are actively metabolizing and reducing Fe(III) available at these sites.

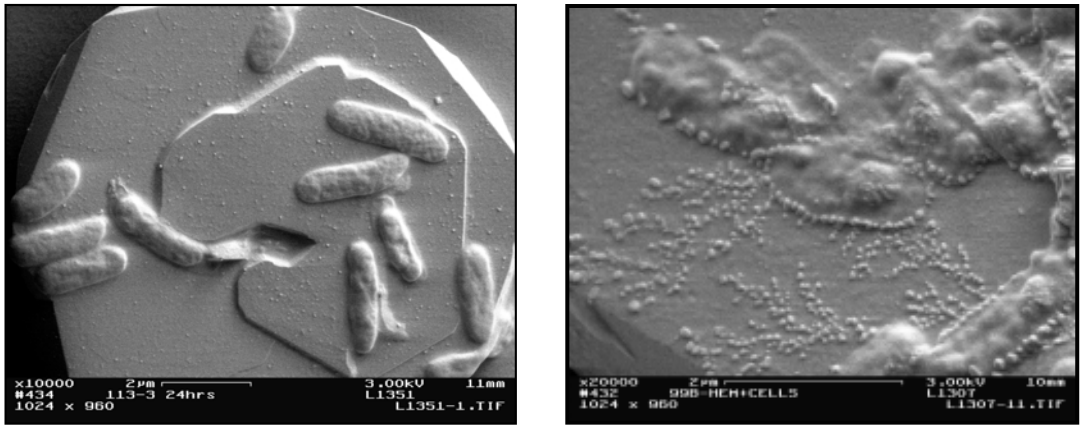

Figure 4. SEM images of S putrefaciens strain BrY on crystals of synthetic tabular hematite after 1 day (left) and 5 days (right). Membrane vesicles, which arise from the outer membrane of Gram-negative bacteria, appear as 100 nm blebs around the perimeter of the cells and are distributed over the hematite surfaces. These vesicles are highly negatively charged and effectively bind cations.

Dissimilatory iron-reducing bacteria enzymatically reduce and dissolve iron oxides, which are common components of corrosion films, and release soluble species of plutonium, Pu(III). Consistent with our previous hypothesis, cell surfaces sorb Pu(III) and remove it from the bulk aqueous phase. However, we incorrectly hypothesized that bacteria with sorbed actinides could be easily detached and recovered from the surfaces that they had colonized and enzymatically altered. In fact, we have demonstrated that although cells do naturally detach from oxide 3 surfaces during their growth cycle, they leave behind negatively charged reactive portions of their outer surface that are strong sorbants for cations. Without a means for recovering both intact bacteria, their subcellular products and associated contaminants, the use of iron-reducing bacteria for decontaminating corroded steel surfaces would not be feasible. Hence, we have targeted an approach that avoids direct contact and attachment of cells to the corrosion films but allows for reduction, dissolution, and sorption of corrosion products and associated actinides. The inability to remove cells and membrane vesicles from oxide surfaces justified our investigation of a bead-based technology for removing Pu from iron oxides that are common corrosion products. The following sections describes recent results obtained from a proof-of-principle experiment.

2.4 DESCRIPTION OF BEAD-BASED TREATMENT

Figure 5 shows the conceptual model of a bead-based system for decontaminating corroded steels. Iron reducing bacteria are encapsulated in small beads of sodium alginate. Encapsulation prevents direct contact between the bacteria and the contaminated oxide surface. Anthraquinone disulfonate (AQDS) is used as a dissolved electron shuttle to carry electrons from the bacteria to Fe(III) and Pu(IV) on the corrosion film. AQDS reduces Fe(III) to Fe(II) and Pu(IV) to Pu(III). The reduced forms of these metals are very soluble and partition to the aqueous phase. The bacterial surface and the sodium alginate sorb and accumulate Fe(II) and Pu(III). The beads, which now contain most of the Pu(III), can be easily separated from the bulk aqueous phase and the uncontaminated steel. The benign process requires no hazardous chemicals or extreme pH conditions.

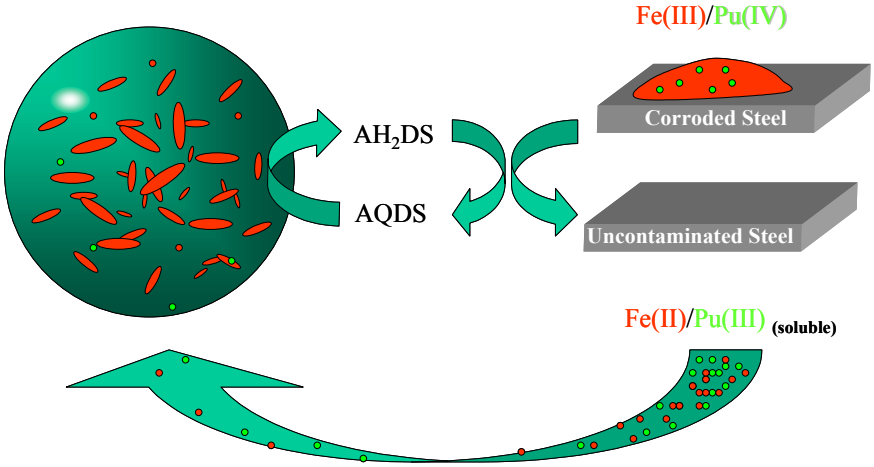

Figure 5 . This illustrates a conceptual model of a bead-based system for decontaminating corroded steels. Metal-reducing bacteria are enrobed in porous alginate beads. Oxidized anthraquinone disulfonate, AQDS, which will serve as a dissolved electron shuttle between immobilized cells and elements in the corrosion film, diffuses into the beads and is enzymatically reduced by the bacteria. The reduced AQDSH diffuses out of the bead and chemically reduces and dissolves Fe(III) and Pu(IV) in the corrosion film. Soluble Fe(II) and Pu(III) sorb to cationic exchange sites within the alginate beads. The beads and accumulated actinides can then be easily separated from the bulk aqueous phase and the uncontaminated steel.

The microbial bead-based technology was tested for its ability to reduce and remove Pu(VI) from Fe(III) oxides. Cells of S. alga strain BrY were enrobed in beads of sodium alginate. The beads, each measuring a few millimeters in diameter, were added to a suspension of synthetic HFO (5 mM) that was co-precipitated with approximately 0.5 mM Pu(IV). AQDS (0.1 mM) was added as the soluble electron shuttle. The contents of the

tubes were made anaerobic by bubbling with N_2 and the tubes were incubated on their side at room temperature. Control tubes lacked either cells or the electron donor. Following 24 hour incubation, beads were separated from the aqueous suspension and analyzed for Pu by liquid scintillation counting. The amount of Pu remaining in the aqueous suspension, which included the liquid medium and any undissolved Fe/Pu precipitates, was also evaluated. A portion of this sample was passed through a 0.036 um membrane filter and the filtrate was analyzed for soluble Pu by scintillation counting. Oxidation state of Pu was determined in each fraction by a modification of the solvent extraction method of Schramke et al., 1989. The results tabulated in Table 1 reveal that bacterial cells embedded in alginate reduced and dissolved 25% of the total amount of Pu that was co-precipitated with the HFO. More than 96% of the Pu that partitioned into the beads was present as Pu(III). Pu(IV) was not reduced and less than 1 % of the total Pu partitioned into the beads for the 3 treatments that served as controls. *These preliminary results clearly indicated the potential of the microbial bead-based technology as part of a decontamination strategy for removing Pu from Fe(III) oxide components of corrosion.*

Table 1. Fate of Pu during the reduction of Fe(III)/Pu(IV) oxides.

Treatment	**Pu in beads**	**Pu in unfiltered suspension**	**Pu in filtered (soluble) fraction**
Cells, AQDS, H_2	25 (96 % as Pu(III))	75	0
Cells, no AQDS, H_2	0.7	99	0
Cells, AQDS, no H_2	0.9	99	0
No cells, AQDS, H_2	0.5	99	0

The bead-based system was also tested for its ability to remove dissolved radionuclides (uranium and technetium) from aqueous media. Figure 6 illustrates that iron reducing bacteria embedded in a porous alginate matrix reduce dissolved Tc(VII) (as pertechnetate ion) to poorly soluble TcO_2. Vials 1 and 2 contain alginate beads that are blackened by TcO_2 precipitates. Vial 3 served as a control and contains beads with no cells. All of the Tc(VII) remained in the aqueous phase. Vials containing dissolved U(VI) in lieu of Tc(VII) yielded similar results. These results clearly demonstrate the potential for removing dissolved radionuclides from solution using an environmentally benign bead-based approach.

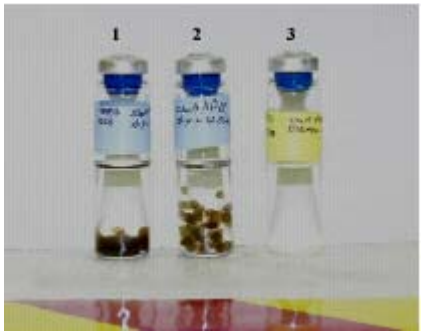

Figure 6. Vials demonstrating the ability of iron-reducing bacteria in alginate beads to remove dissolved Tc(VII) from solution. 100 uM of Tc(VII) were reduced and precipitated within the beads in vials 1 and 2. Vial 3 served as a negative control and lacked bacterial cells. Beads without bacteria are difficult to see because they contain none of the dark Tc(IV) precipitate.

3.0 RELEVANCE, IMPACT, AND TECHNOLOGY TRANSFER

This project targeted scientific questions that highlight gaps in our understanding of how iron reducing bacteria catalyze the reductive dissolution of iron oxides typically associated with corrosion films on mild and stainless steel surfaces. These films represent a major sink for radionuclides and heavy metals used during the processing, transport, and storage of radioactive materials and constitute a significant environmental problem facing DOE. In its present form, the scientific knowledge generated by this project is not directly applicable toward the

decontamination and decommissioning of DOE facilities. However, the results do advance our understanding of the biological processes associated with reductive dissolution of iron oxides and the interaction of radionuclides and heavy metals with bacterial surfaces. Such information contributes to an increasing wealth of knowledge concerning the role of metal reducing bacteria in controlling the fate and transport of inorganic contaminants in saturated subsurface and sedimentary environments and for their *potential* roles in decontamination metal surfaces. Published results from this research project have already impacted the scientific research community and have stimulated the development of collaborations between microbiologists, geochemists, and physicists. Such interactions are vital for linking fundamental science with needs-driven technologies.

Scientific hurdles still exist before a biologically-based means for decontaminating corroded steals can be realized. First, we have only just begun to understand the environmental and genetic factors that regulate the metabolism and physiology of metal reducing bacteria. An awareness of need for a holistic understanding of microbial systems and the environmental/growth parameters that impact the regulation of their physiological activities is reflected in new programs developing within the DOE office of science. In particular, the Genomes to Life program maintains lofty, yet tractable, goals to understand the activity of bacteria by taking a "systems biology" approach. Notably, iron reducing bacteria (Shewanella oneidensis strain MR-1) is a primary target for this program and the researchers it supports. Through a more complete understanding of the biology of this organism, new approaches and insights will certainly be realized concerning the biogeochemical processes important to reductive dissolution of contaminated corrosion scale and, more generally, the fate of radionuclides and heavy metals associated with oxide surfaces..

4.0 PROJECT PRODUCTIVITY

The project demonstrated significant productivity through peer-reviewed publications and advancement of fundamental scientific research questions involving metal reducing bacteria and metal oxide surfaces that they colonize. Many of the objectives related to the interaction of actinides with bacterial surfaces were also addressed. Consistent with our previous hypothesis, cell surfaces sorb Pu(III) and remove it from the bulk aqueous phase. However, we incorrectly hypothesized that bacteria with sorbed actinides could be easily detached and recovered from the surfaces that they had colonized and enzymatically altered. In fact, we demonstrated that although cells do naturally detach from oxide surfaces during their growth cycle, they leave behind negatively charged reactive portions of their outer surface that are strong sorbants for cations. Without a means for recovering both intact bacteria, their subcellular products and associated contaminants, the use of iron reducing bacteria for decontaminating corroded steel surfaces would not be feasible. Hence, we diverged from some proposed goals and targeted an approach that avoids direct contact and attachment of cells to the corrosion films but allows for reduction, dissolution, and sorbtion of corrosion products and associated actinides.

Our preliminary results obtained using the bead-based technology demonstrated that anthroquinone disulfonate, AQDS, serves as a soluble electron shuttle between the enzymes on the bacterial cell surface and Fe(III) and Pu(IV) present in the corrosion film. Soluble Pu(III) released during reduction accumulated within the beads, presumably by sorption of the trivalent cations to alginate and the embedded cells. The beads containing sorbed Pu(III) were then easily separated from the bulk aqueous phase. This environmentally-benign microbiological process avoids the used of hazardous or toxic chemicals, minimizes the volume and toxicity of secondary wastes, and could be applied in situ. Although a renewal proposal that targeted the evaluation of the bead technology for removing actinides from contaminated surfaces was denied, we maintain that the concepts are sound and warrant further consideration.

5.0 PERSONNEL SUPPORTED

This project provided full support for 2 post-docs, partial support for 2 university faculty members, and partial support for 3 national lab staff scientists and associated technical staff. The names and institutions of the collaborating teams are listed below.

University of New Hampshire
Dr. Frank Caccavo (faculty)
Dr. Amitabha Das (Post Doc)

Montana State University
Dr. Gill Geesey (faculty)
Dr. Andrew Neal (post-doc)

Pacific Northwest National Lab
Dr. Yuri Gorby (staff scientist)
Dr. Dhanpat Rai (senior research scientist)
Dr. Jim Fredrickson (senior research scientist)
Mathew Gray (post bachelors)
Jeff McLean (post masters)
Dean Moore (science and engineer associate)
Alice Dohnalkova (science and engineer associate)
Andrew Plymale (science and engineer associate)

6.0 PUBLICATIONS

Rai D, YA Gorby, JK Fredrickson, DA Moore, and M Yui. 2002. Reductive Dissolution of PuO2(am): The Effect of Fe(II) and Hydroquinone. *J. Sol. Chem*. 31(6): 433-453.

Gorby YA, J Mclean, A Dohnalkova, A Korenevsky, K Rosso, E Vinogradov, and TJ Beveridge. 2002. Membrane vesicles form the dissimilatory iron reducing bacterium Shewanella putrefaciens strain CN32. *FEMS Microbial. Lett.* (in revision).

Das A and F Caccavo, Jr. 2001. Adhesion of the dissimilatory Fe(III) - Reducing bacterium Shewanella alga BrY to crystalline Fe(III) oxides. *Curr. Microbiol*. 42:151-154.

Caccavo F and A Das. 2002. Adhesion of Dissimilatory Fe(III)-Reducing Bacteria to Fe(III) Minerals. *Geomicrobiol. J*. 19:161-177.

Das A and F Caccavo, Jr. 2000. Dissimilatory Fe(III) oxide reduction by Shewanella alga BrY requires adhesion. *Curr. Microbiol*. 40:344-347.

Neal, A.L., S. Techkarnjanaruk, A. Dohnalkova, D. McCready, B.M. Peyton, and G.G. Geesey. 2001. Iron sulfides and sulfur species produced at hematite surfaces in the presence of sulfate-reducing bacteria. Geochim. Cosmochim. Acta 65:223-235.

Magnuson, T.S., N. Isoyama, A.L. Hodges-Myerson, G. Davidson, M.J. Maroney, G.G. Geesey, and D.R. Lovley. 2001. Isolation, characterization, and gene sequence analysis of a membrane associated 89 kDa Fe(III) reducing cytochrome c from Geobacter sulfurreducens. Biochem. J. 359:147-152.

Geesey, G.G., A.L. Neal, P.A. Suci, and B.M. Peyton. A review of spectroscopic methods for characterizing microbial transformations of minerals. J. Microbiol. Meth. 51:125-139.

7.0 INTERACTIONS

Yuri Gorby presented *Microbially Promoted Solubilization of Steel Corrosion Products and Fate of Associated Actinides* (04/24/2000 - Invited Speaker) at EMSP National Workshop in Atlanta GA, US with contributions from: YA Gorby, F Caccavo, G Geesey, A Neal, D Rai, A Das, A Dohnalkova, MS Gray, JS Mclean, and JK Fredrickson.

Keynote address: Goldschmidt Geochemistry Conference. May, 2001. Physiological Responses And Environmental Implications Of Fe(Ii)-Induced Inhibition Of Microbial Iron Reduction. Y. A. Gorby, C. Liu, T. J. Beveridge, F. G. Ferris, and J. M. Zachara.

Invited speaker: International Symposium of Ecology and Biogeochemistry. Sept., 2001. Membrane Vesicles from Iron Reducing Bacteria: a Potential Source of Biogenic Nanofossils. YA Gorby and TJ Beveridge.

8.0 TRANSITIONS

None

9.0 PATENTS

None

10.0 FUTURE WORK

The scientific advances realized during the tenure of this project are expected to proliferate into a variety of research avenues involving metal reducing bacteria and their roles and associations with heavy metals and radionuclides. Indeed, several research projects targeting the physiological controls of metal reducing bacteria growing in biofilms and attached to mineral surfaces are already underway. The use as alginate beads as tools for separating, manipulating, and recovering metal reducing bacteria in solid phase suspensions is expected to benefit those interested in investigating biogeochemical processes in the absence of direct microbe-mineral contact. Hopefully, the potential for using bacteria enrobed in alginate beads as a means for recovering heavy metals and radionuclides from aqueous solutions and contaminated surfaces will also receive appropriate attention.

11.0 LITERATURE CITED

Ainsworth, C. C., D. C. Girvin, J. M. Zachara and S. C. Smith (1989). "Chromate adsorption on goethite: effects of aluminum substitution." *Soil Sci. Soc. Am. J.* **53**: 411-418.

AlMahamid, I., K. A. Becraft, N. L. Hakem, R. C. Gatti and H. Nitsche (1996). "Stability of various plutonium valence states in the presence of NTA and EDTA." *Radiochim. Acta* **74**: 129-134.

Amacher, M. C., J. Amacher-Kotuby, H. M. Selim and I. K. Iskan-dar (1986). "Retention and release of metals by soils-evaluation of several models." *Geoderma* **38**: 131-154.

Aringhieri, R., P. Carrai and G. Petruzzelli (1985). "Kinetics of Cu and Cd adsorption by an Italian soil." *Soil Sci. Soc.* **139**: 197-204.

Arnold, R. G., T. J. DiChristina and M. R. Hoffmann (1988). "Reductive dissolution of Fe(III) oxides by *Pseudomonas* sp. 200." *Biotech. Bioeng.* **32**: 1081-1096.

Brown, D.A., B.L. Sherriff, J.A. Sawicki and R. Sparling (1999) "Precipitation of iron minerals by a natural microbial consortium." *Geochim. Cosmochim. Acta* **63**:2163-2169.

Burns, R. G. (1976). "The uptake of cobalt into ferromanganese nodules, soils, and synthetic manganese (IV) oxides." *Geochim. Cosmochim. Acta* **40**: 95-102.

Chen, L., D. B. Chamberlain, C. Conner and G. F. Vandergrift (1997). A survey of decontamination processes applicable to DOE Nuclear Facilities, Argonne National Laboratory.

Choppin, G. R. and B. E. Stout (1989). "Actinide behavior in natural waters." *Sci. of the Total Environ.* **83**: 203-216.

Clark, W. M. (1960). Oxidation-reduction potentials of organic systems. Baltimore, The Williams and Wilkins Co.

Clemens, B. (1993). Radioactive scrap metal: keep it, dump it, or clean it?, University of Tennessee.

Conner, C., D. B. Chamberlain, L. Chen and G. F. Vandergrift (1995). Equipment decontamination: a brief survey of the DOE complex, Argonne National Laboratory.

Cowan, C. E., J. M. Zachara and C. T. Resch (1991). "Cadmium adsorption on iron oxides in the presence of alkaline-earth elements." *Environ. Sci. Technol.* **25**: 437-446.

Davis, J. A. (1978). Surface ionization and complexation at the oxide/water interface, Stanford University.

Davis, J. A., C. C. Fuller and A. D. Cook (1987). "A model for trace metal sorption processes at the calcite surface: adsorption of Cd2+ and subsequent solid solution formation." *Geochim. Cosmochim. Acta* **51**: 1477-1490.

DiChristina, T. J. (1994). "Bioextraction (reductive dissolution) of iron from low-grade iron ores." *Ann. NY Acad. Sci.* **721**: 440-449.

Dillon, C. P. (1995). Corrosion Resistance of Stainless Steels. New York, Marcel Dekker, Inc.

Felmy, A. R., D. Rai, J. A. Schramke and J. L. Ryan (1989). "The solubility of Pu(OH)3 in dilute solutions and in high-ionic-strength chloride brines." *Radiochim. Acta* **48**: 29-35.

Fredrickson, J. K., J. M. Zachara, D. W. Kennedy, H. Dong, T. C. Onstott, N. W. Hinman and S. W. Li (1998). "Biogenic iron mineralization accompanying the dissimilatory bacterial reduction of hydrous ferric oxide." *Geochim. Cosmochim. Acta* **62**:3239-3297.

Fredrickson, J.K., H.M. Kostandarithes, S.W. Li, A.E. Plymale, and M.J. Daly (2000) "Reduction of Fe(III), Cr(VI), U(VI), and Tc(VII) by *Deinococcus radiodurans* R1". *Appl. Environ. Microbiol.* **66**:2006-2011.

Gorby, Y. A. and D. R. Lovley (1992). "Enzymatic uranium precipitation." *Environ. Sci. Technol.* **26**: 205-207.

Grambow, B., E. Smailos, H. Geckeis, R. Müller and H. Hentschel (1996). "Sorption and reduction of U(VI) on iron corrosion products under reducing saline conditions." *Radiochim. Acta* **74**: 149-154.

Hayes, K. F. and J. O. Leckie (1986). Mechanisms of lead ion adsorption at the goethit-water interface. Geochemical processes at mineral surfaces. J. A. a. H. Davis, K.F. Washington, D.C., American Chemical Society.

Jang, L.K., G.G. Geesey, S.L. Lopez, S.L. Eastman, and P.L. Wichlacz (1990) "Use of a gel-forming biopolymer directly dispensed into a loop fluidized bed reactor to remove dissolved copper". *Wat. Res.* **24**:889-897.

Jang, L.K., D. Nguyen and G.G. Geesey (1995) "Selectivity of alginate gel for Cu vs Co". *Wat. Res.* **29**:307-313.

Jenne, E. A. (1977). Trace element sorption by sediments and soil-sites and processes. Symposium of molybdenum in the environment. W. A. P. Chappell, K. New York, Marcel Decker, Inc.

Kinniburgh, P. G. and M. L. Jackson (1981). Cation adsorption by hydrous metal oxides and clay. Adsorption of inorganics at solid-liquid interfaces. M. A. a. R. Anderson, A.J. Ann Arbor, Michigan, Ann Arbor Science Publishers.

Kostka, J. E. and K. H. Nealson (1995). "Dissolution and reduction of magnetite by bacteria." *Environ Sci Technol.* **29**(10): 2535-2540.

Kou, S. (1986). "Concurrent sorption of phosphate and zinc, cadmium, or calcium by a hydrous ferric oxide." *Soil Sci. Soc. Am. J.* **50**: 1412-1419.

Lovley, D. R., J. D. Coates, E. L. Bluntharris, E. J. P. Phillips and J. C. Woodward (1996). "Humic substances as electron acceptors for microbial respiration." *Nature* **382**(6590): 445-448.

Lovley, D. R. and E. J. P. Phillips (1986). "Availability of ferric iron for microbial reduction in bottom sediments of the freshwater tidal Potomac River." *Appl. Environ. Microbiol.* **52**: 751-757.

Lovley, D. R. and E. J. P. Phillips (1988). "Novel mode of microbial energy metabolism: organic carbon oxidation coupled to dissimilatory reduction of iron or manganese." *Appl. Environ. Microbiol.* **54**: 1472-1480.

Lovley, D. R. and E. J. P. Phillips (1992). "Reduction of Uranium by Desulfovibrio desulfuricans." *Appl. Environ. Microbiol.* **58**(3): 850-856.

Macaskie, L. E., B. C. Jeong and M. R. Tolley (1994). "Enzymatically accelerated biomineralization of heavy metals: application to the removal of americium and plutonium from aqueous flows." *FEMS Microbiol. Rev.* **14**(4): 351-367.

McKenzie, R. M. (1967). "The sorption of cobalt by manganese minerals in soils." *Aust. J. Soil Res.* **5**: 235-246.

McKenzie, R. M. (1970). "The reaction of cobalt with manganese dioxide mineral." *Aust. J. Soil Res.* **8**: 97-106.

McKenzie, R. M. (1972). "The sorption of some heavy metals by the lower oxides of manganese." *Geoderma.* **8**: 29-35.

Mills, A. L., J. S. Herman, G. M. G.M. Hornberger and T. D. DeJesus (1994). "Effect of solution ionic strength and iron coatings on mineral grains on the sorption of bacterial cells to quartz sand." *Appl. Environ. Microbiol.* **60**: 3300-3306.

Neal, A.L., S. Techkarnjanaruk, A. Dohnalkova, D. McCready, B.M. Peyton and G.G. Geesey (2001) "Iron sulfides and sulfur species produced at hematite surfaces in the presence of sulfate-reducing bacteria". *Geochim. Cosmochim. Acta* **65**:223-235.

Neilsen, E. H. (1992). Miscellaneous underground radioactive waste tanks, Westinghouse Hanford Company.

Nichols, F. (1995). Feasibility analysis of recycling radioactive scrap steel, MSE, Inc.

Nieves, L. A., S. Y. Chen, E. J. Kohout, R. Nabelssi, R. W. Tilbrook and S. E. Wilson (1995). Evaluation of radioactive scrap metal recycling, Argonne National Laboratory.

Obuekwe, C. O., D. W. S. Westlake, J. A. Plambeck and F. D. Cook (1981). "Corrosion of mild steel in cultures of ferric iron reducing bacterium isolated from crude oil. II. Mechanism of anodic depolarization." *Corrosion (Houston)* **37**: 632-637.

Obuekwe, C. O., D. W. S. Westlake, J. A. Plambeck and F. D. Cook (1981). "Corrosion of mild steel in cultures of ferric iron-reducing bacterium isolated from crude oil: polarization characteristics." *Corrosion* **37**: 461-467.

Obuekwe, C. O., W. S. Westlake, F. D. Cook and J. W. Costerton (1981). "Surface changes in mild steel coupons from the action of corrosion-causing bacteria." *Appl. Environ. Microbiol*. **41**: 766-774.

Phillips, E. J. P., D. R. Lovley and E. E. Roden (1993). "Composition of Non-Microbially Reducible Fe(III) in Aquatic Sediments." *Appl. Environ Microbiol.* **59**(8): 2727-2729.

Rai, D. 1984. Solubility Product of Pu(IV) Hydrous Oxide and Equilibrium Constants of Pu(IV)/Pu(V), Pu(IV)/Pu(VI), and Pu(V)/Pu(VI) Couples. *Radiochimica Acta* 35: 97-108

Rai, D., L. Rao, H. T. Weger, A. R. Felmy, G. R. Choppin, M. Yui. 1999. Thermodynamic Data for Predicting Concentrations of Pu(III), Am(III), and Cm(III) in Geologic Environments. JNC TN8400 99-010. Japan Nuclear Cycle Development Institute, Tokai Works.

Roden, E. E. and J. M. Zachara (1996). "Microbial Reduction of Crystalline Fe(III) Oxides: Influence of Oxide Surface Area and Potential for Cell Growth." *Environ. Sci. Tech* **30**: 1618-1628.

Rusin, P. A., L. Quintana, J. R. Brainard, B. A. Strietelmeier, C. D. Tait, S. A. Ekberg, P. D. Plamer, T. W. Newton and D. L. Clark (1994). "Solubilization of plutonium hydrous oxide by iron-reducing bacteria." *Environ. Sci. Technol.* **28**: 1686-1690.

Sanchez, A. L., J. W. Murray and T. H. Sibley (1985). "The adsorption of plutonium IV and V on goethite." *Geochim. Cosmochim. Acta* **49**: 2297-2307.

Schramke, J. A., D. Rai, G. R. Choppin, and R. W. Fulton. 1989. Determination of Aqueous Plutonium Oxidation States by Solvent Extraction. *J. Radioanal. Nucl. Chem., Articles* 130: 333-346.

Schultz, M. F., M. M. Benjamin and J. F. Ferguson (1987). "Adsorption and desorption of metals on ferrihydrite: reversibility of the reaction and sorption properties of the regenerated soil." *Environ. Sci. Technol.* **21**: 863-869.

Siegrest, H. and Gujer (1985). *Wat. Res.* **19**: 1369-1372.

Stumm, W., R. Kummert and L. Sigg (1980). "A ligand exchange model for the adsorption of inorganic and organic ligands at hydrous oxide interfaces." *Croat. Chem. Acta* **53**: 291-312.

Tsapin, A. I., K. H. Nealson, T. Meyers, M. A. Cusanovich, J. Van Beuumen, L. D. Crosby, B. A. Feinberg and C. Zhang (1996). "Purification and properties of a low-redox-potential tetraheme cytochrome c3 from Shewanella putrefaciens." *J. Bacteriol.* **178**(21): 6386-6388.

Westlake, D. W. S., K. M. Semple and C. O. Obuekwe (1986). Corrosion by ferric iron-reducing bacteria isolated from oil production systems. Biologically Induced Corrosion. S. C. Dexter. Houston, National Association of Corrosion Engineers**:** 193-200.

Yong, P. and L.E. Macaskie (1998) "Bioaccumulation of Lanthanum, uranium and thorium, and use of a model system to develop a method for the biologically-mediated removal of plutonium from solution". *J. Chem. Technol. Biotechnol.* **71**:15-26.

Zachara, J. M., C. C. Ainsworth, C. E. Cowan and C. T. Resch (1989). "Adsorption of chromate by subsurface soil horizons." *Soil Sci. Soc. Am. J.* **53**: 418-428.

Zachara, J. M., D. C. Girvin, R. L. Schmidt and C. T. Resch (1987). "Chromate adsorption on amorphous iron oxyhydroxide in the presence of mafor groundwater ions." *Environ. Sci. Technol.* **21**: 589-594.

12.0 FEEDBACK

None.

13.0 APPENDICES

Appendix A. Reprints of Published Papers

Geomicrobiology Journal, 19:161–177, 2002
Copyright © 2002 Taylor & Francis
0149-0451/02 $12.00 + .00

Adhesion of Dissimilatory Fe(III)-Reducing Bacteria to Fe(III) Minerals

FRANK CACCAVO, JR.

Department of Biology
Whitworth College
Spokane, Washington, USA

AMITABHA DAS

Pacific Northwest National Laboratory
Richland, Washington, USA

The metabolism of dissimilatory iron-reducing bacteria (DIRB) may provide a means of remediating contaminated subsurface soils. The factors controlling the rate and extent of bacterial F(III) mineral reduction are poorly understood. Recent research suggests that molecular-scale interactions between DIRB cells and Fe(III) mineral particles play an important role in this process. One of these interactions, cell adhesion to Fe(III) mineral particles, appears to be a complex process that is, at least in part, mediated by a variety of surface proteins. This study examined the hypothesis that the flagellum serves as an adhesin to different Fe(III) minerals that range in their surface area and degree of crystallinity. Deflagellated cells of the DIRB Shewanella algae *BrY showed a reduced ability to adhere to hydrous ferric oxide (HFO) relative to flagellated cells. Flagellated cells were also more hydrophobic than deflagellated cells. This was significant because hydrophobic interactions have been previously shown to dominate* S. algae *cell adhesion to Fe(III) minerals. Pre-incubating HFO, goethite, or hematite with purified flagella inhibited the adhesion of* S. algae *BrY cells to these minerals. Transposon mutagenesis was used to generate a flagellum-deficient mutant designated* S. algae *strain NF. There was a significant difference in the rate and extent of* S. algae *NF adhesion to HFO, goethite, and hematite relative to that of* S. algae *BrY. Amiloride, a specific inhibitor of Na^+-driven flagellar motors, inhibited* S. algae *BrY motility but did not affect the adhesion of* S. algae *BrY to HFO.* S.algae *NF reduced HFO at the same rate as* S. algae *BrY. Collectively, the results of this study support the hypothesis that the flagellum of* S. algae *functions as a specific Fe(III) mineral adhesin. However, these results suggest that flagellum-mediated adhesion is not requisite for Fe(III) mineral reduction.*

Keywords Fe(III)-reduction, flagellum, adhesion

Subsurface soils and aquifers are contaminated with toxic metals, radionuclides, nitroaromatics, hydrocarbons, and halogenated solvents due to decades of accidental and intentional solid and liquid waste discharge. In response to this problem, there has been intense scientific interest in developing bioremediation technologies that exploit the metabolism of dissimilatory iron-reducing bacteria (DIRB). DIRB couple the oxidation of organic matter

Received 8 August 2001; accepted 6 December 2001.

This work was supported by grant 07-98ER62714 from the Department of Energy Office of Environmental Management. We thank the laboratory of E. Roden at the University of Alabama for assistance in conducting the HFO reduction experiments.

Address correspondence to Frank Caccavo, Jr., Department of Biology, Whitworth College, 300 W. Hawthorne Road, Spokane, WA 99251, USA.

to the reduction of a variety of multivalent metals (Aristovskaya and Zavarsin 1971; Lovley 1991; Lovely 1995a; Lovley 1995b). These organisms are important because they can couple the mineralization of organic contaminants to ferric iron oxide reduction; immobilize metals and radionuclides by direct enzymatic reduction; release adsorbed oxidized or reduced metals and radionuclides associated with insoluble Fe(III) mineral surfaces by reductive dissolution of the Fe(III); or indirectly reduce and immobilize metal and radionuclide contaminants and degrade halogenated solvent and nitroaromatic contaminants by producing reactive Fe(II) from Fe(III) minerals. An understanding of the factors controlling bacterial Fe(III) mineral reduction is therefore essential for predicting the rate of biotransformation and the ultimate fate of metal and radionuclide contaminants during subsurface soil or aquifer bioremediation. However, the factors controlling the rate and extent of bacterial Fe(III) mineral reduction are at present only poorly understood.

The Paradox of Microbial Fe(III) Mineral Respiration

Iron is the fourth most abundant element on Earth (Reeburg 1983). The reduction of Fe(III) is one of the most important chemical changes that occurs in the development of anaerobic soils and sediments (Ponnamperuma 1972). Despite contrasting historical references (Aristovskaya and Zavarsin 1971), a wealth of recent research supports the conclusion that much of the Fe(III) reduction in these environments is enzymatically catalyzed by DIRB (Lovely 1987; Lovely 1991; Lovely 1993; Lovely 1995b; Nealson and Saffarini 1994). Food chains of phylogenetically and physiologically diverse DIRB can completely oxidize complex organic compounds to carbon dioxide with iron serving as the sole electron acceptor (Nealson and Saffarini 1994.) DIRB can therefore play an important role in the geochemical cycling of iron as well as other elements including carbon, sulfur, phosphorous, and trace metals.

The oxidation of organic matter coupled to Fe(III) reduction is an exergonic process. The standard free energy at pH 7 that is available from acetate oxidation coupled to soluble Fe^{3+} reduction (−814 kJ/reaction) is nearly as great as that with oxygen as an electron acceptor (−849 kJ/reaction) and much greater than that with sulfate as an electron acceptor (−52 kJ/reaction) (Lovely and Phillips 1988). Numerous bacteria can gain energy for growth by catalyzing Fe(III) reduction with organic electron donors (Lovley et al. 1997). However, most of the Fe(III) present in low-organic soils and aquifers is in the form of highly insoluble minerals that range in their degree of crystallinity, particle size, surface area, and reactivity (Ponnamperuma 1972; Schwertmann and Taylor 1977). Such minerals include hydrous ferric oxide (HFO), goethite, and hematite.

The rate and extent of dissimilatory Fe(III) mineral reduction, and thus the potential for subsurface soil and aquifer bioremediation by DIRB, are limited by the bioavailability of Fe(III) in these environments (Lovely 1987). Although the metabolism of DIRB is operationally similar to that of oxygen respirers, nitrate reducers, sulfate reducers or methanogens, the unavailability of the Fe(III) in Fe(III) minerals as an electron acceptor may be an important constraint on the ability of DIRB to compete with these organisms for organic carbon. The molecular mechanisms by which DIRB utilize Fe(III) minerals as substrates for growth in natural environments are incompletely understood. Because DIRB exert a significant biogeochemical influence in many anaerobic environments, we hypothesize that they have evolved specific mechanisms to overcome the complex chemical nature of iron and exploit Fe(III) minerals as a potential substrate for anaerobic respiration and growth.

Cell-Mineral Contact as a Mechanism for Surmounting Fe(III) Insolubility

A number of studies have suggested that DIRB cell contact with insoluble Fe(III) minerals plays a role in Fe(III) mineral reduction. Fe(III) minerals separated from DIRB cells by

placing the oxide in dialysis tubing were not reduced (Tugel et al. 1986; Arnold et al. 1988; Lovley and Phillips 1988; Caccavo et al. 1992). Cell-free filtrates from growing cultures of *Shewanella* sp. 200 (Arnold et al. 1988), *Geobacter metallireducens* (Lovely and Phillips 1988), and *Shewanella algae* BrY (Caccavo et al. 1992) did not reduce Fe(III), suggesting that a soluble, iron-reducing intermediate was not produced. Adhesion of *S. alga* BrY cells to Fe(III) bound in anaerobic activated sludge flocs was found to be requisite for Fe(III) reduction (Caccavo et al. 1996). Environmental scanning electron microscopic and confocal laser scanning microscopic studies have shown that *Shewanella putrefaciens* colonizes goethite and ferrihydrite during dissimilatory Fe(III) reduction (Little et al. 1997). *S. putrefaciens* has also been shown to remain passively mobile on Fe(III) mineral coated surfaces, presumably to enhance opportunities for bacteria-iron mineral surface contact (Grantham et al. 1997). Force microscopy has been used to examine the interactions between *S. oneidensis* and goethite (Lower et al. 2001). This study found that under anaerobic conditions, *S. oneidensis* cells respond to the surface of goethite by developing stronger adhesion energies at the cell-mineral interface. A recent study in our laboratory was the first to provide direct evidence that, in the absence of soluble electron shuttles, reversible adhesion is required for insoluble Fe(III) oxide reduction by the DIRB *S. algae* BrY (Das and Caccavo 2000).

The mechanisms by which DIRB adhere to Fe(III) minerals are not completely understood. A Fe(III)-reducing *Shewanella* sp. that attached to and corroded steel oil pipelines was shown to modify the physicochemical environment of the metal by reducing a protective, insoluble Fe(III) surface film. Corrosion resulted from depolarization of the metal anode (Obuekwe et al. 1981b, 1981c), and microscopic studies demonstrated that the *Shewanella* sp. colonized the surface of the steel coupons by means of exopolysaccharide excretion (Obuwkwe et al. 1981a). Scanning electron micrographs of *Shewanella* sp. 200 growing on hematite or goethite also showed that this organism attached to the Fe(III) minerals by what appeared to be extracellular polymer (Arnold et al. 1988). Although both of these studies suggested that extracellular polymers were involved in DIRB colonization of Fe(III) minerals, neither study examined the initial adhesion of the DIRB cells. A more recent study showed that *S. oneidensis* mobilizes a 150-KDa outer membrane protein that specifically interacts with this Fe(III) mineral under conditions suitable for dissimilatory reduction (Lower et al. 2001).

We have focused on using to *S. algae* as a model to study the mechanisms of DIRB adhesion to Fe(III) minerals. This organism can readily and preferentially bind to a range of Fe(III) oxides including HFO, goethite, and hematite (Das and Caccavo 2001). The initial interaction between *S. algae* cells and these Fe(III) oxides can be explained by the Derjaguin-Landau-Verwey-Overbeek (DLVO) theory (Das and Caccavo 2000). Although Roden and Zachara found that the initial rate and long-term bacterial reduction of such minerals are linearly correlated with oxide surface area (Roden and Zachara 1996), such a correlation was not found with regard to adhesion (Das and Caccavo 2001). The initial interaction between *S. algae* cells and Fe(III) oxides is not influenced by electrostatic interactions and appears to be predominated by hydrophobic interactions (Caccavo et al. 1997; Caccavo 1999; Das and Caccavo 2000, Das and Caccavo 2001).

Bulk chemical analysis as well as the surface-specific, spectroscopic probes TOF-SIMS and ESCA were used to compare adhesive *S. algae* BrY cells to an adhesion-deficient *S. algae* mutant (Caccavo et al. 1997). These studies showed that proteins dominated the adhesive cell surface yet the mutant cell surface was dominated by carbohydrate, suggesting that unidentified proteins on the cell surface mediate the adhesion of *S. algae* BrY.

A subsequent study used multiple independent lines of experimental evidence to examine the influence of surface proteins on *S. algae* adhesion to HFO (Caccavo 1999). Cell surface polysaccharide degradation by β-galactosidase had no effect on cell

adhesion, supporting previous findings that the adhesion of *S. algae* to HFO is independent of cell surface polysaccharide. Proteolytic enzyme treatment demonstrated that preincubating *S. algae* BrY cells with *S. griseus* protease or chymotrypsin, but not trypsin, inhibited adhesion. SDS-PAGE analysis of these cells demonstrated that proteolytic digestion with *S. griseus* protease removed a single 50-kDa protein (SP50) from the *S. algae* cell surface, while digestion with chymotrypsin removed proteins of 60 kDa (CT60) and 31 kDa (CT31). The inhibitory effects of protease and chymotrypsin on adhesion and the digestion of specific cell surface proteins by these enzymes suggested that SP50, CT60, and CT31 were putative HFO adhesion molecules. Preincubating HFO with each proteolytic enzyme also supported the role of these proteins in HFO adhesion. Such a treatment resulted in catalytic degradation of cell surface proteins. The inhibitory effect of such degradation on adhesion was significantly greater than the effect of surface coating effects. *S. griseus* protease and chymotrypsin were also capable of removing adhered cells from HFO. Inhibition of protein synthesis by culturing *S. algae* cells in the presence of subminimal inhibitory concentrations of the antibiotic chloramphenicol inhibited the adhesion of those cells to HFO by 46%. Preincubating HFO with proteins extracted from the surface of *S. algae* BrY cells also inhibited cell adhesion by 41%, suggesting that these extracted proteins specifically bound to HFO and competitively inhibited cell adhesion.

Results to date suggest that cell adhesion to Fe(III) minerals is an important and complex process. The studies described here point toward the involvement of multiple surface proteins in Fe(III) mineral adhesion. We continue to work toward elucidating the mechanisms of this process and herein provide evidence that the flagellum is a specific Fe(III) mineral adhesin.

Methods

Culture Conditions and Cell Preparation

Shewanella algae BrY (Caccavo et al. 1992; Rossello-Mora et al. 1994) was grown aerobically in tryptic soy broth (TSB)(30 g/L, Difco Laboratories, Detroit, MI) at 28°C on a rotary shaker at 150 rpm for 15 h. Cells were harvested by centrifugation (5,520 × g, 4°C, 20 min) during the late exponential-early stationary growth phase. Optimal Fe(III) reductase activity is expressed at this stage of growth (Gorby and Bolton 1993). Cells were washed once in anaerobic 30 mM $NaHCO_3$ buffer (pH 7.0) that had been made anaerobic by boiling and cooling under a stream of O_2-free N_2:CO_2 (80%:20%) (Bryant 1972; Balch and Wolfe 1976; Balch et al. 1979). The washed cells were suspended in this same buffer. *E. coli* S17-1(pUI800) (Moore and Kaplan 1989) was kindly provided by Samuel Kaplan (University of Texas Medical School, Houston, TX). *E. coli* S17-1 was grown in Luria-Bertani broth (30 g/L, Difco Laboratories, Detroit, MI) at 37°C and 200 rpm.

Transposon Mutagenesis

The suicide vector pUI800 contains the transposable element Tn*phoA* (Tn5IS*50*L*::phoA*) (Moore and Kaplan 1989; Myers and Myers 1993, 1997). The Tn*phoA* suicide vector was chosen because this system has been successfully used for transposition of closely related *Shewanella* species by other investigators (Myers and Myers 1993, 1997). Conjugal matings between *E. coli* S17-1(pUI800) and a spontaneous, rifampicin-resistant mutant of *S. algae* BrY were conducted using a donor-to-recipient ratio of 1:1 on tryptic soy agar (TSA) (40 g $liter^{-1}$, Difco) at 28°C for 5 h. Transposition was induced and transconjugants were selected by plating mating mixtures onto TSA containing rifampicin (40 $\mu g\ ml^{-1}$) and kanamycin (300 $\mu g\ ml^{-1}$). *S. algae* BrY is Km^s and therefore Km^r was conferred by the

presence of Tn*phoA*. Colony selection of *S. algae* transconjugants was facilitated by the natural red pigmentation of *S. algae* colonies relative to the white color of *E. coli* colonies. Km^r colonies were picked and transferred to TSA plates with rifampicin (40 μg ml^{-1}) and chloramphenicol (Cr) (25 μg ml^{-1}). Cr^r mutants were discarded since they may have harbored pUI800 and might not have undergone transposition.

Screening for Adhesion-Deficient Mutants

Transconjugants were transferred onto plates of soft TSB (0.2% agar) containing rifampicin (40 μg ml^{-1}) and kanamycin (30 μg ml^{-1}) and incubated at 28°C for 13 h (42). Nonmotile cells gave rise to dense pinpoint colonies, while motile *S. algae* formed haloed colonies. Pinpoint colonies were picked and streaked onto TSA plates with the above antibiotics. Motility of these cells was also assayed via phase-contrast microscopy using liquid TSB cultures.

Preparation of Deflagellated Cells

Washed suspensions of *S. algae* BrY cells were deflagellated in a Sorvall Omnimixer for 90 sec at a setting of five (Martin and Savage 1985). The bacteria were separated from the flagella by centrifugation (5,000 × g, 4°C, 30 min). The supernatant containing the flagella was used in the flagellum purification process. The bacterial pellet was washed once, suspended in $NaHCO_3$ buffer, and used in adhesion assays.

Purification of Flagella

The flagellum suspension obtained above was washed by centrifugation (10,000 × g, 4°C, 30 min). The flagella in the resulting supernatant were sedimented by centrifugation (40,000 × g, 4°C, 4 h). The resulting pellet was suspended in 10 mM Tris-HCl buffer (pH 7.0). An aliquot of this suspension (1.7 ml) was applied to a CsCl gradient (0.5 g ml^{-1} layered between equal volumes of 0.6 and 0.4 g ml^{-1} in Tris-HCL buffer). The gradient was centrifuged at 100,000 × g at 4°C for 3 h in a Beckman LB-ultracentrifuge with a SW65K rotor. The gradient tube was then punctured with a syringe and needle and the flagella band was removed and suspended in Tris-HCL buffer. The suspension was placed in the sample reservoir of a 10K Nanosep microconcentrator (Pall Filtron, Northborough, MA) and centrifuged at 14,000 × g at room temperature for 5 min. An aliquot of Tris-HCl buffer was added to the reservoir and the sample was centrifuged again. This process was repeated in order to remove the CsCl from the flagella preparation. The purity of the flagella was assayed by SDS-PAGE and by transmission electron microscopy.

SDS-PAGE

Aliquots of protein samples were heated at 95°C for 10 min in SDS-PAGE sample buffer (BioRad, Hercules, CA). Approximately 5 μg of protein were loaded into each lane of a 12.5% polyacrylamide slab gel and SDS-PAGE was conducted according to the methods of Laemmli (Laemmli 1970). BioRad low molecular weight standards (Mrs, 14,400, 21,500, 31,000, 42,700, 66,200, and 97,400) were used as standards. Proteins were visualized with Coomassie blue. An estimate of molecular size was made by comparing the relative mobility of the purified protein to the proteins of known molecular mass on SDS-PAGE gels.

Transmission Electron Microscopy

Cell suspensions (8.0×10^6 cells ml^{-1}) or flagella were fixed with glutaraldehyde. An aliquot of the suspension (2 μl) was deposited onto a 400-mesh copper grid. An equal volume of 1% uranyl acetate solution was deposited onto the grid and incubated for 2 min. This

solution was then removed by wicking with filter paper. The sample was air dried for 48 h and then examined using a JEOL 100S transmission electron microscope (TEM) at 75 kV.

Adhesion Experiments

Adhesion assays were conducted as described previously (Caccavo et al. 1997; Das and Caccavo 2000). The adhesion buffer was made using anaerobic suspensions of hydrous ferric oxide (Lovley and Phillips 1988), goethite (Roden and Zachara 1996), or hematite (Baker Chemical Co.). Either wild-type or mutant cells (final concentration of 1.80×10^8 cells ml^{-1}) were added to triplicate tubes of adhesion assay buffer containing 8.82×10^{-3} m^2 of HFO, 4.84×10^{-4} m^2 goethite, or 2.39×10^{-4} m^2 hematite. Subsamples were removed over time and analyzed for adhered cells. Similar experiments comparing the adhesion of flagellated or deflagellated *S. algae* BrY cells to HFO were conducted using final cell concentrations of 1.56×10^8 cells ml^{-1} and 1.42×10^8 cells ml^{-1}, respectively. The influence of motility on the adhesion of *S. algae* BrY to HFO was examined by conducting adhesion assays with amiloride (dissolved in dimethyl sulfoxide, Sigma-Aldrich, St. Louis, MO) concentrations ranging from 0 to 1.0 mM. A final concentration of 9.30×10^7 cells ml^{-1} was used. Motility in the presence of amiloride was also examined qualitatively by phase-contrast microscopy. The effect of flagella pre-incubation on adhesion was also examined by incubating the Fe(III) oxides described above with the purified flagella (final concentration of 6 μg of protein ml^{-1}) for 30 min at 150 rpm and room temperature. An adhesion assay was then performed by adding a washed cell suspension (final concentration of 1.69×10^8 cells ml^{-1}) to each tube. The effect of deflagellation on the surface properties of *S. algae* BrY was examined by conducting adhesion assays with 1.43×10^8 cells ml^{-1} (final concentration) and various matrices. Phenyl sepharose (2 ml) or sepharose (2 ml) was washed three times (8,000 $\times$ g, 4°C, 5 min) and suspended in 10 ml $NaHCO_3$ buffer. The Student t-test was used to determine whether statistically significant differences were observed between adhesion assay treatments. Differences were considered significant when p was < 0.05.

Fe(III) Reduction Experiments

Washed cell suspensions of *S. algae* BrY and *S. algae* NF were used as inocula for Fe(III)-NTA and HFO reduction experiments under non-growth conditions. The cell suspensions were rendered anaerobic by bubbling with O_2-free N_2. The medium contained 10 mM lactate and ca. 4.5 mmol Fe(III) L^{-1} in pH 6.8 PIPES buffer. Triplicate tubes were inoculated with ca. 2.5×10^8 cells mL (ca. 0.1 mg protein mL^{-1}). Samples (0.5 mL) were taken with N_2-flushed plastic syringes and added to 5 mL of 0.5M HCl. The Fe(II) content of the HCl extracts was determined after 1 to 2 h using Ferrozine.

Protein Determinations

Protein was measured using the Pierce BCA protein assay reagent kit with albumin standard (Pierce Chemical Co., Rockford, IL).

Results

Effect of Deflagellation on Adhesion

Deflagellated cells of *S. algae* BrY showed a reduced ability to adhere to HFO relative to flagellated cells (Figure 1). There was a significant difference in the rate of adhesion

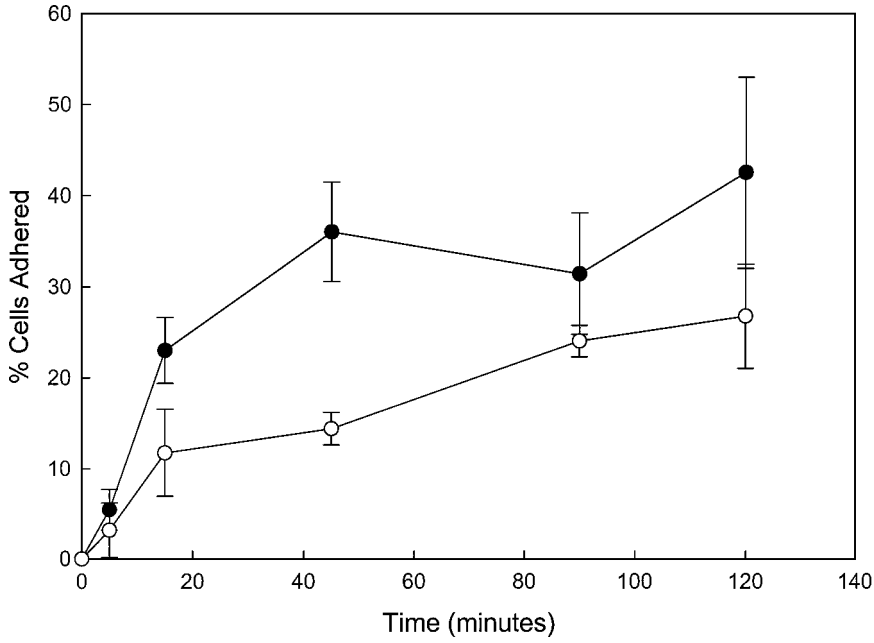

FIGURE 1 Adhesion kinetics of flagellated (●) and deflagellated (○) *S. algae* BrY cells to HFO. Error bars are the standard deviations from the means ($n = 3$).

of deflagellated and flagellated cells ($p = 0.03$). Deflagellation also influenced the surface properties of *S. algae* BrY. Flagellated cells were more hydrophobic than deflagellated cells, as demonstrated by a significant decrease in the ability of deflagellated cells to adhere to the hydrophobic resin phenyl-sepharose (Table 1).

Influence of Purified Flagella on Adhesion

Mechanical shearing and subsequent differential centrifugation of the flagella from *S. algae* BrY resulted in a suspension that, on examination by TEM, appeared to contain mostly flagella (Figure 2A). SDS-PAGE analysis of this preparation showed a single protein band with an apparent molecular weight of 59 kDa (Figure 2B, lane 3).

Pre-incubating HFO, goethite, or hematite with the purified flagella preparation inhibited the adhesion of *S. algae* BrY cells to these minerals by 33%, 76%, and 53%, respectively (Table 2).

TABLE 1 Effect of deflagellation on the surface properties of *S. algae* BrY

	% adhesion[a]		
Treatment	Flagellated cells	Deflagellated cells	*P*
HFO	34.1 ± 1.70	1.81 ± 0.00	0.001
Sepharose CL-4B	0.00 ± 0.00	0.00 ± 0.00	1.000
Phenyl-sepharose CL-4B	15.38 ± 1.04	8.18 ± 0.00	0.040

[a]Values are the means ± standard deviations ($n = 3$).

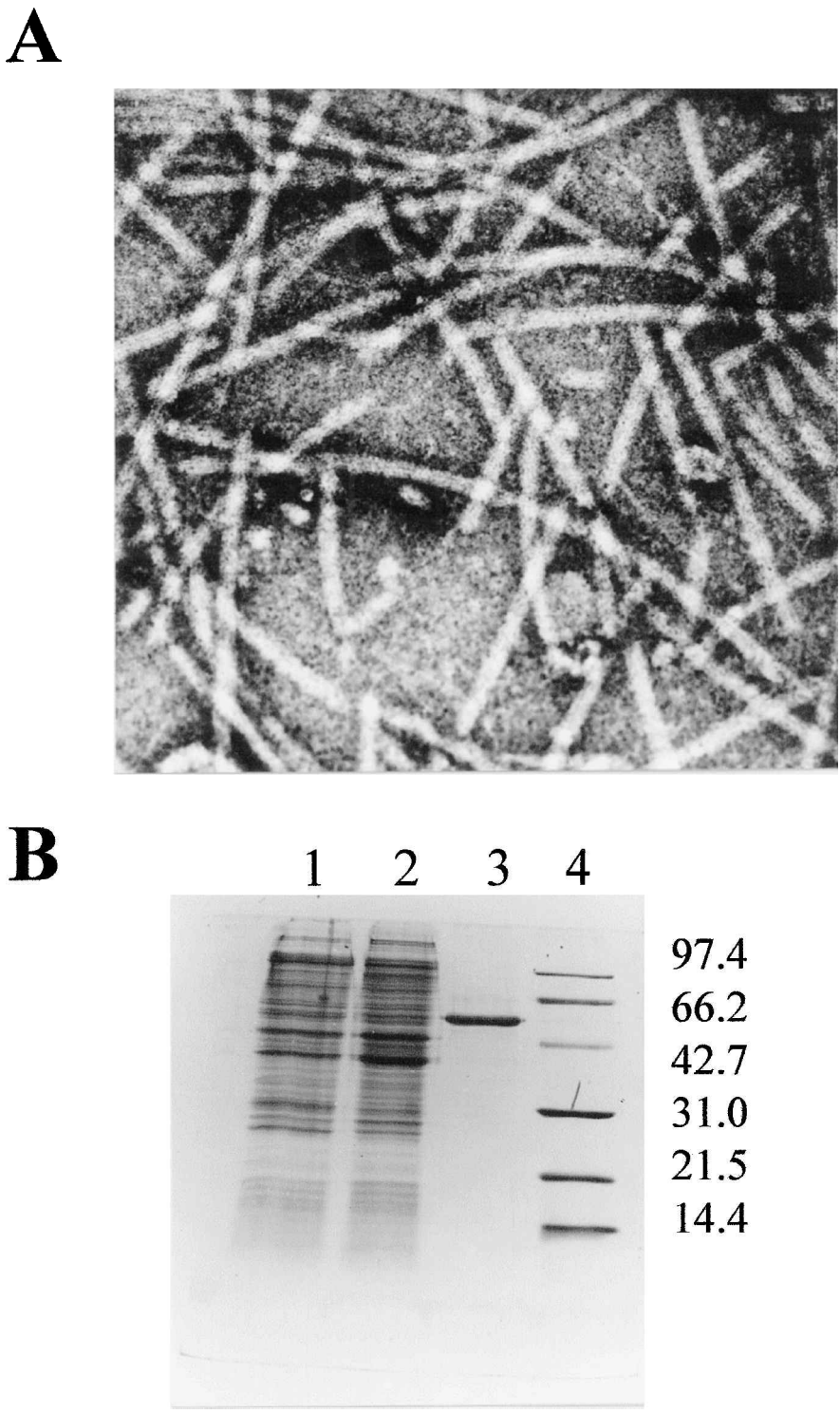

FIGURE 2 (A) Transmission electron micrograph of purified *S. algae* BrY flagella. (B) Coomassie brilliant blue R-250-stained SDS-PAGE analysis. Lanes: 1, *S. algae* NF whole cells; 2, *S. algae* BrY whole cells; 3, purified *S. algae* BrY flagella; 4, molecular mass standards (molecular weights shown on right).

TABLE 2 Adhesion of *S. algae* BrY to Fe(III) oxides with and without flagella pretreatment

	% adhesion[a]		
Fe(III) oxide	No flagella pretreatment	Flagella pretreatment	*P*
HFO	29.0 ± 10.0	19.5 ± 2.36	0.008
Goethite	42.0 ± 13.0	10.0 ± 5.90	0.015
Hematite	30.1 ± 12.4	8.27 ± 7.20	0.037

[a]Values are the means ± standard deviations ($n = 3$).

Isolation of Flagella Mutant

A Km^r, Cr^s transconjugant that formed pinpoint colonies on soft agar plates was isolated. This strain was designated *S. algae* NF. The mutant was confirmed as nonmotile by phase contrast microscopy. TEM analysis demonstrated that the lack of motility in *S. algae* NF was due to the inability of this strain to produce a flagellum (Figure 3B). The wild-type *S. algae* BrY is motile by a single polar flagellum (Figure 3A) (Caccavo et al. 1992). SDS-PAGE analysis of whole cell preparations showed that *S. algae* NF lacked a protein band corresponding to the *S. algae* flagellar protein (Figure 2B, lane 1).

Adhesion of Mutant to Fe(III) Oxides

There was a significant difference in the rate and extent of *S. algae* NF adhesion to HFO relative to *S. algae* BrY (Figure 4A) ($p = 0.005$). There was also a significant difference in the rate and extent of *S. algae* NF adhesion to goethite (Figure 4B) ($p = 0.005$) and to hematite (Figure 4C) ($p = 0.02$) relative to *S. algae* BrY.

Effect of Amiloride on Adhesion to HFO

Phase contrast microscopic analysis showed that amiloride inhibited motility in *S. algae* BrY (data not shown). However, amiloride had no effect on the adhesion of *S. algae* BrY to HFO (Figure 5).

HFO Reduction

Cell suspensions of both *S. algae* strains reduced HFO at the same rate (Figure 6). There was a linear correlation between the time-dependent reduction of HFO by *S. algae* BrY and that by *S. algae* NF (slope = 1.01, $r^2 = 0.9602$). Similar results were obtained for soluble ferric iron reduction (data not shown).

Discussion

The collective findings of our laboratory suggest that *S. algae* adhesion to Fe(III) minerals is mediated by a series of proteins. The results presented in this current study support and refine this conclusion. This study presents three independent lines of evidence that indicate that the flagellum serves as a Fe(III) mineral adhesin.

Flagella are primarily locomotive organelles that have also been shown to function as an adhesive structure (Moens and Vanderleyden 1996). For example, the flagellum was shown to function as a carrier of the moieties that promote adherence of *Vibrio cholerae* to intestinal tissue (Attridge and Rowley 1983). The flagellum is also important in the adhesion of

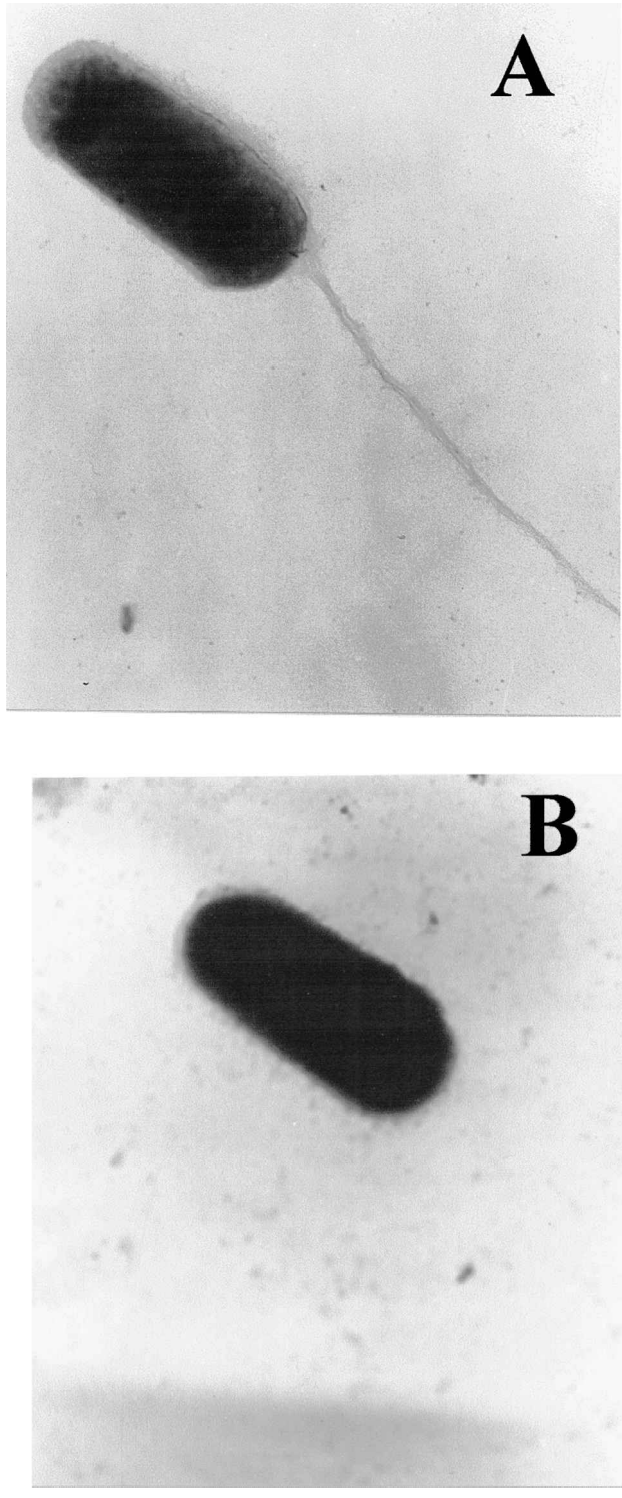

FIGURE 3 Transmission electron micrograph of (A) flagellated wild-type *S. algae* BrY and (B) nonflagellated mutant *S. algae* NF.

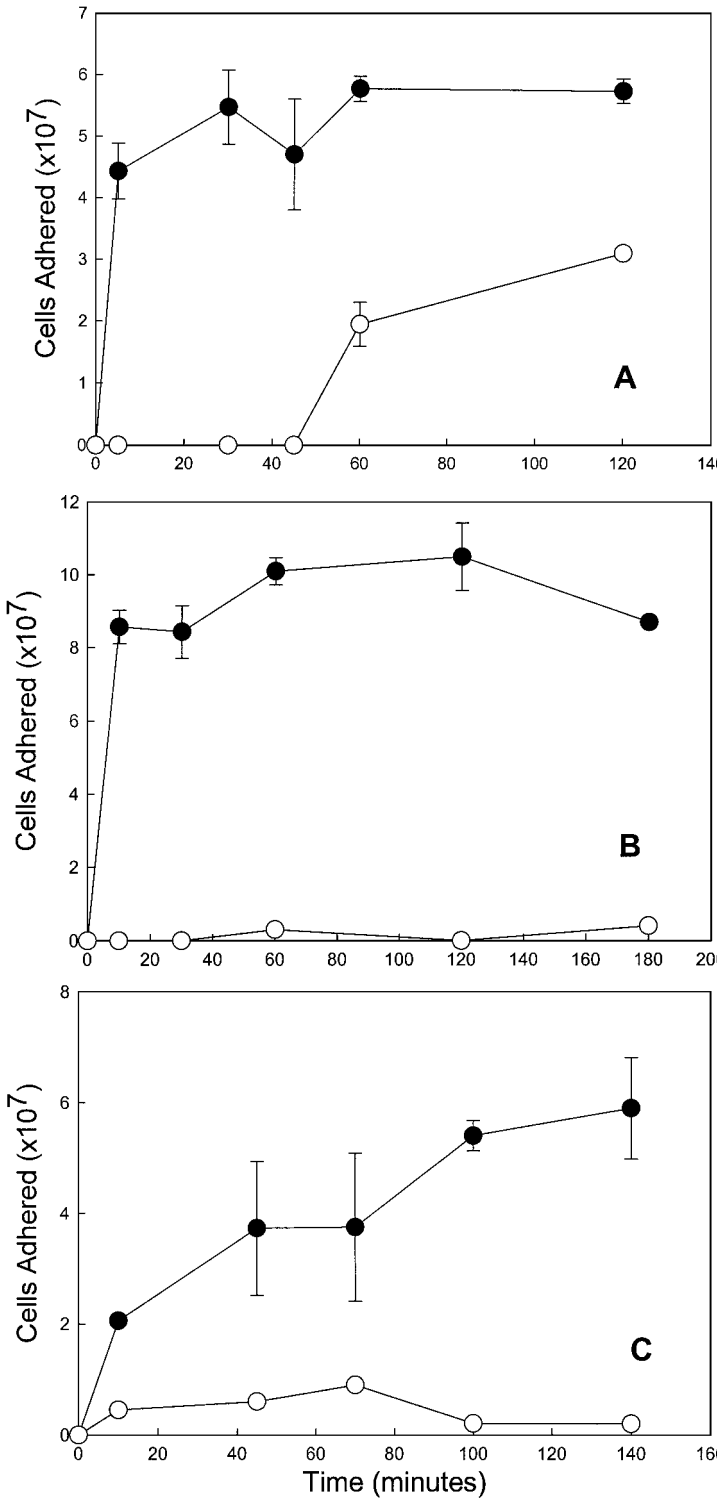

FIGURE 4 Adhesion kinetics of *S. algae* BrY (●) and *S. algae* NF (○) to (A) HFO, (B) goethite, and (C) hematite. Error bars are the standard deviations from the means ($n = 3$).

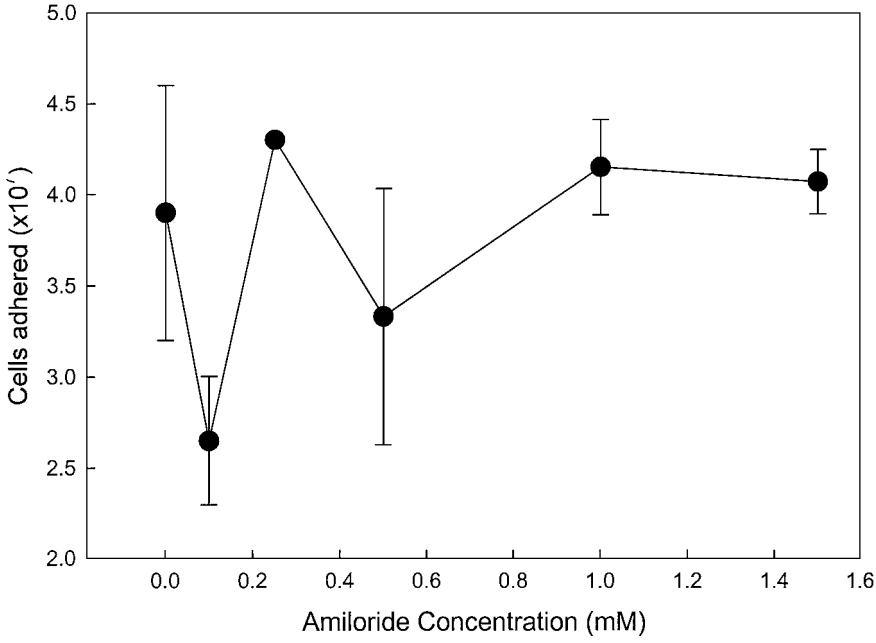

FIGURE 5 Effect of amiloride on adhesion of *S. algae* BrY to HFO. Error bars are the standard deviations from the means ($n = 3$).

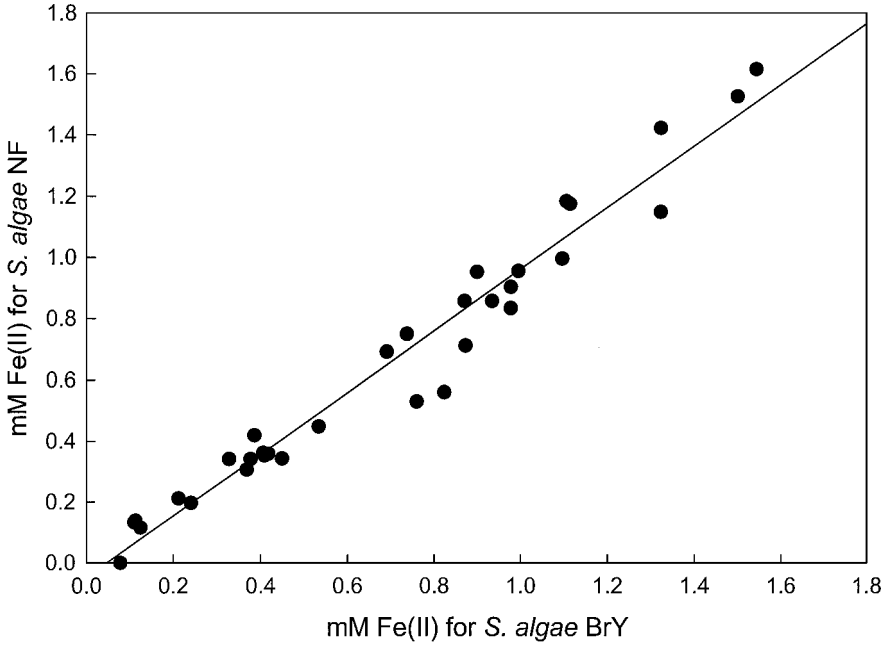

FIGURE 6 Time-dependent reduction of HFO by *S. algae* BrY versus HFO reduction by *S. algae* NF. Datum points represent the mean of triplicate samples from three independent experiments.

Camplyobacter jejuni to the mucosal surface (McSweegan and Walker 1986). Ohmura et al. (1996) have shown that *Thiobacillus ferroxidans* uses a 40-kDa protein located in the flagellum to chemically bond to elemental sulfur particles. In a more recent study, flagella of *Listeria monocytogenes* were shown to act as an adhesive structure during the early stages of attachment to stainless steel (Vatanyoopaisarn et al. 2000). This adhesion was independent of cell motility.

The results presented here suggest that *S. algae* BrY adhesion to HFO is also independent of cell motility. Amiloride, a specific inhibitor of Na^+-driven flagellar motors (Kawagishi et al. 1995), inhibited *S. algae* BrY motility but did not affect the adhesion of *S. algae* BrY to HFO. The finding that deflagellation of *S. algae* BrY resulted in a significant loss in the ability of this organism to adhere to HFO suggests that the flagellum of this organism may function instead as a specific Fe(III) mineral adhesin. Deflagellation also changed the physicochemical properties of the *S. algae* BrY cell surface. The significant decrease in the ability of deflagellated cells to adhere to phenyl-sepharose relative to flagellated cells suggests that the surface of deflagellated cells was less hydrophobic. It is known that the surface of *S. algae* BrY cells is hydrophobic and that initial, reversible adhesion of this organism to Fe(III) minerals is mediated by hydrophobic interactions (Caccavo 1997; Caccavo 1999; Das and Caccavo 2000; Das and Caccavo 2001). The results presented here suggest that the flagellum contributes to the hydrophobic nature of the *S. algae* BrY cell surface.

Additional experimental evidence supporting the role of the flagellum as a Fe(III) mineral adhesin is the finding that purified flagella bound specifically to each of the Fe(III) oxides studied, and significantly inhibited the initial adhesion of *S. algae* BrY cells to these oxides. We have recently shown that a mixture of proteins extracted from the surface of *S. algae* BrY can bind to the surface of HFO and inhibit cell adhesion by up to 41% (Caccavo 1999). The binding of these proteins to HFO was specific, because bound bovine serum albumin did not inhibit adhesion. A 60-kDa protein was among the 28 proteins in this extract that bound to HFO. This protein was also shown to be sensitive to a protease that inhibited *S. algae* BrY adhesion to HFO and was thus identified as CT60, a putative adhesin molecule. The adhesin protein CT60 corresponds in size to the 59-kDa flagelin purified in this study.

The most conclusive evidence supporting the role of the flagellum as a Fe(III) mineral adhesin is the finding that a flagellum-deficient transposon mutant, *S. algae* NF, showed a significantly reduced ability to adhere to all of the oxides studied relative to the wild-type strain. TEM of this strain clearly showed that transposition resulted in the loss of the single, polar flagellum typical of this species.

Adhesion can be described as a two-stage process. Bacteria are initially attracted to a substratum and weakly held at a finite distance from it by a balancing of London van der Waals attraction forces and electrostatic repulsion forces, as described by the DLVO theory (Marshall et al. 1971). This adhesion is reversible and is then followed by irreversible adhesion as the bacterium uses adhesin molecules that overcome the electrostatic repulsion barrier at the substratum (Marshall et al. 1971). This theory may be used to clarify the role that cell adhesion plays in the respiration of insoluble Fe(III) minerals.

The results of the current study demonstrated that HFO reduction by *S. algae* did not require production of the flagellar adhesin. These results support previous findings showing that another adhesion-deficient, mutant strain of *S. algae* (RAD20) reduced HFO at a rate identical to that of the adhesive *S. algae* BrY. Cells of *S. algae* RAD20 initially adhered to the HFO to an extent nearly equal to *S. algae* BrY. However, the *S. algae* RAD20 cells desorbed over the course of the experiment while the *S. algae* BrY cells became firmly adhered. The initial adhesion of both strains was most likely mediated by hydrophobic interactions. However, *S. algae* RAD20 over-produced extracellular polysaccharides that sterically inhibited the interaction of proteinaceous cell surface adhesins with HFO. Although both

S. algae RAD20 and *S. algae* NF were deficient in their ability to adhere to HFO, they both were capable of respiring with HFO at a rate and extent equal to the adhesive *S. algae* BrY. We have previously shown that reversible adhesion mediated by hydrophobic interactions is required for *S. algae* to reduce HFO (Das and Caccavo 2000). It now appears that irreversible adhesion via surface adhesins, like the flagellum, is not required for HFO respiration in this strain. Although loss of the flagellum reduced the overall hydrophobic nature of the *S. algae* NF cell surface, these cells must have been sufficiently hydrophobic to interact with HFO.

Empirical evidence from our and other laboratories clearly indicates that this organism irreversibly adheres to Fe(III) minerals. We have also shown that this adhesion is preferential for Fe(III)-bearing minerals (Caccavo et al. 1996). Since irreversible adhesion is not required for HFO respiration, it is unclear why these cells make a variety of surface proteins used to preferentially and irreversibly adhere to Fe(III) mineral. This represents an interesting and important line of future research.

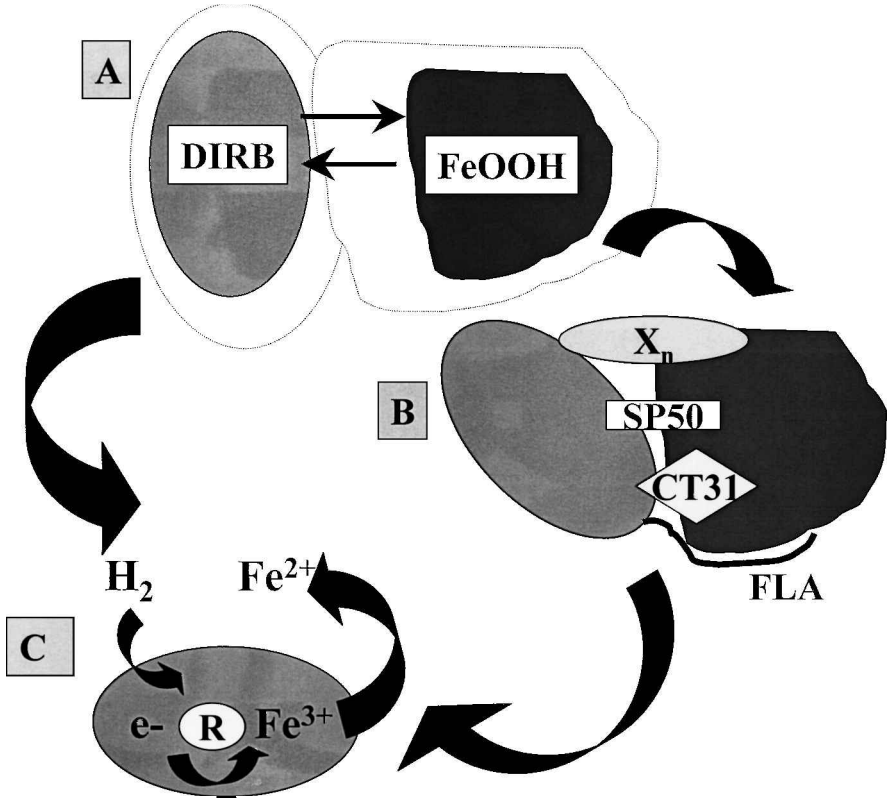

FIGURE 7 Model describing the relationship between DIRB cell adhesion and enzymatic Fe(III) mineral reduction. (A) Hydrophobic interactions (dashed lines) initiate contact between the DIRB cell and the Fe(III) oxide particle. (B) Cell surface proteins mediate the adhesion of the DIRB cell to the Fe(III) particle. The proteins labeled SP50, CT31, and FLA represent identified adhesins. The protein labeled X_n represents additional adhesins that have not yet been identified. The exact number and specific functions of adhesion proteins are not known. (C) Intimate adhesion allows the DIRB cell to couple electron donor (H_2) oxidation to enzymatic reductive dissolution of the Fe(III) mineral particle.

Although flagellum-mediated adhesion is not requisite for HFO respiration, it may significantly influence the transport of DIRB in contaminated, Fe(III)-bearing subsurface environments. This will in turn impact the rate and extent of organic, metal, and radionuclide contaminant biotransformation. The mechanisms and controls on DIRB adhesion to Fe(III) minerals are therefore important considerations for predicting the distribution and activity of DIRB populations in the subsurface, and for assessing the role that soil mineralogical heterogeneities may play in this distribution.

The results of this study further our understanding of the adhesion process by identifying the flagellum of *S. algae* BrY as an adhesin to a variety of Fe(III) minerals. These results help to clarify the role that adhesion plays in Fe(III) mineral respiration and raise new questions about the role that specific adhesins play in the metabolism and ecology of this organism.

Adhesion Model

Recent work suggests that DIRB have evolved specific mechanisms to overcome the complex chemical nature of iron and exploit Fe(III) as a potential substrate for anaerobic respiration and growth. Our central hypothesis is that such adaptations include the production of cell surface proteins that specifically mediate cell adhesion to Fe(III) minerals. Our model for *S. algae* adhesion to Fe(III) minerals is shown in Figure 7. Reversible contact between *S. algae* cells and HFO is initiated by hydrophobic interactions. These initial interactions are requisite for Fe(III) mineral reduction. Specific proteins on the cell surface then mediate the irreversible adhesion of the *S. algae* cell to the Fe(III) oxide. We have identified three of these proteins, the flagellum (CT60), SP50, and CT31, although our data suggest that additional proteins may also be involved. We hypothesize that each protein has a specific, as yet unknown, function in the adhesion process. Data presented in this and previous studies suggest that the rate and extent of Fe(III) mineral reduction by DIRB may not be dependent upon expression of these specific adhesion proteins.

References

Aristovskaya TV, Zavarsin GA. 1971. In: McLaren AD, Skujins J, editors. Biochemistry of iron in soil. New York: Dekker, p 385–408.

Arnold RG, DiChristina TJ, Hoffman MR. 1988. Reductive dissolution of Fe(III) oxides by *Pseudomonas* sp. 200. Biotechnol Bioeng 32:1081–1096.

Attridge SR, Rowley D. 1983. The role of the flagellum in the adherence of *Vibrio cholerae*. J Infect Dis 147:864–872.

Balch WE, Fox GE, Magrum LJ, Woese CR, Wolfe RS. 1979. Methanogens: reevaluation of a unique biological group. Microbiol Rev 43:260–296.

Balch WE, Wolfe RS. 1976. New approach to the cultivation of methanogenic bacteria: 2-mercaptoethanesulfonic acid (HS-CoM)-dependent growth of *Methanobacterium ruminantium* in a pressurized atmosphere. Appl Environ Microbiol 32:781–791.

Bryant MP. 1972. Commentary on the Hungate technique for culture of anaerobic bacteria. Am J Clin Nutr 25:1324–1328.

Caccavo Jr F. 1999. Protein-mediated adhesion of the dissimilatory Fe(III)-reducing bacterium *Shewanella alga* BrY to hydrous ferric oxide. Appl Environ Microbiol 65:5017–5022.

Caccavo Jr F, Blakemore RP, Lovley DR. 1992. A hydrogen-oxidizing, Fe(III)-reducing microorganism from the Great Bay estuary, New Hampshire. Appl Environ Microbiol 58:3211–3216.

Caccavo Jr F, Frølund B, Kloeke F van O, Nielsen PH. 1996. Deflocculation of activated sludge by the dissimilatory Fe(III)-reducing bacterium *Shewanella alga* strain BrY. Appl Environ Microbiol 62:1487–1490.

Caccavo Jr F, Schamberger PC, Keiding K, Nielsen PH. 1997. Role of hydrophobicity in adhesion of the dissimilatory Fe(III)-reducing bacterium *Shewanella alga* to amorphous Fe(III) oxide. Appl Environ Microbiol 63:3837–3843.

Das A, Caccavo Jr F. 2000. Dissimilatory Fe(III) oxide reduction by *Shewanella alga* BrY requires adhesion. Curr Microbiol 40:344–347.

Das A, Caccavo Jr F. 2001. Adhesion of the dissimilatory Fe(III)-reducing bacterium *Shewanella alga* BrY to crystalline Fe(III) oxides. Curr Microbiol 42:151–154.

Ghiorse WC. 1988. Microbial reduction of manganese and iron. In: Zehnder JB, editor. Biology of anaerobic microorganisms. New York: Wiley Interscience, p 305–331.

Gorby YA, Bolton Jr H. 1993. Effects of O_2 on metal-reductase activity and cytochrome content in a facultative Fe(III)-reducing bacterium. Abstracts of the Annual Meeting of the American Society for Microbiology 1993, Washington, DC: 37:368.

Grantham MC, Dove PM, DiChristina TJ. 1997. Microbially catalyzed dissolution of iron and aluminium oxyhydroxide mineral surface coatings. Geochim Cosmochim Acta 61:4467–4477.

Kawagishi I, Maekawa Y, Atsumi T, Homma M, Imae Y. 1995. Isolation of polar and lateral flagellum-defective mutants in *Vibrio alginolyticus* and identification of their flagella driving energy sources. J Bacteriol 177:5158 8–5160.

Laemmli UK. 1970. Cleavage of structural proteins during the assembly of the head of bacteriophage T4. Nature 227:680–685.

Lindsay WL, Schwab AP. 1982. The chemistry of iron in soils and its availability to plants. J Plant Nutr 5:821–840.

Little BJ, Wagner PA, Lewandowski Z. 1997. In: Banfield JF, Nealson KH, editors. Geomicrobiology: interactions between microbes and minerals. Washington, DC: Mineralogical Society of America, p 123–159.

Lovley DR. 1987. Organic matter mineralization with the reduction of ferric iron: a review. Geomicrobiol J 5:375–399.

Lovley DR. 1991. Dissimilatory Fe(III) and Mn(VI) reduction. Microbiol Rev 55:259–287.

Lovley DR. 1993. Dissimilatory metal reduction. Annu Rev Microbiol 47:263–290.

Lovley DR. 1995a. Bioremediation of organic and metal contaminants with dissimilatory metal reduction. J Ind Microbiol 14:85–93.

Lovley DR. 1995b. Microbial reduction of iron, manganese, and other metals. Adv Agron 54:176–217.

Lovley DR, Coates JD, Saffarini D, Lonergan DJ. 1997. In: Iron and related transition metals in microbial metabolism. Chur, Switzerland: Harwood Academic Publishers, p 187–215.

Lovley DR, Phillips EJP. 1988. Novel mode of microbial energy metabolism: organic carbon oxidation coupled to dissimilatory reduction of iron or manganese. Appl Environ Microbiol 54:1472–1480.

Lower SK, Hochella Jr MF, Beveridge TJ. 2001. Bacterial recognition of mineral surfaces: nanoscale interactions between Shewanella and α-FeOOH. Science 292:1360–1363.

Marshall KC, Stout R, Mitchell R. 1971. Mechanism of the initial events in the sorption of marine bacteria to surfaces. J Gen Microbiol 68:337–348.

Martin JH, Savage DC. 1985. Purification and characterization of flagella from *Roseburia cecicola*, an obligately anaerobic bacterium. J Gen Microbiol 131:2075–2078.

McSweegan E, Walker RI. 1986. Identification and characterization of two *Camplyobacter jejuni* adhesins for cellular and mucous substrates. Infect Immun 53:141–148.

Moens S, Vanderleyden J. 1996. Functions of bacterial flagella. Crit Rev Microbiol 22:67–100.

Moore MD, Kaplan S. 1989. Construction of Tn*phoA* gene fusions in *Rhodobacter sphaeroides*: isolation and characterization of a respiratory mutant unable to utilize dimethylsulfoxide as a terminal electron acceptor during anaerobic growth in the dark on glucose. J Bacteriol 171:4385–4394.

Murray JW. 1979. Iron oxides In: Burns RG, editor. Marine minerals. Washington, DC: Mineralogical Society of America, p 47–98.

Myers CR, Myers JM. 1993. Role of menaquinone in the reduction of fumarate, nitrate, iron(III) and manganese(IV) by *Shewanella putrefaciens* MR-1. FEMS Microbiol Lett 114:215–222.

Myers CR, Myers JM. 1997. Cloning and sequencing of *cym*A, a gene encoding a tetraheme cytochrome *c* required for reduction of iron(III), fumarate, and nitrate by *Shewanella putrefaciens* MR-1. J Bacteriol 179:1143–1152.

Nealson KH, Saffarini D. 1994. Iron and manganese in anaerobic respiration: environmental significance, physiology and regulation. Ann Rev Microbiol 48:311–343.

Obuekwe CO, Westlake DWS, Cook FD, Costerton JW. 1981a. Surface changes in mild steel coupons from the action of corrosion-causing bacteria. Appl Environ Microbiol 41:766–774.

Obuekwe CO, Westlake DWS, Plambeck JA, Cook FD. 1981b. Corrosion of mild steel in cultures of ferric iron reducing bacterium isolated from crude oil: polarization characteristics. Corrosion 37:461–467.

Obuekwe CO, Westlake DWS, Plambeck JA, Cook FD. 1981c. Corrosion of mild steel in cultures of ferric iron reducing bacterium isolated from crude oil: mechanism of anodic depolarization. Corrosion 37:632–637.

Ohmura N, Tsugita K, Koizumi J-I, Saiki H. 1996. Sulfur-binding protein of flagella of *Thiobacillus ferrooxidans*. J Bacteriol 178:5776–5780.

Ponnamperuma FN. 1972. The chemistry of submerged soils. Adv Agron 24:29–96.

Reeburg WS. 1983. Rates of biogeochemical processes in anoxic sediments. Ann Rev Earth Planet Sci 11:269–298.

Richardson K, Nixon L, Mostow P, Kaper JB. 1990. Transposon-induced non-motile mutants of *Vibrio cholerae*. J Gen Microbiol 136:717–725.

Roden EE, Zachara JM. 1996. Microbial reduction of crystalline iron(III) oxides: influence of oxide surface area and potential for cell growth. Environ Sci Technol 30:1618–1628.

Rossello-Mora R, Caccavo Jr F, Springer N, Spring S, Osterlehner K, Shuler D, Ludwig W, Amann R, Schleifer KH. 1994. Isolation and taxonomic characterization of a halotolerant facultatively iron-reducing bacterium. Syst Appl Microbiol 17:569–573.

Schwertmann U, Taylor RM. 1977. Iron oxides. In: Dixon JB, Weed SB, editors. Minerals in soil environments. Madison, WI: Soil Science Society of America, p 145–180.

Tugel JB, Hines ME, Jones GE. 1986. Microbial iron reduction by enrichment cultures isolated from estuarine sediments. Appl Environ Microbiol 52:1167–1172.

Vatanyoopaisarn S, Nazli A, Dodd CER, Rees CED, Waites WM. 2000. Effect of flagella on initial attachment of *Listeria monocytogenes* to stainless steel. Appl Environ Microbiol 66:860–863.

CURRENT MICROBIOLOGY Vol. 40 (2000), pp. 344–347
DOI: 10.1007/s002849910068

Current Microbiology
An International Journal
© Springer-Verlag New York Inc. 2000

Dissimilatory Fe(III) Oxide Reduction by *Shewanella alga* BrY Requires Adhesion

Amitabha Das, Frank Caccavo, Jr.

Department of Microbiology, Rudman Hall, University of New Hampshire, Durham, NH 03824, USA

Received: 26 October 1999 / Accepted: 22 November 1999

Abstract. The Derjaguin-Landau-Verwey-Overbeek (DLVO) theory was used to examine the relationship between adhesion and dissimilatory Fe(III) oxide reduction. Adhesion of *Shewanella alga* BrY to hydrous ferric oxide (HFO) was correlated with ionic strength and thus was accurately described by the DLVO theory. Reduction of insoluble HFO was also correlated with KCl concentration. In contrast, there was no correlation between soluble Fe(III) reduction and ionic strength. A correlation between HFO reduction rate and adhesion to HFO was observed. These results provide direct evidence that adhesion is requisite for Fe(III) oxide reduction in the absence of soluble electron shuttles.

Dissimilatory iron-reducing bacteria (DIRB) couple the oxidation of organic matter to the reduction of ferric iron [12, 17, 22]. This metabolism greatly influences the geochemical processes in non-sulfidogenic anaerobic soils and sediments. The low solubility of ferric iron at neutral pH [16, 21] poses a potential metabolic obstacle for the DIRB. They must use a terminal electron acceptor that occurs as a variety of particulate oxides that differ in their surface area, crystallinity, and reactivity [24]. One mechanism that the DIRB may use to overcome this obstacle is adhesion to the Fe(III) oxide particles. Recent studies have clearly demonstrated that DIRB readily and preferentially adhere to Fe(III) oxides [8, 15]. The DIRB *Shewanella alga* BrY produces a complex, proteinaceous system that mediates cell adhesion to hydrous ferric oxide (HFO) [5], and this organism uses different mechanisms to adhere to more crystalline Fe(III) minerals [9].

While the ability of DIRB to adhere to Fe(III) oxides has been well established, the evidence that cell adhesion is a necessary prerequisite for dissimilatory Fe(III) oxide reduction is mostly circumstantial and thus equivocal. Studies with both enrichment cultures and pure cultures of DIRB have suggested that physical contact between the cell and Fe(III) minerals is necessary for dissimilatory Fe(III) mineral reduction. When HFO was separated from DIRB cells by placing the oxide in dialysis tubing, no Fe(III) reduction was observed [1, 6, 19, 26]. Cell-free filtrates from growing cultures of *Pseudomonas* sp. 200 [1], *Geobacter metallireducens* [19], and *S. alga* BrY [6] did not reduce Fe(III) minerals, suggesting that a soluble, iron-reducing intermediate was not produced. Adhesion of *S. alga* BrY cells to anaerobic sludge flocs was found to be necessary for Fe(III) reduction [7]. Environmental scanning electron microscopic and confocal laser scanning microscopic studies have shown that *Shewanella putrefaciens* colonizes goethite and ferrihydrite [15]. Atomic force microscopic studies have shown that *S. putrefaciens* cells attached to Fe(III) oxide-coated silica slides removed portions of the Fe(III) oxide coating by an unknown mechanism [14]. Finally, experiments comparing insoluble Fe(III) reduction rates between *S. alga* BrY and an adhesion-deficient strain of this species suggested that contact, but not irreversible adhesion, was required for insoluble Fe(III) reduction [8].

The purpose of this study was to determine whether a direct correlation between DIRB adhesion and dissimilatory Fe(III) oxide reduction exists.

Materials and Methods

Culture conditions and cell preparation. *Shewanella alga* BrY is a Gram-negative rod that was isolated from anaerobic sediments of the Great Bay estuary, New Hampshire [6, 23]. *S. alga* BrY was grown aerobically in 100 ml of tryptic soy broth (30 g/L, Difco Laboratories, Detroit, MI) at 28°C on a rotary shaker at 150 rpm for 15 h. Cells were harvested by centrifugation (5520 *g*, 4°C, 20 min) during the late exponential–early stationary growth phase. Optimal Fe(III) reductase activity is expressed at this stage of growth [13]. Cells were washed once in anaerobic 10 mM HEPES-buffer (*N*-[2-hydroxyethyl]piperazine-

Correspondence to: F. Caccavo, Jr.

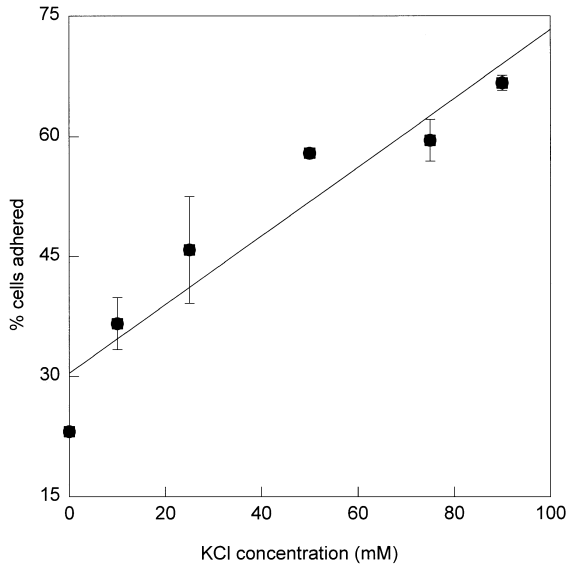

Fig. 1. Adhesion of *S. alga* BrY to HFO as a function of KCl concentration. Error bars represent the standard deviations from the means (n = 3). The line was drawn with SigmaPlot (Jandel Scientific) and represents a linear regression analysis using the least squares method [11]. The equation for the line was y = 0.429x + 30.39.

N′-[2-ethanesulfonic acid]), pH 7.0, that had been made anaerobic by boiling and cooling under a stream of O_2-free N_2 [2–4]. The washed cells were suspended in this same buffer.

Adhesion assay. The adhesion assay was conducted as described previously [8] in anaerobic HEPES buffer with HFO (1 mM) and varying concentrations of potassium chloride. The final cell concentration in the adhesion assays was 1.5×10^9 cells ml^{-1}. The initial pH of the adhesion assay buffers did not vary by more than 0.05 units. Adhesion assays were also conducted at different KCl concentrations with HFO-free buffer. These controls showed that ionic strength did not influence cell sedimentation. All adhesion assays were performed in triplicate.

Iron reduction assays. Tubes of anaerobic HEPES buffer containing either HFO or soluble ferric citrate and varying KCl concentrations were inoculated with *S. alga* BrY cell suspensions. The final cell concentrations for HFO and ferric citrate were 1.5×10^9 and 2.8×10^9 cells ml^{-1}, respectively. Hydrogen (10 ml) was added to the headspace of the tubes to provide an electron donor. The initial pH of the Fe(III) buffers did not vary by more than 0.07 units. Fe(III) reduction was monitored by measuring the accumulation of Fe(II) over time. Samples were removed from the tubes with syringes and needles [4] and extracted in 0.5 *N* HCl for 15 min. The amount of Fe(II) solubilized after this extraction was determined with Ferrozine as previously described [19]. All iron reduction experiments were performed in triplicate.

Results and Discussion

We used the Derjaguin-Landau-Verwey-Overbeek (DLVO) theory [10, 26] to determine whether DIRB cell adhesion is necessary for Fe(III) oxide reduction. The DLVO theory treats bacteria as colloids and evaluates the changes in free energy between the cell surface and solid particles as a function of separation distance. When a bacterial cell approaches a solid particle, it experiences physicochemical forces traditionally associated with adsorption theory [27]. Both *S. alga* BrY and HFO are negatively charged [8, 9], and thus the adhesion of *S. alga* cells to HFO particles is influenced by electrostatic repulsion. However, according to DLVO theory, increasing the ionic strength of the adhesion buffer will serve to balance these repulsive forces, decrease the potential energy to the secondary minimum, and allow the DIRB cell to more readily occupy reversible adsorption sites on the HFO particle. Figure 1 demonstrates that *S. alga* BrY adhesion to HFO can be accurately described by DLVO theory. The percentage of *S. alga* BrY cells that adhered to HFO increased in linear proportion to the concentration of balancing electrolyte (KCl) in the adhesion buffer ($r^2 = 0.90$).

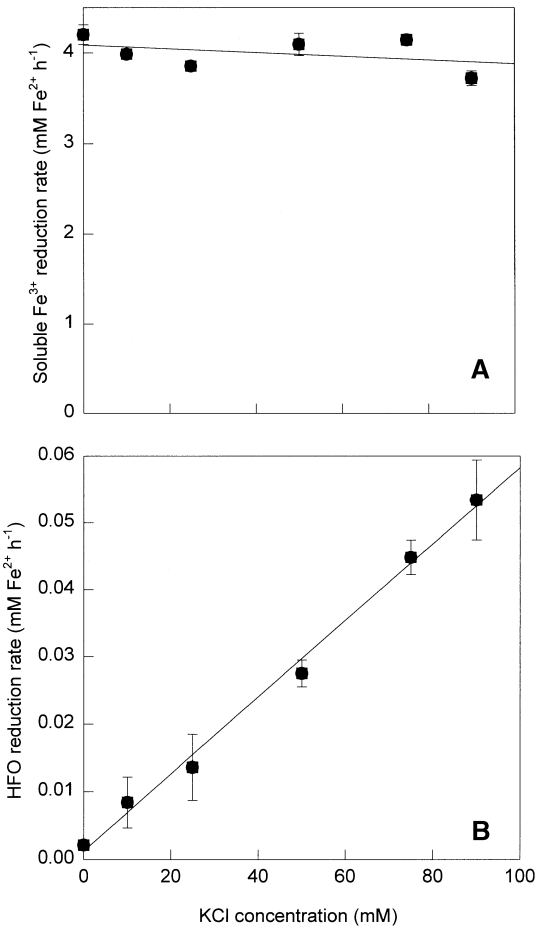

Fig. 2. Reduction of (A) soluble ferric citrate and (B) insoluble HFO by *S. alga* BrY as a function of KCl concentration. Error bars represent the standard deviations from the means (n = 3). The lines were drawn using SigmaPlot (Jandel Scientific) and represent linear regression analyses using the least squares method [11]. The equations for the lines were y = −0.002x + 4.087 and y = 5.698x + 1.221 for plots A and B, respectively.

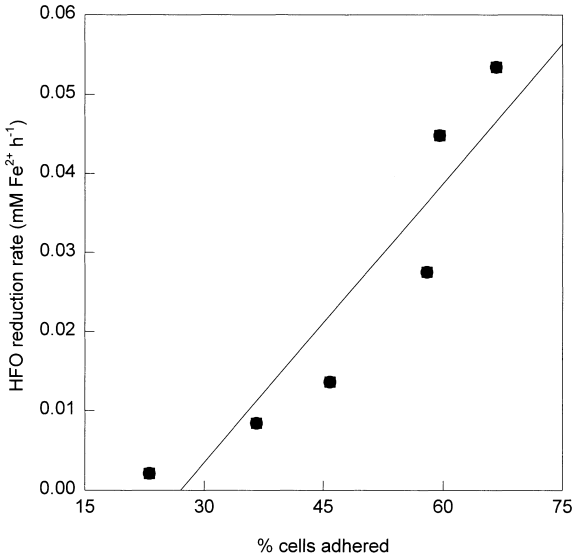

Fig. 3. The relationship between *S. alga* BrY adhesion to HFO and HFO reduction rate. The line was drawn with SigmaPlot (Jandel Scientific) and represents a linear regression analysis using the least squares method [11]. The equation for the line was $y = 1.175x + -0.031$.

The ability of *S. alga* BrY to reduce insoluble HFO was correlated with KCl concentration (Fig. 2B) ($r^2 = 0.99$). However, buffer ionic strength had no effect on the ability of *S. alga* BrY cells to reduce soluble Fe(III) (Fig. 2A), and the soluble Fe(III) reduction rate was poorly correlated with the concentration of KCl ($r^2 = 0.16$). Since KCl had no influence on *S. alga* reduction of soluble Fe(III), we can assume that KCl did not affect components of the electron transport chain or the terminal Fe(III) reductase. The positive influence of KCl on HFO reduction rate is thus consistent with DLVO theory. As ionic strength increases, the location at which reversible sorption occurs as a result of balanced attractive and repulsive forces between cell and Fe(III) particle is forced closer to the actual mineral surface [20]. This would allow the *S. alga* BrY cells greater access to HFO adsorption sites and stimulate the HFO reduction rate. This hypothesis is supported by the data shown in Fig. 3. A correlation between adhered cells and HFO reduction rates based on buffer ionic strength was observed ($r^2 = 0.90$).

The metabolic versatility of DIRB has focused scientific attention on developing bioremediation technologies based on this metabolism [17]. However, the effective application of such technologies has been hindered by a lack of information on the mechanisms by which DIRB overcome the low solubility of Fe(III) and respire with Fe(III) minerals. Recent research has suggested that soluble organic compounds, such as humic acids, can shuttle electrons between DIRB cells and insoluble Fe(III) oxides [18]. Such a mechanism would allow DIRB to overcome the low bioavailability of Fe(III) oxides and exploit them as electron acceptors. However, humic acids are not always available in the environments in which DIRB are active, and such a process cannot explain microbial Fe(III) reduction in defined culture media.

The information presented in this study narrows the fundamental gap in our understanding of the factors controlling the rate and extent of bacterial Fe(III) mineral reduction. This is the first study to demonstrate that *S. alga* BrY adhesion to and reduction of HFO can be described by the DLVO theory. Additionally, the results presented here provide the first direct evidence that, in the absence of soluble electron shuttles, reversible adhesion is required for insoluble Fe(III) oxide reduction by DIRB. On the basis of these results, it is now evident that cell adhesion is one of the rate-limiting steps in the dissimilatory reduction of Fe(III) oxides. We anticipate that this information can be used to model the transport of DIRB and the kinetics of bacterial Fe(III) mineral reduction in both pristine and contaminated anaerobic environments. Such models will be essential to the effective application of this metabolism in bioremediation.

ACKNOWLEDGMENTS

This work was supported by grant 07-98ER62714 from the Department of Energy, Office of Environmental Management. We thank Yuri Gorby from Pacific Northwest National Laboratory for critically reviewing the manuscript.

Literature Cited

1. Arnold RG, DiChristina TJ, Hoffman MR (1988) Reductive dissolution of Fe(III) oxides by *Pseudomonas* sp. 200. Biotechnol Bioeng 32:1081–1096
2. Balch WE, Wolfe RS (1976) New approach to the cultivation of methanogenic bacteria: 2-mercaptoethanesulfonic acid (HS-CoM)-dependent growth of *Methanobacterium ruminantium* in a pressurized atmosphere. Appl Environ Microbiol 32:781–791
3. Balch WE, Fox GE, Magrum LJ, Woese CR, Wolfe RS (1979) Methanogens: reevaluation of a unique biological group. Microbiol Rev 43:260–296
4. Bryant MP (1972) Commentary on the Hungate technique for culture of anaerobic bacteria. Am J Clin Nutr 25:1324–1328
5. Caccavo F Jr (1999) Protein-mediated adhesion of the dissimilatory Fe(III)-reducing bacterium *Shewanella alga* BrY to hydrous ferric oxide. Appl Environ Microbiol, in press
6. Caccavo F Jr, Blakemore RP, Lovley DR (1992) A hydrogen-oxidizing, Fe(III)-reducing microorganism from the Great Bay estuary, New Hampshire. Appl Environ Microbiol 58:3211–3216
7. Caccavo F Jr, Frølund B, van O. Kloeke F, Nielsen PH (1996) Deflocculation of activated sludge by the dissimilatory Fe(III)-reducing bacterium *Shewanella alga* strain BrY. Appl Environ Microbiol 62:1487–1490
8. Caccavo F Jr, Schamberger PC, Keiding K, Nielsen PH (1997) Role of hydrophobicity in adhesion of the dissimilatory Fe(III)-reducing bacterium *Shewanella alga* to amorphous Fe(III) oxide. Appl Environ Microbiol 63:3837–3843

9. Das A, Caccavo F Jr (1999) Adhesion of the dissimilatory Fe(III)-reducing bacterium *Shewanella alga* BrY to crystalline Fe(III) oxides. Appl Environ Microbiol, submitted
10. Derjagium BV, Landau L (1941) Theory of the stability of strongly charged lyphobic sols and of the adhesion of strongly charged particles in solutions of electrolytes. Acta Physicochim URSS 14:633–662
11. Draper N, Smith H (1981) Applied regression analysis, 2nd edn. New York: John Wiley & Sons, Inc.
12. Ghiorse WC (1988) Microbial reduction of manganese and iron. In: Zehnder JB (ed) Biology of anaerobic microorganisms. New York: John Wiley, pp 305–331
13. Gorby YA, Bolton H Jr (1993) Effects of O_2 on metal-reductase activity and cytochrome content in a facultative Fe(III)-reducing bacterium. Abstracts of the Annual Meeting of the American Society for Microbiology 1993:37
14. Grantham MC, Dove PM (1996) Investigation of bacterial-mineral interactions using Fluid Tapping Mode™ atomic force microscopy. Geochim Cosmochim Acta 13:2473–2480
15. Grantham MC, Dove PM, DiChristina TJ (1997) Microbially catalyzed dissolution of iron and aluminium oxyhydroxide mineral surface coatings. Geochim Cosmochim Acta 61:4467–4477
16. Lindsay WL, Schwab AP (1982) The chemistry of iron in soils and its availability to plants. J Plant Nutr 5:821–840
17. Lovley DR (1995) Microbial reduction of iron, manganese, and other metals. Adv Agron 54:176–217
18. Lovley DR, Blunt-Harris EL (1999) Role of humic-bound iron as an electron transfer agent in dissimilatory Fe(III) reduction. Appl Environ Microbiol 65:4252–4254
19. Lovley DR, Phillips EJP (1988) Novel mode of microbial energy metabolism: organic carbon oxidation coupled to dissimilatory reduction of iron or manganese. Appl Environ Microbiol 54:1472–1480
20. Mills AL, Herman JS, Hornberger GM, DeJesus TH (1994) Effect of solution ionic strength and iron coatings on mineral grains on the sorption of bacterial cells to quartz sand. Appl Environ Microbiol 60:3300–3306
21. Murray JW (1979) Iron oxides In: Burns RG (ed), Marine minerals. Washington, D.C.: Mineralogical Society of America, pp 47–98
22. Nealson KH, Saffarini D (1994) Iron and manganese in anaerobic respiration: environmental significance, physiology and regulation. Annu Rev Microbiol 48:311–343
23. Rossello-Mora R, Caccavo F Jr, Springer N, Spring S, Osterlehner K, Shuler D, Ludwig W, Amann R, Schleifer KH (1994) Isolation and taxonomic characterization of a halotolerant facultatively iron-reducing bacterium. Syst Appl Microbiol 17:569–573
24. Schwertmann U, Taylor RM (1977) Iron oxides. In: Dixon JB, Weed SB (eds) Minerals in soil environments. Madison, WI: Soil Science Society of America, pp 145–180
25. Travis CC, Etnier EL (1981) A survey of sorption relationships for reactive solutes in soil. J Environ Qual 10:8–17
26. Tugel JB, Hines ME, Jones GE (1986) Microbial iron reduction by enrichment cultures isolated from estuarine sediments. Appl Environ Microbiol 52:1167–1172
27. Verwey EJW, Overbeek JG (1948) Theory of the stability of lyphobic colloids. Amsterdam: Elsevier
28. Weber WJ, McGinley PM, Katz LE (1991) Sorption phenomena in subsurface systems: concepts, models and effects on contaminant fate and transport. Water Res 5:499–528

Pergamon

Geochimica et Cosmochimica Acta, Vol. 65, No. 2, pp. 223–235, 2001
Copyright © 2001 Elsevier Science Ltd
Printed in the USA. All rights reserved
0016-7037/01 $20.00 + .00

PII S0016-7037(00)00537-8

Iron sulfides and sulfur species produced at hematite surfaces in the presence of sulfate-reducing bacteria

ANDREW L. NEAL[1,*] SOMKIET TECHKARNJANARUK[1,†] ALICE DOHNALKOVA,[2] DAVID MCCREADY,[2] BRENT M. PEYTON,[3] and GILL G. GEESEY[1,4]

[1]Center for Biofilm Engineering, Montana State University, Bozeman, MT 59717, USA
[2] Environmental Molecular Sciences Laboratory, Pacific Northwest National Laboratory, Richland, WA 99352, USA
[3]Center for Multiphase Environmental Research, Washington State University, Pullman, WA 99164, USA
[4]Department of Microbiology, Montana State University, Bozeman, MT 59717, USA

(*Received March* 6, 2000; *accepted in revised form August* 11, 2000)

Abstract—In the presence of sulfate-reducing bacteria (*Desulfovibrio desulfuricans*) hematite (α-Fe_2O_3) dissolution is affected potentially by a combination of enzymatic (hydrogenase) reduction and hydrogen sulfide oxidation. As a consequence, ferrous ions are free to react with excess H_2S to form insoluble ferrous sulfides. X-ray photoelectron spectra indicate binding energies similar to ferrous sulfides having pyrrhotite-like structures (Fe2$p_{3/2}$ 708.4 eV; S2$p_{3/2}$ 161.5 eV). Other sulfur species identified at the surface include sulfate, sulfite and polysulfides. Thin film X-ray diffraction identifies a limited number of peaks, the principal one of which may be assigned to the hexagonal pyrrhotite (102) peak (d = 2.09 Å; 2θ = 43.22°), at the hematite surface within 3 months exposure to sulfate-reducing bacteria (SRB). High-resolution transmission electron microscopy identifies the presence of a hexagonal structure associated with observed crystallites. Although none of the analytical techniques employed provide unequivocal evidence as to the nature of the ferrous sulfide formed in the presence of SRB at hematite surfaces, we conclude from the available evidence that a pyrrhotite stiochiometry and structure is the best description of the sulfides we observe. Such ferrous sulfide production is inconsistent with previous reports in which mackinawite and greigite were products of biological sulfate reduction (Rickard 1969a; Herbert et al., 1998; Benning et al., 1999). The apparent differences in stoichiometry may be related to sulfide activity at the mineral surface, controlled in part by H_2S autooxidation in the presence of iron oxides. Due to the relative stability of pyrrhotite at low temperatures, ferrous sulfide dissolution is likely to be reduced compared to the more commonly observed products of SRB activity. Additionally, biogenic pyrrhotite formation will also have implications for geomagnetic field behavior of sediments. *Copyright © 2001 Elsevier Science Ltd*

1. INTRODUCTION

Any sulfur compound with an oxidation state greater than S^{2-} (i.e., S^0, S^{4+} and S^{6+}) has the potential to act as terminal electron acceptor in biologic oxidation of organic compounds (Goldhaber and Kaplan, 1974). Whilst assimilatory sulfate-reduction is commonplace, dissimilatory sulfate-reduction is carried out by a specialized group of nutritionally diverse organisms known collectively as anaerobic sulfate-reducing bacteria (SRB), including the genus *Desulfovibrio*. The observed activity of SRB in diverse habitats, including freshwater (Smith and Klug, 1981) and marine (Jørgensen, 1977) sediments, subsurface aquifers (Olson et al., 1981) and hydrothermal vent systems (Baross and Deming, 1983) points to their environmental significance.

The geological significance of SRB activity derives from the production of H_2S, resultant from sulfate-reduction, and its subsequent reaction with Fe^{2+} (the most abundant sulfide binding ion in typical reducing sediments) to form ferrous sulfides. Such sulfides are common components of both recent and ancient sediments and include the tetragonal, sulfur-deficient Fe^{2+}-sulfide, mackinawite (FeS-$Fe_{1.07}S$, Lennie et al., 1995a), the mixed-valence thiospinel, greigite (Fe_2^{3+}, Fe^{2+} S_4, Vaughan and Ridout, 1971) and the Fe^{2+}-polysulfide, pyrite (FeS_2). Iron sulfide mineral formation can be significant, annually an estimated 3.9×10^{13} g of pyrite-S are deposited in deltaic and anoxic continental shelf sediments (Berner, 1982). Sulfide production by SRB also has implications for steel corrosion (Hamilton, 1991) and bioremediation of heavy metal pollution in anoxic environments (Miller, 1950; Bacon et al., 1980; Webb et al., 1998).

Ferrous sulfides resulting from SRB activity have been studied previously and described as mackinawite and/or greigite (Rickard, 1969a; Herbert et al., 1998; Benning et al., 1999). In the aforementioned studies, ferrous sulfides were produced by free-living bacteria in liquid culture with added ferrous ions. However, most subsurface bacterial activity is likely to be associated with surfaces (Ghiorse and Wilson, 1988; Costerton et al., 1995), for example, the majority (98%) of bacteria in a Cape Cod aquifer were found to be attached (Harvey et al., 1984). We have therefore chosen to study ferrous sulfide production by bacteria associated with hematite surfaces.

In this study we identify ferrous sulfides produced by *Desulfovibrio desulfuricans* associated with hematite (α-Fe_2O_3) surfaces. The iron oxides goethite, lepidocrocite, ferrihydrite

*Author to whom correspondence should be addressed (andy_n@erc.montana.edu).
† *Present address:* Biochemical Engineering and Pilot Plant Research and Development Unit, National Center for Genetic Engineering and Biotechnology, Pilot Plant Development and Training Institute, King Mongkut University of Technology, Thouburi Thakham, Baugkhuntien, Bangkok, Thailand 10150.

and hematite are important Fe(III)-containing constituents of soils and sediments (Appelo and Postma 1996). The specular hematite used for these experiments lends itself to manipulation both during bacterial culture and subsequent chemical analysis. Dissimilatory bacterial sulfate reduction, using lactate as the electron donor, is described in Eqn. 1 (Thauer et al., 1977),

$$2\ \text{Lactate} + SO_4^{2-} + H^+ \rightarrow 2\ \text{Acetate} + 2CO_2 + 2H_2O + HS^-. \quad (1)$$

With no ferrous salts added to the growth medium, aq. $[Fe^{2+}]$ is potentially dependent upon a combination of indirect (*sensu.* Brown et al. 1999) reductive dissolution of hematite by hydrogen sulfide analogous to generalized goethite dissolution (Eqn. 2, Pyzik and Sommer, 1981);

$$8Fe_2O_3 + 8H_2S + 32H^+ \rightarrow 16Fe^{2+}_{(aq.)} + S_8^0 + 24H_2O \quad (2)$$

and direct reduction due to cell associated hydrogenase activity (Eqn. 3, Robert and Berthelin 1986; Le Gall et al., 1994)

$$Fe_2O_3 + 6H^+ + 2e^- \rightarrow 2Fe^{2+}_{(aq.)} + 3H_2O. \quad (3)$$

With the aim of investigating ferrous sulfide chemistry resulting from SRB activity at iron oxide surfaces (as opposed to liquid culture) we present X-ray photoelectron spectroscopic, X-ray diffraction and transmission electron microscopic evidence that the ferrous sulfides differ from those phases previously identified (i.e., mackinawite and greigite). Although an unequivocal assignment is insoluble, the techniques suggest that the surface associated precipitates are best described as pyrrhotite-like.

2. METHODS

2.1. Organisms and Culture

Two *Desulfovibrio desulfuricans* strains were used in the experiments described here, G20 and Essex 6 (ATCC 29577, NCIMB 8307, Postgate and Campbell, 1966). G20 was derived from *D. desulfuricans* G100A (Wall et al., 1993). Both strains were a gift of Dr. J. Wall, University of Missouri. A green fluorescent protein (GFP) reporter gene construct was used to visualize cells of *D. desulfuricans* strain G20. In our laboratory, the *IncQ* plasmid pdsk519 encoding for GFP-*mut2* (Matthysse et al., 1996) was modified for chloramphenicol resistance and mobilized into G20 with GFP expression under control of the constitutive *npt2* promoter. The *mut2* derivative of the wild type GFP gene confers a 30-fold increase in chromophore fluorescence intensity (Cormack et al., 1996). Use of such recombinant organisms allows in situ, non-destructive visualization of bacteria at surfaces avoiding artifacts such as changes in surface chemistry caused by more traditional staining methods (e.g., DAPI, see review by Errampalli et al., 1999).

D. desulfuricans, a facultative anaerobe, was grown in batch culture in 25 mL anaerobic serum bottles with butyl rubber septa and aluminum crimp caps (Wheaton, Millville, NJ) in Lactate Medium C (Butlin et al., 1949; Postgate, 1963). Lactate Medium C contains 8 ml l^{-1} 60% sodium lactate syrup, 4.5 g l^{-1} Na_2SO_4, 2 g l^{-1} $MgSO_4$, 1 g l^{-1} yeast extract, 1 g l^{-1} NH_4Cl, 0.5 g l^{-1} K_2HPO_4 and 0.06 g l^{-1} $CaCl_2$ ($\Sigma[SO_4^{2-}] = 40$ mM) in distilled, deionized water and adjusted to pH 7 with 6N NaOH. Na-thioglycollate ($C_2H_3O_2SNa$) and ascorbic acid were added at a concentration of 0.01 g l^{-1} to poise E_h of the medium at circa. −100 mV. All media was sterilized by autoclave at 121°C for 20 min. The medium was supplemented with chloramphenicol (20 μg ml^{-1}) to maintain selective pressure for plasmid retention by the cells. *D. desulfuricans* Essex 6 was also grown in the absence of SO_4^{2-} employing pyruvate fermentation with fumarate as the electron acceptor (Postgate and Campbell, 1966; Magee et al., 1978). The medium contains 4.5 g l^{-1} Na-fumarate (35 mM), 3.5 g l^{-1} Na-pyruvate (34 mM), 1.6 g l^{-1} $MgCl_2$, 1 g l^{-1} NH_4Cl, 1 g l^{-1} yeast extract, 0.5 g l^{-1} KH_2PO_4 and 0.1 g l^{-1} $CaCl_2$ (pH 7). Reductants were again added to poise medium E_h. Preliminary experiments have demonstrated that Essex 6 is unable to couple the oxidation of pyruvate to thioglycollate reduction. Thus the effect of *D. desulfuricans* presence at the hematite surface in the absence of sulfate (and therefore H_2S), could be assessed.

2.2. Materials and Experimentation

Natural specular hematite (α-Fe_2O_3) from Bahia, Brazil was used for this study, a gift of Dr. K. Rosso (Pacific Northwest National Laboratory, Richland, WA). Hematite samples (dimensions approximately $5 \times 3 \times 0.2$ mm) were washed before use in distilled, deionised water to remove particulate surface contamination.

The potential reductive effect of Na-thioglycollate and ascorbic acid as well as any possible photoreduction of hematite in the medium was evaluated by incubating a hematite sample in Lactate Medium C without the addition of bacteria for seventeen days at room temperature (23–26°C). Additionally samples were exposed to Lactate Medium C in the presence of G20 or Essex 6 for 17 d and to Essex 6 for three months. Other treatments included Essex 6 in sulfate-free medium and Lactate medium C in the absence of bacteria but with the addition of approximately 150 μM H_2S. Hematite samples were added to serum bottles before autoclaving. Following incubation, hematite samples with associated precipitates were removed from the culture medium and observed using epifluorescent microscopy to evaluate the presence/absence of SRB, after which they were washed in O_2-free distilled, deionised water and dried under a stream of N_2 before being mounted and placed in the XPS vacuum chamber.

2.3. Instrumentation

2.3.1. Optical microscopy

Observation of bacteria attached to the hematite surface was made using an Olympus BX60 microscope equipped with an infinity-corrected, long working distance water immersion objective lens (40×, NA = 0.55, Nikon Inc., Torrence, CA) and 100 W Hg-vapor discharge lamp. Reflected differential interference contrast (DIC) images were captured using a U-DICR polarizer (Olympus America Inc., Lake Success, NY), fluorescence images with a WIBA filter block (460–490 nm excitation; 505 nm dichroic mirror; 515–550 nm emission; Olympus America Inc.). Video capture was performed using an Image-Point™ monochrome, Peltier cooled (+10 °C) CCD camera (Photometrics Ltd., Tuscon, AZ) and Image-Pro Plus™ software (Media Cybernetics, Silver Springs, MD).

2.3.2. X-ray photoelectron spectroscopy

X-ray photoelectron spectroscopy (XPS) was performed on a Model 5600ci spectrometer (Perkin Elmer Inc., Eden Prairie, MN). The instrument was calibrated employing the Au4$f_{7/2}$, Cu2$p_{3/2}$ and Ag3$d_{5/2}$ photopeaks with binding energies of 83.99, 932.66 and 368.27 eV respectively. A 5 eV flood gun was used to offset charge accumulation on the samples. A consistent 800 μm diameter area was analyzed on all surfaces using a monochromatized AlK_α X-ray source (1486.6 eV) at 300 W and a pass energy of 93.9 eV for broad scans, 29.35 eV for high-resolution scans (nominal resolution = 0.3 eV). The system was operated at a base pressure of 10^{-8}–10^{-9} τ. To correct for sample charging, all reported literature-based binding energies have been referenced to the adventitious C1*s* peak observed on hematite exposed to Lactate Medium C in the absence of bacteria at 285.1 eV.

Fe2$p_{3/2}$ spectra were analyzed using a multiplet splitting model derived from consideration of electrostatic and spin-orbit interactions (Gupta and Sen, 1974; Gupta and Sen, 1975). We have however followed the practice of McIntyre and Zetaruk (1977), Pratt et al. (1994a) and Pratt et al. (1994b) in fitting only three major peaks to the Fe^{2+}-S spectrum, ignoring two minor peaks at elevated binding energies (E_b). Fe^{3+}-O spectra have been fitted using four peaks, consistent with the aforementioned authors. S2*p* spectra have been fitted employing asymmetric doublets (ΔE_b 1.18 eV) reflecting the spin-orbit splitting of S2$p_{3/2}$ and S2$p_{1/2}$ photopeaks. Following baseline subtraction (Shirley, 1972), curves were fit employing combinations of Lorenztian

Table 1. XPS reference binding energies of iron and sulfur species encountered at the hematite surface.

Species	Mineral	Binding energy (eV)[a]	FWHM[b] (eV)	Reference
Fe2$p_{3/2}$				
Fe^{3+}-O	hematite (α–Fe_2O_3)	711.1		McIntyre and Zetaruk, 1977
		711.3		Junta-Rosso and Hochella, 1996
		711.0		Asami et al., 1976
Fe^{2+}-S	pyrrhotite ($Fe_{0.89}S$)	708.5		Buckley and Woods, 1985
	pyrrhotite (Fe_7S_8)	707.8	2.3	Jones et al., 1992
		707.6	1.6	Pratt et al., 1994b
		707.5	1.6	Pratt et al., 1994a
	greigite (Fe_2^{3+}, $Fe^{2+}S_4$)	707.3	1.6	Herbert et al., 1998
	mackinawite ($Fe_{1+x}S$)	707.8		Lennie and Vaughan, 1996
	pyrite (FeS_2)	707.5		Buckley and Woods, 1987
Fe^{3+}-S	pyrrhotite (Fe_7S_8)	708.9	1.3	Pratt et al., 1994b
		709.3		Pratt et al., 1994a
	greigite (Fe_2^{3+}, Fe^{2+} S_4)	709.2	1.4	Herbert et al., 1998
S2p				
S^{2-}	greigite (Fe_2^{3+}, Fe^{2+} S_4)	161.0	1.3	Herbert et al., 1998
	pyrrhotite ($Fe_{0.89}S$)	161.6		Buckley and Woods, 1985
	pyrrhotite (Fe_7S_8)	161.4	1.9	Jones et al., 1992
		161.3	0.9–1.2	Pratt et al., 1994a
		161.3	1.3	Pratt et al., 1994b
	mackinawite ($Fe_{1+x}S$)	162.4		Lennie and Vaughan, 1996
	pyrite (FeS_2)	162.8		Buckley and Woods, 1987
S_2^{2-}		162.5		Mycroft et al., 1990
		162.3	1.3	Pratt et al., 1994b
S_n^{2-}		163.8		Hyland and Bancroft, 1989
		163.3	0.9–1.2	Pratt et al., 1994a
		163.3	2.2	Pratt et al., 1994b
$S_2O_3^{2-}$		164.0		Manocha and Park, 1977
		164.0	1.3	Pratt et al., 1994b
S^0		164.4	0.9–1.2	Pratt et al., 1994a
		164.2		Hyland and Bancroft, 1989
SO_3^{2-}		166.5		Wagner et al., 1992
		166.5	0.9–1.2	Pratt et al., 1994a
SO_4^{2-}		168.3	0.9–1.2	Pratt et al., 1994a
		168.6	1.4	Pratt et al., 1994b
		168.8	2.0	Jones et al., 1992
$S_2O_3^{2-}$		169.7		Manocha and Park, 1977

[a] All E_b are referenced to a C1s of 285.1 eV
[b] Full width at half maximum

and Gaussian line shapes. Table 1 contains Fe2$p_{3/2}$ and S2p E_b from previous studies, referenced to the adventitious C1s of 285.1 eV.

2.3.3. X-ray diffraction

Thin film X-ray diffraction was carried out on precipitates at the hematite surface using a Phillips X'Pert MPD (Phillips Analytical, Natick, MA) incorporating a vertical theta-theta goniometer (220 mm radius) and a long fine focus ceramic X-ray tube with a Cu anode. The instrument was operated at a power of 40 kV, 50 mA, using CuK_α radiation (λ = 1.541 Å). Parallel beam optics were employed with a Gutmann mirror providing a high intensity, parallel collimated incident beam. The receiving optics comprised a 0.09 radian parallel plate collimator and proportional counter detector. The sample was mounted at room temperature on an Anton-Paar TTK 450 thin-film stage under vacuum ($\sim 2 \times 10^{-2}$ τ). Diffractograms were run over the 2θ range 5°–75° with a (constant) angle of incidence (Ω) of 2.5°. Diffraction pattern analysis was performed using Jade 5™ software (Materials Data Inc., Livermore, CA) with comparison to the Joint Committee on Powder Diffraction Standards (JCPDS) database.

2.3.4. High resolution TEM (HR-TEM)

Hematite samples with associated precipitates were anaerobically embedded in hard grade LR White™ resin, and cured for six hours at 60°C. Hardened blocks were sectioned in an anaerobic glove box using a Leica UltraCut R microtome (Leica Microsystems Inc., Deerfield, IL). In an attempt to minimize sample compression and hematite fracture during sectioning, a Diatome Ultra 35° knife was used in favor of the more common 45° knife (see Jesior 1986). The lower angle edge resulted in sections without hematite fracture of sufficient area to investigate the attached biofilm precipitates. Fifty nanometer thick sections were collected at room temperature on copper grids supported with lacey carbon film and observed at 200 kV using a JEOL 2010 high-resolution analytical electron microscope (JEOL USA Inc., Peabody, MA). High-resolution images were collected and analyzed by DigitalMicrograph® 3 software (Gatan Inc., Pleasanton, CA).

3. RESULTS

3.1. Evaluation of Culture Medium and Bacteria Attached to Hematite

Throughout incubation, culture media were visually evaluated for the formation of ferrous sulfides in suspension as a black discoloration of the normally straw-colored (due to the inclusion of yeast extract in the medium) solution. In no treatment was such discoloration observed, suggesting that if any ferrous sulfide production had taken place it was confined to the hematite surfaces. Epifluorescent microscopic observation con-

(a)

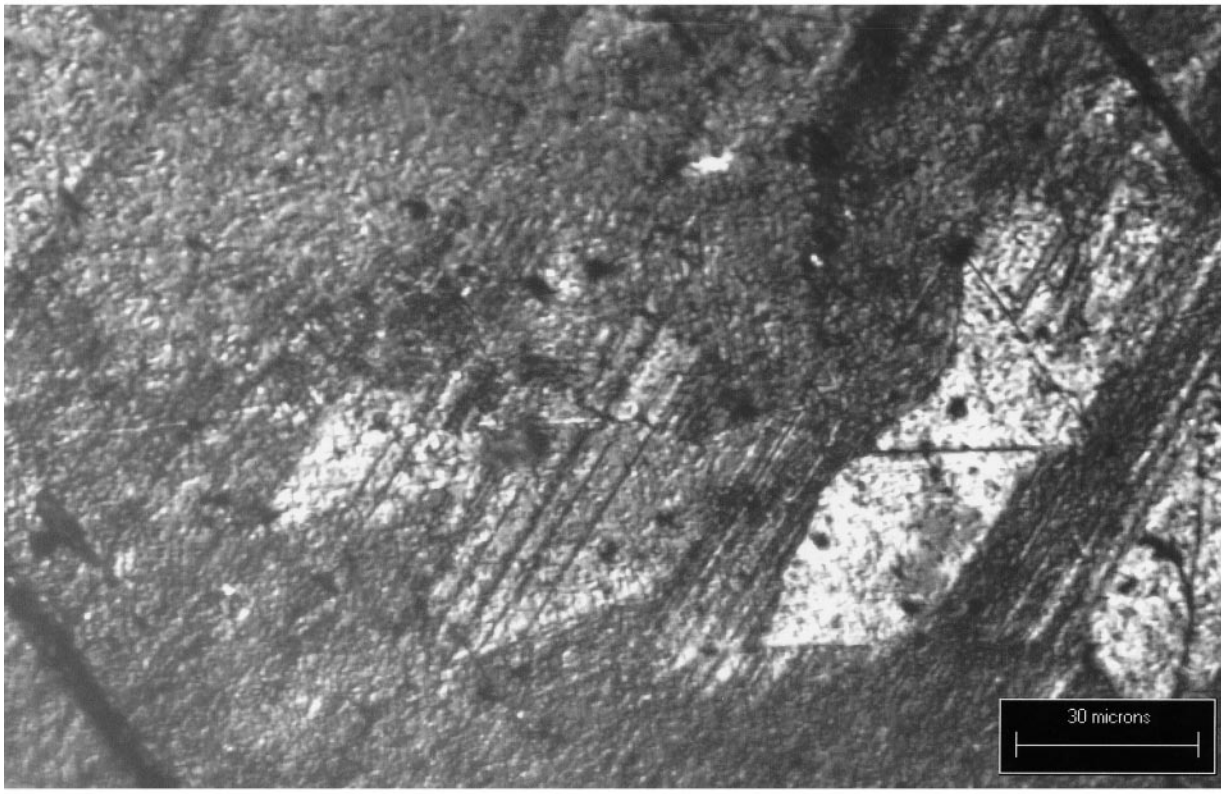

(b)

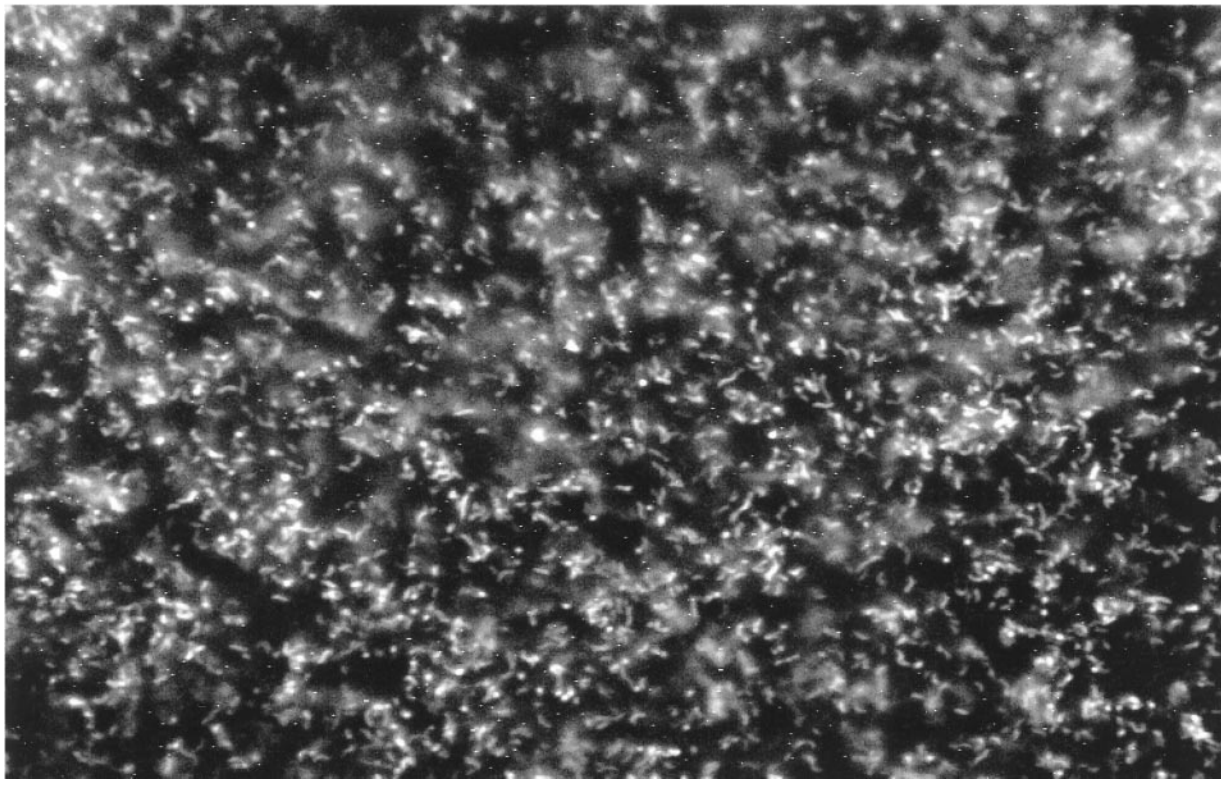

Fig. 1. Reflected DIC (above) and corresponding epifluorescence (below) photomicrographs of *Desulfovibrio desulfuricans* G20 (pNpt2CmGFP) attached to a hematite surface after 17 d in culture. The scale bar associated with the DIC image is representative of both images. 40× long working distance, water immersion lens. DIC image, 32 msec exposure, 4 dB gain, Epifluorescent image, 10 sec exposure, 4 dB gain.

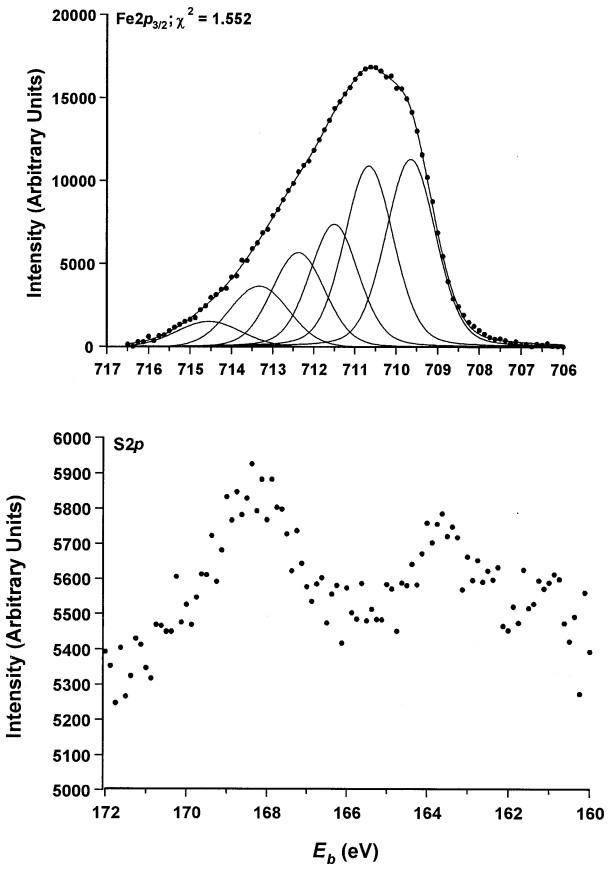

Fig. 2. XPS spectra of hematite surface exposed to growth medium in the absence of sulfate-reducing bacteria. Fe2$p_{3/2}$; component photopeaks are fitted representing Fe^{3+}-O of the hematite surface, the peak weighted average is 710.9 eV. S2*p*; despite the low signal to noise ratio, photopeaks representative of sulfate (*circa.* 168 eV), elemental sulfur/thiosulfate (*circa.* 164 eV) can be distinguished. Component bands were fitted to the Fe2$p_{3/2}$ spectrum following baseline subtraction (see Section 2.3 for details on baseline substraction and curve fitting). Adventitious C1s = 285.1 eV.

firmed the association of *D. desulfuricans* with the precipitates formed at the mineral surfaces (Fig. 1). No bacteria were observed on sterile mineral surfaces.

3.2. XPS Spectra of Hematite Surfaces

3.2.1. Sterile hematite surface

The presence of adventitious C and N was observed on the hematite surface, no doubt resulting from exposure to the growth medium but also potentially, from fluid infiltration between adjacent hematite platelets in the original hematite crystal (Junta-Rosso and Hochella, 1996). The Fe2$p_{3/2}$ region is shown in Figure 2 together with the results of curve fitting. In accordance with McIntyre and Zetaruk (1977) a pair of narrow photopeaks separated by 1.2 eV best fit the steep leading edge of the Fe2*p* region (χ^2 = 1.55). The Fe^{3+}-O peak weighted average is 710.9 eV, consistent with published hematite XPS spectra (Asami et al., 1976; McIntyre and Zetaruk, 1977; Junta-Rosso and Hochella, 1996). A photopeak in the O1*s* core region at 529.9 eV was attributed to O^{2-} of hematite (Junta-Rosso and Hochella, 1996, data not shown). Although at every step of sample preparation care was taken to avoid sample oxidation, assessment of the degree of oxidation (if any) was not possible because precipitates were analyzed in situ at the hematite surface and the O^{2-} photopeak of the substratum confounds the identification of oxidized species potentially associated with precipitates. Since the primary product of SRB activity on the hematite surface was expected to be ferrous sulfide, the S2*p* region was also studied on the unexposed surface. Despite a low signal-to-noise ratio, weak photopeaks were observed at circa 164 eV, 168 eV and at 161 eV (Fig. 2). These photopeaks can be attributed to $S_8^0/S_2O_3^{2-}$ (Hyland and Bancroft, 1989, Manocha and Park, 1977) and SO_4^{2-} (Jones et al., 1992) and S^{2-} (Buckley and Woods, 1985; Pratt et al., 1994a,b) species respectively, presumably resulting from sulfate adsorption from the growth medium and the reductive effect of medium associated Na-thioglycollate both on the hematite surface and sulfate. Some reduction and sulfide formation therefore occurs in the absence of bacteria however, as will be demonstrated, the degree of reduction is inconsequential relative to reduction and sulfide production in the presence of SRB.

3.2.2. Hydrogen sulfide exposed hematite surface

The Fe2$p_{3/2}$ region exhibited a contribution at low E_b indicative of Fe^{2+} (Fig. 3). Curve fitting employed the hematite model established from the unexposed surface (Fe^{3+}-O, see Fig. 2), with the addition of a principal photopeak at 708.7 eV (FWHM = 1.4 eV) and two multiplets 0.9 eV either side of the major peak (χ^2 = 1.24, see Fig. 3). The E_b of the principal peak is in good agreement with the Fe2$p_{3/2}$ Fe^{2+}-S photopeak collected on pyrrhotite by Buckley and Woods (1985, see Table 1). Since the Fe^{3+}-S component of the putative pyrrhotite (Pratt et al., 1994a,b) is likely to be confounded with the Fe^{3+}-O component of hematite, whilst accepting the lack of adherence to the pyrrhotite model, no attempt was made to include these photopeaks in the curve fitting procedure. Instead, corroborating evidence was sought in the S2*p* core region for the identification of the ferrous sulfide.

The S2*p* region is potentially complicated by contributions from monosulfide (S^{2-}), disulfide (S_2^{2-}) and polysulfide (S_n^{2-}) species (Hyland and Bancroft, 1989). S^{2-} and S_2^{2-} peaks originate from S-Fe bonds whilst S_n^{2-} peaks originate from S-S bonds. To obtain a good fit to the data (χ^2 = 1.33), we have adopted the approach of previous authors (Pratt et al. 1994a; Herbert et al., 1998) in fitting doublets (ΔE_b 1.18 eV) for S_2^{2-} and S_n^{2-} to the high E_b tail in the S2*p* core region. The principal S2$p_{3/2}$ photopeak was identified at 167.9 eV (FWHM = 1.3 eV) corresponding to SO_4^{2-}, undoubtedly likely due to adsorption of sulfate from the growth medium, accompanied by a second peak corresponding to SO_3^{2-} at 166 eV (FWHM = 1.3 eV) (Wagner et al., 1992). Minor photopeaks at 161.4 (FWHM = 1.3 eV) and 163.2 eV (FWHM = 1.2 eV) were ascribed to S^{2-} and S_2^{2-} respectively (Mycroft et al., 1990; Pratt et al., 1994a; Pratt et al., 1994b). Whilst the S^{2-} and S_2^{2-} may potentially be due to interactions with other cations in the growth medium (for example Mg^{2+} and Na^{2+}) the position of the monosulfide peak is again similar to pyrrhotite-like structures (Buckley and Woods, 1985; Jones et al., 1992; Pratt et al., 1994a; Pratt et al., 1994b).

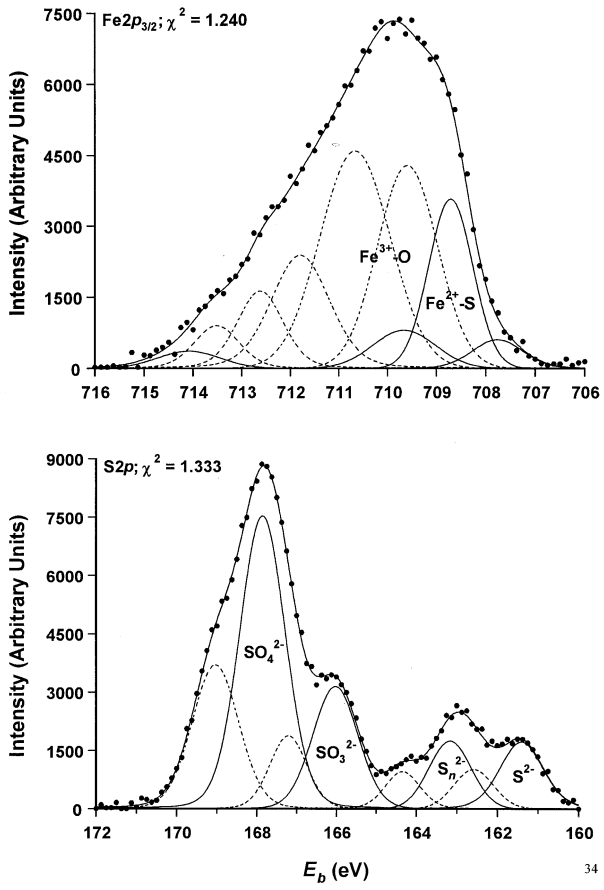

Fig. 3. XPS spectra of hematite surface exposed to hydrogen sulfide. Fe2$p_{3/2}$; Fe^{2+}-S contributions are indicated by solid lines, Fe^{3+}-O contributions by broken lines. The Fe^{2+}-S maximum is at 708.7 eV. S2*p*; S-species are represented by multiplet peaks representing the S2$p_{3/2}$ and S2$_{1/2}$ spin states, S2$p_{3/2}$ contributions for the S-species indicated are respented by solid lines, the corresponding S2$p_{1/2}$ contributions by broken lines. Component bands were fitted to both spectra following baseline subtraction. (See Section 2.3 for details on baseline subtraction and curve fitting). Adventitous Cls = 285.1 eV.

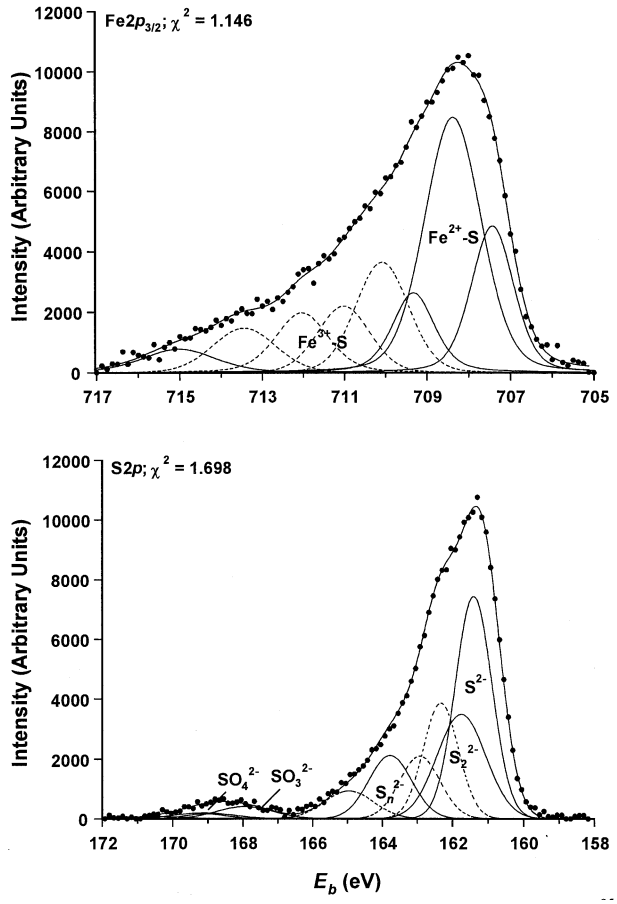

Fig. 4. XPS spectra of hematite sulface exposed to the sulfate-reducing bacterium *Desulfovibrio desulfuricans* Essex 6 for 17 d. Fe2$p_{3/2}$; Fe^{2+}-S contributions are indicated by solid lines, Fe^{3+}-S contributions by broken lines. The Fe^{2+}-S maximum is at 708.4 eV. S2*p*; S-species are represented by multiplet peaks representing the S2$p_{3/2}$ and S2$p_{1/2}$ spin states, S2$p_{3/2}$ contribution for the S-species indicated are represented by solid lines, the corresponding S2$p_{1/2}$ contributions by broken lines. Component bands were fitted to both spectra following baseline subtraction. (See Section 2.3 for details on baseline subtraction and curve fitting). Adventitious C1s = 285.1 eV.

3.2.3. SRB exposed hematite surface

Broad scan spectra (not shown) suggested C1*s* and N1*s* peak intensities were increased (relative to O1*s*) on all hematite surfaces exposed to *D. desulfuricans* (compared to unexposed surfaces) and a prominent photopeak was present in the C1*s* core region at ~288 eV. Such surface differences can be accounted for by, among other things, organic species associated with bacteria (i.e., proteins, lipids, polysaccharides etc., see Rouxhet and Genet, 1991).

The XPS spectra of the hematite surface exposed to Essex 6 in the presence of sulfate suggested that the sulfide layer was of sufficient thickness to mask any hematite-related signal (see Fig. 4). The Fe^{2+}-S photopeak was identified at 708.4 eV (FWHM = 1.5 eV, $\chi^2 = 1.15$). In the S2*p* region, the S^{2-} peak was identified at 161.3 eV (FWHM = 1.6 eV), the S_2^{2-} peak at 162.5 eV (FWHM = 1.3 eV), S_n^{2-} at 163.9 eV (FWHM = 1.4 eV) and SO_4^{2-} at 168 eV (FWHM = 1.4 eV, $\chi^2 = 2.63$).

The Fe2*p* spectrum of G20 exposed hematite exhibited a shoulder at low E_b, the position of which was determined at 708.4 eV (FWHM = 1.4 eV, $\chi^2 = 1.72$). In the S2*p* region, the monosulfide S2$p_{3/2}$ peak is at 161.5 eV (FWHM = 1.3 eV), the S2$p_{3/2}$ S_2^{2-} peak at 162.2 eV (FWHM = 1.3 eV) and the S2$p_{3/2}$ S_n^{2-} peak at 163.6 eV (FWHM = 1.9 eV). The high E_b region was resolved into two pairs of multiplets, the S2$p_{3/2}$ peaks being at 166.7 eV (FWHM = 1.7 eV) and 168 eV (FWHM = 1.8 eV). These peak positions were suggestive of SO_3^{2-} and SO_4^{2-} respectively.

Interestingly, the hematite surface exposed to Essex 6 in the absence of medium-SO_4^{2-} (but containing sodium thioglycollate as a reductant and hence a potential source of sulfur) indicated not only a lack of metal sulfide species but the presence of $S_8^0/S_2O_3^{2-}$ and S_n^{2-} (peak maxima ~164 and ~170 eV) and SO_4^{2-}/SO_3^{2-} (peak maximum ~169 eV, Fig. 5).

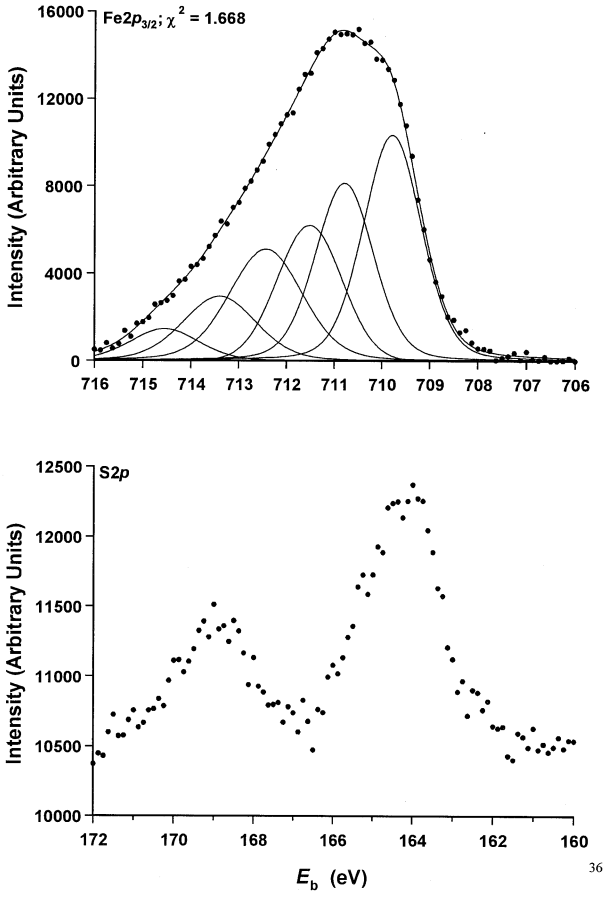

Fig. 5. XPS spectra of hematite surface exposed to Essex 6 in growth medium sulfate-lacking. Fe2$p_{3/2}$; the spectrum is suggestive of hematite Fe^{3+}-O, *cf.* Fig. 2. S2*p*; despite the low signal to noise ratio, photopeaks representative of elemental sulfur, thiosulfate can be distinguished. Adventitious C1s = 285.1 eV.

3.3. X-ray Diffraction of Precipitated Iron Sulfides

Thin film X-ray diffraction of precipitates on the hematite sample exposed to bacteria for 17 d indicated a broad peak at low angle suggestive of amorphous material and an absence of crystal structure associated with the precipitate. Following 3 months incubation in bacterial culture peaks were identified associated with precipitates on the hematite surface with *d*-spacings of 1.28, 1.81, 2.04 and 2.09 Å (2θ, 74.04°, 50.32°, 44.46° and 43.22° respectively, see Figure 6). The low number of peaks identified may result from a lack of heterogeneous orientation of the crystals at the hematite surface as well as the presence of small unobservable crystallites. With so few lines assignment of an unequivocal crystal structure is difficult, however the principal 2.09 Å (43.22° 2θ) peak may be assigned to the hexagonal pyrrhotite (102) peak (Lennie et al., 1995b). We remain cautious concerning this assignment however because minor peaks at such angles are a common feature of ferrous sulfides as well as S_8^0. Even so, XRD suggests that a crystal phase forms at the hematite surface in under three months.

3.4. HR-TEM of Precipitated Iron Sulfides

High magnification HR-TEM images of the hematite surface incubated for 3 months illustrate the presence of numerous crystals with regions of overgrowth (Fig. 7). Lattice spacings of 2.6, 3.8 and 5.1 Å were consistently measured for the observed crystals however, again unequivocal assignment to a particular phase was not possible. However, Fourier transformation of the 5.1 Å lattice spacing, the most commonly observed, yielded a hexagonal crystal structure (Fig. 8) adding weight to the identification of the ferrous sulfide phase as a putative pyrrhotite.

4. DISCUSSION

4.1. Ferrous Sulfide Production by Sulfate-Reducing Bacteria at Hematite Surfaces

The production of ferrous sulfides by SRB is dependent upon Fe^{2+} release from the hematite surface, affected potentially both by direct (i.e., hydrogenase) and indirect (i.e., H_2S oxidation) processes. Reaction between ferrous ions and excess H_2S subsequently results in ferrous sulfide production. Although none of the analytical techniques employed here (XPS, thin film XRD and HR-TEM) provide unequivocal evidence (either on their own or in combination) as to the nature of the ferrous sulfide formed in the presence of SRB at hematite surfaces, we conclude from the available evidence that a pyrrhotite stiochiomertry and structure is the best description of the sulfides we observe. This observation is at variance with previous studies of SRB ferrous sulfide production, although it is not without precedent; pyrrhotite is observed in anoxic marine sediments (Kobayashi and Nomura, 1972; Roberts and Turner, 1993; Horng et al., 1998) and at the surface of corroding iron and steel in H_2S-rich environments (Meyer et al., 1958; Berner, 1964; Ringas and Robinson, 1988). Moreover, low temperature pyrrhotite formation has been observed in laboratory studies (Berner, 1964; Sweeney and Kaplan, 1973).

The production of ferrous sulfides has long been used to identify SRB in mixed and single species culture (Butlin et al., 1949). Rickard (1969a) described the initial production of mackinawite and subsequently, greigite by *Desulfovibrio desulfuricans* Canet 41 in medium containing 182 mM $Fe^{2+}_{(aq.)}$. More recently, using a mixed bacterial culture and 14 μM $Fe^{2+}_{(aq.)}$, Herbert et al. (1998) have again identified mackinawite and greigite and Benning et al. (1999) have described mackinawite formation by *D. desulfuricans* ATCC 29578 (ferrous iron content unspecified). Magnetotactic bacteria, with close affiliations to SRB (DeLong et al., 1993), have been shown to produce intracellular mackinawite and greigite (Pósfai et al., 1998; Frankel et al., 1998; Schüler and Frankel, 1999).

Pyrite is understood to replace mackinawite by reaction between FeS and S_8^0 or S_n^{2-} (Berner 1964; Berner, 1970; Rickard 1969b; Taylor et al., 1979; Luther, 1991; Schoonen and Barnes, 1991b; Wilkin and Barnes, 1996; Benning et al., 2000) following the amorphous FeS $\rightarrow$ mackinawite $\rightarrow$ greigite $\rightarrow$ pyrite sequence. Previous studies have described little or no pyrite formation in SRB batch cultures despite significant accumulation of precursor ferrous sulfides (Rickard, 1969a; Herbert et al., 1998; Benning et al., 1999). An exception has been described by Donald and Southam (1999) who report that pyrite formation from FeS is accelerated in the presence of

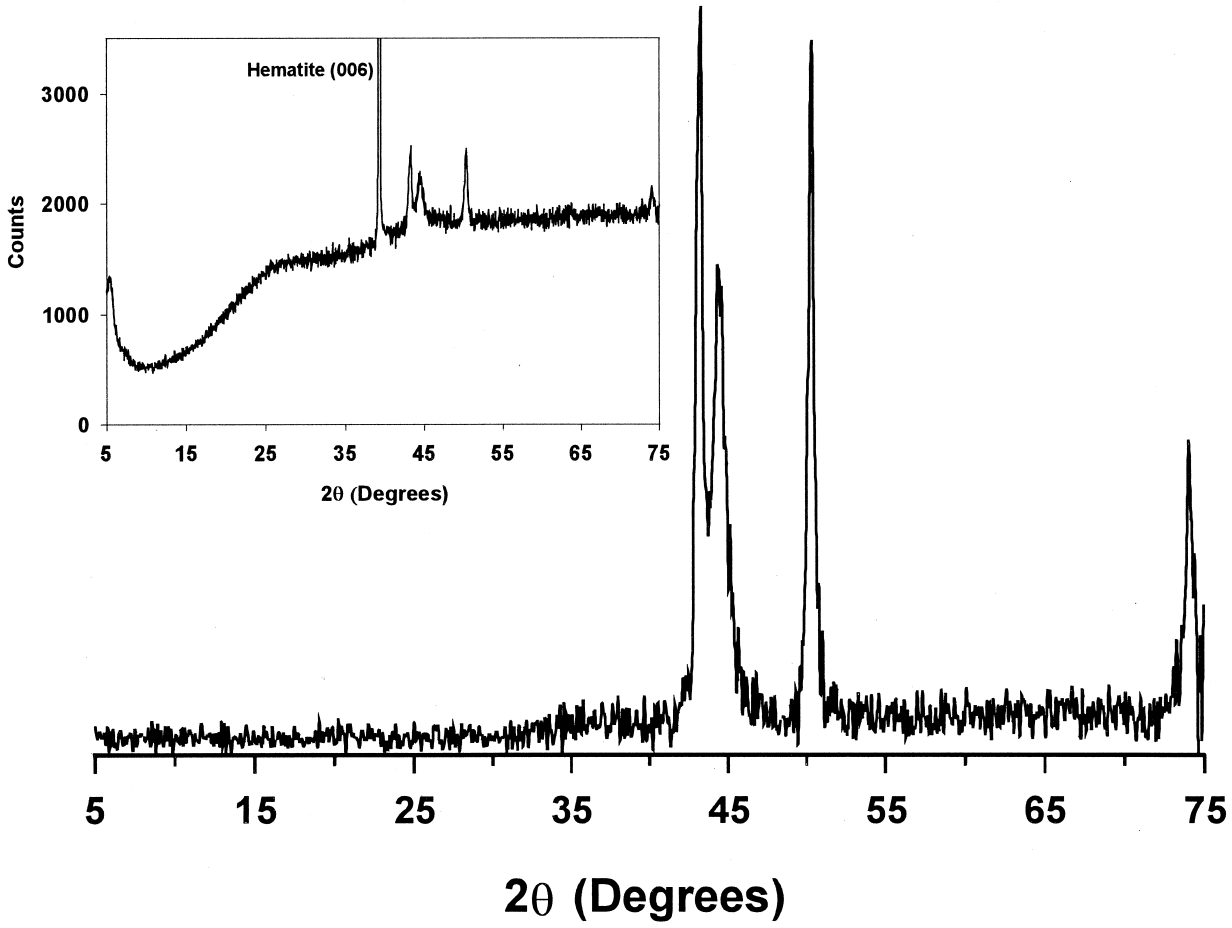

Fig. 6. Background subtracted XRD trace from the precipitate formed at a hematite surface in the presence of sulfate-reducing bacteria following 3 months of incubation. The hematite (006) peak has also been subtracted. Peaks are observed at 43.22° (d = 2.09Å), 44.46° (d = 2.04Å), 50.32° (d = 1.81Å) and 74.04° (d = 1.28Å). Inset—untransformed XRD trace indicating the relative intensities of the precipitate associated peaks compared to the hematite peak.

SRB, compared to abiotic processes, an apparent consequence of nucleation of pyrite on inner and outer surfaces of the cell envelope. However, despite the presence of oxidized sulfur species, in no instance was pyrite observed at the hematite surfaces in this study (FeS_2; Fe2$p_{3/2}$ 707.5 eV, S2$p_{3/2}$ 162.8 eV, Buckley and Woods, 1987). This fact may corroborate our identification of the ferrous sulfide as pyrrhotite since in the presence of oxidized sulfur species mackinawite and/or greigite, were they present, would be expected to transform to pyrite relatively quickly.

One significant difference between previous experiments and this study is the amount of $Fe^{2+}_{(aq.)}$ in the growth media. Whilst $SO^{2-}_{4(aq).}$ concentrations (and therefore likely subsequent H_2S concentrations) in the four studies range from 32 mM (Herbert et al., 1998) to 50 mM (Rickard, 1969a), $Fe^{2+}_{(aq.)}$ concentrations vary greatly between 182 mM (Rickard, 1969a) and an unknown but potentially low concentration in this study arising from the low dissolution rate of hematite (Byrne and Kester, 1976; dos Santos and Stumm, 1992). $Fe^{2+}_{(aq.)}$ supply could potentially play a role in determining the resultant ferrous sulfide stoichiometry. Thermodynamic calculations suggest the greigite stability field is particularly sensitive to changes in the $H_2S_{(aq.)}$: $Fe^{2+}_{(aq.)}$ ratio (Anderko and Shuler, 1997). Specifically, at a fixed Fe^{2+} molality of 10 mM kg^{-1}, greigite is not formed below 40 mM kg^{-1} H_2S (Anderko and Shuler, 1997). Berner (1971) also indicates that with sulfide activity (pS^{2-}) as the controlling factor the pyrrhotite stability field exists at lower pS^{2-} relative to pyrite (at equivalent E_h, see also Lord and Church, 1983). These sources place emphasis on pS^{2-} in determining the nature of the ferrous sulfide formed under particular circumstances, rather than the availability of ferrous ions. Since autooxidation of H_2S is likely to occur at the hematite surface (see dos Santos Afonso and Stumm, 1992; Herszage and dos Santos Afonso, 2000) the potential exists for pS^{2-} to be reduced in close proximity to the mineral surface. Visual inspection of the culture media indicates that ferrous sulfide formation is limited to the mineral surface—the very place where we might expected the most reduced pS^{2-}.

Alternatively the greigite stability field lies above the H^+/H_2 redox equilibrium, suggesting the mackinawite → greigite → pyrite sequence is thermodynamically unfeasible in strong reducing environments (Anderko and Shuler, 1997), indeed there is now considerable empirical evidence suggesting the conversion of mackinawite to pyrite requires an oxidant, i.e., S^0_8 or

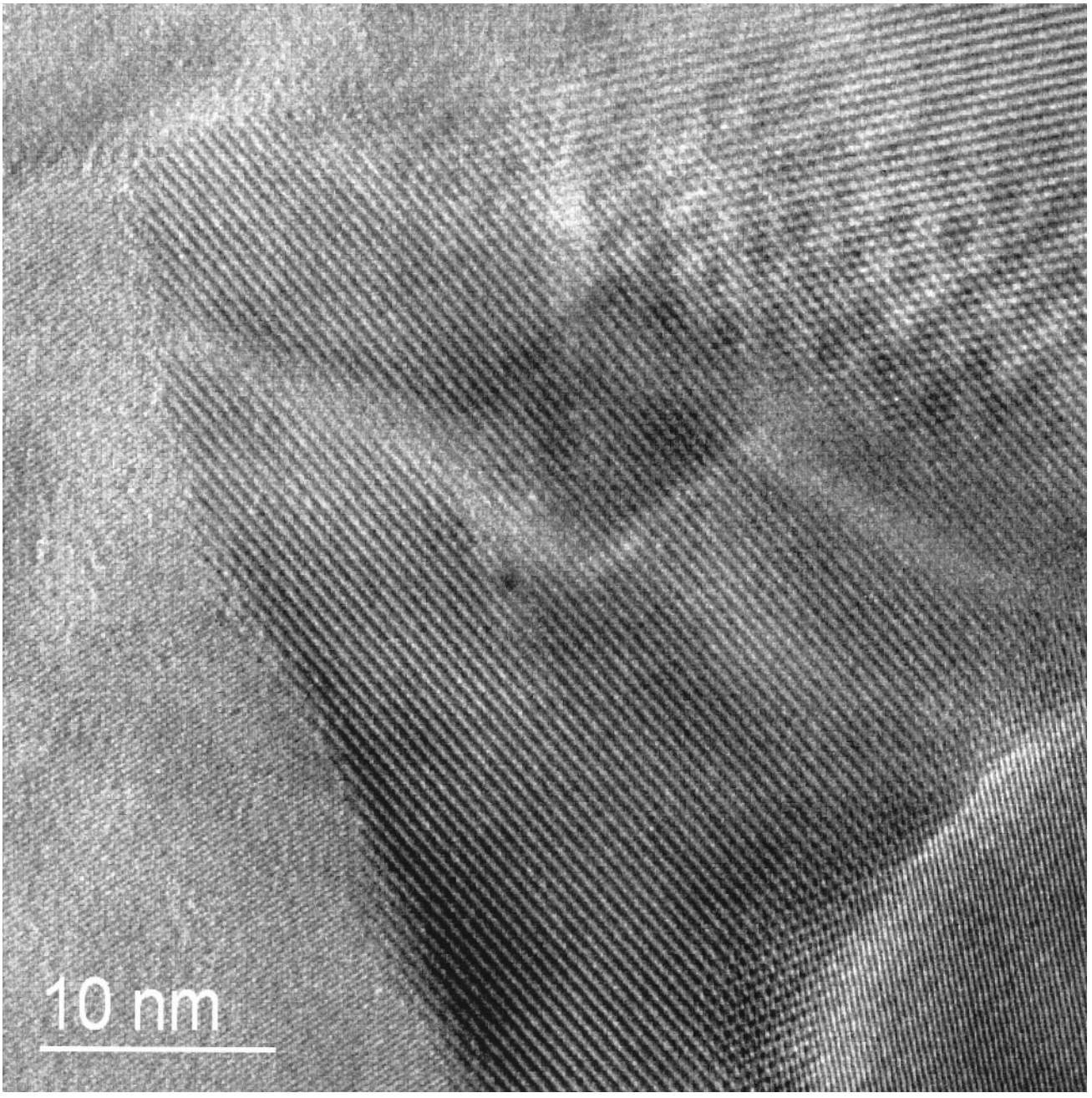

Fig. 7. HR-TEM micrograph of crystal phases present at a hematite surface in the presence of sulfate-reducing bacteria following 3 months of incubation. Several crystals are visible with regions of overgrowth in between. D-spacings of 2.6, 3.8 and 5.1 Å were consistently measured for the crystal phases at the surface.

polysulfides (for example Berner, 1970; Schoonen and Barnes, 1991a,b; Wilkin and Barnes, 1996; Benning et al., 2000). Thus, the apparent stoichiometric differences in ferrous sulfides produced could arise either from reduced pS^{2-}, or from the generation of an extremely reducing environment at the mineral surface in the presence of SRB. Since XPS indicates that precipitates formed at the hematite surface upon addition of H_2S in the absence of bacteria had equivalent E_b to those formed in the presence of SRB we conclude that pS^{2-} may exert more influence over formation of a particular phase than E_h, although we should not discount the potential control of E_h completely. Assessment of pFe^{2+} is not trivial. Metal ions are likely to interact with bacterial membranes (Fein et al., 1997), and extracellular polymers (Geesey and Jang, 1989; Barker and Banfield, 1996), both phenomena are likely to reduce the availability of free ferrous ions within bacterial biofilms. With regard to pS^{2-}, we are currently attempting to assess sulfide concentrations at mineral surfaces employing microelectrodes.

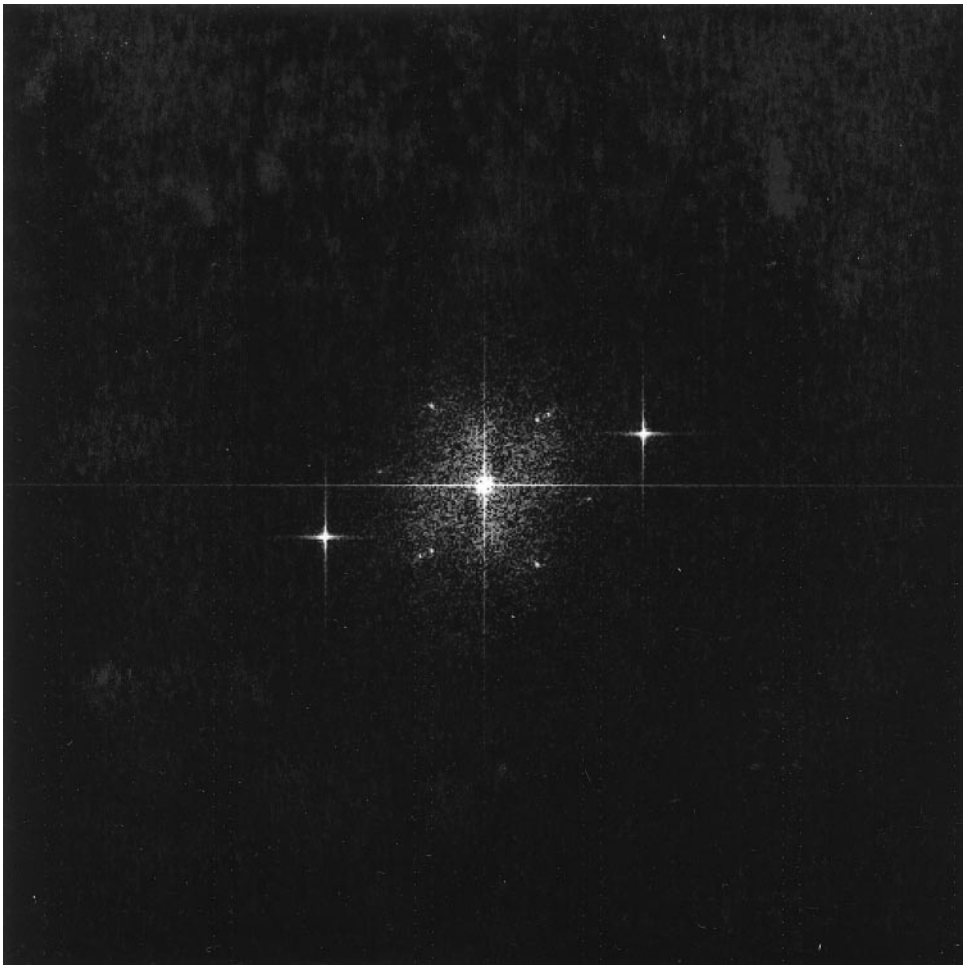

Fig. 8. Fourier transformation of the 5.1 Å lattice pattern in Figure 7 suggesting a hexagonal crystal structure.

4.2. Sulfur Species other than Fe-Sulfide Present at the Hematite Surface

Reductive dissolution of hematite by H_2S (Eqn. 2) is complex and although the products are often described as Fe-sulfide and elemental sulfur there are in fact many intermediates. Studies show these to include S_n^{2-}, SO_3^{2-}, SO_4^{2-} and $S_2O_3^{2-}$ (Pyzik and Sommer, 1981; dos Santos Afonso and Stumm, 1992; Davydov et al., 1998; Herszage and dos Santos Afonso, 2000) as well as S_8^0 (dos Santos Afonso and Stumm, 1992). Tetra- and pentasulfides are likely to be the only stable polysulfides in the culture medium (Giggenbach, 1972). Hematite dissolution is surface-controlled, the rate dependent upon the concentration of reductant(s) at the surface. Surface complexation models (Yates et al., 1974; Sulzberger et al., 1989) point to the significance of surface functional groups in mineral dissolution. Specifically for hematite, dos Santos Afonso and Stumm (1992) postulate the formation of FeS^- and FeSH surface complexes by exchange of O^{2-} for S^{2-} and SH^-, these new surface groups would then undergo electron transfer. The existence of SH^- groups at the hematite surface has been confirmed using FTIR spectroscopy (Davydov et al., 1998). Since Fe^{2+}-O^{2-} bonds in the hematite lattice are weakened in the process, $Fe^{2+}_{(aq.)}$ is released from the surface.

XPS spectra of all the hematite surfaces exposed to H_2S-practicing SRB revealed the presence of SO_3^{2-} and SO_4^{2-} as well as S_n^{2-}, at no time were peaks indicative of S_8^0 or thiosulfate observed. However, on the two hematite surfaces not exposed to H_2S, i.e., the surface exposed only to Lactate medium C in the absence of SRB and the surface exposed to Essex 6 growing in the absence of medium-SO_4^{2-}, peaks consistent with S_8^0 and $S_2O_3^{2-}$ were observed coincident with surface associated SO_4^{2-}. Reduction of hematite by H_2S (or Fe-sulfide, Tiller and Booth, 1962) precludes the accumulation of elemental sulfur and thiosulfate at the surface. A likely explanation is the reaction between elemental sulfur and sulfhydryl ions (HS^-) forming polysulfides (Teder 1971). At the same time both $S_2O_3^{2-}$ and SO_3^{2-} may disproportionate to SO_4^{2-} (Jørgensen, 1990; Canfield and Thamdrup, 1994; Habicht et al., 1998).

4.3. Implications of Pyrrhotite and Polysulfide Formation at Iron Oxide Surfaces

Iron sulfides have an important role to play in both the sulfur and iron cycles (Lovley, 1993; Nealson and Saffarini, 1994). The final product of iron sulfide formation, pyrite (FeS_2) (Rickard, 1969b; Berner, 1970; Berner, 1984), is stable (Lennie and

Vaughan 1996), although even pyrite is susceptible to dissolution by the Fe-oxidizers *Thiobacillus ferrooxidans* and *Leptospirillum ferrooxidans* (Bennett and Tributsch, 1978; Crundwell, 1996; Edwards et al., 1998). Intermediate species, i.e., mackinawite and greigite, being metastable at low temperatures (Lennie and Vaughan, 1996) are therefore likely to have an important influence upon the iron and sulfur balance. Fluctuations in ambient [Fe^{2+}] or [S^{2-}] (Anderko and Shuler 1997), pH (Brookins, 1988; Anderko and Shluer, 1997) or oxidation (Morse, 1991; Holmes, 1999) are likely to result in dissolution of sulfide precipitates. Such potential dissolution attains greater significance when one considers that other, potentially toxic, elements are often co-precipitated with Fe (Miller, 1950). The formation of pyrrhotite, a species considered stable at low temperatures (Kissin and Scott, 1982), will greatly limit the dissolution of Fe, S and other co-precipitates caused by environmental fluctuations in Fe, S and O_2. Polysulfides, being reduced species, represent a reactive form of elemental sulfur and together with monosulfides are responsible for maintaining trace metal concentrations in anoxic sediments at relatively high concentrations (Brooks et al., 1968; Presley et al., 1972).

Potential pyrrhotite formation by SRB also has implications for paleomagnetic studies of geomagnetic field behavior (Laj et al., 1991; Tauxe, 1993). Ferrous sulfide formation results in part from the dissolution of iron oxide minerals, thus the relative amounts of diagenetic ferrimagnetic minerals (i.e., pyrrhotite and greigite) compared to authigenic ferrimagnetic minerals (i.e., magnetite) are important considerations for the interpretation of paleomagnetic records. Roberts and Turner (1993) have identified pyrrhotite, together with greigite, associated with recent fine-grained sediments. They conclude that these phases exist as a result of interrupted sulfidation of precursor ferrous sulfides (i.e., arrested pyritization) due to low permeability of fine-grained sediments. Our results suggest that low sediment permeability need not be required for pyrrhotite formation but that low sulfide activity due to sulfide autooxidation at iron oxide surfaces may also result in pyrrhotite formation.

Thus, the presence of SRB at a hematite surface results in mineral dissolution and the formation of the stable iron sulfide pyrrhotite and reactive polysulfides resultant from excess H_2S production. Such a mechanism is consistent with observations by Morse and Cornwell (1987) that iron sulfides may exist principally as scales upon other minerals in sediments. Sulfide/polysulfide formation by SRB has the potential to greatly affect S, Fe and other trace metal concentrations in anoxic soils and sediments, of significance not only to the S and Fe cycles but also to the bioavailability of toxic trace metals and paleomagnetism.

Acknowledgments—XPS was performed at the Interfacial Chemical Analysis Laboratory at Montana State University. This research was supported by the Office of Biologic and Environmental Research, U. S. Department of Energy as part of the Natural and Accelerated Bioremediation Research Program (grant # ER 62630-3339). A portion of this work was performed at the Environmental Molecular Sciences Laboratory, a national scientific user facility sponsored by the Energy's Office of Biological and Environmental Research (OBER) and Pacific Northwest National Laboratory. This research was also supported by the OBER Natural and Accelerated Bioremediation Research Program. The authors are grateful to three anonymous reviewers whose thoughtful comments greatly improved the original manuscript.

Associate editor: D. J. Wesolowski

REFERENCES

Anderko A. and Shuler P. J. (1997) A computational approach to predicting the formation of iron sulfide species using stability diagrams. *Comput. Geosci.* **23,** 647–658.

Appelo C. A. J. and Postma D. (1996) Geochemistry, groundwater and pollution. A. A. Balkema, Rotterdam.

Asami K., Hashimoto K., and Shimodaira S. (1976) X-ray photoelectron spectrum of Fe^{2+} state in iron oxides. *Corrosion Sci.* **16,** 35–45.

Bacon P. B., Brewer P. G., Spencer D. W., Murray J. W., and Goddard J. (1980) Lead-210, polonium-210, manganese and iron in the Cariaco Trench. *Deep-Sea Res.* **27A,** 119–135.

Barker W. W. and Banfield J. F. (1996) Biologically versus inorganically mediated weathering reactions: Relationships between minerals and extracellular microbial polymers in lithobiontic communities. *Chem. Geol.* **132,** 55–69.

Baross J. A. and Deming J. W. (1983) Growth of 'black smoker' bacteria at temperatures of at least 250°C. *Nature* **303,** 423–426.

Bennett J. C. and Tributsch H. (1978) Bacterial leaching patterns on pyrite crystal surfaces. *J. Bacteriol.* **134,** 310–317.

Benning L. G., Wilkin R. T., and Konhauser K. O. (1999) Iron monosulphide stability: Experiments with sulphate reducing bacteria. In *Geochemistry of the Earth's Surface* (ed. H. Ármannsson) pp. 429–432. A. A. Balkema, Rotterdam.

Benning L. G., Wilkin R. T., and Barnes H. L. (2000). Reaction pathways in the Fe-S system below 100°C. *Chem. Geol.* **167,** 25–51.

Berner R. A. (1964) Iron sulfides formed from aqueous solutions at low temperatures and pressures. *J. Geol.* **72,** 293–306.

Berner R. A. (1970) Sedimentary pyrite formation. *Am. J. Sci.* **268,** 1–23.

Berner R. A. (1971) Principles of chemical sedimentology. McGraw-Hill, New York.

Berner R. A. (1982) Burial of organic carbon and pyrite sulfur in the modern ocean: Its geochemical and environmental significance. *Am. J. Sci.* **278,** 451–473.

Berner R. A. (1984) Sedimentary pyrite formation: An update. *Geochim. Cosmochim. Acta* **48,** 605–615.

Brookins D. G. (1988) Eh-pH Diagrams for Geochemistry. Springer-Verlag, New York.

Brooks R. R., Presley B. J., and Kaplan I. R. (1968) Trace elements in interstitial waters of marine sediments. *Geochim. Cosmochim. Acta* **32,** 397–414.

Brown G. E., Henrich V. E., Casey W. H., Clark D. L., Eggleston C., Felmy A., Goodman D. W., Grätzel M., Maciel G., McCarthy M. I., Nealson K. H., Sverjensky D. A., Toney M. F., and Zachara J. M. (1999) Metal oxide surfaces and their interactions with aqueous solutions and microbial organisms. *Chem. Rev.* **99,** 77–174.

Buckley A. N. and Woods R. (1985) X-ray photoelectron spectroscopy of oxidized pyrrhotite surfaces. I. Exposure to air. *Appl. Surf. Sci.* **22/23,** 280–287.

Buckley A. N. and Woods R. (1987) The surface oxidation of pyrite. *Appl. Surf. Sci.* **27,** 437–452.

Butlin K. R., Adams M. E., and Thomas M. (1949) The isolation and cultivation of sulphate-reducing bacteria. *J. Gen. Microbiol.* **3,** 49–59.

Byrne R. H. and Kester D. R. (1976) Solubility of hydrous ferric oxide and iron speciation in seawater. *Mar. Chem.* **4,** 255–274.

Canfield D. E. and Thamdrup B. (1994) The production of ^{34}S-depleted sulfide during bacterial disproportionation of elemental sulfur. *Science* **266,** 1973–1975.

Cormack B. P., Valdivia R. H., and Falkow S. (1996) FACS-optimized mutants of the green fluorescent protein (GFP). *Gene* **173,** 33–38.

Costerton J. W., Lewandowski Z., Caldwell D. E., Korber D. R., and Lappin-Scott H. M. (1995) Bacterial biofilms. *Ann. Rev. Microbiol.* **49,** 711–745.

Davydov A., Chaung K. T., and Sanger A. R. (1998) Mechanism of H_2S oxidation by ferric oxide and hydroxide surfaces. *J. Phys. Chem. B.* **102,** 4745–4752.

DeLong E. F., Frankel R. B., and Bazylinski D. A. (1993) Multiple evolutionary origins of magnetotaxis in bacteria. *Science.* **259,** 803–806.

Donald R. and Southam G. (1999) Low temperature anaerobic bacterial diagenesis of ferrous monosulfide to pyrite. *Geochim. Cosmochim. Acta* **63,** 2019–2023.

Edwards K. J., Schrenk M. O., Hamers R., and Banfield J. F. (1998)

Microbial oxidation of pyrite: Experiments using microorganisms from an extreme acidic environment. *Am. Mineral.* **83,** 1444–1453.

Errampalli D., Leung K., Cassidy M. B., Kostrzynska M., Blears M., Lee H., and Trevors J. T. (1999) Applications of the green fluorescent protein as a molecular marker in environmental organisms. *J. Microbiol. Methods* **35,** 187–199.

Fein J. B., Daughney C. J., Yee N. and Davis T. A. (1997) A chemical equilibrium model for metal adsorption onto bacterial surfaces. *Geochim. Cosmochim. Acta* **61,** 3319–3328.

Frankel R. B., Bazylinski D. A., and Schüler D. (1998) Biomineralization of magnetic iron minerals in bacteria. *Supramolec. Sci.* **5,** 383–390.

Geesey G. G. and Jang L. (1989) Interactions between metal ions and capsular exopolymers. In *Metal ions and Bacteria* (eds. T. J. Beveridge and R. J. Doyle) Chap. 11, pp. 325–357. Wiley-Interscience.

Ghiorse W. C. and Wilson J. T. (1988) Microbial ecology of the terrestrial subsurface. *Adv. Appl. Microbiol.* **33,** 107–172.

Giggenbach W. (1972) Optical spectra and equilibrium distribution of polysulfide ions in aqueous solution at 20°C. *Inorg. Chem.* **11,** 1201–1207.

Goldhaber M. B. and Kaplan I. R. (1974) The sulfur cycle. In *The Sea—Ideas and Observations on Progress in the Study of the Seas* (ed. E. D. Goldberg). pp. 569–655. Wiley Interscience.

Gupta R. P. and Sen S. K. (1974) Calculation of multiplet structure of core *p*-vacancy levels. *Phys. Rev. B* **10,** 71–77.

Gupta R. P. and Sen S. K. (1975) Calculation of multiplet structure of core *p*-vacancy levels. II. *Phys. Rev. B* **12,** 15–19.

Habicht K. S., Canfield D. E., and Rethmeier J. (1998) Sulfur isotope fractionation during bacterial reduction and disproportionation of thiosulfate and sulfite. *Geochim. Cosmochim. Acta* **62,** 2585–2595.

Hamilton, W. A. (1991) Sulphate-reducing bacteria and their role in microbially influenced corrosion. In *Microbially influenced corrosion and biodeterioration* (ed. N. J. Dowling et al.). pp. i–iv. Institute for Applied Microbiology.

Harvey R. W., Smith R. L., and George L. (1984) Effect of organic contamination upon microbial distribution and heterotrophic uptake in a Cape Cod, Mass., aquifer. *Appl. Environ. Microbiol.* **48,** 1197–1202.

Herbert R. B., Benner S. G., Pratt A. R., and Blowes D. W. (1998) Surface chemistry and morphology of poorly crystalline iron sulfides precipitated in media containing sulfate-reducing bacteria. *Chem. Geol.* **144,** 87–97.

Herszage J. and dos Santos Afonso M. (2000). The autooxidation of hydrogen sulfide in the presence of hematite. *Colloids Surf. A* **168,** 61–69.

Holmes J. (1999) Fate of incorporated metals during mackinawite oxidation in sea water. *Appl. Geochem.* **14,** 277–281.

Horng C. S., Torii M., Shea K. S., and Kao S. J. (1998) Inconsistent magnetic polarities between greigite- and pyrrhotite/magnetite-bearing marine sediments from the Tsailiano-chi section, southwestern Taiwan. *Earth Planet. Sci. Lett.* **164,** 467–481.

Hyland H. M. and Bancroft G. M. (1989) An XPS study of gold deposition at low temperatures on sulphide minerals: Reducing agents. *Geochim. Cosmochim. Acta* **53,** 367–372.

Jesior J. C. (1986) How to avoid compression. *J. Ultrastruc. Mol. Struc. Res.* **95,** 210–217.

Jones C. F., Lecount S., Smart R. St. C., and White T. (1992) Compositional and structural alteration of pyrrhotite surfaces in solution: XPS and XRD studies. *Appl. Surf. Sci.* **55,** 65–85.

Jørgensen B. B. (1977) The sulfur cycle of a coastal marine sediment (Limfjorden, Denmark). *Limnol. Oceanogr.* **22,** 814–831.

Jørgensen B. B. (1990) A thiosulfate shunt in the sulfur cycle of marine sediments. *Science* **249,** 152–154.

Junta-Rosso J. L. and Hochella M. F. (1996) The chemistry of hematite {001} surfaces. *Am. Mineral.* **60,** 305–314.

Kissin S. A. and Scott S. D. (1982) Phase relations involving pyrrhotite below 350°C. *Econ. Geol.* **77,** 1739–1754.

Kobayashi K. and Nomura M. (1972) Iron sulfides in the sediment cores from the Sea of Japan and their geophysical implications. *Earth Planet. Sci. Lett.* **16,** 200–208.

Laj C., Mazaud A., Weeks R., Fuller M., and Herrero-Bervera E. (1991) Geomagnetic reversal paths. *Nature* **351,** 447.

Le Gall J., Payne W. J., Chen L., Liu M. Y., and Xavier A. V. (1994) Localization and specificity of cytochromes and other electron transfer proteins from sulfate-reducing bacteria. *Biochimie* **76,** 655–665.

Lennie A. R., Redfern S. A. T., Schofield P. F., and Vaughan D. J. (1995a) Synthesis and Rietveld crystal structure refinement of mackinawite, tetragonal FeS. *Mineral. Mag.* **59,** 677–683.

Lennie A. R., England K. E. R., and Vaughan D. J. (1995b) Transformation of synthetic mackinawite to hexagonal pyrrhotite: A kinetic study. *Am. Mineral.* **80,** 960–967.

Lennie A. R. and Vaughan D. J. (1996) Spectroscopic studies of iron sulfide formation and phase relations at low temperatures. In *Mineral Spectroscopy: A Tribute to Roger G. Burns* (ed. M. D. Dyar et al.). pp. 117–131. The Goechemical Society (Special Publication No. 5).

Lord C. J. and Church T. M. (1983) The geochemistry of salt marshes: Sedimentary ion diffusion, sulfate reduction, and pyritization. *Geochim. Cosmochim. Acta* **47,** 1381–1391.

Lovley D. R. (1993) Dissimilatory metal reduction. *Ann. Rev. Microbiol.* **47,** 263–290.

Luther G. W. III (1991) Pyrite synthesis via polysulfide compounds. *Geochim. Cosmochim. Acta* **55,** 2839–2849.

Magee E. L., Ensley B. D., and Barton L. L. (1978) An assessment of growth yields and energy coupling in *Desulfovibrio. Arch. Microbiol.* **117,** 21–26.

Manocha A. S. and Park R. L. (1977) Flotation related ESCA studies on PbS surfaces. *Appl. Surface Sci.* **1,** 129–141.

Matthysse A. G., Stretton S., Dandie C., McClure N. C., and Goodman A. E. (1996) Construction of GFP vectors for use in Gram-negative bacteria other than *Escherichia coli. FEMS Microbiol. Lett.* **145,** 87–94.

McIntyre N. S. and Zetaruk D. G. (1977) X-ray photoelectron spectroscopic studies of iron oxides. *Anal. Chem.* **49,** 1521–1529.

Meyer F. H., Riggs O. L., McGlasson R. L., and Sudbury J. D. (1958) Corrosion products of mild steel in hydrogen sulfide environments. *Corrosion* **14,** 69–75.

Miller L. P. (1950) Formation of metal sulfides through the activities of sulfate-reducing bacteria. *Contr. Boyce Thompson Inst. Plant Res.* **16,** 85–89.

Morse J. W. (1991) Oxidation kinetics of sedimentary pyrite in seawater. *Geochim. Cosmochim. Acta* **55,** 3665–3667.

Morse J. W. and Cornwell, J. C. (1987) Analysis and distribution of iron sulfide minerals in recent anoxic marine sediments. *Mar. Chem.* **22,** 55–69.

Mycroft J. R., Bancroft G. M., McIntyre N. S., Lorimer J. W., and Hill I. R. (1990) Detection of sulphur and polysulphides on electrochemically oxidized pyrite surfaces by X-ray photoelectron spectroscopy and Raman spectroscopy. *J. Electroanal. Chem.* **292,** 139–152.

Nealson K. H. and Saffarini D. (1994) Iron and Manganese in anaerobic respiration: Environmental significance, physiology, and regulation. *Ann. Rev. Microbiol.* **48,** 311–343.

Olson G. J., Dockins W. S., McFeters G. A. and Inverson W. P. (1981) Sulfate-reducing and methanogenic bacteria from deep aquifers in Montana. *Geomicrobiol. J.* **2,** 327–340.

Pósfai M., Buseck P. R., Bazylinski D. A., and Frankel R. B. (1998) Iron sulfides from magnetotactic bacteria: Structure, composition and transitions. *Am. Mineral.* **83,** 1469–1481.

Postgate J. R. (1963) Versatile medium for the enumeration of sulfate-reducing bacteria. *Appl. Microbiol.* **11,** 265–267.

Postgate J. R. and Campbell L. L. (1966) Classification of *Desulfovibrio* species, the nonsporulating sulfate-reducing bacteria. *Bacteriol. Rev.* **30,** 732–738.

Pratt A. R., Muir I. J., and Nesbitt H. W. (1994a) X-ray photoelectron and Auger electron spectroscopic studies of pyrrhotite and mechanism of air oxidation. *Geochim. Cosmochim. Acta* **58,** 827–841.

Pratt A. R., Nesbitt H. W. and Muir I. J. (1994b) Generation of acids from mine waste: Oxidative leaching of pyrrhotite in dilute H_2SO_4 solutions at pH 3.0. *Geochim. Cosmochim. Acta* **58,** 5147–5159.

Presley B. J., Kolodny Y., Nissenbaum A., and Kaplan I. R. (1972) Early diagenesis in a reducing fjord, Saanich Inlet, Br. Colombia, II. Trace element distribution in interstitial water and sediments. *Geochim. Cosmochim. Acta* **36,** 1073–1090.

Pyzik A. J. and Sommer S. E. (1981) Sedimentary iron monosulfides: Kinetics and mechanism of formation. *Geochim. Cosmochim. Acta* **45,** 687–698.

Rickard D. T. (1969a) The microbiological formation of iron sulphides. *Stokholm Contrib. Geol.* **20,** 49–66.

Rickard D. T. (1969b) The chemistry of iron sulphide formation at low temperatures. *Stokholm Contrib. Geol.* **20,** 67–95.

Ringas C. and Robinson F. P. A. (1988) Corrosion of stainless steel by sulfate-reducing bacteria—electrochemical techniques. *Corrosion* **44,** 391–396.

Robert M. and Berthelin J. (1986) Role of biological and biochemical factors in soil mineral weathering. In *Interactions of soil minerals with natural organics and microbes* (ed. P. M. Huang and M. Schnitzer). Chap. 12, pp. 453–495. Soil Science Society of America, Madison, WI. (Special Publication No. 17).

Roberts A. P. and Turner G. M. (1993) Diagenetic formation of ferrimagnetic iron sulfide minerals in rapidly deposited marine sediments, South Island, New Zealand. *Earth Planet. Sci. Lett.* **115,** 257–273.

Rouxhet P. G. and Genet M. J. (1991) Chemical composition of the microbial cell surface by X-ray photoelectron spectroscopy. In *Microbial Cell Surface Analysis. Structural and Physiochemical Methods* (ed. N. Mozes et al.). Chap. 8, pp. 173–220. VCH Publications Inc., Baton Rouge.

dos Santos Afonso M. and Stumm W. (1992) Reductive dissolution of iron(III) (hydr)oxides by hydrogen sulfide. *Langmuir* **8,** 1671–1675.

Schoonen M. A. A. and Barnes H. L. (1991a) Reactions forming pyrite and marcasite from solution: I. Nucleation of FeS_2 below 100°C. *Geochim. Cosmochim. Acta* **55,** 1495–1504.

Schoonen M. A. A. and Barnes H. L. (1991b) Reactions forming pyrite and marcasite from solution: II. Via FeS_2 precursors below 100°C. *Geochim. Cosmochim. Acta* **55,** 1505–1514.

Schüler D. and Frankel R. B. (1999) Bacterial magnetosomes: Microbiology, biomineralization and biotechnological applications. *Appl. Microbiol. Biotechnol.* **52,** 464–473.

Shirley D. A. (1972) High-resolution X-ray photoemission spectrum of the valence bands of gold. *Phys. Rev. B* **5,** 4709–4714.

Smith A. D. and Klug M. J. (1981) Electron donors utilized by sulfate-reducing bacteria in eutrophic lake sediments. *Appl. Env. Microbiol.* **42,** 116–121.

Sulzberger B., Suter D., Siffert C., and Banwart S. (1989) Dissolution of Fe(III) (hydr)oxides in natural waters: Laboratory assessment of the kinetics controlled by surface coordination. *Mar. Chem.* **28,** 127–144.

Sweeney R. E. and Kaplan I. R. (1973) Pyrite framboid formation: laboratory synthesis and marine sediments. *Econ. Geol.* **68,** 618–634.

Tauxe L. (1993) Sedimentary records of relative paleointensity of the geomagnetic field: Theory and practice. *Rev. Geophys.* **31,** 319–354.

Taylor P., Rummery T. E., and Owen D. G. (1979) On the conversion of mackinawite to greigite. *J. Inorg. Nucl. Chem.* **41,** 595–596.

Teder A. (1971) The equilibrium between elementary sulfur and aqueous polysulfide solutions. *Acta Chem. Scand.* **25,** 1722–1728.

Thauer, R. K., Jungermann, K., and Decker, K. (1977) Energy conservation in chemotrophic anaerobic bacteria. *Bacteriol. Rev.* **41,** 100–180.

Tiller A. K. and Booth G. H. (1962) Polarization studies of mild steel in cultures of sulfate-reducing bacteria. II. Thermophilic organisms. *Trans. Faraday Soc.* **58,** 110–115.

Vaughan D. J. and Ridout M. S. (1971) Mössbauer studies of some sulfide minerals. *J. Inorg. Chem.* **33,** 741–746.

Wagner C. D., Riggs W. M., Davies L. E., Moulder J. F., and Mailenberg G. M. (1992) Handbook of X-ray photoelectron spectroscopy. Perkin-Elmer.

Wall J. D., Rapp-Giles B. J., and Rousset M. (1993) Characterization of a small plasmid from *Desulfovibrio desulfuricans* and its use for shuttle vector construction. *J. Bacteriol.* **175,** 4121–4128.

Webb, J. S., McGinness, S., and Lappin-Scott, H. M. (1998) Metal removal by sulfate-reducing bacteria from natural and constructed wetlands. *J. Appl. Microbiol.* **84,** 240–248.

Wilkin R. T. and Barnes H. L. (1996) Pyrite formation by reactions of iron monosulfides with dissolved inorganic and organic sulfur species. *Geochim. Cosmochim. Acta* **60,** 4167–4179.

Yates D. E., Levine S., and Healy T. (1974) Site-binding model of the electrical double layer at the oxide/water interface. *J. Chem. Soc., Faraday Trans. 1.* **70,** 1807–1818.

Isolation, characterization and gene sequence analysis of a membrane-associated 89 kDa Fe(III) reducing cytochrome *c* from *Geobacter sulfurreducens*

Timothy S. MAGNUSON*†[1], Naohito ISOYAMA*†, Allison L. HODGES-MYERSON‡, Gerard DAVIDSON§, Michael J. MARONEY§, Gill G. GEESEY*† and Derek R. LOVLEY‡

*Department of Microbiology, P.O. Box 3520, Montana State University, Bozeman, MT 59717-3520, U.S.A., †Center for Biofilm Engineering, 366 EPS Building, Montana State University, Bozeman, MT 59717-3980, U.S.A., ‡Department of Microbiology, Morrill Science Center, University of Massachusetts, Amherst, MA 01003, U.S.A., and §Department of Chemistry, University of Massachusetts, Amherst, MA 01003, U.S.A.

Geobacter sulfurreducens is capable of anaerobic respiration with Fe(III) as a terminal electron acceptor via a membrane-bound Fe(III) reductase activity associated with a large molecular mass cytochrome *c*. This cytochrome was purified by detergent extraction of the membrane fraction, Q-Sepharose ion-exchange chromatography, preparative electrophoresis, and MonoQ ion-exchange chromatography. Spectrophotometric analysis of the purified cytochrome reveals a *c*-type haem, with no evidence of haem *a*, haem *b* or sirohaem. The cytochrome has an M_r of 89000 as determined by denaturing PAGE, and has an isoelectric point of 5.2 as determined by analytical isoelectric focusing. Dithionite-reduced cytochrome can donate electrons to Fe(III)-nitrilotriacetic acid and synthetic ferrihydrite, thus demonstrating that the cytochrome has redox and thermodynamic properties required for reduction of Fe(III). Analysis using cyclic voltammetry confirmed that the reduced cytochrome can catalytically transfer electrons to ferrihydrite, further demonstrating its ability to be an electron transport mediator in anaerobic Fe(III) respiration. Sequence analysis of a cloned chromosomal DNA fragment revealed a 2307 bp open reading frame (*ferA*) encoding a 768 amino acid protein corresponding to the 89 kDa cytochrome. The deduced amino acid sequence (FerA) translated from the open reading frame contained 12 putative haem-binding motifs, as well as a hydrophobic N-terminal membrane anchor sequence, a lipid-attachment site and an ATP/GTP-binding site. FerA displayed 20% or less identity with amino acid sequences of other known cytochromes, although it does share some features with characterized polyhaem cytochromes *c*.

Key words: electron transport protein, iron reductase, metal respiration.

INTRODUCTION

Dissimilatory iron-reducing bacteria are increasingly recognized as an ecologically and environmentally important group of micro-organisms [1–4]. Progress is being made toward the understanding of their biochemistry and physiology, particularly with the genera *Shewanella* and *Geobacter*, both of which are being studied intensively in terms of the biochemistry and physiology of Fe(III) reduction [2,5–17]. It is currently hypothesized that *c*-type cytochromes play an important role in dissimilatory metal reduction by metal-respiring micro-organisms. The strongest evidence that supports this hypothesis is the thermodynamic and redox properties of the metal-reducing cytochromes that have been characterized thus far [18,19]. One possible model for the electron transport pathway from organic compounds (or hydrogen) to Fe(III) involves a membrane-associated respiratory chain coupled to membrane-bound cytochromes that serves as terminal metal reductases [10,20]. This situation has been demonstrated for Fe(III) and U(VI) reductase activity in *Geobacter sulfurreducens* [7,10,21], and in *Shewanella putrefaciens* [14,15,22–24].

Members of the family Geobacteraceae are of particular interest because of their ability to degrade petroleum hydrocarbons, as well as their ability to reduce radionuclides, such as uranium [21,25]. Representative members of the Geobacteraceae include *G. metallireducens* strain GS-15 and *G. sulfurreducens* strain PCA, both of which are Gram-negative anaerobes capable of using a variety of organic acids and aromatic compounds as electron donors [2]. These organisms share a unique metabolic feature, namely the ability to couple metal [Fe(III), U(VI), and Mn(IV)] reduction with energy transduction and ATP synthesis. A model organism for the study of dissimilatory metal reduction has been *G. sulfurreducens* strain PCA [26]. This organism has the ability to use formate, acetate and hydrogen as electron donors, and can respire on fumarate, Mn(IV) (as MnO_2) and Fe(III) [as both Fe(III)-citrate and insoluble Fe(III) oxyhydroxides] [2,26]. Preliminary research established that the enzyme complex responsible for this process resided in the cell membrane of the organism, and contained a cytochrome *c* component that acts as an electron transport mediator to Fe(III) [10]. The emphasis of the present paper is the purification and characterization of this cytochrome, the cloning and sequencing of its structural gene, and its description as a novel iron-reducing protein.

MATERIALS AND METHODS

Organism and culture conditions

G. sulfurreducens strain PCA (A.T.C.C. 51573) was obtained from our laboratory culture collection. It was cultured under

Abbreviations used: IEF, isoelectric focusing, ORF, open reading frame.

[1] To whom correspondence should be addressed, at the Department of Biological Sciences, Idaho State University, 921 South 8th Avenue, Pocatello, ID, U.S.A. (e-mail magntimo@isu.edu).

The nucleotide sequence data reported will appear in DDBJ, EMBL, GenBank® and GSDB Nucleotide Sequence Databases under the accession number AY033095.

© 2001 Biochemical Society

strict anaerobic conditions on modified freshwater medium, containing 20 mM sodium acetate as the electron donor and carbon source, and either 50 mM Fe(III) or 40 mM fumarate as the electron acceptor [26]. *G. sulfurreducens* was mass-cultured in 10-litre glass carboys under N_2/CO_2 (4:1). Late log-phase cells were harvested via centrifugation and the pellet was resuspended in 20 mM Tris/HCl (pH 7.5)/10 % glycerol, and frozen at −80 °C until use for protein preparation.

Purification of the membrane-bound cytochrome *c*

All manipulations were carried out aerobically at 4 °C. Cell suspensions (containing about 10 g wet weight of cell paste) of *G. sulfurreducens* were thawed and deoxyribonuclease I (40 units/ml), ribonuclease A (10 μg/ml) and lysozyme (0.1 mg/ml) were added. The cell suspension was incubated at 37 °C for 30 min, and then disrupted with a French pressure cell at 40000 kPa. After two passes through the cell, the crude cell extract was clarified by centrifugation at 7000 ***g*** for 20 min. The supernatant was removed and centrifuged at 105000 ***g*** for 1 h to pellet the membrane fraction. The supernatant (soluble fraction) was removed and the pellet (membrane fraction) resuspended in buffer A (20 mM Tris/HCl, pH 7.5, 10 % glycerol and 0.1 mg/ml dodecyl β-D-maltoside). The protein concentration of the membrane suspension was determined, and adjusted to 10.0 mg/ml with buffer A. The membrane suspension was then extracted with dodecyl β-D-maltoside at a ratio of 1 mg of detergent/mg of protein. Detergent was added from a 5 % aqueous stock solution. Extraction was carried out for 1 h at 4 °C with stirring, after which insoluble material was pelleted by ultracentrifugation for 1 h at 105000 ***g***. The supernatant (detergent extract) was reserved and the pellet discarded.

Detergent extract (400 mg) was loaded on to a column of Q-Sepharose Fast Flow ion-exchange media (column dimensions 2.5 cm × 40 cm) equilibrated with buffer A. Bound proteins were eluted with a linear gradient of 0–0.6 M NaCl (300 ml total volume). Fractions (5.0 ml) were collected and assayed for Fe(III) reductase activity [10] and cytochrome content (A_{409}). The cytochrome *c* was eluted at approx. 0.3 M NaCl. Fractions containing cytochrome were pooled and concentrated with a Filtron Ultrasette tangential flow ultrafiltration device (Filtron, Northborough, MA, U.S.A.) equipped with a 30 kDa cut-off membrane. The pool from the ion-exchange chromatography step was desalted against 1 × stacking gel buffer (0.125 M Tris/HCl, pH 6.8, 10 % glycerol and 0.5 % *N*-lauroylsarcosine) on a Sephadex G-25 column (2.5 cm × 40 cm), and then resolved on a PrepCell Preparative electrophoresis apparatus (Bio-Rad). A Tris-buffered system [27,28] was used, with some modifications. Stacking and resolving gels contained 0.5 % *N*-lauroylsarcosine and 10 % glycerol. A 4 % acrylamide, 10 mm high × 37 mm diameter stacking gel and 6 % acrylamide, 60 mm high × 37 mm diameter resolving gel was used. Approx. 60–80 mg of protein was loaded on to the gel. Electrophoresis conditions were 20 W constant power for approx. 15 h with cooling. Fractions (6 ml) were collected by elution with buffer A at a flow rate of 0.7 ml/min. Fractions were analysed by non-denaturing gel electrophoresis, and fractions containing cytochrome *c* were pooled and concentrated with a Filtron Ultrasette. The final 'polishing' step in the purification involved ion-exchange chromatography on a MonoQ HR5/5 anion-exchange column (Amersham Pharmacia Biotech). Samples from the preparative electrophoresis step were first desalted against buffer A on a HiPrep Fast Desalting Column (Amersham Pharmacia Biotech) and then loaded on to the MonoQ column (5 mg of protein in 1.0 ml). Bound proteins were eluted with a 20 ml linear gradient of 0–2.0 M NaCl in buffer A. Fractions (1.0 ml) were collected and analysed for presence of 89 kDa cytochrome. Fractions containing the cytochrome were pooled and concentrated, and stored at −80 °C.

Biophysical and biochemical characterization

Proteins were routinely analysed by non-denaturing and denaturing (SDS) PAGE [27,28]. Fractions containing cytochrome *c* were identified by haem staining of SDS/PAGE gels [29]. Analytical isoelectric focusing (IEF) was performed on precast vertical IEF gels (Novex, San Diego, CA, U.S.A) with a pH range of 3–10. IEF standards covered the range 4.45–9.6, and were obtained from Bio-Rad. Purified cytochrome was characterized using UV-visible spectrophotometry using a Shimadzu UV-2401-PC dual-beam spectrophotometer. Pyridine haemochrome analysis was performed as described in [30]. After addition of NaOH and pyridine to protein samples, the oxidized form of the protein was obtained by addition of 3 μl of 0.1 M potassium ferricyanide solution. The spectrum was recorded, and the protein was then reduced by the addition of sodium dithionite from a 0.1 M stock solution prepared in 0.1 M sodium bicarbonate buffer, pH 7.0. The haem *c* content was calculated using the absorption coefficient of 30.1 $mM^{-1} \cdot cm^{-1}$ for the α-peak (reduced) at 550 nm [30]. Extraction and determination of flavin nucleotides was performed by acid extraction and HPLC analysis [31].

Measurement of Fe(III) reducing activity

For measurement of direct reduction of Fe(III) compounds by reduced cytochrome *c*, spectrophotometric and electrochemical methods were employed. For spectrophotometric measurement of Fe(III) reduction by the cytochrome, the protein was diluted to 0.1 mg/ml total protein in buffer A and titrated with small aliquots (2–5 μl) of 0.1 M sodium dithionite until reduction of the *c*-type cytochrome was observed (15–30 μl was typically required for reduction). Aliquots of 0.1 M Fe(III)-nitrilotriacetic acid or 0.1 M ferrihydrite suspension were then added (5–10 μl) and the spectrum was re-recorded. Cyclic voltammetry was performed on a BAS CV-50-S electrochemistry workstation with accompanying data analysis software. A three-electrode (platinum reference, saturated calomel and glassy carbon) anaerobic cell was used, and redox analysis was done using a thin-film membrane entrapment method [18]. Protein was dissolved in electrolyte solution (0.1 M Tris/HCl, pH 7.5) containing 0.1 mg/ml dodecyl maltoside. Parameters for the analysis were: scan rate 10 mV/s, protein concentration 2.0 mg/ml, the gross mid-point potential was estimated by calculating the average of the anodic and cathodic peak potentials ($E_o' = 1/2(E_{pa} + E_{po})$). For experiments measuring electron transfer to ferrihydrite, ferrihydrite suspension [10 % (w/v)] was mixed with the cytochrome at varying concentrations, spotted on to the electrode, and the experiment repeated. Peak potentials and currents were determined by computer analysis, and a second-order rate constant was calculated using peak potentials and currents from a series of experiments with varying scan rates and iron concentrations.

Cloning of the structural gene encoding the 89 kDa cytochrome *c*

Internal amino acid sequences of the 89 kDa cytochrome *c* were obtained by tryptic digest of electroblotted cytochrome followed by automated Edman degradation sequencing [32]. *G. sulfurreducens* chromosomal DNA was prepared by the method of Ausabel et al. [33]. PCR primers were obtained from amino acid

© 2001 Biochemical Society

sequences and used to amplify a segment of *G. sulfurreducens* chromosomal DNA. The primers used had the sequences 5′-CKACKGCKCCBTTSTAYCAYAAYAC-3′ (forward) and 5′-CCAGTCBAGGAADATNGTRTTVGG-3′ (reverse). PCR was performed as described in [33]. PCR products were analysed and purified on agarose gels, cloned into the cloning vector pCR-TOPO (Invitrogen), and subsequently sequenced using automated dye-termination methods. Sequences were analysed using Genetics Computer Group software.

In order to clone the gene encoding the 89 kDa cytochrome, a genomic library of *G. sulfurreducens* was constructed using the cosmid vector pDDC1 [34]. Approx. 1000 transfectants were screened by colony hybridization with a probe that was prepared by PCR incorporation of fluorescein-11-dUTP into the 230 bp amplicon. One clone, pCC901 (containing an 11 kb fragment), was used for all further analysis. Sequencing of the 89 kDa cytochrome gene was performed bi-directionally using pCC901 as template. Primers for sequencing were designed using the DNA sequence data from the original PCR product. The DNA was sequenced using an ABI Prism 310 Genetic Analyzer (PE biosystems) at the Thermal Biology Institute sequencing facility at Montana State University. The raw sequence data were assembled using Sequencher 3.1 sequence analysing software (Gene Codes Corporation, Ann Arbor, MI, U.S.A.). Sequence analysis was performed using the Biology Workbench NCSA version 3.2 (http://workbench.sdsc.edu/). Non-redundant GenBank® and SwissProt databases were used for DNA and amino acid sequence comparison.

Materials and chemicals

Gel filtration molecular-size standards were obtained from Sigma. Electrophoresis standards were from Bio-Rad Laboratories. DEAE-Sepharose Fast Flow chromatography media were obtained from Pharmacia Amersham Biotech. All other reagents were of analytical grade.

RESULTS

Purification and characterization of the 89 kDa membrane-associated cytochrome *c*

A combination of chromatographic and electrophoretic steps led to the purification of the large-molecular-mass membrane-bound *c*-type cytochrome from *G. sulfurreducens* (Figure 1). Typical yields were approx. 1 mg of protein per 10 g wet weight of cell mass. The cytochrome is found mainly in the cell membrane (approx. 70% by mass), although it is also detected in smaller amounts in the soluble fraction. This cytochrome is present in slightly higher amounts in cells grown with Fe(III) than with cultures grown on fumarate (Figure 1), but purification is more difficult with cells from Fe(III)-grown cultures, since they carry a high amount of Fe(II) mineral precipitates. SDS/PAGE analysis confirmed that the final product of the purification is pure, and contains a haem-staining protein band with an M_r of 89000 (Figure 1). Pyridine haemochrome analysis of the cytochrome confirms the presence of haem *c* in the protein, with absorbance maxima (reduced protein) of 413 nm, 534 nm and 550 nm (Figure 2). When haem groups were quantified with the pyridine haemochrome method, a value of 14 haems/mol of protein was obtained. No other redox-active cofactors (FAD, FMN, Fe–S etc.) were detected by chemical or spectrophotometric means. The isoelectric point of the pure protein determined by analytical IEF is 5.2. Spectrophotometric analysis of the oxidation/reduction reactions with Fe(III) is shown in Figure 3. A distinct reoxidation of the cytochrome was observed when

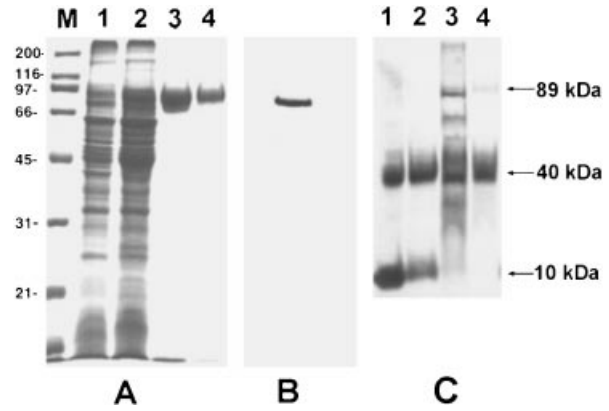

Figure 1 Electrophoretic analysis of cytochromes in *G. sulfurreducens*

(**A**) Denaturing electrophoresis analysis of fractions obtained from the purification of FerA. Lane M, molecular size standards (kDa): lane 1, 5 μg of membrane extract; lane 2, 5 μg of membrane extract; lane 3, 1 μg of PrepCell FerA cytochrome pool; lane 4, 1 μg of MonoQ FerA cytochrome pool. The gel was stained with silver. (**B**) Purified cytochrome *c* (1 μg) stained for haem. (**C**) Denaturing gel electrophoresis of cytochromes found in *G. sulfurreducens* subcellular fractions. Lane 1, soluble fraction from Fe(III)-grown culture; lane 2, soluble fraction from fumarate-grown culture; lane 3, membrane fraction from Fe(III)-grown culture; lane 4, membrane fraction from fumarate-grown culture. The gel was stained for haem *c*, and 40 μg of protein was loaded in each lane. The image was processed using Adobe Photoshop 5.0 for PC.

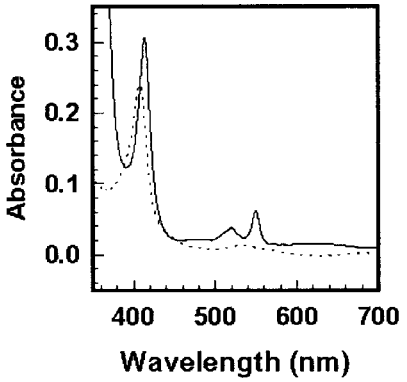

Figure 2 UV-visible pyridine haemochrome spectra of purified FerA in oxidized (broken line) and reduced (solid line) states

Note α and β peaks (reduced) at 550 and 535 nm respectively.

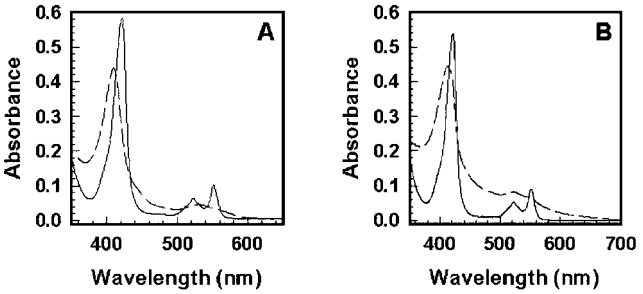

Figure 3 UV-visible redox spectral analysis of electron transfer from reduced FerA to Fe(III) compounds

Broken lines represent oxidized cytochrome; solid lines represent reduced cytochrome. (**A**) Cytochrome with soluble Fe(III)-NTA, (**B**) Cytochrome with insoluble ferrihydrite.

© 2001 Biochemical Society

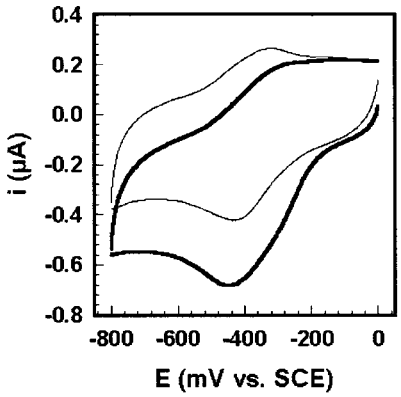

Figure 4 Cyclic voltammograms of FerA without ferrihydrite (thin line) and with 10% (w/v) ferrihydrite suspension (thick line)

Experimental conditions are given in the Materials and methods section.

```
         *        20         *        40         *        60         *
MSRKVTKYSAVLAVSLFAAALAGCGSENKEGTVGTGPGGVATVGDTACVQCHSAVVDPLTGESIITQYTR :  70

         80         *       100         *       120         *       140
SFHYSKGVGCEGCHGGGAQHNGVGPLPFPLAGQSEAQIAARCASCHNGVIAPLSSSPNFVNGNHANPFGG : 140

         *       160         *       180         *       200         *
EEAKENLCSRCHSHEGAIFGAQAGFTGDGNILRNAAYQPVYPQDPETFNVMTCATCHQHGGAQRQVFTQI : 210

       220         *       240         *       260         *       280
STAGVPNSRRTVAWDPNRNSINDQYDLCTSCHTVNTMTGTLIGSGNVLQIFTSNAVGSGTKSVTTAPFYH : 280

         *       300         *       320         *       340         *
NTRWFRTLPSTHYDFPESKTTASGTTIEGYVIRRNTANPCFDCHGHEFQTNTRRLAGADRPNTIFLDWGQ : 350

       360         *       380         *       400         *       420
SAHGGKLLQAKVAAAALASSGAAEVDDVMKAGATDATAPGWTHYNWDDTASRGACQRCHTSTGASNFLNN : 420

         *       440         *       460         *       480         *
PAGYDRTGAGNSFTHLAGWTSSNKRSDQNELLYCWGCHTNAGTGELRNPGAITENYAGVNSTSTGTTGTA : 490

       500         *       520         *       540         *       560
VTISYPDIAGSNVCMTCHLGREAGENIKAITDADGILGFVNSHYLAAGGQLFGKTGYEYATRSYAKPTPF : 560

         *       580         *       600         *       620         *
AHDKIGTAAAPGTGTNGPCAGCHMTTPNSHSFLPVTKDGTGAVTAITSTACATCHAGAYALTPEALTAEE : 630

       640         *       660         *       680         *       700
EEYVASLEALKAALAGKGILFFNAHPYFYRDTNANGIGDPGELVSSNAFTNWAGVYGLALWKDVMGAAFN : 700

         *       720         *       740         *       760
ANLLIHDPGGYAHNRFYVKRLIWDSIDFIYDGVLNSDVTAAIDAQVTATRLDSATATAAKAYLGTTRP : 768
```

Figure 5 Deduced amino acid sequence of FerA

The lipid attachment site is **double-underlined**, haem-binding sites are **underlined**, and histidine residues are in **bold**; the ATP-GTP-binding site is in **wavy-underline**. Amino acid sequences corresponding to the internal amino acid sequence data from the purified protein are in **dash underline**.

Fe(III) was added to the reduced cytochrome. Electrochemistry experiments estimate a gross redox potential of −190 mV (versus standard hydrogen electrode), based on the average of experimental oxidation and reduction values. Experiments with insoluble Fe(III)-oxides (ferrihydrite) confirm that the cytochrome can transfer electrons to Fe(III), as judged by the characteristic difference between the voltammograms with and without Fe(III) (Figure 4). The specific evidence for electron transfer to ferrihydrite is the diminished reduction peak at −350 mV, and the increased oxidation peak at −420 mV, presumably due to reoxidation of both the cytochrome and the Fe(II) in solution. Kinetic analysis determined a second-order rate constant of $1 \times 10^3\ M^{-1} \cdot s^{-1}$.

Cloning and sequence analysis of *ferA*, the gene encoding the 89 kDa cytochrome *c*

Screening of a genomic library (approx. 1000 clones) with a probe corresponding to an internal DNA sequence of the gene encoding the cytochrome resulted in the isolation of five positive clones. Of these, a single clone, pCC901, was retained for further study. The clone contained a DNA insert of approx. 11 kb, and the presence of the desired sequence in pCC901 was confirmed by PCR analysis using the same degenerate primers used in initial isolation of the gene fragment. Sequencing was initiated by using the intact cosmid as template with primers designed from the 230 bp amplicon sequence. A primer walking strategy was subsequently used to design further primers for sequencing. Sequence analysis of cosmid pCC901 revealed a 2307 bp open reading frame (ORF) with a putative Shine–Dalgano site (AGGA) located 10 bp upstream from the start codon of the ORF. No known RNA polymerase-binding sites upstream of the ORF were detected, but a possible consensus sequence may exist in the −59 to −33 region. The ORF, designated *ferA*, encodes a protein of 768 amino acids, with a predicted molecular protein mass of 80.5 kDa (Figure 5). Amino acid sequence data from the purified protein exactly matched regions of the deduced amino acid sequence of *ferA*, thus confirming that the gene in fact encodes the 89 kDa cytochrome *c* of *G. sulfurreducens*. The nucleotide sequence of the PCR amplicon generated from the protein sequence-based degenerate primers also matched a portion of the gene sequence, further supporting the conclusion that *ferA* encodes the 89 kDa cytochrome *c*. The deduced amino acid sequence of the FerA protein contains 12 *c*-type haem-binding motifs (CXXCH), as well as a lipid-attachment site and an ATP/GTP-binding site.

```
                    *        20         *        40         *        60         *
MtrF  : MNKFASFTTQYSLVL---LIATLLSACGGSDGDDGSPGEPGKP--PAMTISSLNISVDKVAISDGIAQVD :  65
OmcA  : MMKRFNFNTATKAVLGAGLLSLLLTGCGGSDGKDGEDGKPGVVGVNINSTSTLKAKFTNATVDAGKVTVN :  70
MtrC  : --MMNAQKSKIALLLAASAVTMALTGCGGSSGNNGNDGSDGGE--PAGSIQTLNLDITKVSYENGAPMVT :  66
FerA  : ---MSRKVTKYSAVLAVSLFAAALAGCG-SENKEGTVGTGPGGVATVGDTACVQCHSAVVDPLTGESIIT :  66
NrfA  : -------MTKFKLLLAGSLVAIVSMGLLASNINEREKERVALNKTAHSQGIKGKAMSEEWARYYPRQFDS :  63
Hmc   : -----MRNGRTLLRWAGVLAATALIGVGGFWSQGTTKALPEGPGEKRADLIEIGAMERFGKLDLPKVAFR :  65
Fcc   : MKKMNLAVCIATLVGTAGLMGTAVAADNLAEFHVQNQECDSCHTPDGELSNDSLTYENTQCVSCHGTLAE :  70
MtrA  : ---------------------------------------------MKNCLKVKNLLPALTITMAMSAVM :  24
                                 1
```

Figure 6 Alignment of the N-terminal region of outer and periplasmic cytochromes *c* used in anaerobic respiration

OmcA, MtrC, MtrF, outer membrane cytochromes from *S. oniedensis*; MtrA, soluble cytochrome from *S. oniedensis*; Hmc, high-mass cytochrome from *D. vulgaris*; Fcc, fumarate reductase from *S. fridgidimarina*; NrfA, nitrate reductase from *Wollinella succinogenes*. Dark and light shading represent amino acid identity (exact match) and amino acid similarity (similar side chain), respectively.

© 2001 Biochemical Society

Amino acid sequence comparisons indicated that FerA had 19.2 % identity with MtrA from *S. putrefaciens* MR-1 [35], 19.1 % identity with the 16-haem *c*-type cytochrome Hmc from *Desulfovibrio vulgaris* [36] and 15.2 % identity with the 9-haem *c*-type cytochrome 9Hcc from *D. desulfuricans* [37]. Alignment of the N-terminal regions of FerA with a variety of membrane and periplasmic respiratory cytochrome is shown in Figure 6. A shared LXXC lipid-attachment motif is seen with all membrane-associated respiratory proteins (MtrA, MtrC, MtrF, OmcA and FerA), but not with soluble cytochromes FccA and NrfA. Haem-binding site distribution seems to be random in FerA, whereas a more clustered pattern exists for OmcA, 9Hcc and Hmc. A Kyte–Doolittle hydrophobicity plot of FerA indicated a strongly hydrophobic region near the N-terminal of the amino acid sequence. Otherwise, hydrophobic and hydrophilic residues were mixed, with no strong evidence for transmembrane spanning regions of higher hydrophobicity.

DISCUSSION

Dissimilatory metal reduction by micro-organisms is believed to be mediated by membrane-bound cytochromes [6,9,11,12,14, 16,17,23]. In *S. putrefaciens*, outer membrane *c*-type cytochromes are thought to be components for the electron transport to Fe(III) [9,11,12,14,16,17] and Mn(IV) [23]. In *G. sulfurreducens*, Fe(III) reductase activity has been purified as an enzyme complex [7,10], which contained a single *c*-type cytochrome. In addition to these findings, it has also been suggested that a small soluble cytochrome *c* may act as an electron shuttle between the membrane respiratory complexes and Fe(III) outside the cell [8]. Upon further study, however, this does not appear to be the case [13]. A recently discovered [21] 40 kDa membrane cytochrome *c* in *G. sulfurreducens* may also play a role in electron transport to Fe(III) and other metals, although this protein has not yet been purified or extensively characterized.

Purification of the Fe(III) reductase activity from *G. sulfurreducens* led to the identification and purification of the 89 kDa cytochrome *c*. Pyridine haemochrome analysis of the purified protein gave a high estimation of the number of haems, possibly due to the fact that polyhaem cytochromes with large amounts of haem are difficult to analyse using this technique. This was the case for the 16-haem cytochrome *c* from *D. desulfuricans* [38], where sequence data were used to definitively determine the number of haems in the protein. It can be concluded from sequence data that the 89 kDa cytochrome of *G. sulfurreducens* has 12 haem *c* moieties. In addition, cofactor analysis did not detect any presence of either FAD or FMN, and spectrophotometric analysis did not reveal any other cofactors. Thus the cytochrome *c* is not similar to the flavocytochrome fumarate reductase from *S. oniedensis*, or any characterized sirohaem bisulphite reductases. Electrochemistry experiments with the 89 kDa cytochrome *c* and ferrihydrite gave very similar results to those seen with cytochrome c_7 from *Desulfuromonas acetoxidans* (E'_o approx. -200 mV) and ferrihydrite [19]. It should be noted that the electrochemistry experiments did not resolve individual mid-point potentials of the haems in the protein, but they did give reliable data regarding the overall redox properties of FerA. Kinetic analysis confirmed that the 89 kDa cytochrome *c* can catalytically reduce insoluble Fe(III) oxides, with the second-order rate constant comparable with those obtained for cytochromes *c* from *Desulfovibrio* spp. and Fe(III) oxides [18]. Based in this evidence, the cytochrome falls into Ambler's Class III [39] cytochrome group, since it is a polyhaemic low-redox-potential cytochrome *c*. This cytochrome shares these features with some *c*-type cytochromes from sulphate-reducing bacteria, as well as other metal-reducing bacteria. It also has the features presumably required for it to be a metal reductase, namely a membrane location, a low redox potential and an ability to reduce Fe(III) compounds [18]. The results of the present study clearly demonstrate that the 89 kDa cytochrome *c* of *G. sulfurreducens* can serve as an electron-transport mediator in the dissimilatory reduction of Fe(III) by this organism.

DNA and amino acid sequences have been reported for polyhaem cytochromes in sulphate-reducing [36,37,40,41] and iron-reducing bacteria [10,16,24]. The present study has characterized the first gene sequence encoding a cytochrome from *G. sulfurreducens*. This gene, designated *ferA*, encodes the 89 kDa *c*-type cytochrome, FerA, which was purified from Fe(III) reductase complex [10]. The lines of evidence supporting this conclusion are: (i) internal amino acid sequence from the purified native protein exactly matches the deduced amino acid sequence from the cloned gene; (ii) the predicted mass of the cytochrome is 80.5 kDa, and the corrected mass including haem and lipoprotein moieties is 86 kDa, which coincides with the experimental molecular mass of 89 kDa for the native protein as determined by SDS/PAGE; and (iii) the predicted isoelectric point of the protein is 5.6, coinciding with the experimental value of 5.2 for the purified protein. In addition, the gene sequence obtained matched a contig in the partially completed *G. sulfurreducens* genome (http://www.tigr.org), further supporting the accuracy of the sequence data. The CXXCH haem-binding motif found in all *c*-type cytochromes was also present in FerA, based on the deduced amino acid sequence of *ferA*. In addition to the haem-binding motifs, computer analysis also predicted a lipid-attachment site, as well as an ATP/GTP-binding site. While the significance of the lipid-attachment site is more obvious (see below), the reason for the existence of an ATP/GTP-binding site is less clear. An ATP/GTP-binding site is not present in any cytochromes supposedly involved in metal reduction, including MtrA, OmcA and Hmc. ATP binding by the cytochrome could play a role in some type of active transport process, perhaps involving Fe(III)/Fe(II). The presence of this site appears to be unique among putative metal-reducing *c*-type cytochromes.

A BLAST search of GenBank®/SwissProt found no DNA base sequence of high similarity to *ferA*. Comparisons using FASTA revealed, however, that FerA is at least partially identical with MtrA, a *c*-type cytochrome presumed to play a role in Fe(III) reduction in *S. putrefaciens* [35]. In contrast with the clustered distribution of haem-binding sites within cytochromes such as the c_3-type cytochromes Hmc and 9Hcc [37,41], the 12 *c*-type haem-binding motifs in FerA were distributed more evenly throughout the protein. These results suggest that FerA does not have high secondary-structural similarity to OmcA or these c_3-type cytochromes. FerA, like OmcA in *S. putrefaciens*, lacks the CXXCHH haem-binding motif found in c_3-type cytochromes such as Hmc and 9Hcc in *D. vulgaris* and *D. desulfuricans* respectively. However, there are a sufficient number of neighbouring histidine residues to participate in hexaco-ordinate bis-histidinyl haem-binding. Hydropathy-plot analysis of FerA revealed a hydrophobic domain at the N-terminus, consistent with a signal peptide/membrane anchor sequence. Previous work [24] indicated that this lipid-attachment site (LXXC) near the N-terminus of the mature protein serves as a hydrophobic anchor for attachment of OmcA to the membrane. This structural feature may serve a similar role for FerA. Secondary-structure prediction programs failed to detect consistently any other transmembrane domains in FerA, however. It thus appears that FerA may be anchored to the membrane via its N-terminus, but the remainder of the protein extends into the aqueous environment outside the outer membrane. In summary, this work

© 2001 Biochemical Society

represents the first characterization of a cytochrome *c* involved in dissimilatory Fe(III) reduction in a *Geobacter* isolate. The cytochrome *c*, designated FerA, has physiological, thermodynamic and biochemical properties that allow it to serve as a Fe(III) reductase protein.

We thank M. Coppi (University of Massachusetts) for preparation of amino acid sequencing samples, the Macromolecular Sequence Facility at Harvard University for amino acid sequencing, and E. Gelke (University of Massachusetts) and M. Bateson (Montana State University) for sequencing assistance. This research was supported by Department of Energy grants ER-62719 (to G.G.G.) and DE-FG02-97ER62475 (to D.R.L.), National Science Foundation grants ECC8907039 (to G.G.G.) and DEB 9523932 (to D.R.L.), and NIH Grant No. GM38829 (to M.J.M.).

REFERENCES

1 Lovley, D. R. and Coates, J. D. (2000) Novel forms of anaerobic respiration of environmental relevance. Curr. Opin. Microbiol. **3**, 252–256
2 Lovley, D. R., Coates, J. D., Saffarini, D. A. and Lonergan, D. J. (1997) Dissimilatory iron reduction. In Iron and Related Transition Metals in Microbial Metabolism (Winkelman, G. and Carrano, C. J., eds.), pp. 187–215, Harwood Academic Publishers, Switzerland
3 Snoeyenbos-West, O. L., Nevin, K. P., Anderson, R. T. and Lovley, D. R. (2000) Enrichment of *Geobacter* species in response to stimulation of Fe(III) reduction in sandy aquifer sediments. Microb. Ecol. **39**, 153–167
4 Rooney-Varga, J. N., Anderson, R. T., Fraga, J. L., Ringelberg, D. and Lovley, D. R. (1999) Microbial communities associated with anaerobic benzene degradation in a petroleum-contaminated aquifer. Appl. Environ. Microbiol. **65**, 3056–3063
5 Mikoulinskaia, O., Akimenko, V., Galouchko, A., Thauer, R. K. and Hedderich, R. (1999) Cytochrome *c*-dependent methacrylate reductase from *Geobacter sulfurreducens* AM-1. Eur. J. Biochem. **263**, 346–352
6 Akfar, E. and Fukumori, Y. (1999) Purification and characterization of triheme cytochrome c_7 from the metal-reducing bacterium, *Geobacter metallireducens*. FEMS Microbiol. Lett. **175**, 205–210
7 Gaspard, S., Vazquez, F. and Holliger, C. (1998) Localization and solubilization of the Iron(III) reductase of *Geobacter sulfurreducens*. Appl. Environ. Microbiol. **64**, 3188–3194
8 Seeliger, S., Cord-Ruwisch, R. and Schink, B. (1998) A periplasmic and extracellular *c*-type cytochrome of *Geobacter sulfurreducens* acts as a ferric iron reductase and as an electron carrier to other acceptors or to partner bacteria. J. Bacteriol. **180**, 3686–3691
9 Gordon, E. H., Pike, A. D., Hill, A. E., Cuthbertson, P. M., Chapman, S. K. and Reid, G. A. (2000) Identification and characterization of a novel cytochrome c_3 from *Shewanella frigidimarina* that is involved in Fe(III) respiration. Biochem. J. **349**, 153–158
10 Magnuson, T. S., Hodges-Myerson, A. L. and Lovley, D. R. (2000) Characterization of a membrane-bound NADH-dependent Fe^{3+} reductase from the dissimilatory Fe^{3+}-reducing bacterium *Geobacter sulfurreducens*. FEMS Microbiol. Lett. **185**, 205–211
11 Dobbin, P. S., Butt, J. N., Powell, A. K., Reid, G. A. and Richardson, D. J. (1999) Characterization of a flavocytochrome that is induced during the anaerobic respiration of Fe^{3+} by *Shewanella frigidimarina* NCIMB400. Biochem. J. **342**, 439–448
12 Field, S. J., Dobbin, P. S., Cheesman, M. R., Watmough, N. J., Thomson, A. J. and Richardson, D. J. (2000) Purification and magneto-optical spectroscopic characterization of cytoplasmic membrane and outer membrane multiheme *c*-type cytochromes from *Shewanella frigidimarina* NCIMB400. J. Biol. Chem. **275**, 8515–8522
13 Lloyd, J. R., Blunt-Harris, E. L. and Lovley, D. R. (1999) The periplasmic 9.6-kilodalton *c*-type cytochrome of *Geobacter sulfurreducens* is not an electron shuttle to Fe(III). J. Bacteriol. **181**, 7647–7649
14 Myers, C. R. and Myers, J. M. (1992) Localization of cytochromes to the outer membrane of anaerobically grown *Shewanella putrefaciens* MR-1. J. Bacteriol. **174**, 3429–3438
15 Myers, C. R. and Myers, J. M. (1993) Ferric reductase is associated with the outer membrane of anaerobically grown *Shewanella putrifaciens* MR-1. FEMS Microbiol. Lett. **108**, 15–22
16 Myers, C. R. and Myers, J. M. (1997) Outer membrane cytochromes of *Shewanella putrifaciens* MR-1: spectral analysis, and purification of the 83-kDa *c*-type cytochrome. Biochim. Biophys. Acta **1326**, 307–318
17 Tsapin, A. I., Nealson, K. H., Meyers, T., Cusanovich, M. A., Van Beuumen, J., Crosby, L. D., Feinberg, B. A. and Zhang, C. (1996) Purification and properties of a low-redox-potential tetraheme cytochrome c_3 from *Shewanella putrifaciens*. J. Bacteriol. **178**, 6386–6388
18 Lojou, E., Bianco, P. and Bruschi, M. (1998) Kinetic studies on the electron transfer between various *c*-type cytochromes and iron (III) using a voltammetric approach. Electrochim. Acta **43**, 2005–2013
19 Lojou, E., Bianco, P. and Bruschi, M. (1998) Kinetic studies on the electron transfer between bacterial *c*-type cytochromes and metal oxides. J. Electroanal. Chem. **452**, 167–177
20 Lovley, D. R. (2000) Fe(III) and Mn(IV) reduction. In Environmental Metal-Microbe Interactions (Lovley, D. R., ed.), pp. 3–30, ASM Press, Washington DC
21 Lloyd, J. R., Sole, V. A., Van Praagh, C. V. and Lovley, D. R. (2000) Direct and Fe(II)-mediated reduction of technetium by Fe(III)-reducing bacteria. Appl. Environ. Microbiol. **66**, 3743–3749
22 Myers, J. M. and Myers, C. R. (2000) Role of the tetraheme cytochrome CymA in anaerobic electron transport in cells of *Shewanella putrefaciens* MR-1 with normal levels of menaquinone. J. Bacteriol. **182**, 67–75
23 Myers, J. M. and Myers, C. R. (2001) Role for outer membrane cytochromes OmcA and OmcB of *Shewanella putrefaciens* MR-1 in reduction of manganese dioxide. Appl. Environ. Microbiol. **67**, 260–269
24 Myers, J. M. and Myers, C. R. (1998) Isolation and sequence of *omcA*, a gene encoding a decaheme outer membrane cytochrome *c* of *Shewanella putrefaciens* MR-1, and detection of *omcA* homologs in other strains of *S. putrefaciens*. Biochim. Biophys. Acta **1373**, 237–251
25 Lovley, D. R. (1993) Dissimilatory metal reduction. Annu. Rev. Microbiol. **47**, 263–290
26 Caccavo, F., Lonergan, D. J., Lovley, D. R., Davis, M., Stolz, J. F. and McInerney, M. J. (1994) *Geobacter sulfurreducens* sp. nov., a hydrogen- and acetate-oxidizing dissimilatory metal-reducing microorganism. Appl. Environ. Microbiol. **60**, 3752–3759
27 Hames, B. D. and Rickwood, R. (1989) Gel Electrophoresis of Proteins: A Laboratory Manual, IRL Press, New York
28 Laemmli, U. K. (1970) Cleavage of structural proteins during the assembly of the head of bacteriophage T4. Nature (London) **227**, 680–685
29 Thomas, P. E., Ryan, D. and Levin, W. (1976) An improved staining procedure for the detection of the peroxidase activity of cytochrome P-450 on sodium dodecyl sulfate polyacrylamide gels. Anal. Biochem. **75**, 168–176
30 Berry, E. A. and Trumpower, B. L. (1987) Simultaneous determination of hemes *a*, *b*, and *c* from pyridine hemochrome spectra. Anal. Biochem. **161**, 1–15
31 Hausinger, R. P., Honer, J. F. and Walsh, C. (1986) Separation of flavins and flavin analogs by high-performance liquid chromatography. Methods Enzymol. **122**, 199–209
32 LeGendre, N. and Matsudaira, P. T. (1989) Purification of proteins and peptides by SDS-PAGE. In A Practical Guide to Protein and Peptide Purification for Microsequencing (Matsudaira, P. T., ed.), pp. 52–69, Academic Press, Inc., New York
33 Ausabel, F. M., Brent, R., Kingston, R. E., Moore, D. D., Seidman, J. G., Smith, J. A. and Struhl, K. (1997) Current Protocols in Molecular Biology, John Wiley and Sons, Inc., New York
34 Wall, J. D. (1993) Genetics of the sulfate-reducing bacteria. In The Sulfate Reducing Bacteria: Contemporary Perspectives (Odom, J. M. and Singleton, R., eds.), pp. 77–87, Springer-Verlag, New York
35 Beliaev, A. and Saffarini, D. (1999) *Shewanella putrefaciens mtrB* encodes an outer membrane protein required for Fe(III) and Mn(IV) reduction. J. Bacteriol. **180**, 6292–6297
36 Pollock, W. B., Loutfi, M., Bruschi, M., Rapp-Files, B. J., Wall, J. D. and Voordouw, G. (1991) Cloning, sequencing, and expression of the gene encoding the high-molecular-weight cytochrome *c* from *Desulfovibrio vulgaris* Hildenborough. J. Bacteriol. **173**, 220–228
37 Matias, P. M., Coelho, R., Pereira, I. A. C., Coelho, A. V., Thompson, A. W., Sieker, I. C., Gall, J. L. and Carrondo, M. A. (1999) The primary and three-dimensional structures of a nine-heme cytochrome *c* from *Desulfovibrio desulfuricans* reveal a new member of the Hmc family. Structure **7**, 119–130
38 Higuchi, Y., Yagi, T. and Voordouw, G. (1994) Hexadecaheme cytochrome *c*. Methods Enzymol. **243**, 155–165
39 Ambler, R. P. (1984) The structure and classification of cytochromes *c*. In From Cyclotrons to Cytochromes: Essays in Molecular Biology and Chemistry (Kaplan, N. O. and Robinson, A., eds.), pp. 263–280, Academic Press, New York
40 Magro, V., Pieulle, L., Forget, N., Guigliarelli, B., Petillot, Y. and Hatchikian, E. C. (1997) Further characterization of the two tetraheme cytochromes c_3 from *Desulfovibrio africanus*: nucleotide sequences, EPR spectroscopy, and biological activity. Biochim. Biophys. Acta **1342**, 149–163
41 Voordouw, G. (1993) Molecular biology of the sulfate-reducing bacteria. In The Sulfate-Reducing Bacteria: Contemporary Perspectives (Odom, J. M. and Singleton, R., eds.), pp. 88–130, Springer-Verlag, New York

Received 7 March 2001/1 May 2001; accepted 6 July 2001

© 2001 Biochemical Society

ELSEVIER

Journal of Microbiological Methods 51 (2002) 125–139

Journal of Microbiological Methods

www.elsevier.com/locate/jmicmeth

Review article

A review of spectroscopic methods for characterizing microbial transformations of minerals

Gill G. Geesey [a,b,*], Andrew L. Neal [c], Peter A. Suci [a], Brent M. Peyton [d]

[a] *Department of Microbiology and Center for Biofilm Engineering, Montana State University, Bozeman, MT 59717-3520, USA*
[b] *Biotechnology Department, Idaho National Engineering and Environmental Laboratory, Idaho Falls, ID 83415-2203, USA*
[c] *Department of Microbiology, Montana State University, Bozeman, MT 59717-3520, USA*
[d] *Department of Chemical Engineering, Center for Multiphase Environmental Research, Washington State University, Pullman, WA 99164-2710, USA*

Received 17 September 2001; received in revised form 28 February 2002; accepted 28 February 2002

Abstract

Over the past decade, advances in surface-sensitive spectroscopic techniques have provided the opportunity to identify many new microbiologically mediated biogeochemical processes. Although a number of surface spectroscopic techniques require samples to be dehydrated, which precludes real-time measurement of biotransformations and generate solid phase artifacts, some now offer the opportunity to either isolate a hydrated sample within an ultrahigh vacuum during analysis or utilize sources of radiation that efficiently penetrate hydrated specimens. Other nondestructive surface spectroscopic techniques permit determination of the influence of microbiological processes on the kinetics and thermodynamics of geochemical reactions. The ability to perform surface chemical analyses at micrometer and nanometer scales has led to the realization that bacterial cell surfaces are active sites of mineral nucleation and propagation, resulting in the formation of both stable and transient small-scale surface chemical heterogeneities. Some surface spectroscopic instrumentation is now being modified for use in the field to permit researchers to evaluate mineral biotransformations under in situ conditions. Surface spectroscopic techniques are thus offering a variety of opportunities to yield new information on the way in which microorganisms have influenced geochemical processes on Earth over the last 4 billion years.
© 2002 Elsevier Science B.V. All rights reserved.

Keywords: Biogeochemistry; Spectroscopic techniques; Microorganisms

1. Introduction

Biogeochemistry is a discipline of great importance to our understanding of Earth's evolution and the potential for bioremediation of metal-contaminated and radionuclide-contaminated subsurface sites. Recent advances in this area have been largely due to the application of surface-sensitive spectroscopic techniques to studies on microbe–mineral interactions and more specifically the role of microbial activities on metal, radionuclide and mineral oxidation state that in turn influences their solubility and reactivity toward other components in surface sediments, soils and subsurface environments. These techniques provide

* Corresponding author. Department of Microbiology and Center for Biofilm Engineering, Montana State University, Bozeman, MT 59717-3520, USA. Tel.: +1-208-526-2233; fax: +1-208-526-0828.

E-mail address: gill_g@erc.montana.edu (G.G. Geesey).

0167-7012/02/$ - see front matter © 2002 Elsevier Science B.V. All rights reserved.
PII: S0167-7012(02)00045-3

useful molecular and atomic information at single cell or microcolony scale. Some spectroscopic techniques such as Raman imaging can be used to obtain chemical maps of a mineral surface under fully hydrated conditions important for preservation of the integrity of biological systems involved in mineral transformations. This review describes advances in our understanding of inorganic mineral transformations by microorganisms in nature and under controlled laboratory conditions that are based on surface spectroscopy. The review also identifies features and limitations of the different spectroscopic techniques that are relevant to studies on microbe–mineral interactions.

2. Background

Biogeochemical research in recent years has changed the way we view life on Earth and in particular has expanded greatly our views on microbial ecology and diversity. These advances have, in part, resulted from our need to identify novel approaches to contain and detoxify hazardous waste that is buried in subsurface environments. The discovery in the 1980s of a subsurface biosphere containing viable and potentially active microbial populations spawned a large number of investigations to evaluate their value in contaminant detoxification, immobilization and stabilization. We are now at a point where interdisciplinary research is essential, and fields of science that previously have not been engaged in common activities must come together to solve these challenging problems.

Historically, mineral transformations involving microorganisms were evaluated from a priori knowledge of the solid phase mineralogy, and measurements of solution phase chemistry were used to infer microbiological modification of the solid phase. For example, dissimilatory iron reduction is typically assessed by the Ferrozine assay (Stookey, 1970; Viollier et al., 2000), which is used to quantify the amount of Fe(II) in solution (Kazem and Lovley, 2000; Roden et al., 2000). When insoluble products are formed during mineral biotransformation, these products are solubilized prior to solution phase analysis (Roden and Zachara, 1996; Fredrickson et al., 2000). Solution phase assays have also been used to evaluate biotransformations of minerals containing other elements such as Cr(VI), Mn(IV), and U(VI) (Francis et al., 1994; Kazem and Lovley, 2000; Wielinga et al., 2001).

Recently, microbiological studies have utilized solid phase minerals synthesized in the laboratory for better control over the mineral structure of the starting material. Synthetic iron oxides, including goethite (α-FeOOH), lepidocrocite (γ-FeOOH), ferrihydrite ($Fe_5OH_8 \cdot 4H_2O$) and hematite (α-Fe_2O_3) have been prepared for assessment of metal reduction by microorganisms (Cornell and Schwertmann, 1996). The preparation of amorphous MnO_2 has been described by Lovley and Phillips (1988), while the production of birnessite (δ-MnO_2) films has been reported by Brulé et al. (1980). Because these preparations have been well characterized and appear to be similar to naturally occurring minerals, they are convenient to use in controlled laboratory studies.

The approach described above was used by Roden et al. (2000) to compare the rate and extent of bacterial reductive dissolution of a synthetic crystalline Fe(III) oxide-coated sand under batch culture and continuous-flow column reactor culture conditions. In this study, X-ray diffraction (XRD) was used to characterize the goethite-like mineral structure of the Fe oxide coating before solubilization by the Fe(III)-reducing bacterium *Shewanella putrefaciens* strain CN32. The results demonstrated the importance of advective removal of Fe(II) from the vicinity of the bacterial cell surface on the extent of Fe reduction and biomass production.

Generally, solution phase analysis yields limited information on the nature of the inorganic solids formed in the presence of microorganisms or the inorganic material adsorbed to surface-associated microbial biomass. Knowledge and control of the aqueous phase chemistry and hydrodynamics and application of mathematical models can overcome this limitation of solution phase analysis to quantify sorption of dissolved metal ions to a solid phase. By employing a bioreactor to control hydrodynamics, an aqueous phase with defined chemistry, and a chemical equilibrium model (MINEQL), Nelson et al. (1995) simulated the influence of the surface-associated microbial population on Pb distribution between the aqueous phase and the biofilm components on iron oxide and glass surfaces. The results indicated that only 10–20% of the Pb adsorbed to biofilm were

associated with cells and that the bulk of Pb adsorption sites in the biofilm were associated with extracellular polymeric material. In this case, solid phase analysis would have provided independent evidence to support the model predictions of Pb distribution between cell and extracellular polymeric components.

In summary, solution phase analyses provide information on total and reduced metal and radionuclide concentrations, are amenable to determination of rates of biotransformation of chemical species that reside external to the cell, and permit assessment of sorption and precipitation phenomena. Restricting analyses to the solution phase, however, limits the type of information one can obtain on the chemical transformations that occur at mineral or other solid surfaces where biological oxidation or reduction may lead to the formation of surface complexes undetectable in solution.

3. Solid phase mineralogical and chemical analysis

Analysis of the solid phase on which microbially induced biotransformations occur offers the opportunity to obtain a wealth of biogeochemical information that cannot be acquired through solution phase analysis. Many solid phase-associated biogeochemical processes can be evaluated by surface spectroscopic analysis. Ideally, reactors used for biotransformation studies should accommodate both solution phase and solid phase analyses. Wielinga et al. (2001) used a stirred-flow reactor to recover both the solid and the solution phases to determine the reduction rates of Cr(VI) in the presence of iron (hydr)-oxides and dissimilatory iron-reducing bacteria (DIRB). A filter at the top of the reactor retained the biomass and insoluble inorganic material for subsequent solids analysis while allowing the liquid phase and soluble components such as Cr(VI) and Fe(II) in the reactor effluent to be recovered for solution phase assays.

3.1. X-ray diffraction

X-ray diffraction has been used for many years to determine the symmetry of crystals and to measure lattice parameters to high accuracy and has been used extensively to identify geological material through crystal structure. In fact, generation of interpretable XRD patterns can only be obtained for material displaying a crystalline structure (Table 1). The diffraction pattern obtained from a sample is then compared with that of known minerals provided by databases such as the International Center for Diffraction Data for sample identification or by theoretical interpretation. The depth of penetration of the X-rays varies with X-ray source, sampling angle, and the type of mineral. Using a CuK_α source at a 30° sampling angle, the penetration depth for hematite is approximately 3 μm, whereas with a MoK_α source at a 90° sampling angle, the penetration depth for alumina is approximately 675 μm. Slurries of solid phase material exposed to cultures of microorganisms are typically recovered and subjected to analysis by powder XRD after drying on a glass slide in the appropriate gas phase. The distance between crystalline layers (*D*-spacing) obtained from X-ray diffractograms has been used to identify uraninite (UO_2) as a product of microbiological uranyl acetate and metaschoepite reduction (Fredrickson et al., 2000). This approach cannot be used to identify uraninite as a product of solid phase U(VI) reduction, however. XRD was also used to demonstrate that siderite ($FeCO_3$) is a product of magnetite (Fe_3O_4) reduction by Fe-reducing bacteria in bicarbonate-buffered medium (Dong et al., 2000), whereas Brown et al. (1997) used powder XRD to demonstrate that hematite is a product of magnetite biotransformation. Palladium-loaded microbial biomass, after washing with organic solvents and air drying, was evaluated by XRD to demonstrate the feasibility of elemental Pd recovery using sulfate-reducing bacteria (Lloyd et al., 1998). Neal et al. (2001) employed thin-film XRD, where the precipitate is observed as a surficial film, to identify a hexagonal pyrrhotite (Fe_7S_8) structure associated with ferrous sulfides formed by sulfate-reducing bacterial biofilms on hematite. In other studies, precipitates of iron sulfides formed in the presence of sulfate-reducing bacteria yielded powder XRD patterns that lacked reflections indicative of crystalline iron sulfide phases (Herbert et al., 1998).

The lack of well-defined crystalline phases among precipitates formed as a result of microbial activity often limits the utility of XRD in characterizing inorganic reaction products. Also, the large beam size associated with XRD requires relatively large quantities of material to produce a pattern. Precipitates formed in liquid microbial cultures are typically

Table 1
Features of different surface analytical techniques used to investigate microbe–mineral interactions

Technique	Elements	Detection limit	Spatial resolution	Penetration depth	Aqueous phase	Oxidation state	Coordination chemistry	Spatial information	Structural information	Limitations	Features
XRD	Those forming crystals	2%	100 nm	3–675 μm	No	Yes	Inorganic	No	Yes	Crystalline phases only	Mineralogy characterization
Synchrotron-XRD	Fe minerals to date		100 nm		Yes	Yes	Inorganic	Yes	Yes	Crystalline phases only	Mineral transformation reactions in situ
SEM-EDS	Atomic no. >8	10^{-15} g (0.1–1%)	0.3 μm	1 μm	No	No	No	Yes	Limited	Limited chemical/mineral information	Spatial relationships between elements, microbes and solid phase; quantitative analysis
TEM-EDS	Atomic no. >8	10^{-15} g (0.1–1%)	10–100 nm	Thin section (10–100 nm)	No	No	No	Yes	Limited	Same as SEM-EDS	High-resolution spatial relationships between elements, microbes and solid phase
HR-TEM electron diffraction	Those forming crystal phases	10^{-16} g	100 nm	Thin section (10–100 nm)	No	No	No	Yes	Yes	Crystalline phases only	Structure of nanometer-size crystals; spatial relationships between crystals and microbial structures
EF-TEM	Atomic no. >1		10 nm	Thin section (10–100 nm)	No	No	No	Yes	Yes	Elemental imaging	Identification of amorphous and crystalline phases; spatial relationships between inorganic phase and microbial cell structures
EELS	Atomic no. >1	10^{-20} g; (300 atoms in case of phosphorus)	10 nm	Thin section (10–50 nm)	Yes	Yes	Yes	Yes	No	Thin specimen required; requires knowledge of atomic and solid-state physics, electron optics and electronics	Identification of oxidation states of metals associated with hydrated microbial cells

XPS	most	Tens of micrometers	Tens of Angstroms	No	Yes	Yes	No	No	Interference from surface contamination	Surface sensitive, oxidation state, organic and inorganic compounds
Raman	Those involved in bonds yielding large Stoke's shift	10 μm	70 μm in water; near surface	Yes	Yes	Yes	Yes	Limited	Dissolved solutes must be in 1–5% concentration range	Spatial information on dissolved and precipitated organic and inorganic material; nondestructive, real-time sampling of biological material
XANES	Hard X-rays: metals, actinides; Soft X-rays: C, O, N, Si	Tens of nanometers	Tens of micrometers	Yes	Yes	No	Yes	Yes	Beamline accessibility	Information on average local structure; oxidation state of a metal or radionuclide
EXAFS	Same as XANES	Tens of nanometers	Tens of micrometers	Yes	No	Yes	Yes	Yes	Beamline accessibility	Information on average short-range order around an element in non crystalline material
X-PEEM	Metals, actinides, C, O, N, Si	Tens of nanometers	Thin section (tens of micrometers)	Yes	Yes	No	Yes	No	Not yet applied to microbe–metal interactions	Evaluation at specific depths
Mössbauer	Fe, Ni, Zn, Ge, Kr, Rb, Ru, Sn, Sb, Te, I, Cs, La, Hf, W, Re, Os, Ir, Pt, Au, Hg, Tl, Ra, Th, Pa, Np, U, Pu, Am, Cm		Surface atoms, 10–20 μm	No	Yes	Yes	Yes	Yes	Not applicable to some elements or minerals of interest	Resolution of different Fe minerals when present in same sample

spread over a surface to dry before XRD interrogation in order to accommodate the limited depth of penetration of the electron beam into the sample, thus disrupting spatial relationships between the microorganisms and the different mineral phases that are present. Samples containing complex mixtures of crystalline phases or of a predominant amorphous nature are difficult to interpret. However, XRD can provide positive identification of those mineral phases that display crystalline structure.

3.2. In situ time-resolved X-ray diffraction using synchrotron X-ray source

Recently, the use of synchrotron radiation to enhance the brilliance of X-rays has made it possible to preserve spatial relationships and follow mineral transformation reactions in situ (Table 1). Anoxic and oxic reactions during abiotic pyrite formation were followed for the first time in a Fe-S system using in situ time-resolved X-ray diffraction by Cahill et al. (2000). In one set of experiments, the incident X-ray beam was reduced to 1.0×0.5 mm, and the X-rays diffracted from the sample were collected on a translating image plate system. The reaction cell consisted of a 0.7-mm horizontally mounted quartz capillary mounted on a Huber four-circle goniometer. A full diffraction pattern was collected from a portion of the imaging plate, the plate was translated to expose a fresh area of the sample, and a new diffraction pattern was collected. With this translating image plate system, time resolution for these experiments was 5 min or less. Using this approach, it was demonstrated that mackinawite ($Fe_{1+x}S$) is the only Fe-S phase to occur during heating to 120 °C in the presence of H_2S under anoxic conditions. However, with the controlled introduction of small quantities of oxygen, mackinawite rapidly transformed to greigite (Fe_3S_4) and then to pyrite (FeS_2) with goethite (α-FeOOH) present throughout the heating period. Typically, XRD of solid samples at a synchrotron source can detect less than 1.0% by weight of a secondary phase. However, with interference from water and the steel sample cell of the translating image plate system, the detection limit was estimated to be closer to 5.0%. It may be possible to reconfigure the reaction chamber in order to incorporate a biological component in studies of nucleation reactions of FeS and other minerals.

3.3. Mössbauer spectroscopy

Application of Mössbauer spectroscopy to investigate chemical and physical phenomena of surfaces began in 1964 with studies involving iron and tin. Mössbauer spectroscopy is based on nuclear transformations involving recoilless gamma resonance fluorescence (radiation, absorption, scattering), most successfully in isotopes having long-lived low-lying excited nuclear energy states, ^{57}Fe being of particular utility. The Mössbauer effect can be detected by monitoring radiation, which is resonantly reemitted by the absorber after resonance absorption of the incident γ-rays. Although Mössbauer spectroscopy has focused primarily on ^{57}Fe and Sn using ^{57}Co and ^{119}Sn radiation sources, it can be applied to a wide range of elements (Table 1). Mössbauer spectroscopy provides information on a broad range of chemical and physical phenomena at solid surfaces (Table 2). Chemical shifts and quadruple splitting in Mössbauer spectra of iron compounds can be used to identify those compounds and the Fe oxidation state. Mössbauer conversion electron spectroscopy has been used to determine qualitatively and quantitatively various iron oxides and oxyhydroxides like magnetite, hematite, wustite and α-FeOOH, β-FeOOH and γ-FeOOH, even when these different minerals coexist in the sample (Gutlick et al, 1978). ^{57}Fe Mössbauer spectroscopy can also yield depth-selective Mössbauer spectra over 10–20 μm by changing from one type of backscattered radiation to another (i.e., resonantly scattered γ-rays, L shell conversion electrons, K_α X-rays, and K_L Auger electrons). The conversion electrons and Auger electrons yield spectra of the <1000 atoms proximal to the surface of a sample, making it a

Table 2
Chemical and physical phenomena interrogated by Mössbauer spectroscopy (Gutlick et al., 1978)

Surface atoms
Electronic state and local symmetry
Magnetic properties
Intramolecular and intermolecular vibrations
Surface diffusion
Adsorption processes
Chemistry of surface compounds
Catalysis
Topochemical reactions
Boundary effects on internal atoms of a solid

useful technique to study oxide films. Mössbauer has been used to good effect in both laboratory and environmental samples to identify iron carbonate (siderite) and green rust formation in laboratory culture by *S. putrefaciens* strain CN32 (Kukkadapu et al., 2001) and in recent anoxic sediments from the Seine estuary (Boughriet et al., 1997).

3.4. High-resolution electron diffraction

High-resolution transmission electron microscopy (HR-TEM) has been used to obtain images and structural information of very small (nanometer-size) crystalline particles, including those associated with mineral-transforming bacteria (Fig. 1). At high magnification, lattice fringes can be resolved whose spacing is used to deduce crystal structure. Convergent beam diffraction (CBD) is accomplished using an incident-beam diameter of the order of 20 nm. Besides providing information on crystal symmetry, CBD can be used to measure small (0.1%) changes in lattice parameters due to atomic concentration gradients. Features of this technique are presented in Table 1. Watson et al. (2000) used the spacing of the lattice rings to deduce a greigite structure in nanometer-size crystals formed by sulfate-reducing bacteria in the presence of sulfate and iron. Similarly, Neal et al. (2001) used electron diffraction data to resolve a hexagonal structure associated with iron sulfides produced by sulfate-reducing bacteria on hematite, which supported X-ray diffraction data consistent with a pyrrhotite phase.

Selected area electron diffraction (SAED) has been used to obtain electron diffraction patterns from crystals on the order of 0.1 μm in size. SAED was employed by Posfai et al. (1998) to characterize single crystal iron sulfides formed within magnetotactic bacteria. Donald and Southam (1999) used SAED to identify micrometer-sized cubic minerals associated with sulfate-reducing bacteria as [111] pyrite, having an observed *d*-spacing of 3.14 Å. Theoretically, one can use this technique to distinguish between an intracellular and a cell surface site of crystal initiation. However, it is often difficult to prepare sufficiently thin sections of sample without disrupting the organic–mineral interface.

3.5. Energy-dispersive X-ray spectroscopy (EDS)

Energy-dispersive X-ray spectroscopy is used in conjunction with electron microscopy to identify elemental composition, relative abundance and distribution within a sample at high spatial resolution (Table 1). EDS does not distinguish oxidation state of elements, which is important in demonstrating the biotransformation of a mineral. When used with a scanning electron microscope (SEM), the level of resolution is on the order of 1 μm and when used with a transmission electron microscope (TEM) can achieve a resolution on the order of 0.1 μm. The EDS

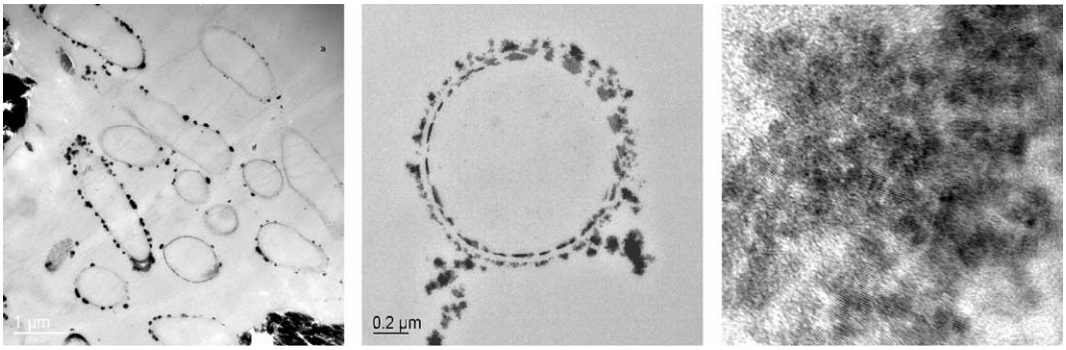

Fig. 1. TEM low (left) and high (center) magnification image of a thin section of the metal-reducing bacterium *S. algae* strain BrY incubated in an anaerobic solution containing 100 mM uranyl acetate. This unstained preparation clearly reveals the presence of uranium precipitates on the cell surface and within the periplasmic region of this Gram-negative bacterium. Extracellular precipitates resulting from the reduction of dissolved U(VI) to highly insoluble U(VI) exhibit *d*-spacing of 3.0Å, as shown by high-resolution lattice fringe imaging, and are consistent with the reduced uranium oxide uraninite (right). Courtesy of Yuri Gorby, Bruce Weilinga and Alice Dohnalkova.

energy-dispersive detector partitions and quantifies X-rays emitted from the specimen when probed with the electron beam. Element discrimination is based on the fact that each element emits X-rays of a characteristic energy. Elements lighter than boron cannot be detected using standard EDS, and many elements must be at levels 100 ppm or greater to produce a detectable signal. Because the electrons bombarding a sample at typical energies of ~ 15 keV can penetrate on the order of 1 μm into the specimen, the emitted X-rays provide information on elemental composition of the bulk material. Before analysis under high vacuum, samples must be dehydrated. Spatial relationships between biological and mineral components may be disrupted during dehydration, even when steps are taken to stabilize biological structures through chemical fixation.

Donald and Southam (1999) employed SEM-EDS to determine the extent of conversion of FeS to FeS_2 at the surface of cells of sulfate-reducing bacteria based on relative abundance of Fe and S at these locations. Lloyd et al. (2001) used TEM-EDS to demonstrate that the products of Cr(VI) reduction and Te(IV) reduction were associated with cells of sulfate-reducing bacteria. Lloyd et al. (2000) used TEM-EDS to demonstrate the precipitation of Tc at the periphery of Tc-reducing cells of *Geobacter sulfurreducens*. McLean and Beveridge (2001) and McLean et al. (2000) successfully imaged a Cr-reducing pseudomonad by TEM-EDS without fixation or staining due to the electron density contributed by the reduced Cr species adsorbed to the cell. Thus, EDS has become a valuable means of resolving spatial relationships between microbial cells and specific elements associated with mineral phases.

3.6. Energy-filtering transmission electron microscopy (EF-TEM)

Energy-filtering transmission electron microscopy is a powerful new method for detecting and identifying inorganic precipitates formed in the presence of microorganisms. An electron energy filter is used to filter out all inelastically scattered electrons in the precipitate, thus eliminating chromatic aberration from the final image. A two-dimensional elemental image is produced from thin specimens with nanometer resolution in less than 1 min (Table 1). The method can be used for chemical characterization of both crystalline and amorphous materials that nucleate at the surface of a bacterial cell. The technique has been successfully used to characterize secondary phases in steels (Warbichler et al., 1998). Barker and Banfield (1998) employed EF-TEM to resolve discrete zones of biogeochemical weathering of silicate mineral assemblages containing lichen communities.

3.7. Electron energy loss spectroscopy (EELS)

Electron energy loss spectroscopy is one of the many techniques that can be used to determine structure and/or chemical composition of a solid (Table 1). EELS provides information about chemical, crystallographic, and electronic structure of an element. EELS compares the differences in fine structure of absorption edges (or white lines) of metals in standards of known oxidation state to determine the oxidation state of metal atoms at high spatial resolution. Absorption edges, such as the $L_{2,3}$ absorption edge, are produced by excited electron dipole transitions between core $2p_{3/2}$ and core $2p_{1/2}$ spin-orbit split levels to unoccupied $3d$ levels. Spectra of different $3d^n$ configurations differ and can be used to identify valance state. The minimum detectable concentration or mass fraction is 60 ppm for Ca in a carbon matrix using this technique (Egerton, 1986). In recent years, electron microscopists have used EELS as a method of light-element microanalysis, for which purpose a simple magnetic-prism spectrometer mounted beneath a conventional TEM with scanning transmission electron microscopy facilities is sufficient. Daulton et al. (in press) used EELS to determine the oxidation state of Cr associated with metal encrusted cells of *Shewanella oneidensis* strain DSP10 under hydrated conditions.

3.8. X-ray photoelectron spectroscopy (XPS)

Of the spectroscopic techniques included here, X-ray photoelectron spectroscopy is one of the more established techniques, applicable to both mineral (Hochella 1988) and microbial (Rouxhet and Genet 1991; van der Mei et al., 2000) surfaces (Table 1). XPS exploits the unique energies of photoelectrons liberated from atoms of different elements within a sample exposed to stimulating X-rays. Any electron

with a binding energy lower than that of the stimulating radiation (1486.6 eV for an AlK_α source, 1256.6 eV for an MgK_α source) may be ejected from a sample. Analysis of the ejected photoelectrons provides elemental and chemical state information. XPS generally probes a few tens of angstroms and is therefore considered a *near-surface* probe. This "surface sensitivity" may be problematic when studying mineral surfaces and associated microbial cells because the chemistry of interest may be buried under other material. At low resolution, XPS provides data similar to EDS (see above) describing elemental abundance in a sample. High-resolution spectra yield information about the valence state of elements present.

Despite potential problems arising from the surface sensitivity of XPS, the technique is used to good effect in probing bacterial–metal interactions. Association of Fe with exopolymers of *Desulfovibrio indonensis* (Beech et al., 1999) and a *Burkholderia* sp. (Johansson and Saastamoinen, 1999) has been identified. Depletion of Fe at the surface of hornblende by an *Arthrobacter* species was detected using XPS by comparing Fe/Si ratios of samples exposed to bacteria to ratios of unexposed samples (Kalinowski et al., 2000). Francis et al. (1994) employed a curve fitting algorithm to the peaks in the U4*f* core region of the spectrum to demonstrate reduction of U(VI) by a *Clostridium* sp. Curve fitting of peaks in the Fe2*p* regions of XPS spectra of precipitates produced during growth of *Desulfovibrio* spp. consisted of mixed valence Fe(II)/Fe(III) sulfides that resembled greigite and pyrrhotite (Herbert et al., 1998; Neal et al., 2001).

3.9. Raman spectroscopy

Raman spectroscopy, like infrared spectroscopy, probes quantum state transitions associated with molecular vibrations but relies upon scattering of the incident light rather than absorption (as is the case with infrared). An organic or inorganic molecule, which has an inducible dipole moment, has the potential to produce a Raman spectrum having unique albeit complex features that permit positive identification. Raman has been used to probe the surfaces of metal sulfides exposed to microbial populations known to be important in pyrite dissolution at the Richmond Mine at Iron Mountain in northern California (Edwards et al., 2000). Comparison of Raman spectra of the surface of a single pyrite crystal exposed to the microbial populations with the spectra of a pyrite surface exposed to sterile acid solution under otherwise similar conditions revealed three peaks at 470, 217, and 151 cm^{-1} when the microorganisms were present, which were not present under abiotic conditions. The peaks were characteristic of orthorhombic (S_8^0) sulfur. Calibration of the Raman data indicated that the sulfur layer was on the order of several hundred angstroms thick if distributed uniformly across the surface.

Raman spectroscopy was also employed to compare the species of the sulfur deposited on marcasite (FeS_2) and arsenopyrite ($AsFeS_2$) mineral surfaces in the presence of a sulfur-oxidizing bacterial isolate and in the presence of sterile acid solution. In contrast to pyrite, the surfaces of these other minerals accumulated elemental sulfur (S_8^0) under abiotic conditions but not in the presence of the bacterial isolate (Edwards et al., 2000). These results encouraged reconsideration of a widely accepted mechanism of sulfide mineral dissolution involving sequential oxidation of surface sulfur atoms to form thiosulfate anion, which is then liberated along with Fe^{2+} ions into the bulk aqueous solution (Singer and Stumm, 1968).

The laser beam can be highly focused using a microprobe to obtain Raman spectra at high spatial resolution. Cooney et al. (1999) used this approach to probe the complex geochemistry of the Martian meteorite ALH84001. Raman spectroscopy was used to look for evidence of biochemical signatures of the submicroscopic structures associated with the meteorite. Raman imaging was employed by Boughriet et al. (1997) to identify FeS and pyrite formation in anaerobic sediments from the Seine estuary. By combining Raman microprobe and confocal microscopy, Pasteris et al. (2001) showed that S_8^0 was precipitated intracellularly in the bacterial endosymbionts of the clam *Calyptogena*.

Shortcomings in the sensitivity of Raman spectroscopy are driving the development of instruments with deep ultraviolet (UV) lasers with excitation wavelengths between 224.3 and 248.6 nm. Many organic molecules have electronic adsorption bands, which fall in this range, and coupling of these electronic and vibrational transitions leads to a significant increase in

spectral intensity termed resonance Raman scattering. Many of the molecules, in microbial cells for which resonance Raman is pertinent, have a ring structure, such as the amino acids tryptophan and tyrosine and the nucleic acids guanine, adenine and cytosine. Even though these molecules are found in all cells, resonance Raman spectra vary among species and over different phase of growth in cultures at cell densities between 10^8 and 10^{10} cells/ml (Wu et al., 2001). The utility of deep UV excitation is further emphasized by employing the native fluorescence arising from cellular components (again, amino acids and nucleic acids) to visualize cells as well as to collect resonance Raman spectra. Using this combination, single cells of *S. oneidensis* have been imaged in situ in real time on unpolished surfaces of calcite and in a Mars soil analogue (Storrie-Lombardi et al., 2001). Lasers, which excite in the deep UV, are of little utility in collecting spectra from inorganic molecules that are more typically excited with visible radiation such as the 514.4 and 676.4 nm lines from Ar^+ and HeNe lasers, respectively.

Because Raman is relatively insensitive to water, high-quality spectra can be readily obtained for fully hydrated samples. Suci et al. (2001) used Raman microscopy to determine nondestructively in real time the concentration of an antimicrobial agent at different locations within a yeast biofilm growing on a germanium surface in the presence of a flowing aqueous phase. By combining native fluorescence imaging and resonance Raman spectroscopy using deep UV excitation for detection of biological constituents with nonresonance Raman spectroscopy using visible excitation for detection of the mineral phases, it should be possible to evaluate mineral transformations at the cellular level under hydrated conditions.

3.10. X-ray absorption spectroscopy

X-ray absorption spectroscopy has evolved as a means to study surface chemistry under fully hydrated conditions. In X-ray absorption spectroscopy, the intensity of a transmitted beam of X-rays is measured as a function of incident wavelength. A synchrotron is used to produce high-energy electrons, which are then captured by a bending device and manipulated to enhance the brilliance of generated X-rays. X-ray absorption edges occur at an incident energy close to the binding energy of the core electrons of an atom. These absorption edges are analogous to the ionization edges seen in electron energy loss spectra. Fine structure is present in the near-edge region as well as in a region up to several hundred electron volts beyond the edge. Near-edge information is captured by X-ray absorption near-edge spectroscopy (XANES), while information at energies further from the edge is captured by extended X-ray absorption fine structure (EXAFS). Fine structure provides information on the immediate atomic environment and is used to determine interatomic distances relative to a known element even in the case of amorphous samples (Table 1). Synchrotron radiation offers the means to determine the number and identity of coordinating atoms and using model compounds bond angles around an element of interest. Such information is often critical for establishing mechanisms of biotransformations of a mineral by microorganisms.

Beamlines at synchrotron radiation facilities worldwide are becoming increasingly available to evaluate oxidation state and coordination chemistry of atoms of metals, minerals and radionuclides transformed by microorganisms. The high-energy (hard) X-rays from synchrotron sources can penetrate samples that are tens of micrometers in thickness while maintained in a fully hydrated environment. For example, the density and distribution of elements such as chromium and potassium have been obtained in a fully hydrated environment at the resolution of a single bacterial cell using synchrotron X-ray absorption spectroscopy (Fig. 2). Alternatively, low-energy (soft) X-ray absorption techniques are more sensitive to the lighter physiological elements such as C, O, N and Si, but progress in this area has been slow due to specimen charging under X-ray illumination. For detailed reviews on the experimental aspects of X-ray absorption spectroscopy and geological applications of synchrotron radiation, the reader is referred to Meitzner (1998) and Henderson et al. (1995), respectively.

3.11. X-ray absorption near-edge structure

X-ray absorption near-edge structure, typically within 40 eV of the absorption edge, is sensitive to both electronic and molecular (or cluster) structure, providing information on the average local structure and to some extent oxidation state of a metal or

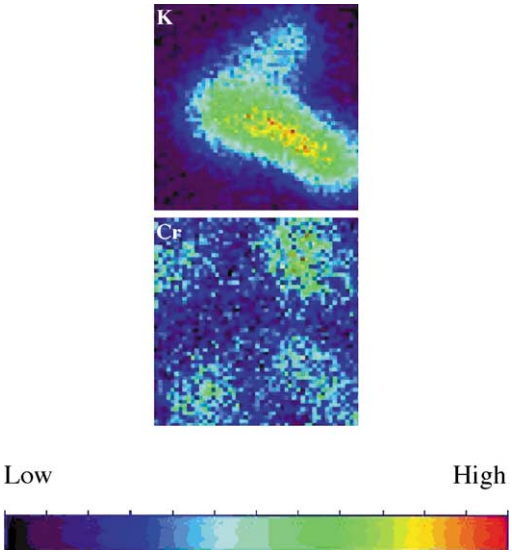

Fig. 2. Potassium (top) and chromium (bottom) elemental maps obtained by synchrotron X-ray absorption spectroscopy at sector 2 at the Advanced Photon Source at Argonne National Laboratory showing spatial relationship between a hydrated bacterial cell (*P. fluorescens*), as defined by potassium density, and chromium precipitated on the outside of the cell. Each image is 25 μm^2. Courtesy of B. Lai, Z. Cai, J. Maser, P. Ilinski, D. Legnini, W. Rodrigues, W. Yun, S.T. Pratt and K.M. Kemner (Argonne National Laboratory), M.A. Schneegurt and C.S. Culpa, Jr. (University of Notre Dame) and K.H. Nealson (California Institute of Technology).

radionuclide (Table 1). In general, near-edge absorption features represent transitions to unoccupied electronic levels successively higher in energy, with modulations due to selection rules, as well as multiple scattering phenomena (Durham, 1988). A linear relationship has been shown to exist between the fraction of an element in a solid and relative XANES energy edge (Bertsch et al., 1994). A shift to higher energy with respect to the XANES energy edge indicates an increase in the average oxidation state of an element.

Samples of biological material for XANES or EXAFS analysis may be inserted in a chamber sealed with Mylar film. Alternatively, a small amount of solid sample can be placed in the well of a Lucite plate and sealed with Kapton (polyimide) tape before exposure to the radiation source (Fredrickson et al., 2000). Some chambers have been modified to control the composition of the gas phase to achieve anaerobic conditions.

Francis et al. (1994) utilized XANES to reproduce XPS results indicating the reduction of U(VI) by anaerobic cultures of a *Clostridium* sp. Whereas the XPS results suggested a U reduction product with a valence of 4^+, XANES data suggested a more reduced oxidation state. Because XANES can probe to greater depths in the sample than is possible with XPS, comparison of results obtained by these two spectroscopic techniques may offer a means to distinguish the oxidation state of an element residing at different locations on or within a bacterial cell.

XANES was used to characterize the solid phase of mineral suspensions in U(VI)-containing aqueous media inoculated with dissimilatory metal-reducing bacteria (Fredrickson et al., 2000). U-L_3 edge XANES revealed that microbiologically reduced solids were predominantly in the U(IV) oxidation state. XANES was also used by these authors to demonstrate microbial reduction of U(VI) in crystalline metaschoepite to a tetravalent form of U.

XANES was used to study the structural properties of strongly magnetic iron sulfide produced in the presence of sulfate-reducing bacteria (Watson et al., 2000). By comparing the Fe K-edge spectrum of this biologically derived material to that of several iron sulfide model compounds, these investigators suggested the magnetic iron sulfide material most closely resembled that of mackinawite, in which the Fe is tetrahedrally coordinated to four S atoms.

Wielinga et al. (2001) employed Cr *K*-edge XANES to determine valence state of Cr associated with the solid phases produced in a stirred-flow reactor containing iron (hydr)-oxides and dissimilatory iron-reducing bacteria. XANES analysis verified that all of the Cr present was in the reduced Cr(III) state and offered preliminary structural data indicating that the reduced Cr was associated with Fe hydroxides. Bargar et al. (2000) used in situ XANES to characterize the intermediates and products of Mn(II) oxidation by spores of a marine *Bacillus* sp. in a flow-through reaction cell described by Villinski et al. (1999). After agitating bacterial spores in an anoxic $MnCl_2$ solution for a period of time to allow adsorption of Mn(II) to the bacterial cells, the bacterial suspension was circulated through the reactor at the same time an air-equilibrated Mn(II) solution was introduced and X-ray absorption spectra were measured continuously throughout the subsequent oxida-

tion reaction. Only MnO_2 was detected during the oxidation reaction even though Mn(III)/(II/III) oxides were predicted to be more stable than MnO_2 under these conditions. This approach permits detection of short-lived (>10–60 min) intermediates that occur at abundances >5–10%.

3.12. Extended X-ray absorption fine structure

Extended X-ray absorption fine structure provides information on average short-range order around an element of interest and has been used to characterize interactions between atoms within solution phase metal–organic complexes (Table 1). EXAFS revealed that the U and Fe of a U/Fe/citrate ternary complex are coordinated through carboxylate and hydroxyl groups to the citric acid molecules with chelation of Fe to U occurring through a *m*-citrato bridge (Dodge and Francis, 1997). EXAFS can also be used to identify complexation reactions between metal ions and organic molecules, such as those produced by microorganisms proposed for in situ mobilization and immobilization of radionuclide contaminants in subsurface environments. The reader is referred to a recent review by Charnock (1995) for additional information on the biological applications of EXAFS spectroscopy.

EXAFS is well suited to structural analysis of noncrystalline materials, providing short-range order information in the absence of X-ray diffraction patterns. Using this approach, Suzuki et al. (2001) showed that the local structures around ferric ions in ferric oxyhydroxides are disordered, although the atomic local structures of Fe-O behave as local structural units. Because the reaction products of microbiologically influenced inorganic precipitation reactions at mineral surfaces often have limited crystallinity, EXAFS offers a means of characterizing the nature of these products. Lloyd et al. (2000) employed EXAFS to verify microbiological reduction of technetium (VII) as the pertechnetate ion (TcO_4^-) to Tc(IV) as $TcO_2 \cdot H_2O$. Technetium reduction occurred indirectly via biogenic magnetite formation and directly via a hydrogen-dependent mechanism. EXAFS has also been used in conjunction with XANES to characterize bacterially derived magnetic iron sulfides (Watson et al., 2000). In this study, EXAFS fitting parameters supported XANES data, suggesting that Fe is mainly tetrahedrally coordinated and likely to be in the form of mackinawite.

3.13. Soft X-ray spectromicroscopy

Soft X-ray transmission microscopy allows high-resolution, through-sample observations of reactions in a wet environment at normal pressure. Originally developed for imaging wet biological material, this technique has expanded its applications to industrial chemistry and environmental science. Interactions between X-ray photons and electrons in the sample produce contrast, which can be displayed as a microscopic image. While phase contrast is used to some extent, photoelectric absorption is the primary mechanism for producing contrast. For each element, absorption varies with X-ray photon energy. Contrast depends primarily upon the difference between absorption by the solid and liquid phases in a sample. The spectroscopic capabilities of the soft X-ray microscope compare the image from a more absorbing region of an element of interest with that obtained from a less absorbing "edge" region. The instrument operates optimally (43 nm resolution) when imaging samples of up to 10 mm in thickness but has been used successfully for samples up to 50 mm in thickness. Details of the technique have been published by Meyer-Ilse (1999).

Spectroscopic capabilities in the soft X-ray range (1–50 nm) permit evaluation at specific depths, thus allowing characterization of reaction products at the interface of an oxide film and base metal in a fully hydrated aqueous environment (Kurtis et al., 2000). The corrosion of iron in water has been studied by this technique by sandwiching a mixture of iron filings and polystyrene beads between two silicon nitride windows mounted on a sample carrier. Iron distribution maps were produced by this approach that revealed locations of iron corrosion. Although this technique has potential to yield novel information on mineral–microbe interactions, to our knowledge, it has not yet been applied in this area.

3.14. X-ray photoelectron emission spectromicroscopy (X-PEEM)

X-ray photoelectron emission spectromicroscopy has developed into a tool to investigate magnetic

properties of materials, microchemistry of cells and tissues, bacteria and their metabolic by-products, and elements that are highly localized minerals (Table 1). X-PEEM can achieve lateral resolution of 20 nm while providing information on elemental composition through total yield XANES. Labrenz et al. (2000) used X-PEEM in conjunction with other spectroscopic techniques to identify nanometer-diameter sphalerite (ZnS) particles formed within biofilms of aerotolerant sulfate-reducing bacteria. X-PEEM confirmed the presence of sulfide and sulfate within the cell-associated mineral aggregate. X-PEEM was used successfully to interrogate the valence state of Mn in a 1-mm thick rock (De Stasio et al., 2000; 2001). X-PEEM has also been applied to wet samples confined in a sealed cell that can be installed in a ultrahigh vacuum system.

X-PEEM interrogation of dehydrated samples composed of lighter elements is restricted by sample charging. Gilbert et al. (2001) attempted to overcome the problem of charging in ultrathin samples of biogenic silica in a cyanobacterial mat under ultrahigh vacuum by inducing photoconductivity. In this case, they used near-UV laser illumination in conjunction with Si L-edge X-ray photoelectron emission spectroscopy to investigate Si mineral chemistry. While the electron yield from the Si was elevated by this approach, the image obtained was highly distorted and the internal structures were obscured. Sample charging thus remains a largely unresolved problem for X-PEEM analysis of most biological material.

4. Conclusions

Microbial transformations of minerals can be investigated by a variety of surface spectroscopic techniques. In addition to identifying and mapping the distribution of elements on a surface (EDS and soft X-ray TEM), some surface-sensitive spectroscopic techniques can resolve the oxidation state of an element (XPS, EELS and X-PEEM) and provide information on the identity of neighboring atoms and their orientation (XANES and EXAFS). That some of these techniques can obtain this information from hydrated samples offers the opportunity to characterize biological reactions involving mineral oxidation and reduction and the adsorption and precipitation processes accompanying these redox reactions (X-PEEM, RS, EELS, XANES and EXAFS). These techniques will become increasingly useful for determining the range of biogeochemical transformations in which subsurface microorganisms participate and the conditions under which microorganisms may be exploited to remediate metal-contaminated and radionuclide-contaminated sites in subsurface environments.

Acknowledgements

The authors gratefully acknowledge financial support provided by the Natural and Accelerated Bioremediation Research Program (NABIR), Office of Biological and Environmental Research (grant nos. DE-FG03-98ER62630/A001 and DE-FG03-01ER63270) and Environmental Management Science Program (EMSP) (grant no. FG07-98ER62719), U.S. Department of Energy.

References

Bargar, J.R., Tebo, B.M., Villinski, J.E., 2000. In situ characterization of Mn(II) oxidation by spores of the marine *Bacillus* sp. strain SG-1. Geochim. Cosmochim. Acta 64, 2775–2778.

Barker, W.W., Banfield, J.F., 1998. Zones of chemical and physical interaction at interfaces between microbial communities and minerals: a model. Geomicrobiol. J. 15, 223–244.

Beech, I.B., Zinkevich, V., Tapper, R., Gubner, R., Avci, R., 1999. Study of the interaction of sulfate-reducing bacteria exopolymers with iron using X-ray photoelectron spectroscopy and time-of-flight secondary ionization mass spectrometry. J. Microbiol. Methods 36, 3–10.

Bertsch, P.M., Hunter, D.B., Sutton, S.R., Bajt, S., Rivers, M.L., 1994. In situ chemical speciation of uranium in soils and sediments by micro X-ray absorption spectroscopy. Environ. Sci. Technol. 28, 980–984.

Boughriet, A., Figueiredo, R.S., Laureyns, J., Recourt, P., 1997. Identification of newly generated iron phases in recent anoxic sediments: ^{57}Fe Mössbauer and microRaman spectroscopic studies. J. Chem. Soc., Faraday Trans. 93, 3209–3215.

Brown, D.A., Sherriff, B.L., Sawicki, J.A., 1997. Microbial transformation of magnetite to hematite. Geochim. Cosmochim. Acta 61, 3341–3348.

Brulé, D.G., Brown, J.R., Bancroft, G.M., Fyfe, W.S., 1980. Cation adsorption by hydrous manganese dioxide: a semi-quantitative X-ray photoelectron spectroscopic (ESCA) study. Chem. Geol. 28, 331–339.

Cahill, C.L., Benning, L.G., Barnes, H.L., Parise, J.B., 2000. In situ time resolved X-ray diffraction of iron sulfides during hydrothermal pyrite growth. Chem. Geol. 167, 53–63.

Charnock, J.M., 1995. Biological applications of EXAFS spectroscopy. Radiat. Phys. Chem. 45, 385–391.

Cooney, T.F., Scott, E.R.D., Krot, A.N., Sharma, S.K., Yamaguchi, A., 1999. Vibrational spectroscopic study of minerals in the Martian meteorite ALH84001. Am. Mineral. 84, 1569–1576.

Cornell, R.M., Schwertmann, U., 1996. The Iron Oxides: Structure, Properties, Reactions, Occurrences and Uses. VCH, New York, NY.

Daulton, T.L., Little, B.J., Lowe, K., Jones-Meeham, J., 2001. In situ environmental cell—transmission electron microscopy study of microbial reduction of chromium (VI) using electron energy loss spectroscopy. Microsc. Microanal. 7, 470–485.

De Stasio, G., Gilbert, B., Nelson, T., Hansen, R., Wallace, J., Mercanti, D., Capozi, M., Baudat, P.A., Perfetti, P., Margaritondo, G., Tonner, B.P., 2000. Feasibility tests of transmission X-ray photoelectron emission microscopy (X-PEEM) of wet samples. Rev. Sci. Instrum. 71, 11–14.

De Stasio, G., Gilbert, B., Frazer, B.H., Nealson, K.H., Conrad, P.G., Livi, V., Labrenz, M., Banfield, J.F., 2001. The multidisciplinarity of spectromicroscopy: from geomicrobiology to archaeology. J. Electron Spectrosc. Relat. Phenom. 114–116, 997–1003.

Dodge, C.J., Francis, A.J., 1997. Biotransformation of binary and ternary citric acid complexes of iron and uranium. Environ. Sci. Technol. 37, 3062–3067.

Donald, R., Southam, G., 1999. Low temperature anaerobic bacterial diagenesis of ferrous monosulfide to pyrite. Geochim. Cosmochim. Acta 63, 2019–2023.

Dong, H., Fredrickson, J.K., Kennedy, D.W., Zachara, J.M., Kukkadapu, R.K., Onstott, T.C., 2000. Mineral transformation associated with the microbial reduction of magnetite. Chem. Geol. 169, 299–318.

Durham, P.J., 1988. Theory of XANES. In: Koningsberger, D.C., Prins, R. (Eds.), X-ray Absorption: Principles, Applications, Techniques of EXAFS, SEXAFS and XANES. Wiley, New York, pp. 53–84.

Edwards, K.J., Bond, P.L., Druschel, G.K., McGuire, M.M., Hamers, R.J., Banfield, J.F., 2000. Geochemical and biological aspects of sulfide mineral dissolution: lessons from Iron Mountain, California. Chem. Geol. 169, 383–397.

Egerton, R.F., 1986. Electron Energy-Loss Spectroscopy in the Electron Microscope. Plenum, New York, NY, pp. 1–25.

Francis, A.J., Dodge, C.J., Lu, F., Halada, G.P., Clayton, C.R., 1994. XPS and XANES studies of uranium reduction by *Clostridium* sp. Environ. Sci. Technol. 28, 636–639.

Fredrickson, J.K., Zachara, J.M., Kennedy, D., Duff, M.C., Gorby, Y.A., 2000. Reduction of U(VI) in goethite (α-FeOOH) suspensions by a dissimilatory metal-reducing bacterium. Geochim. Cosmochim. Acta 64, 3085–3098.

Gilbert, B., Margaritondo, G., Douglas, S., Nealson, K.H., Egerton, R.F., Rempfer, G.F., De Stasio, G., 2001. XANES microspectroscopy of biominerals with photoconductive charge compensation. J. Electron Spectrosc. Relat. Phenom. 114–116, 1005–1011.

Gutlick, P., Link, R., Trautwein, A., 1978. Mössbauer Spectroscopy and Transition Metal Chemistry. Springer-Verlag, New York, NY, pp. 238–243.

Henderson, C.M.B., Cressey, G., Redfern, S.A.T., 1995. Geological applications of synchrotron radiation. Radiat. Phys. Chem. 45, 459–481.

Herbert Jr., R.B., Benner, S.G., Pratt, A.R., Blowes, D.W. 1998. Surface chemistry and morphology of poorly crystalline iron sulfides precipitated in media containing sulfate-reducing bacteria. Chem. Geol. 144, 87–97.

Hochella, M.F., 1988. Auger electron and X-ray photoelectron spectroscopies. Rev. Miner. 18, 573–637.

Johansson, L.-S., Saastamoinen, T., 1999. Investigating early stages of biocorrosion with XPS: AISI 304 stainless steel exposed to *Burkholderia* species. Appl. Surf. Sci. 144–145, 244–248.

Kalinowski, B.E., Liermann, L.J., Brantley, S.L., Barnes, A., Pantang, C.G., 2000. X-ray photoelectron evidence for bacteria-enhanced dissolution of hornblende. Geochim. Cosmochim. Acta 64, 1331–1343.

Kasem, K., Lovley, D.R., 2000. Reduction of Fe(III), Mn(IV), and toxic metals at 100 °C by *Pyrobaculum islandicum*. Appl. Environ. Microbiol. 66, 1050–1056.

Kukkadapu, R.K., Zachara, J.M., Smith, S.C., Fredrickson, J.K., Liu, C., 2001. Dissimilatory bacterial reduction of Al-substituted goethite in subsurface sediments. Geochim. Cosmochim. Acta 65, 2913–2924.

Kurtis, K.E., Meyer-Ilse, W., Monteiro, P.J.M., 2000. Soft X-ray spectromicroscopy for in situ study of corrosion. Corros. Sci. 42, 1327–1336.

Labrenz, M., Druschel, G.K., Thomsen-Ebert, T., Gilbert, B., Welch, S.A., Kemner, K.M., Logan, G.A., Summons, R.E., De Stasio, G., Bond, P.L., Lai, B., Kelly, S.D., Banfield, J.F., 2000. Formation of sphalerite (ZnS) deposits in natural biofilms of sulfate-reducing bacteria. Science 290, 1744–1747.

Lloyd, J.R., Yong, P., Macaskie, L.E., 1998. Enzymatic recovery of elemental palladium by using sulfate-reducing bacteria. Appl. Environ. Microbiol. 64, 4607–4609.

Lloyd, J.R., Sole, V.A., Van Praagh, C.V.G., Lovley, D.R., 2000. Direct and Fe(II)-mediated reduction of technetium by Fe(II)-reducing bacteria. Appl. Environ. Microbiol. 66, 3743–3749.

Lloyd, J.R., Mabbett, A.N., Williams, D.R., Macaskie, L.E., 2001. Metal reduction by sulfate-reducing bacteria: physiological diversity and metal specificity. Hydrometallurgy 59, 327–337.

Lovley, D.R., Phillips, E.J.P., 1988. Novel mode of microbial energy metabolism: carbon oxidation coupled to dissimilatory reduction of iron and manganese. Appl. Environ. Microbiol. 54, 472–1480.

McLean, J.S., Beveridge, T.J., 2001. Chromate reduction by a Pseudomonad isolated from a site contaminated with chromated copper arsenate. Appl. Environ. Microbiol. 67, 1076–1084.

McLean, J.S., Beveridge, T.J., Phipps, D., 2000. Isolation and characterization of a chromium-reducing bacterium from a chromated copper arsenate-contaminated site. Environ. Microbiol. 2, 611–619.

Meitzner, G., 1998. Experimental aspects of X-ray absorption spectroscopy. Catal. Today 39, 281–291.

Meyer-Ilse, W., 1999. X-ray microscopy and microanalysis. Encyclopedia of Applied Physics. VCH Publishers, New York, NY, pp. 324–341.

Neal, A.L., Techkarnjanaruk, S., Dohnalkova, A., McCready, D., Peyton, B.M., Geesey, G.G., 2001. Iron sulfides and sulfur spe-

cies produced at hematite surfaces in the presence of sulfate-reducing bacteria. Geochim. Cosmochim. Acta 65, 223–235.

Nelson, Y.M., Waihung, L., Lion, L.W., Shuler, M.L., Ghiorse, W.C., 1995. Lead distribution in a simulated aquatic environment: effects of bacterial biofilms and iron oxide. Water Res. 29, 1934–1944.

Pasteris, J.D., Freeman, J.J., Goffredi, S.K., Buck, K.R., 2001. Raman spectroscopic and laser scanning confocal microscopic analysis of sulfur in living sulfur-precipitating marine bacteria. Chem. Geol. 180, 2–18.

Posfai, M., Buseck, P.R., Bazylinski, D.A., Frankel, R.B., 1998. Iron sulfides from magnetotactic bacteria: structures, composition, and phase transition. Am. Mineral. 83, 1469–1481.

Roden, E.E., Zachara, J.M., 1996. Microbial reduction of crystalline Fe(III) oxides: role of oxide surface area and potential for cell growth. Environ. Sci. Technol. 30, 1618–1628.

Roden, E.E., Urrutia, M.M., Mann, C.J., 2000. Bacterial reductive dissolution of crystalline Fe(III) oxide in continuous-flow column reactors. Appl. Environ. Microbiol. 66, 1062–1065.

Rouxhet, P.G., Genet, M.J., 1991. Chemical composition of the microbial cell surface by X-ray photoelectron spectroscopy. Microbial Cell Surface Analysis. VCH, New York, NY, pp. 173–220.

Singer, P.C., Stumm, W., 1968. Kinetics of the oxidation of ferrous iron. Bitumenous Coal Research. Proceedings of the 2nd Symposium on Coal Mine Drainage Research. National Coal Association, Pittsburgh, PA, pp. 12–34.

Stookey, L.L., 1970. Ferrozine—a new spectrophotometric reagent for iron. Anal. Chem. 42, 779–781.

Storrie-Lombardi, M.C., Hug, W.F., McDonald, G.D., Tsapin, A.I., Nealson, K.H., 2001. Hollow cathode ion lasers for deep ultraviolet Raman spectroscopy and fluorescence imaging. Rev. Sci. Instrum. 72, 4452–4459.

Suci, P.A., Geesey, G.G., Tyler, B.J., 2001. Integration of Raman microscopy, differential interference contrast microscopy, and attenuated total reflection Fourier transform infrared spectroscopy to investigate chlorhexidine spatial and temporal distribution in *Candida albicans* biofilms. J. Microbiol. Methods 46, 193–208.

Suzuki, S., Suzuki, T., Kimura, M., Takagi, Y., Shinoda, K., Tohji, K., Waseda, Y., 2001. EXAFS characterization of ferric oxyhydroxides. Appl. Surf. Sci. 169–170, 109–112.

van der Mei, H.C., de Vries, J., Busscher, H.J., 2000. X-ray photoelectron spectroscopy for the study of microbial cell surfaces. Surf. Sci. Rep. 39, 1–24.

Villinski, J.E., O'Day, P.A., Corley, T.L., Conklin, M.H., 1999. A flow-through cell for in situ, real time X-ray absorption spectroscopy studies of geochemical reactions. In: D.W. Morganwalp, H.T. Buxton (Eds.), U.S. Geological Survey Toxic Substance Hydrology Program, Proceedings of the Technical Meeting, Charleston, SC, March 8–12, 1999. Vol. 1, Contamination from Hard Rock Mining. U.S. Geological Survey Water-Resources Investigations Report 99-4018, pp. 217–225.

Viollier, E., Inglett, P.W., Hunter, K., Roychoudhury, A.N., van Capellan, P., 2000. The ferrozine method revisited: Fe(II)/Fe(III) determination in natural waters. Appl. Geochem. 15, 785–790.

Warbichler, P., Hofer, F., Hofer, P., Letofsky, E., 1998. On the application of energy-filtering TEM in materials science: III. Precipitates in steel. Micron 29 (1), 63–72.

Watson, J.H.P., Cressey, B.A., Roberts, A.P., Ellwood, D.C., Charnock, J.M., Soper, A.K., 2000. Structural and magnetic studies on heavy-metal-adsorbing iron sulfide nanoparticles produced by sulfate-reducing bacteria. J. Magn. Magn. Mater. 214, 13–30.

Wielinga, B., Mizuba, M.M., Hansel, C.M., Fendorf, S., 2001. Iron promoted reduction of chromate by dissimilatory iron-reducing bacteria. Environ. Sci. Technol. 35, 522–527.

Wu, Q., Hamilton, T., Nelson, W.H., Elliott, S., Sperry, J.F., Wu, M., 2001. UV Raman spectral intensities of *E. coli* and other bacteria excited at 228.9, 244.0, and 248.2 nm. Anal. Chem. 73, 3432–3440.

Geomicrobiology Journal, 19:179–207, 2002
Copyright © 2002 Taylor & Francis
0149-0451/02 $12.00 + .00

Biomineralization of Poorly Crystalline Fe(III) Oxides by Dissimilatory Metal Reducing Bacteria (DMRB)

JOHN M. ZACHARA
RAVI K. KUKKADAPU
JAMES K. FREDRICKSON
YURI A. GORBY
STEVEN C. SMITH

Pacific Northwest National Laboratory
Richland, Washington, USA

*Dissimilatory metal reducing bacteria (DMRB) catalyze the reduction of Fe(III) to Fe(II) in anoxic soils, sediments, and groundwater. Two-line ferrihydrite is a bioavailable Fe(III) oxide form that is exploited by DMRB as a terminal electron acceptor. A wide variety of biomineralization products result from the interaction of DMRB with 2-line ferrihydrite. Here we describe the state of knowledge on the biotransformation of synthetic 2-line ferrihydrite by laboratory cultures of DMRB using select published data and new experimental results. A facultative DMRB is emphasized (*Shewanella putrefaciens*) upon which most of this work has been performed. Key factors controlling the identity of the secondary mineral suite are evaluated including medium composition, electron donor and acceptor concentrations, ferrihydrite aging/recrystallization status, sorbed ions, and co-associated crystalline Fe(III) oxides. It is shown that crystalline ferric (goethite, hematite, lepidocrocite), ferrous (siderite, vivianite), and mixed valence (magnetite, green rust) iron solids are formed in anoxic, circumneutral DMRB incubations. Some products are well rationalized based on thermodynamic considerations, but others appear to result from kinetic pathways driven by ions that inhibit interfacial electron transfer or the precipitation of select phases. The primary factor controlling the nature of the secondary mineral suite appears to be the Fe(II) supply rate and magnitude, and its surface reaction with the residual oxide and other sorbed ions. The common observation of end-product mineral mixtures that are not at global equilibrium indicates that microenvironments surrounding respiring DMRB cells or the reaction-path trajectory (over Eh-pH space) may influence the identity of the final biomineralization suite.*

Keywords biogenic Fe(II), biomineralization, crystalline Fe(III) oxides, dissimilatory iron reduction, ferrihydrite, ferrous iron minerals, Mössbauer spectroscopy

Received 19 December 2000; accepted 16 November 2001.

Research was supported by the Office of Basic Energy Sciences (OBES)—Geosciences Program, U.S. Department of Energy (DOE). Pacific Northwest National Laboratory is operated for the DOE by Battelle Memorial Institute under Contract DE-AC06-76RLO 1830.

This work was supported by the U.S. Department of Energy, Office of Basic Energy Sciences, Engineering and Geosciences Division. The research was performed at the W.R. Wiley Environmental Molecular Sciences Laboratory, a national scientific user facility sponsored by the U.S. Department of Energy's Office of Biological and Environmental Research located at Pacific Northwest National Laboratory. It is operated for the U.S. Department of Energy by Battelle Memorial Institute under Contract DE-AC06-76RL01830.

Address correspondence to John M. Zachara, Pacific Northwest National Laboratory, P.O. Box 999, Mail Stop K8-96, Richland, WA 99352, USA. E-mail: john.zachara@pnl.gov

Poorly crystalline Fe(III) oxides are common secondary weathering products found in soils, unsaturated and saturated subsurface materials, aquatic sediments, and geologic materials. One common form of poorly crystalline Fe(III) oxide is ferrihydrite (Childs 1992), the subject of this paper. Ferrihydrites are typically finely divided, exhibit high surface area, and often exist as particle coatings on rock fragments that have served as Fe-sources in soils and subsurface sediments, as suspended material in groundwater, and as water-column precipitates near oxic-anoxic interfaces in natural waters (Whittmore and Langmuir 1975; Schwertmann et al. 1982; Fortin et al. 1993). They precipitate readily, form abiotically or biotically by Fe(II) oxidation and Fe(III) hydrolysis (Cornell and Schwertmann 1996), and are often associated with biologic materials and organic matter in natural waters (Fortin et al. 1993; Perret et al. 2000). Ferrihydrite functions as a sorbent and repository for both contaminants and nutrients, acts as redox and proton buffering phase in soil and sediment porewaters and groundwaters, and is a precursor for the formation of the common crystalline Fe(III) oxides (goethite, hematite).

Ferrihydrite is especially important as an electron acceptor in soils, sediments, and aquifers because it is more bioavailable to dissimilatory metal reducing bacteria (DMRB) then crystalline ones (Lovley et al. 1991; Lovley and Phillips 1986; Phillips et al. 1993). The bioavailable Fe(III) fraction in sediments qualitatively correlates with ammonium oxalate extractable Fe(III) (Fe_o) (Lovley and Phillips 1987). Mineralogic analyses (X-ray diffraction, Mössbauer spectroscopy) indicate that Fe_o, in turn, approximates the ferrihydrite content of a soil or sediment (Campbell and Schwertmann 1984, 1985; Cornell and Schwertmann 1996). Both specimen and natural crystalline Fe(III) oxides are bioreducible by DMRB to a certain degree (Lovley et al. 1991; Roden and Zachara 1996; Zachara et al. 1998; Kukkadapu et al. 2001), and their extent of reduction appears related to surface area (Roden and Zachara 1996), thermodynamic factors (Postma and Jakobsen 1996; Liu et al. 2001a), degree of structural disorder (Zachara et al. 1998), and extent of surface passivation by sorbed Fe(II) (Roden and Zachara 1996). In batch suspensions with DMRB, ferrihydrite is often fully reduced or transformed to secondary ferrous containing mineral solids (e.g., Fredrickson et al. 1998; Fredrickson et al. 2001) whereas goethite and hematite are only partially reduced (Zachara et al. 1998). Water advection enhances the extent of crystalline Fe(III) oxide reduction (Roden and Urrutia 1999; Roden et al. 2000), perhaps through relaxation of thermodynamic constraints or surface passivation. Results to date indicate that poorly crystalline Fe(III) oxides support greater amounts of electron donor oxidation by DMRB than crystalline ones, all other factors held constant.

DMRB solubilize poorly crystalline Fe(III) oxides as $Fe^{2+}_{(aq)}$ or transform them to ferrous containing solid phases during bioreduction. Reported secondary products of ferrihydrite bioreduction include: siderite ($FeCO_3$; Mortimer and Coleman 1997; Fredrickson et al. 1998), magnetite (Fe_3O_4; Lovley 1991; Mortimer and Coleman 1997; Mortimer et al. 1997), vivianite [$Fe_3(PO_4)_2 \cdot 8H_2O$] (Fredrickson et al. 1998), and green rust {$[Fe^{II}_{(6-x)} Fe^{III}_{(x)}(OH)_{12}]^{x+}[(A^{2-})_{x/2} \cdot yH_2O]^{x-}$} (Fredrickson et al. 1998; Parmar et al. 2001). The biomineralization products are important in that they influence the overall thermodynamics of the bioreduction reaction, and consequently its extent (Zachara et al. 1998). Also, biomineralization is integral to the rate and kinetics of the overall bioreduction process. The secondary products may assist bioreduction by removing or lowering the thermodynamic activity of reaction byproducts [e.g., Fe(II)], or may retard bioreduction by coating or passivating the residual Fe(III) oxide or DMRB surface (Liu et al. 2001a, 2001b). Biomineralization products may also sequester trace elements associated with the original oxide by coprecipitation or surface complexation (Zachara et al. 2001).

Here we address the biotransformation of ferrihydrite by DMRB with emphasis on secondary mineral formation. A synthetic, 2-line ferrihydrite is used as a qualitative surrogate

of an important component of the bioavailable iron oxide fraction in soils, sediments, and geologic material. This material is used in unreacted state, and after coreaction with a number of anionic and cationic solutes to produce ferrihydrites of greater environmental relevance. We begin with a review on the nature of ferrihydrite, and its thermodynamic relationships to other Fe-solids that represent potential transformation products. Experimental information is then provided on the identity of biomineralization products resulting from the action of DMRB on 2-line ferrihydrite. Chemical and biologic factors are evaluated that appear to control the biomineralization process. It is shown that a complex array of both ferric and ferrous iron phases are formed when DMRB utilize 2-line ferrihydrite as a terminal electron acceptor, and that the primary controlling factor is the respiration-driven biogenic Fe(II) supply rate. Although many of the products may be well rationalized based on thermodynamic considerations, others appear to result from kinetic pathways with unique biotic signature. The level of scientific understanding is found to be insufficient to allow prediction of the final phase assemblage, and key areas are identified where research is needed.

Background

The Nature of Ferrihydrite

As noted in the introduction, acid ammonium oxalate (AAO) extractable Fe (Fe_o) qualitatively correlates with the bioavailable Fe(III) fraction, and the ferrihydrite content of a soil or sediment. Natural Fe(III) oxides span a wide range of crystallinity, structure, size, and solubility. Whereas AAO preferentially dissolves ferrihydrite over goethite and hematite (Schwertmann et al. 1982; Campbell and Schwertmann 1985), the dissolution kinetics of a particular Fe(III) oxide in AAO is strongly dependent on these properties and consequently extraction time is a key variable in controlling the phase specificity and extent of extraction. Wang et al. (1993), for example, observed that ferrihydrite was extracted by AAO within 30 min, while longer extraction times (e.g., 50–180 min) dissolved lepidocrocite of progressively increasing size. More crystalline or Si-containing ferrihydrite may require greater than 120 min of extraction for complete removal (Schwertmann 1973). Magnetite and small particle goethite may also dissolve to certain degree in AAO. Consequently, the AAO technique as typically applied with a 2-h extraction time (Lovley and Phillips 1987) is not a quantitative or uniquely selective extractant of ferrihydrite or any other Fe(III) oxide phase for that matter.

Ferrihydrites exhibit a continuum in structure from amorphous to partly crystalline. The term hydrous ferric oxide (HFO, e.g., Dzombak and Morel 1990) is applied to a material synthesized in the laboratory by rapid hydrolysis of a Fe(III) salt solution, with approximately 4- to 8-h aging at pH 7. This material may be amorphous (protoferrihydrite) or exhibit two broad X-ray diffraction (XRD) maxima (2-line ferrihydrite). HFO and 2-line ferrihydrite are often used synonymously (Cornell and Schwertmann 1996). A more crystalline variety (6-line ferrihydrite) is prepared by heat-induced hydrolysis (Cornell and Schwertmann 1991). These 2- and 6-line ferrihydrites represent end members to a continuum that span a range in X-ray diffraction patterns and physical characteristics that result from differences in synthesis conditions. As noted by Childs (1992), the XRD peaks of ferrihydrite are broad and weak and the number of resolvable diffraction lines depends on sample preparation, the diffraction instrument and its operation conditions, and interpretation. The 2- and 6-line ferrihydrites precipitate under different conditions and the 2-line variety apparently does not transform to the 6-line variety with time (Cornell and Schwertmann 1996).

The molecular structure of ferrihydrite has been investigated by various techniques including XRD, Mössbauer spectroscopy, and X-ray scattering/X-ray absorption (Pankhurst

and Pollard 1992; Stanjek and Weidler 1992; Manceau and Drits 1993), without great consensus (see review by Cornell and Schwertmann 1996). Six-line ferrihydrite is believed to exhibit a defective hematite structure with significant Fe(III) vacancies and considerable sorbed water (Towe and Bradley 1967; Chukhrov et al. 1973; Russell et al. 1979). Two-line ferrihydrite is more disordered and is thought to consist of coherent domains of four planar $Fe(O,OH)_6$ groups (Feitknecht et al. 1973). The high degree of disorder and large water content leads to a variable stoichiometric composition for ferrihydrite that has proved difficult to characterize. Stanjek and Weidler (1992), for example, proposed a bulk formula of $Fe_{1.55}O_{1.66}(OH)_{1.33}$.

Thermodynamic Stability and Phase Transformations Under Oxidizing Conditions

Under oxidizing conditions, ferrihydrites are thermodynamically unstable with respect to crystalline Fe(III) oxides including maghemite (γ-Fe_2O_3), lepidocrocite (γ-FeOOH), hematite (α-Fe_2O_3), and goethite (α-FeOOH) (Figure 1). Ferrihydrite is described in Figure 1 as $Fe(OH)_3$ for ease of computation. Other, more complex stoichiometric formula have been proposed including $Fe(OH)_{2.35}$ from solubility studies (Fox 1988, 1988a) and $Fe_2O_3 \cdot 2FeOOH \cdot 2.6H_2O$ from infrared spectroscopy (Russell 1979). These different stoichiometric representations of ferrihydrite do not change the fact that this phase is less stable than the crystalline Fe(III) oxides. Factors controlling the rate and extent of ferrihydrite conversion to crystalline Fe(III) oxides have been extensively studied in the laboratory (see review by Cornell and Schwertmann 1996) and involve pH, foreign inorganic and organic ions, temperature, and others. Both 2- and 6-line ferrihydrites begin crystallization toward goethite (primarily) and hematite in laboratory suspensions at room temperature over periods of weeks to months. Such crystallization is accompanied by changes in internal structure and water content, morphology and particle size, surface area, concentrations of undercoordinated surface sites, and thermodynamic properties such as solubility (Schindler et al. 1963). These changes that accompany aging and crystallization are likely to influence the bioreducibility of the poorly crystalline Fe(III) oxide and the nature and identity of secondary mineral products.

Coprecipitated silica, organic material, and trace metal cations retard the crystallization of ferrihydrites to goethite and hematite in laboratory suspensions (Cornell and Schwertmann 1996). These constituents bind strongly to hydroxylated Fe(III) centers and inhibit crystallization by functioning as chemical defects that block the formation of continuous arrays of Fe and O atom centers. Silica and organic material are believed to play a central role in the stabilization of ferrihydrite in soil (Carlson and Schwertmann 1981; Childs 1992). Natural ferrihydrites from both soil and lake environments invariably contain Si (up to 9 mol%) and significant organic material (Fortin et al. 1993; Tessier et al. 1996; Perret et al. 2000). Ferrihydrite is most commonly reported in volcanic ash, podzolic, and hydromorphic soils; soils or sediments containing soluble organic materials and silicate; relatively young, water-containing geologic deposits such as Holocene tills; hydrogeologic environments where ferrigenous groundwaters may be oxidized; and as a water column precipitates in seasonably anoxic lakes. Longer weathering periods and higher temperatures promote organic matter oxidation and transformation of ferrihydrite to lepidocrocite, hematite, and/or goethite.

Thermodynamic Stability Under Reducing Conditions

With decreasing oxidation potential, ferrihydrites become thermodynamically unstable with respect to various ferrous containing solid phases. Magnetite (Fe_3O_4) and siderite ($FeCO_3$) are the most stable ferrous containing mineral solids. The actual phase formed is dependent

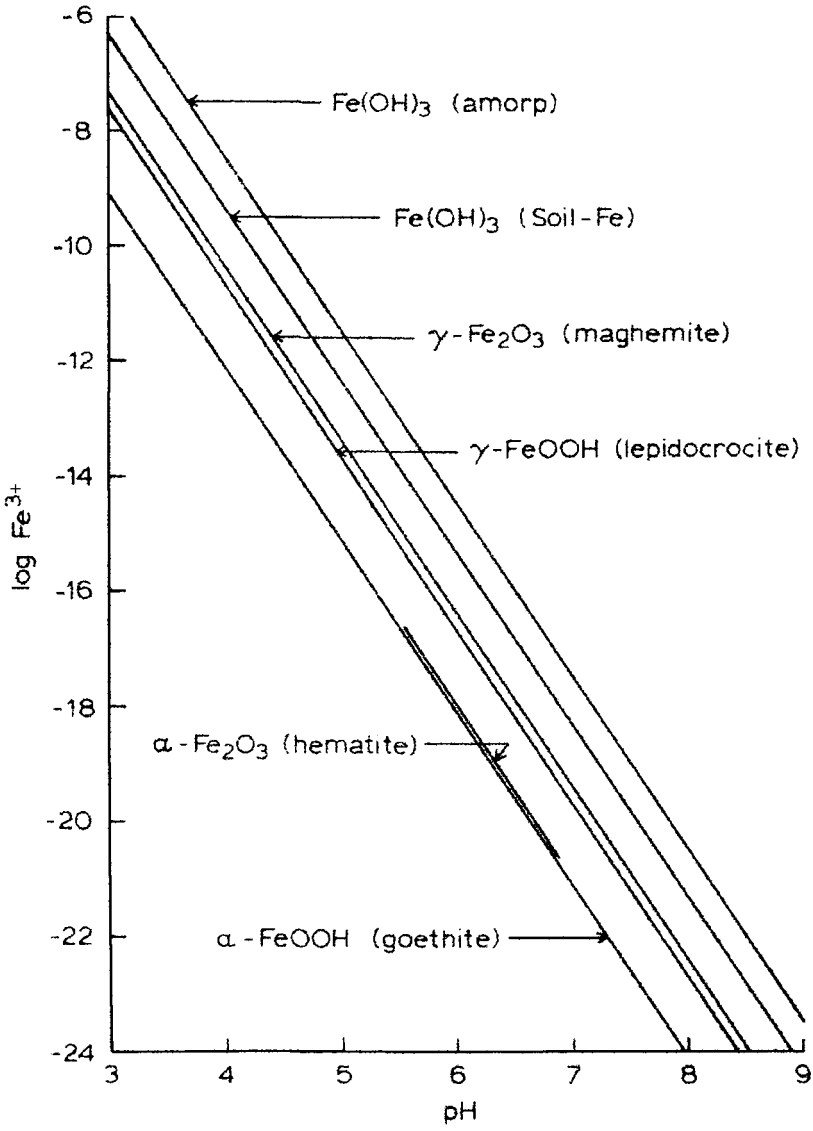

FIGURE 1 Thermodynamic stability of Fe(III) oxides under oxidizing conditions expressed as solubility. The most stable phase is that which supports the lowest Fe^{3+} activity (e.g., goethite given the used thermodynamic data). From Lindsay (1979). Ferrihydrite is approximated with the stoichiometric formula of $Fe(OH)_3$.

on pH, redox potential (pe or Eh), and carbonate concentration or CO_2 partial pressure. These relationships can be conveyed through a stability diagram (Figure 2), of which there are many variants (see, for example, Garrels and Christ 1965; Lindsay 1979; Génin et al. 1998a, 1998b). As shown in Figure 2, a decreasing redox potential at circumneutral pH with 1 mmol/L of HCO_3^- favors the thermodynamic transformation of ferrihydrite first to magnetite and then to siderite at lower Eh ($\approx -.125$ V). High pH tends to favor the formation of Fe_3O_4, whereas lower pH and increasing carbonate favor $FeCO_3$.

Green rusts are mixed valence [Fe(II)/Fe(III)] layered hydroxides that exhibit a pyroaurite structure. In the laboratory they are synthesized by air oxidation of ferrous hydroxide

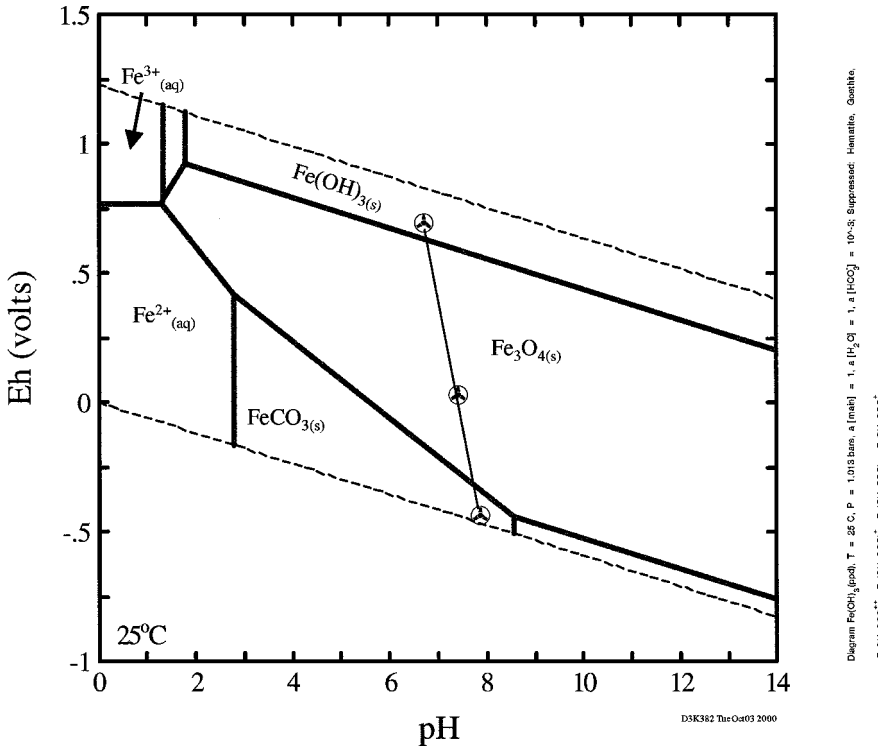

FIGURE 2 Thermodynamic stability of ferrihydrite [stoichiometry assumed as $Fe(OH)_3$] with respect to magnetite (Fe_3O_4) and siderite ($FeCO_3$) as a function of redox potential (Eh) and pH. HCO_3^{3-} was fixed at 10^{-3} mol/L. A reaction path for the bioreduction of 2-line ferrihydrite at circumneutral pH is noted that leads to magnetite and siderite formation. Note that the stability field of Fe_3O_4 is much reduced if goethite and hematite are considered stable phases rather than $Fe(OH)_3$.

precipitates (Vins et al. 1987; Drissi et al. 1995; Génin et al. 1998a) and by other procedures including reaction of $Fe^{2+}_{(aq)}$ with ferrihydrite (Hansen and Poulsen 1999). Green rusts are reduced precursors to lepidocrocite (γ-FeOOH, Schwertmann and Fechter 1994). Green rusts are reported as microbially induced corrosion products of steel and as reduced Fe-phases in hydromorphic soils (Génin et al. 1998b). They have also been reported as biomineralization products of ferrihydrite (Fredrickson et al. 1998; Parmar et al. 2001) and lepidocrocite. Just as ferrihydrite is a metastable phase to both goethite and hematite, green rusts are metastable to magnetite and siderite (Génin et al. 1998b) and, consequently, do not exhibit a stability region in Figure 2. However, their identification in hydromorphic soils (Trolard et al. 1997; Génin et al. 1998b) indicates temporal periods of environmental stability (or persistent metastability). The reader is directed to Génin et al. (1998a, 1998b) for stability diagrams of green rust in relation to goethite, lepidocrocite, and ferrous iron phases.

Experimental Methods and Procedures

Ferrihydrite (2-line) was prepared by precipitation with alkali (Cornell and Schwertmann 1991) to pH 7-8 using either ferric nitrate or ferric chloride. Ferrihydrites coprecipitated

with Ni or Co

$$\left[X_{Me} = \left(\frac{Me}{Me + Fe}\right) = 0.05\right]$$

where Me = Ni(II) or Co(II) were prepared in a similar manner from acidic salt solutions containing 5 mol% Ni(II) or Co(II). The solids were washed with either 0.1 mol/L $NaClO_4$ or deionized water to remove nitrate or chloride.

Anoxic suspensions of *Shewanella putrefaciens* strain CN32 (Dr. David Boone, Subsurface Microbial Culture Collection, Portland State University) were prepared as described by Fredrickson et al. (1998). The bacterial cells were harvested at late log growth phase (16 h growth) and washed three times in the desired pH buffer solution. Following the third wash, cells were re-suspended in the appropriate buffer at pH 6.8. Anoxic gas (N_2) was sparged through the cell suspension for approximately 15 min prior to inoculation of the ferrihydrite suspensions. The target concentration of CN32 was 2×10^8 cfu/mL in suspension with ferrihydrite, unless otherwise noted.

Several variations of growth media and headspace atmosphere were used depending on experimental objectives (Table 1). After combining the components, the pH was adjusted to 6.8 using NaOH and filter sterilized with a 0.2 μm syringe filtration system. Growth media was added to the ferrihydrite suspensions the same day as the CN32 cells.

TABLE 1 Media compositions for bioreduction experiments

	Concentration (mmol/L)			
Component	Media 1	Media 2	Media 3	Media 4
KCl	1.34	1.34	1.34	1.34
NH_4Cl	28	28	28	28
$CaCl_2$	0.68	0.68	0.68	0.68
$NaClO_4$	50	—	—	—
NaH_2PO_4	—	0.4	—	—
Trace minerals	—	Yes[a]	—	—
e^- donor	Lactic acid; 30	Lactic acid; 0.5 Lactic acid; 30	H_2 H_2	H_2 H_2
MES[b]	—	—	50	50
$NaHCO_3$	—	30	—	30
PIPES[c]	30	—	—	—
Me-HFO	50	50 150	20	20
Incubation temperature	30°C	~23°C	30°C	30°C
Headspace	N_2	N_2:CO_2 80:20	N_2 N_2:CO_2 99:1 N_2:CO_2 98:2 N_2:CO_2 95:5 N_2:CO_2 90:10 N_2:CO_2 80:20	N_2 N_2:CO_2 90:1 N_2:CO_2 98:2 N_2:CO_2 95:5 N_2:CO_2 90:10 N_2:CO_2 80:20

[a] See Fredrickson et al. (1998) Table 1 for a listing of trace minerals and their concentrations.
[b] [2-(*N*-morpholino)ethanesulfonic acid].
[c] [*N*-(2-hydroxyethyl)piperazine-N′-(2-ethanesulfonic acid)].

Variable Electron Donor (Lactate): Electron Acceptor [Fe(III)] Ratio

Three combinations of donor/acceptor were used: 0.5/150, 0.5/50, and 30/50 mmol/L lactate/ferrihydrite, respectively (Media 2 in Table 1). The ferrihydrite used in this experiment had been stored for 3 d since precipitation and the suspension was washed with deionized water prior to initiation of bioreduction. Incubation was performed in 60-mL serum bottles containing 50 mL of suspension at room temperature (~23°C) for approximately 20 d. The mineral residue at experiment termination was analyzed by XRD and Mössbauer spectroscopy after drying under anoxic conditions.

Influence of Variable pCO_2

Serum bottles (160 mL) containing 50 mL of 20 mmol/L ferrihydrite suspension in either MES [2-(*N*-morpholino)ethanesulfonic acid] or bicarbonate buffer (Table 1, Media 3 and 4, respectively) were purged with oxygen-free N_2 or mixtures of N_2:CO_2 (Table 1, Media 3 and 4) for 15 min prior to inoculation. The serum bottles were sealed with thick butyl rubber stoppers and aluminum crimp seals. Washed cells of CN32 were added through the stoppers to a final concentration of 7.5×10^7 cfu/mL. Hydrogen gas (40 cm^3) was added to the serum bottles to provide an electron donor. The suspensions were incubated at 30°C and 50 rpm. After Fe(III) reduction ceased (5 d), concentrations of Fe(II) in the aqueous phase and weak acid (0.5 mol/L HCl) extract were determined as described by Fredrickson et al. (1998). The suspension pH was determined under an anoxic atmosphere using a glass combination pH microelectrode (Microelectrodes, Inc., Bedford, NH). The mineral residue was dried under anoxic conditions and analyzed by XRD.

Influence of Aging and Metal Coprecipitation

Ferrihydrite and ferrihydrite coprecipitated with 5% Ni(II) or Co(II) was aged for 7 months at room temperature in pH 7.0, 0.25 mol/L $NaNO_3$. The aged materials were washed extensively to remove NO_3 and were then inoculated with CN32 in Media 1 (Table 1) to evaluate the comparable reducibility of the aged to the unaged materials. Ten mL of suspension in a 20-mL headspace vial were incubated with CN32 (10^8 cfu/mL) at 30°C for 33 d. The bioreduced suspensions were handled under an anoxic atmosphere in an environmental chamber. Approximately 6.8 mL of a composite sample from five replications were filtered, washed, and dried under anoxic conditions in preparation for Mössbauer and XRD analysis.

Mixtures of Fe(III) Oxides

A portion of freshly precipitated 2-line ferrihydrite suspension was heated at 70°C for 16 d (Ford et al. 1997) to produce a ferric oxide mixture containing 18% ferrihydrite, 42% goethite, and 40% hematite as determined by spectral area analysis of the Mössbauer pattern. Ten mL of suspension in a 20 mL headspace vial was incubated with CN32 at 30°C for 33 d in Media 1 (Table 1). The bioreduced mineral residue was prepared for Mössbauer and XRD analysis as described previously.

Mössbauer Analyses

Subsamples of the unreduced and bioreduced ferrihydrites were analyzed using ^{57}Fe Mössbauer spectroscopy. The bioreduced mineral residues were filtered; washed with deoxygenated, deionized H_2O and then acetone; and then dried under anoxic conditions. The dried powders (unreduced and bioreduced) were mixed with petroleum jelly, sealed with tape or Arlon polymer, and left in the anoxic chamber until analysis. Spectra were collected

at variable temperatures using ~50 mCi (1.85 MBq) ^{57}Co/Rh single-line thin sources. The Mössbauer bench (MB-500; WissEL, Germany) was equipped with a dual Mössbauer drive system to gather data simultaneously for two experiments. The velocity transducer (MVT-1000; WissEL) was operated in the constant-acceleration mode (23 Hz, ± 10 mm/sec). Data were acquired on 1,024 channels and then folded to 512 channels to give a flat background and a zero-velocity position corresponding to the center shift (CS or δ) of a metallic-Fe foil at room temperature. Calibration spectra were obtained with a 20 μm thick α-Fe foil (Amersham, England) placed in exactly the same position as the samples to minimize any geometry error. The transmitted radiations were recorded with the Ar-Kr proportional counters. The unfolded spectra were folded and evaluated with the Recoil program (University of Ottawa, Canada) using the Voigt-based hyperfine parameter distribution method (Rancourt and Ping 1991). The intensity ratio of the h_1/h_3 and h_2/h_3 lines of the sextet were fixed at 3 and 2, respectively.

Results and Discussion

A number of factors have been observed to influence the secondary mineral suite resulting from the bioreduction of ferrihydrite including: aqueous chemistry, electron donor and acceptor concentrations, extent of ferrihydrite aging, adsorbed or coprecipitated ions, and co-associated crystalline Fe(III) oxides. Here, we show the influence of these factors on the identity and morphology of biomineralization products formed. DMRB function primarily at circumneutral pH range and our evaluation was performed in the pH range of 6–8. Through this assessment we identified the primary geochemical and microbiologic controls on biomineralization.

Laboratory Models

Biotransformations of ferrihydrite have been commonly studied at circumneutral pH in media buffered with either PIPES (1,4-piperazinediethanesulfonic acid) or bicarbonate buffer to maintain constant hydrogen ion activity. Other buffers such as MES [2-(4-morpholine)ethane sulfonic acid] are used less frequently to access lower pH. The bioreduction reactions approximated below with hydrogen or lactate as the electron donor consume protons and elevate the suspension pH with time, especially when initial Fe(III) concentrations are high and bioreduction is extensive. Again, we use the most simplistic representation of ferrihydrite stoichiometry for ease of reaction balancing.

$$\mathrm{Fe(OH)_{3(s)}} + 1/2\mathrm{H_2} + 2\mathrm{H^+} = \mathrm{Fe^{2+}} + 3\mathrm{H_2O} \tag{1}$$

$$\begin{aligned}\mathrm{Fe(OH)_{3(s)}} &+ 1/4\mathrm{CH_3CHOHCOO^-} + 7/4\mathrm{H^+} \\ &= \mathrm{Fe^{2+}} + 1/4\mathrm{CH_3COO^-} + 1/4\mathrm{HCO_3^-} + 10/4\mathrm{H_2O}\end{aligned} \tag{2}$$

Increasing pH promotes the formation of oxide, hydroxide, carbonate, and phosphate mineral phases that are observed as biomineralization products. The composition of media used for bioreduction studies vary (see, for example, Kostka and Nealson 1995; Fredrickson et al. 1998; Zachara et al. 2001), and may include trace metals (with SO_4^{2-} as the charge compensating anion), vitamins, N (NH_4Cl, ≈1.0 mmol/L), P (PO_4^{3-} at 0.4–4.0 mmol/L), and K (KCl, ≈1.0 mmol/L) depending on whether the media is intended to support growth or not. Media preparations containing trace metals and vitamins typically contain in excess of 1.0 mmol/L SO_4^{2-}. Although SO_4^{2-} does not generally function as an electron acceptor for DMRB, it may enhance the formation of green rust.

To date, the bioreduction of poorly crystalline Fe(III) oxide has been studied primarily with 2-line ferrihydrite as the electron acceptor. The preferred synthesis method has been by hydrolysis of acid ferric salt solutions. Although natural ferrihydrites often form by oxidation of ferrous containing waters (Childs 1992), this synthesis route has not often been applied for specimen ferrihydrite because of the potential for joint lepidocrocite precipitation. When facultative DMRB are to be studied, many investigators avoid the use of $Fe(NO_3)_3$ salts for hydrolytic 2-line ferrihydrite synthesis, in favor of $FeCl_3 \cdot nH_2O$, to avoid potential NO_3^- carryover from the solids that could provide facultative DMRB with an alternative electron acceptor. The chloride ion, however, promotes akaganeite (β-FeOOH) formation below pH 5 (Schwertmann and Cornell 1991), and the resulting solid must be analyzed carefully to confirm the presence of the desired Fe(III) oxide. However, little attention has generally been paid to documenting the true mineralogic nature of the starting material which may vary with aging time and other vagaries of the synthesis process including base addition rate, pH, temperature, electrolyte ion, and so forth.

Aqueous Chemistry

The solution and media conditions exert a strong effect on the nature of ferrous-containing biomineralization products formed from 2-line ferrihydrite (Table 2). As discussed later, the electron donor to acceptor ratio is also important, and all studies discussed in this section utilized 30 mmol/L to 50 mmol/L ferrihydrite as the electron acceptor and excess electron donor in the form of lactate or $H_{2(g)}$.

Bicarbonate buffer promotes siderite formation ($FeCO_3$) through mass action effects [e.g., $Fe^{2+} + HCO_3^- = FeCO_{3(s)} + H^+$] (Table 2). Abiotic studies indicate that siderite precipitation is 98% complete in 4 h when mmol/L solutions of Fe^{2+} and bicarbonate are mixed at pH 7.2 (Thornber and Nickel 1976). This precipitation rate is comparable to, or possibly faster than, the biotic reduction rate (Liu et al. 2001a). It was not uncommon in the studies of Fredrickson et al. (1998) to observe complete conversion of poorly crystalline Fe(III) to siderite. Biogenic siderite is observed as rhombohedral crystallites ranging in size from 0.5 to 2.0 μm (Figure 3a).

Fine-grained magnetite is a most common product of the bioreduction of ferrihydrite by DMRB (Lovley et al. 1987; Mortimer and Coleman 1997; Fredrickson et al. 1998). Magnetite exhibits a large stability field relative to 2-line ferrihydrite as the redox potential

TABLE 2 Secondary solid phases resulting from the bioreduction of 2-line ferrihydrite by *S. putrefaciens*, strain CN32 from Fredrickson et al. (1998)

Buffer	HCO_3[a]	HCO_3[a]	PIPES[a]	PIPES[a]
Final pH[b]	7.4	7.1	7.8	7.1
PO_4^{3-}[c]	4.0×10^{-3}	0	4.0×10^{-3}	0
% of total Fe(II) reduced[d]	62%	33%	28%	11%
Secondary mineral phases[e]	Siderite, vivianite	Siderite, magnetite[f]	Poorly crystalline[g]	Magnetite

[a] Buffer concentration was 30 mmol/L.
[b] After 20 d incubation.
[c] Final concentration was at least 10× less in both treatments.
[d] After 20 d incubation.
[e] By XRD.
[f] Magnetite is a minor component.
[g] Greenish-blue color consistent with green rusts.

a. Siderite ($FeCO_3$)

1 μm

b. Magnetite (Fe_3O_4)

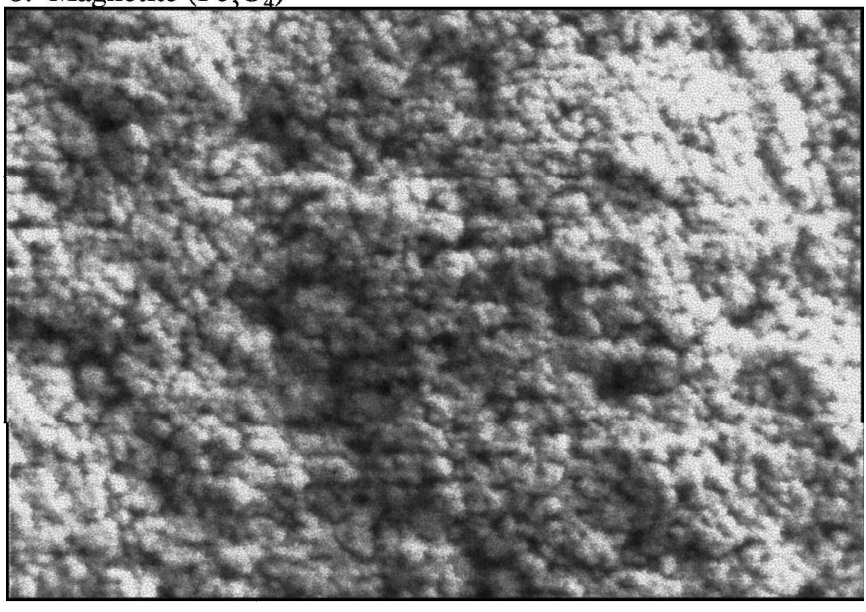

500 nm

FIGURE 3 Scanning electron micrographs of biogenic magnetite and siderite coated with ferrihydrite. Samples are from the experiment summarized in Figure 4. Scale as noted.

is decreased (Figure 2), and is a more stable phase than ferrihydrite under anoxic conditions. Biogenic magnetite exists as aggregates of nm-sized crystallites (Figure 3b; Fredrickson et al. 1998), retaining morphologic and size features of 2-line ferrihydrite. The size and morphology of biogenic magnetite indicates that it forms by topotactic conversion of 2-line ferrihydrite driven by Fe(II) sorption (Ardizzone and Formaro 1983; Mann et al. 1989; Fredrickson et al. 1998). Biogenic magnetite forms in both bicarbonate and organic acid buffers (Mortimer and Coleman 1997; Fredrickson et al. 1998).

An anoxic suspension of 2-line ferrihydrite that is inoculated with DMRB and spiked with an electron donor at circumneutral pH rapidly enters the stability field of magnetite regardless of whether bicarbonate is present or not (e.g., note reaction path in Figure 2). Magnetite can form rapidly under requisite bioreductive conditions, which appears to involve a moderate Fe(II) flux that sorbs to and reacts with the residual ferrihydrite. The formation of magnetite sequesters the remaining Fe(III) in a relatively stable, inverse spinel structure. It is not known whether biogenic magnetite, once formed, can be bioreduced to siderite, or whether siderite formation requires specific conditions such as a high respiration/Fe(II) flux rate that precludes magnetite formation. Kostka and Nealson (1995) showed that magnetite bioreduction by *S. putrefaciens* was feasible below pH 7 in a specific medium formulation (MR-1). The results of Dong et al. (2000) indicated that biogenic magnetite could be bioreduced by DMRB to siderite, but small quantities of residual ferrihydrite in the magnetite may have contributed to siderite formation.

An example of the conditions leading to magnetite and siderite formation is shown in Figure 4 where the bioreduction (by *S. putrefaciens*, strain CN32) of 2-line ferrihydrite (20 mmol/L) was studied as a function of N_2:CO_2 ratio (100:0–80:20) in MES and bicarbonate buffers with H_2 as the electron donor. In all cases, the mineral/buffer suspension was equilibrated with gas before inoculation with organisms and e-donor. The biomineralization products that resulted (as determined by XRD, data not shown) were almost identical in both buffers. Magnetite was observed as the primary product below a N_2:$CO_{2(g)}$ ratio of approximately 90:10. At a ratio of 90:10, a mixture of phases was observed including crystalline Fe(III) oxides (goethite, lepidocrocite) as well as magnetite and siderite. At a N_2:CO_2 ratio of 80:20, siderite was the only bioreduction product. The pH of all treatments increased with bioreduction. There was not a direct correlation between Fe(II) produced and pH increase because protons were also released by mineral precipitation.

Model calculations and chemical analyses showed that both these buffer systems were in equilibrium with $CO_{2(g)}$ and contained equivalent bicarbonate concentrations at the same pH (Table 3). The results strongly indicate that the formation of siderite does not proceed through a magnetite intermediate. Rather, higher HCO_3^- concentrations (18–40 mmol/L) appear to prevent topotactic conversion to magnetite through aqueous complexation of Fe(II), or surface complexation of HCO_3^- that inhibits Fe_3O_4 formation and/or accelerates nucleation of $FeCO_{3(s)}$. Under such conditions, $FeCO_{3(s)}$ precipitates as large rhombohedral precipitates in a groundmass of fine-grained ferrihydrite, indicating homogeneous precipitation after the initial nucleation phase (Figure 3a). The results indicated that small differences in initial and final pH may influence the identity of the secondary products, but more definitive studies are required. The Figure 4 data do not allow comment on whether the respiration/reduction rate varied between the treatments with different $CO_{2(g)}$ pressures and/or whether kinetic issues were important.

The use of mmol/L concentrations of PO_4^{3-} as a nutrient often leads to vivianite [$Fe_3(PO_4)_2 \cdot 8H_2O$] precipitation as Fe(II) is produced during bioreduction. Much of the added PO_4^{3-} is initially sorbed by the Fe(III) oxide (Fredrickson et al. 1998, 2001), and the sorbed PO_4^{3-} appears to be directly incorporated into vivianite during bioreduction. Vivianite precipitates rapidly in DMRB suspensions at circumneutral pH (Zachara

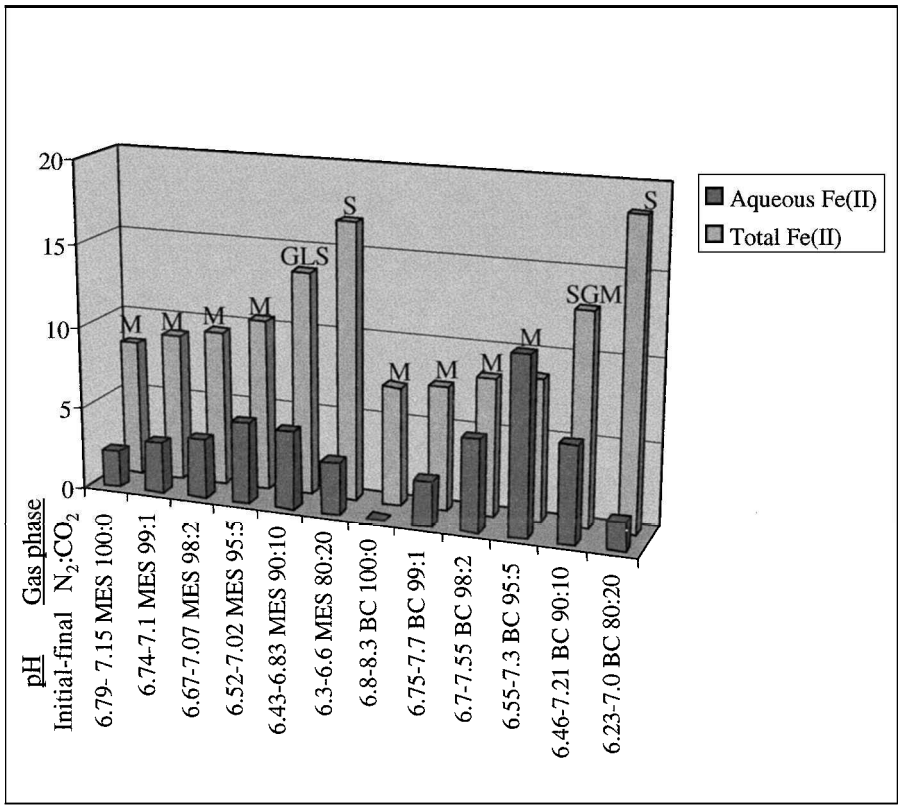

FIGURE 4 Total (0.5 N HCl extractable) and aqueous Fe(II) in a bioreduction experiment with 2-line ferrihydrite (20 mmol/L), H_2 gas, variable CO_2 pressure, and either bicarbonate (BC) or MES buffer. Observed biomineralization products identified by letter: M = magnetite, G = goethite, L = lepidocrocite, and S = siderite. Initial and final pH values and gas pressure are as noted. Carbonate concentrations are given in Table 2.

et al. 1998), typically forming 5–10 μm prismatic crystallites. Its precipitation is observed in both bicarbonate and organic acid buffers. Because nutrient PO_4^{3-} is typically added at concentrations well below that of the poorly crystalline Fe(III) oxide, the vivianite is found in association with other biogenic solids. The low solubility of vivianite (Al-Borno and Tomson 1994) combined with its rapid precipitation kinetics allows it to form before siderite in bicarbonate buffer (Zachara et al. 1998). There is no evidence for direct microbial involvement in the precipitation of either siderite or vivianite other than through Fe(II) supply.

In addition to promoting vivianite formation, PO_4^{3-} inhibits the nucleation of magnetite in both abiotic (Couling and Mann 1985) and DMRB inoculated (Fredrickson et al. 1998) systems. The inhibitory effect may result from the strong surface complexation of PO_4^{3-} that impedes the internal recrystallization of 2-line ferrihydrite to magnetite (Couling and Mann 1985). The adsorption density and aqueous concentration range over which PO_4^{3-} inhibits magnetite formation has not been established. Green rust (in association with vivianite) has been observed as a biomineralization product of 2-line ferrihydrite (50 mmol/L) only in the presence of PO_4^{3-} (4.4 mmol/L) and AQDS (0.10 mmol/L, anthraquinone disulfonate, an electron shuttle) in carbonate-deficient buffer (Fredrickson et al. 1998; Figure 5). The formation of metastable green rust is apparently facilitated by PO_4^{3-} that inhibits magnetite formation; AQDS that accelerates the respiration, reduction, and Fe(II) supply rate; and

TABLE 3 Total CO_2 (mmol/L) in aqueous phase with variable pH and CO_2 partial pressure (atm)*

pH	PCO_2	0.01	0.02	0.05	0.1	0.2
6.0		0.49	0.98	2.45	4.90	9.80
6.1		0.52	1.05	2.64	5.29	10.58
6.2		0.57	1.15	2.89	5.78	11.57
6.3		0.64	1.28	3.20	6.40	12.81
6.4		0.71	1.43	3.59	7.19	14.38
6.5		0.81	1.63	4.08	8.17	16.35
6.6		0.94	1.88	4.70	9.41	18.83
6.7		1.09	2.19	5.48	10.97	21.95
6.8		1.29	2.58	6.47	12.94	25.88
6.9		1.54	3.08	7.70	15.41	30.83
7.0		1.85	3.70	9.26	18.53	37.06
7.1		2.24	4.49	11.22	22.45	44.90
7.2		2.73	5.47	13.69	27.39	54.78
7.3		3.36	6.72	16.80	33.61	67.23
7.4		4.14	8.29	20.72	41.45	82.90
7.5		5.13	10.26	25.66	51.32	102.64

*The data in the table are specific to Figure 4. Total aqueous CO_2 only includes H_2CO_3, HCO_3^-, CO_3^{2-} species, equilibrium constants at 25°C were used in calculations, and the calculated values were not corrected for ionic strength.

SO_4^{2-} (from the trace metal solution), Cl^- (from the nutrient solution), and CO_3^{2-} (from lactate oxidation) to function as intercalating anions. An abiotic analogue study observed the formation of green rust under comparable conditions of Fe(II), PO_4^{3-}, pH, and ferrihydrite concentration (Hansen and Poulsen 1999). As noted by Hansen and Poulsen (1999), vivianite, not green rust, is the stable end product and the long-term persistence of green rust is determined by the available PO_4^{3-} concentration. A phosphate deficiency relative to vivianite stoichiometry will stabilize green rust.

Electron Acceptor to Donor Ratio

A wide range of electron acceptor to donor ratios may exist in soil or sediment. The electron donor may be in excess or deficient relative to the poorly crystalline Fe(III) oxide fraction. Electron donors for DMRB include $H_{2(g)}$ and low molecular weight organic acids (e.g., lactate, acetate) that are typically in low concentration in porewater or groundwater. Because of their low concentration (e.g., $<10^{-4}$ mol/L) and the large solid-liquid ratio of natural soil-water systems (typically >2 kg/L), the electron donor may often be deficient relative to the electron acceptor when concentrations at a single time point are compared. However, because the electron donors are water-soluble, advective flux over longer time periods in natural systems may supply total concentrations of electron donor that exceed the stationary concentration of poorly crystalline Fe(III) oxides.

The electron donor to acceptor ratio can affect the biomineralization products resulting from the action of DMRB on 2-line ferrihydrite. Shown in Figure 6 are transmission Mössbauer spectra of 2-line ferrihydrite aged for 8 h (a), and after contact with *S. putrefaciens*, CN32, for 20 d under anoxic conditions in 30 mmol/L bicarbonate buffer with lactate as the electron donor (b–e). Three electron donor:acceptor ratios are shown,

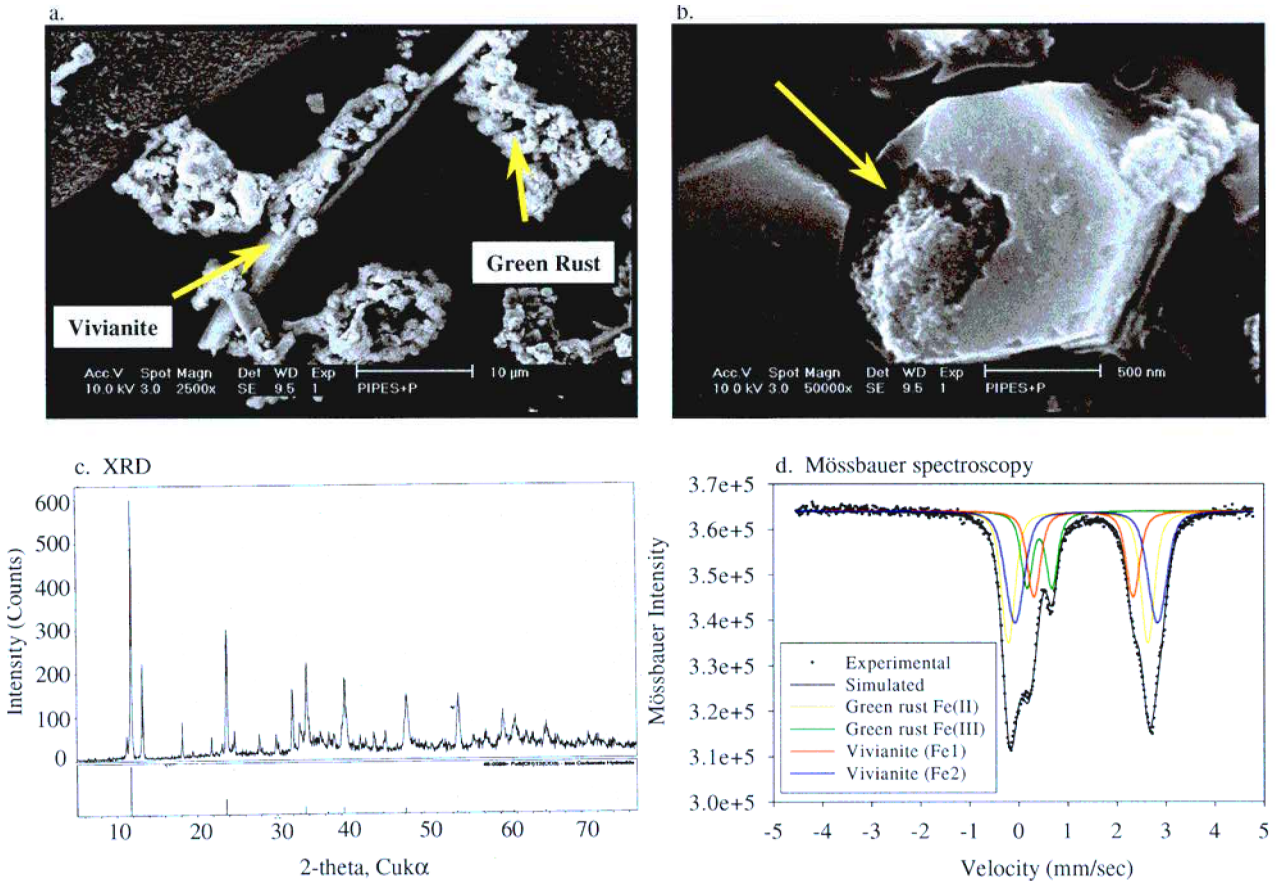

FIGURE 5 Biogenic green rust. (a) green rust coassociated with vivianite, (b) high magnification of a green rust particle showing residual 2-line ferrihydrite, (c) XRD of the phase assemblage measured under anoxic conditions, and (d) the Mössbauer spectrum along with Voight-based fitting of the potential contributions of vivianite and green rust. The Mössbauer analysis of this phase mixture is complicated because each solid contains Fe in two structurally distinct sites.

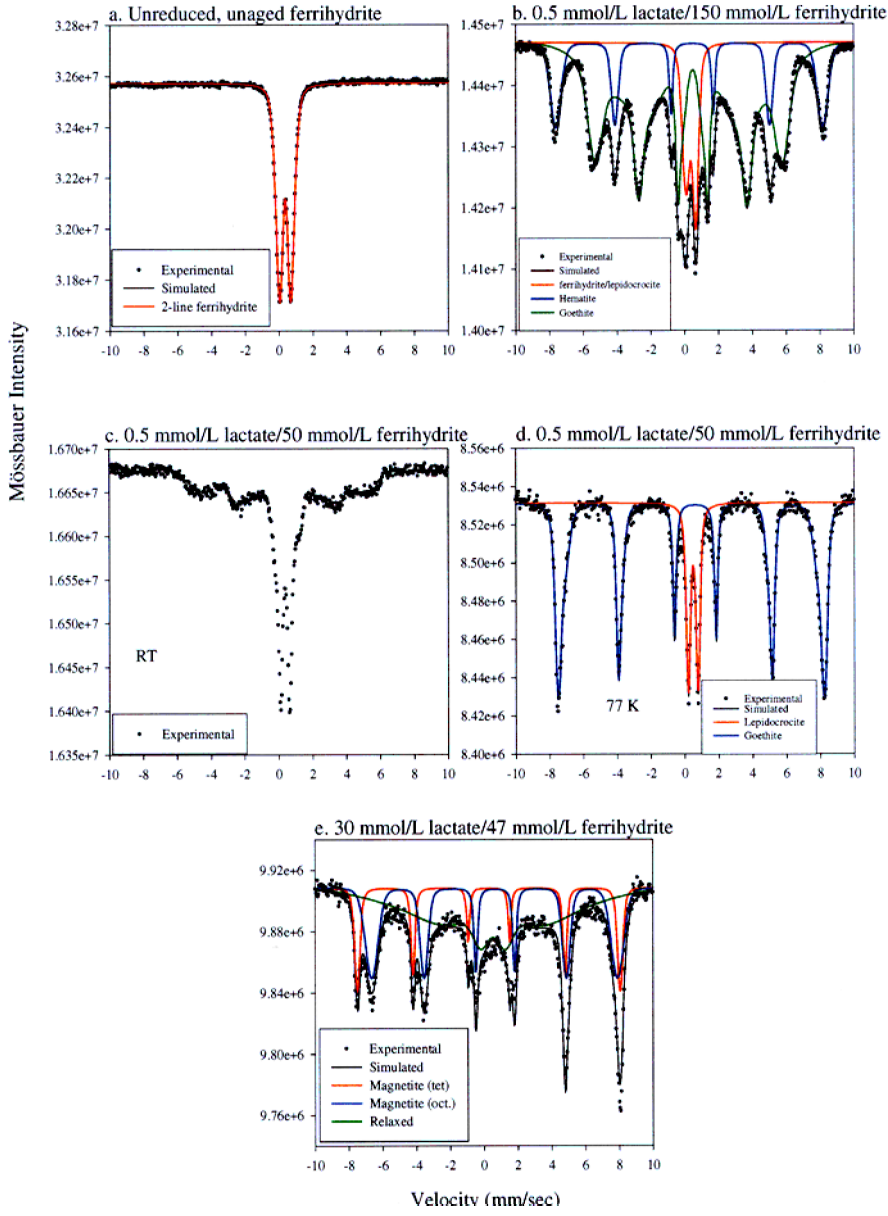

FIGURE 6 Room temperature (RT) Mössbauer spectrum of 2-line ferrihydrite, (a) and of ferrihydrite subject to bioreducing conditions (in 30 mmol/L bicarbonate buffer) with variable e-donor:acceptor ratios (b–e). (b) RT spectrum of 0.5 mmol/L lactate and 150 mmol/L ferrihydrite, (c) RT spectrum of 0.5 mmol/L lactate and 50 mmol/L ferrihydrite, (d) 77 K spectrum of 0.5 mmol/L lactate and 50 mmol/L ferrihydrite, and (e) RT spectrum of 30 mmol/L lactate and 47 mmol/L ferrihydrite. Voight-based model simulations are shown by solid line along with contributing mineral phases. Mag(TET) and Mag(OCT) refer to the tetrahedral and octahedral sites of magnetite.

from deficient (0.5 mmol/L lactate/150 mmol/L ferrihydrite) to excess (30 mmol/L lactate/47 mmol/L ferrihydrite). The Mössbauer spectrum for the 2-line ferrihydrite (Figure 6a) was consistent with previously reported ones (Murad and Schwertmann 1980). Striking are the differences between the biomineralization products. When ferrihydrite was at great excess (0.5 mmol/L lactate/150 mmol/L ferrihydrite, Figure 6b), it was transformed to a complex mixture of Fe(III) oxides including hematite, goethite, lepidocrocite, and more crystalline ferrihydrite. Well-formed crystalline Fe(III)-oxide phases, hematite and goethite, were the dominant biotransformation phases on a mass basis. At a lower electron donor to acceptor ratio (0.5 mmol/L lactate/50 mmol/L ferrihydrite), the oxide was transformed to a mixture of at least two components as inferred by room temperature Mössbauer spectroscopy (Figure 6c), a magnetically ordered phase with an incipient sextet, and a paramagnetic doublet phase. These components were further resolved by study at 77°K (Figure 6d) into a mixture of small particle-size goethite and lepidocrocite. Small particle goethite was the mass dominant phase. Finally, when the electron donor was in excess (Figure 6e), the 2-line ferrihydrite was almost fully transformed to fine-grained magnetite, with a small residual concentration of 6-line ferrihydrite (relaxed component).

The Mössbauer spectrum of biogenic magnetite (Figure 6e) and the modeling of the potentially present phases and their distribution involves complexity that deserves comment. The high center background in the Mössbauer spectrum may result from a size effect of nm-sized magnetite particles that can induce "collapse" of the spectrum (McNab et al. 1968) or from the presence of another iron phase that could include maghemite or a more crystalline form of ferrihydrite (e.g., 6-line). The Voight-based modeling technique that was used to simulate the spectra in Figure 6 involves the application of as many as 30 different parameters, and, consequently, there is rarely a unique fit of any given Mössbauer spectrum (e.g., alternate models may give the same sum of squares). We have elected to describe the high baseline effect as resulting from the contribution of a 6-line ferrihydrite phase (relaxed component in Figure 6e) because the resulting lorentzian line widths for the simulated magnetite phase were more realistic. The mineralogic implication of this fit is that DMRB activity may induce crystallization of 2-line ferrihydrite to 6-line ferrihydrite. Further studies, including temperature variant Mössbauer measurements are needed, however, for validation.

The results in Figure 6 demonstrate that iron-reducing bacteria may promote the transformation of poorly crystalline Fe(III) oxides to crystalline ones (hematite, goethite, and lepidocrocite) as well as to ferrous-containing crystalline phases (magnetite). These mineral transformations are believed to result from the reaction of biogenic $Fe^{2+}_{(aq)}$ with the residual ferrihydrite; however, cysteine, a sulfur containing amino-acid, has also been observed to induce the recrystallization of ferrihydrite to goethite (Cornell and Schneider 1989). When the electron donor is at low concentration relative to the Fe(III) oxide, small amounts of $Fe^{2+}_{(aq)}$ are released through the reductive process that strongly sorb to the residual oxide at circumneutral pH (see $Fe^{2+}_{(aq)}$ sorption data in Fredrickson et al. 1998). Low concentrations of sorbed Fe^{2+} have been observed to catalytically promote the recrystallization of poorly crystalline Fe(III) oxides to thermodynamically more stable goethite (Fischer 1972), possibly through reductive dissolution (Cornell and Schwertmann 1996). Our observations above indicate that hematite and lepidocrocite, which are also more thermodynamically stable than 2-line ferrihydrite but crystallize by different mechanisms, may also result as products from this process. The differences in mineralization products between the 0.5 mmol/L lactate/150 mmol/L ferrihydrite and 0.5 mmol/L lactate/50 mmol/L ferrihydrite are not easily explained and imply that the adsorption density of biogenic Fe^{2+} and the kinetic rate of supply may influence the crystalline structure and particle size of the resulting Fe(III) oxide. Finally, when the electron donor is in excess, higher levels of biogenic Fe^{2+}

are generated that saturate the ferrihydrite surface inducing conversion to magnetite (Fe_3O_4; Ardizzone and Formaro 1983; Mann et al. 1989).

Influence of Foreign Ions

In the preceding section it was shown that thermodynamically favored crystalline Fe(III) oxides may result from the action of DMRB on poorly crystalline Fe(III) oxides. Those experiments (Figure 6) utilized synthetic 2-line ferrihydrites free of impurities. In natural environments, however, ferrihydrites may contain coprecipitated trace metals and/or phosphate and silica (Carlson and Schwertmann 1981; Fox 1989; Fortin et al. 1993), and/or coreacted organic materials (Perret et al. 2000). These impurities generally act to stabilize ferrihydrites in natural environments, preventing their long-term recrystallization to more stable goethite and hematite.

Shown in Figure 7 are room-temperature Mössbauer spectra for aged, 2-line ferrihydrite and aged 2-line ferrihydrites substituted with either 5 mol% Ni(II) or Co(II) (Zachara et al. 2001). The unreduced, aged 2-line ferrihydrite contains microcrystalline goethite as an aging/transformation product (Figure 7a), while coprecipitated Ni(II) and Co(II) prevents ferrihydrite recrystallization (Figure 7c, e). The mineralogic products resulting from the activity of DMRB (*S. putrefaciens*, CN32) on these poorly crystalline Fe(III) oxides varies dramatically (Figure 7b, d, and f). These experiments were performed with excess electron donor, for example, 30 mmol/L lactate and 50 mmol/L ferrihydrite in pH 7 PIPES buffer. The dominant bioreduction product of the aged 2-line ferrihydrite was fine-grained goethite (Figure 7b) in combination with a small amount of magnetite. The Ni(II)-substituted ferrihydrite resisted bacterial reduction (Figure 7d). Co(II)-ferrihydrite was biotransformed to a nonstoichiometric magnetite (Figure 7f) in mixture with Co-substituted 2- and 6-line ferrihydrite. Nonstoichiometry was implied by the larger tetrahedral peak height of magnetite that indicated either partial oxidation or Co(II) substitution.

Coreacted ions that retard ferrihydrite crystallization apparently have different effects on ferrihydrite bioavailability to DMRB and the nature of the resulting mineralization products. Both Co(II) and Ni(II) prevented the crystallization of goethite during both the aging process and during bioreduction (Figure 7). Co(II) promoted the transformation to magnetite. Ni(II), in contrast, prevented the use of ferrihydrite as an electron acceptor. This latter effect appeared to be a mineral/chemical one in that Ni(II) did not induce adverse physiologic effects on CN32 (Fredrickson et al. 2001). These striking differences may result from the contrasting electronic properties of Ni(II) and Co(II/III). The half-cell potential of the Co(II)/Co(III) couple (1.48 V) is well above that of Fe(II/III) (0.67 V; Zachara et al. 2001), and the polyvalent character of Co and its redox potential may facilitate electron transfer into ferrihydrite aggregates. Redox inert Ni(II) apparently blocks electron transduction to and within the ferrihydrite structure.

Sorbed anions including PO_4^{3-} and H_4SiO_4 also inhibit ferrihydrite crystallization to goethite and hematite (Carlson and Schwertmann 1981; Cornell et al. 1987; Reeves and Mann 1991; Galvez et al. 1999). This effect results from strong oxyanion surface complexation to, or coprecipitation with, ferrihydrite that may block structural ordering. In spite of the inhibitory effect of PO_4^{3-} on both ferrihydrite crystallization and magnetite formation, its presence as a nutrient at surface saturating concentrations did not appreciably slow or accelerate the bioreduction rate of ferrihydrite at a P/Fe ratio of 0.088 (Fredrickson et al. 1998). Sorbed, redox-inert PO_4^{3-} does not block electron transduction to the solid as observed for Ni(II). Rather, it appears to enhance the extent of bioreduction by removal of potentially passivating byproducts, such as Fe(II) through vivianite precipitation.

Given the observed importance of sorbed Si in stabilizing ferrihydrites in terrestrial environments, a Si-containing (2 mol%), 2-line ferrihydrite was synthesized by coprecipitation

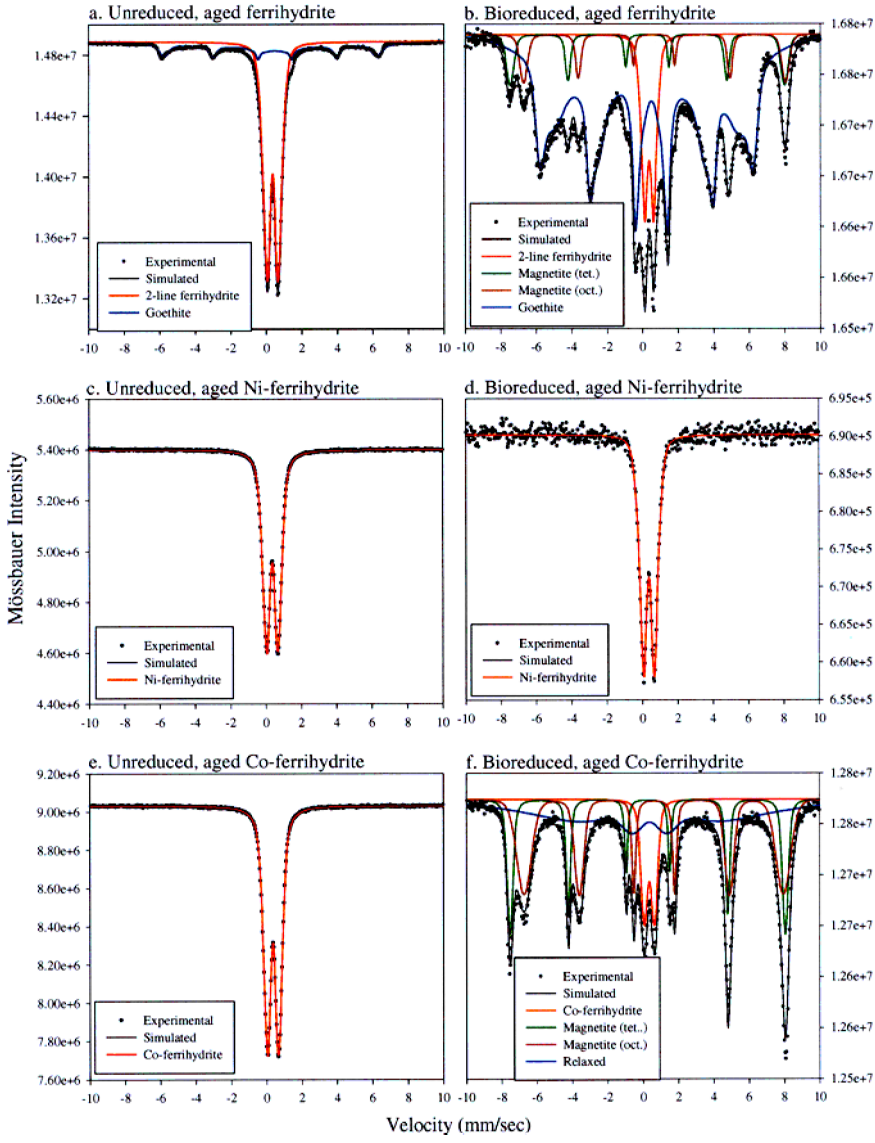

FIGURE 7 Room temperature Mössbauer spectra of unreduced and bioreduced, (a) and (b) aged ferrihydrite, (c) and (d) Ni-spiked ferrihydrite, and (e) and (f) Co-spiked ferrihydrite. The bioreduction experiments were performed in PIPES buffer. Voight-based model simulations are shown by solid line along with contributing mineral phases. Mag(TET) and Mag(OCT) refer to the tetrahedral and octahedral sites of magnetite.

to evaluate its behavior under Fe(III)-reducing conditions promoted by DMRB. The anoxic incubation with CN32 was performed identically to those reported in Figure 7 (50 mmol/L 2-line ferrihydrite, 30 mmol/L lactate, pH 7 PIPES buffer, and no PO_4^{3-}), and samples of the residual oxide were subsampled after 1, 8, and 28 d of incubation. The XRD and Mössbauer spectra of the starting Si-ferrihydrite were identical to pure ferrihydrite (not shown, e.g., Figure 6a). XRD and Mössbauer analyses of the bioreduced solids indicated rapid conversion of Si-containing ferrihydrite to fine-grained magnetite within 1 day of incubation with DMRB (Figure 8). Greenalite, a ferrous silicate, was not observed in any of the bioreduced

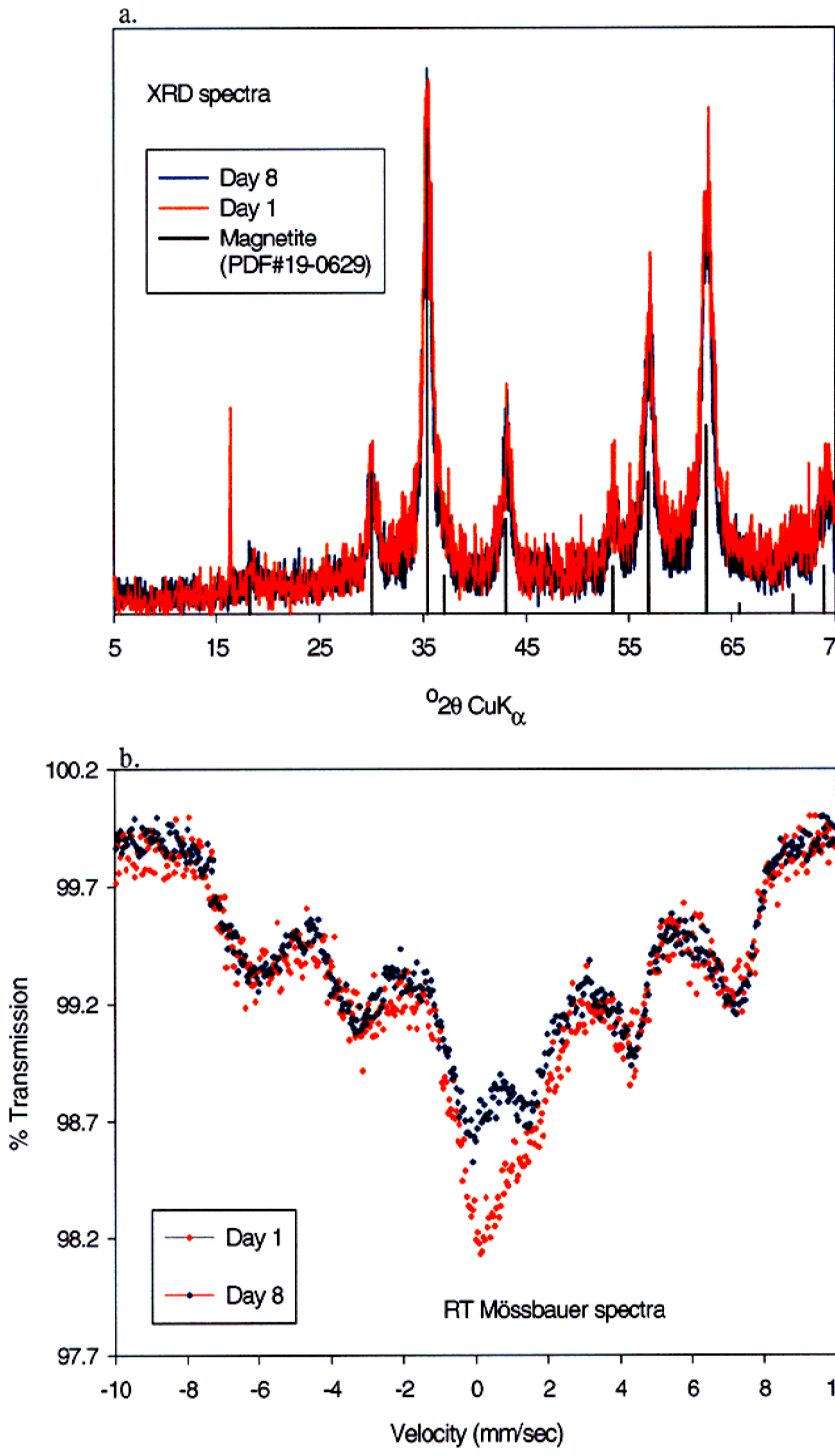

FIGURE 8 X-ray diffraction (a) and room temperature Mössbauer spectra (b) of bioreduced 2-line ferrihydrite containing 2 mol% Si. Shown are samples collected after 1 and 8 days of incubation of 50 mmol/L ferrihydrite with CN32 in pH 7 PIPES buffer with 30 mmol/L lactate.

samples. The 1-day sample contained some residual ferrihydrite (singlet at approximately 0 mm/sec) that was further reduced between days 1 and 8. The fine-grained character of the magnetite (<10 nm) was indicated by the collapsed nature of the Mössbauer spectra (Figure 8a; compare Figure 8a to Figure 6c). The rapid conversion of the Si-ferrihydrite to magnetite indicates that, unlike PO_4^{3-}, H_4SiO_4 does not inhibit magnetite formation. Moreover, the presence of sorbed/coprecipitated H_4SiO_4 at the concentration studied had no inhibitory effect on ferrihydrite reduction, and it may, in fact, have stimulated the rate of ferrihydrite conversion. These results markedly contrast with the inhibitatory effect of H_4SiO_4 on ferrihydrite crystallization to goethite and hematite under oxidizing conditions. These four examples indicate that it is not currently possible to generalize on the effects of coreacted ions on ferrihydrite bioreducibility and mineral transformation.

Bioreduction in Mixtures of Fe(III) Oxides

Fe(III) oxides in soils, subsurface sediments, and geologic materials often exist as phase mixtures of poorly crystalline and crystalline phases (e.g., Bigham et al. 1991). Such mixtures result from the metastable/transitory nature of ferrihydrite with respect to goethite and hematite. Over time, ferrihydrite will transform to thermodynamically more stable hematite and goethite, even if stabilized by adsorbed/coprecipitated impurities. The transition is controlled by a variety of environmental factors including pH, temperature, organic matter content, and possible microbiologic effects (Cornell and Schwertmann 1996).

Whereas the crystalline Fe(III) oxides are bioreducible to a degree by DMRB (Roden and Zachara 1996; Zachara et al. 1998; Kukkadapu et al. 2001), the poorly crystalline Fe(III) oxides are more bioavailable (Lovely and Phillips 1986, 1987). The enhanced bioavailability of ferrihydrite over the crystalline oxides is clearly shown in Figure 9 where a mixture of hematite, goethite, and 2-line ferrihydrite (50 mmol/L total Fe) was subject to reduction by *S. putrefaciens* (10^8 cells/mL of CN32) under anoxic conditions in PIPES buffer with excess electron donor (30 mmol/L lactate). In Figure 9a, the three starting oxides are clearly differentiated by transmission Mössbauer spectroscopy. This mixture was obtained by heating 2-line ferrihydrite for 10 d at 70°C. After 32 d incubation, the Mössbauer doublet associated with 2-line ferrihydrite has been removed by bioreduction, and the goethite sextet strengthened relative to hematite (Figure 9b). Our results cannot resolve whether the enhanced goethite Mössbauer signal (Figure 9b) resulted from additional goethite formation during incubation or from the partial bioreduction of hematite relative to goethite.

Unlike the results for 30 mmol/L lactate and 50 mmol/L 2-line ferrihydrite in Figure 6e where magnetite was formed, no Fe(II)-containing mineral products were produced in the experiment shown in Figure 9. In contrast, the Fe(II) was evolved to the aqueous phase where it sorbed to the residual goethite and hematite surfaces. At experiment termination, 8 mmol/L of Fe(III) had been reduced and, of this, 5 mmol/L was present in the aqueous phase and 3 mmol/L was sorbed to the crystalline Fe(III) oxides. While the observations imply that crystalline Fe(III) oxides may impede biomineralization of 2-line ferrihydrite by sorption of biogenic Fe(II), we note that small amounts of 2-line ferrihydrite (e.g., 5–10 mmol/L with 30 mmol/L lactate) are also fully solubilized by CN32 when crystalline Fe(III) oxides are not present. This solubilization may be facilitated by the excess concentration of lactate, which is a weak complexant of $Fe^{2+}_{(aq)}$.

A Conceptual Model Based on Laboratory Studies

The laboratory biomineralization studies of 2-line ferrihydrite reported to date support a conceptual model where the rate of supply and total concentration of biogenic Fe(II) is the primary determinant of the nature of secondary mineralization products (Figure 10).

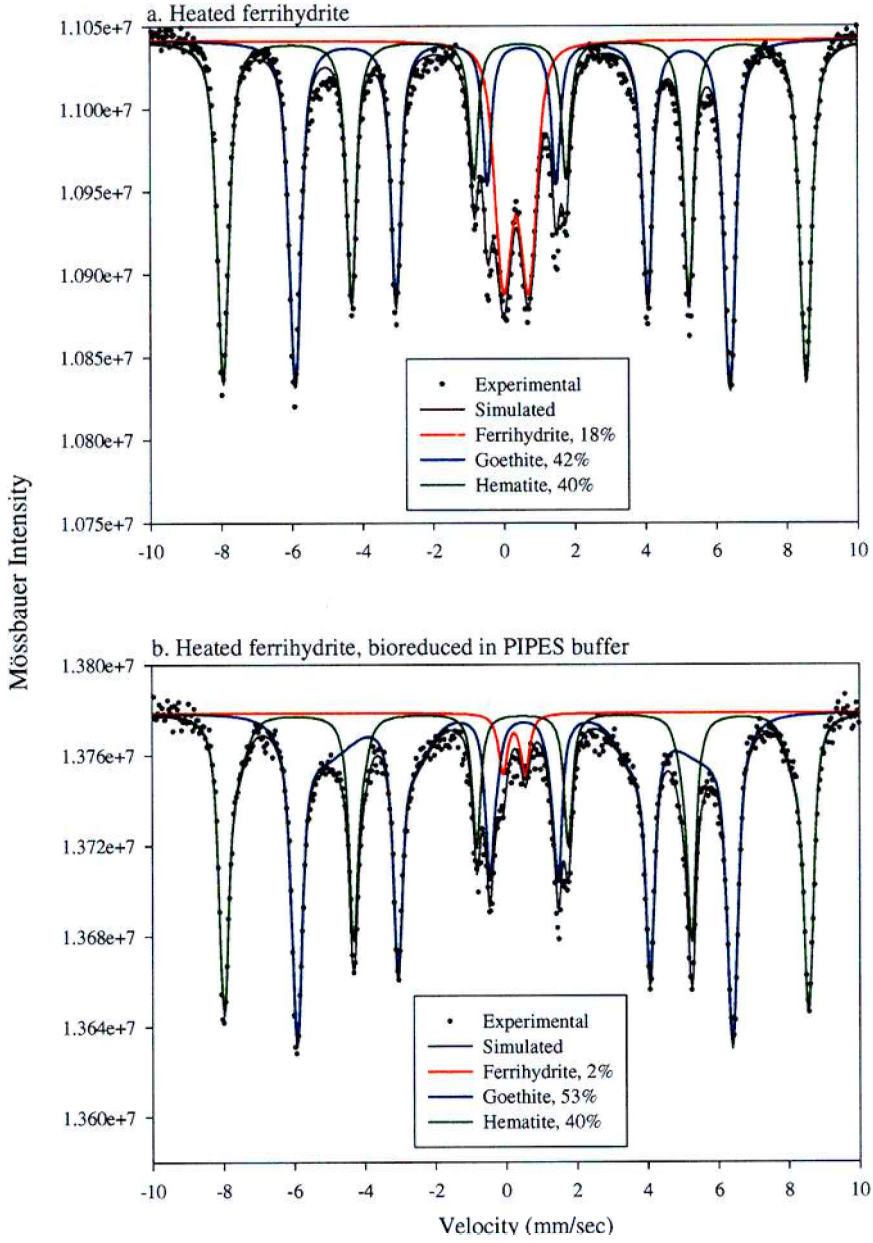

FIGURE 9 Room temperature (RT) Mössbauer spectrum of 2-line ferrihydrite that had been heated at 70°C for 10 h, (a) showing presence of ferrihydrite, goethite, and hematite. RT Mössbauer spectrum of bioreduced, heated 2-line ferrihydrite (50 mmol/L initial) with excess electron donor (30 mmol/L), (b) showing loss of ferrihydrite peak. Voight-based model simulations are shown by solid line along with contributing mineral phases. Mass percentages calculated from spectral areas.

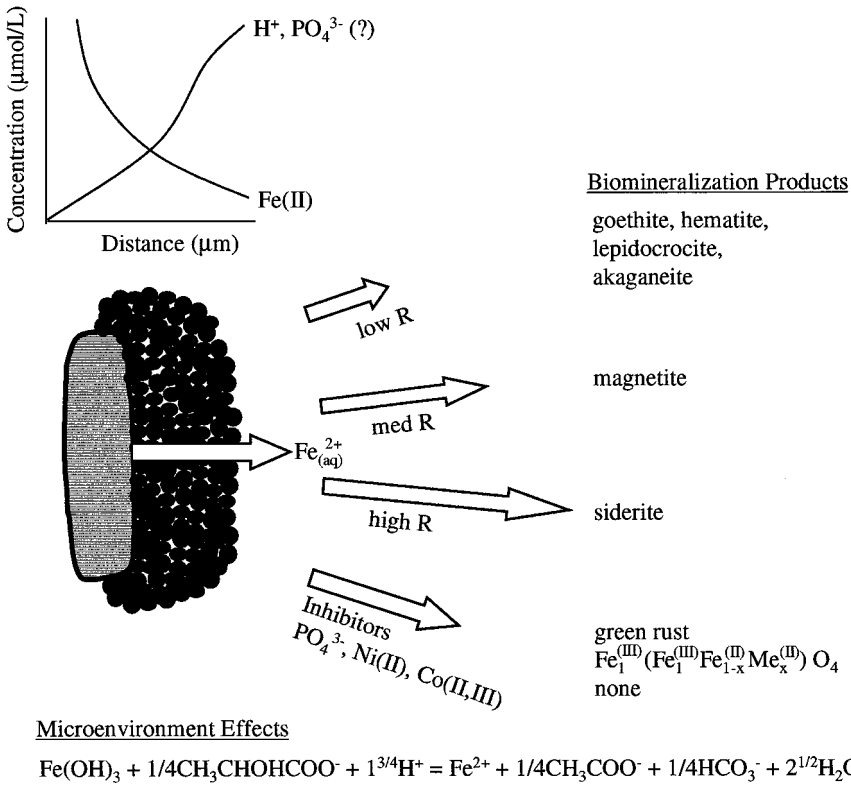

FIGURE 10 Conceptual model of ferrihydrite biomineralization showing aggregated ferrihydrite nanoparticles around the DMRB and vectors to represent the magnitude and rate of biogenic Fe(II) flux (R). A gradient of Fe(II), OH^-, coreacted ions, and electron donor oxidation products is assumed to exist from the organism surface out to the bulk media.

Electron microscopy of ferrihydrite/DMRB suspensions indicates that nm-sized ferrihydrite particles aggregate and cluster around DMRB cells at circumneutral pH (Y. Gorby, unpublished data). This bacterial aggregation is visibly obvious and leads to the flocculation of the ferrihydrite suspension.

The cellular oxidation of the electron donor generates an electron flux into the aggregated ferrihydrite, presumably at or near the organism interface. It is important to note that very little is known about the biochemical aspects of these systems, particularly with regard to the mechanisms by which Fe(III) is reduced at the membrane-oxide interface. The intracellular respiration reaction combined with electron transfer generates a gradient (a microenvironment) of Fe(III) oxide dissolution products [Fe(II), OH; or PO_4^{3-}/H_4SiO_4 or trace metals if adsorbed or coprecipitated with ferrihydrite] and electron donor oxidation products (e.g., acetate and bicarbonate from lactate) that diffuse outward through the aggregated ferrihydrite. The reaction products [e.g., Fe(II), HCO_3^-] may form aqueous complexes, adsorb/complex to the residual oxide or cell surface and promote mineral transformation, or react in some other manner. The circumneutral pH conditions typically used for these bioreduction studies favor the strong sorption of Fe(II), PO_4^{3-}, H_4SiO_4, and HCO_3^- by the residual ferrihydrite surface (Fredrickson et al. 1998, 2001; Zachara et al. 1998). The hydrogen ion activity may be significantly lower in the aggregated ferrihydrite microenvironment than in the bulk media as a result of Fe(III) oxide dissolution (reactions 1 and 2). The higher pH of the microenvironment is conducive to recrystallization of Fe(III)

oxides (Schwertmann and Murad 1983; Cornell and Schwertmann 1996) and the formation of ferrous iron solids.

The formation of crystalline Fe(III) oxides occurs when the reduction rate is slow, and the sorption density of Fe(II) is low on the residual ferrihydrite. This Fe(II) catalyzed abiotic reaction is very sensitive to pH and Fe(II) concentration (Fischer 1972) with maximum rates occurring near pH 6.5. Magnetite appears as the primary biomineralization product when the reduction rate increases and more Fe(II) is produced. This observation may also be explained on abiotic grounds (Ardizzone and Fomaro 1983; Mann et al. 1989). Magnetite formation is promoted by sorptive surface saturation of the ferrihydrite. Perhaps the crystallization vectors of goethite/hematite and magnetite are competitive. Siderite formation is encouraged by rapid reduction rates and mmol/L concentrations of bicarbonate that function as ligands for the solid phase and, possibly, inhibitors of magnetite formation.

The role of biosorption and the cell surface on the reductive phase transformations of ferrihydrite are unclear. Although it is known that Fe^{2+} sorbs significantly to the DMRB surface (Urrutia et al. 1998; Liu et al. 2001b), it is not known whether this sorption is instrumental in the nucleation of secondary phases. Electron microscopy has yet to show phase morphologies consistent with a direct microbial role in the precipitation of siderite, vivianite, green rust, or the crystalline Fe(III) oxides; although studies of sufficient detail have not been performed.

The formation of hematite, goethite, and magnetite sequesters residual Fe(III) in mineralogic environments that are less bioavailable than ferrihydrite. This reduction in bioavailability reflects differences in the free energies of the newly formed phases in relation to the electron donor, as well as the crystalline structure of the Fe(III)-containing phases and its effect on reductive dissolution rates as compared to ferrihydrite. These transformations act to slow or terminate further bioreduction even if excess electron donor is present.

Spatial and temporal chemical heterogeneity are two potential explanations for the common observation of mixtures of biomineralization products (e.g., goethite with siderite and/or magnetite) that are in global disequilibrium (Figures 4 and 7). Local spatial heterogeneity in chemical conditions surrounding respiring DMRB (microenvironments and chemical gradients) may allow the simultaneous precipitation of different mineral phases. In Figure 10, for example, chemical conditions may be conducive to the formation of one mineral phase near the ferrihydrite/DMRB interface, and another phase near the ferrihydrite/bulk solution interface as a result of a concentration gradient in Fe(II) and OH^-. Alternatively, temporally evolving chemical conditions as electron equivalents are liberated from the electron donor by respiration may create a reaction path that traverses Eh-pH space (e.g., Figure 2). Biomineralization phases that precipitate early in the incubation, but that are slowly reactive once formed (e.g., hematite, goethite, and magnetite), may be a relict of the reaction path and indicative of previous conditions.

The effect of coreacted ions on the bioreductive phase transformation of ferrihydrite is not easily generalized because of insufficient research and highly variable chemical behavior. The influence of adsorbed anions and cations on the abiotic transformation of 2-line ferrihydrite to crystalline Fe(III) oxides has been summarized by Cornell and Schwertmann (1996). Under reducing conditions promoted by DMRB, the coreacted ions may be solubilized, they may engage in solid-state reaction with biogenic Fe(II)[e.g., PO_4^{3-} to form vivianite or H_4SiO_4 to form greenalite ($Fe_3Si_2O_5(OH)_4$)], or they may coprecipitate in biogenic secondary phases (e.g., Co(II) or Ni(II) with vivianite, siderite, magnetite, or green rust; Fredrickson et al. 2001; Parmar et al. 2001; Zachara et al. 2001). Solubilized ligands (e.g., PO_4^{3-} or organic material) may complex Fe(II), lowering solution phase activities and mineral phase supersaturation, or may react with growth sites on nucleating biomineral surfaces influencing their precipitation kinetics. For these reasons, coreacted ions may have

important kinetic effects by either stimulating (e.g., Co) or retarding (e.g., Ni) biomineralization, or promoting the formation of different phases (e.g., PO_4^{3-}/vivianite or green rust) through inhibition or mass action effects. Water advection (Roden and Urrutia 1999; Roden et al. 2000) or associated sorbing mineral phases (e.g., Kukkadapu et al. 2001) as exist in sediment or soil may also influence the biomineralization process by removing Fe(II) from the bulk fluid phase and steepening the diffusional gradient within the DMRB-ferrihydrite aggregate (Figure 10). These effects, like that of aqueous complexation, may suppress biomineralization by preventing requisite degrees of supersaturation of Fe(II)-containing phases.

The conceptual model in Figure 10 is most relevant to suspensions of synthetic fine-grained ferrihydrite as investigated in this study. The physical model may differ appreciably in soils or subsurface sediments where ferrihydrite microprecipitates exist in close association with surfaces that have functioned as precipitation templates or Fe sources, or in freshwater sediments where ferrihydrite flocs of complex and varied morphology may form containing bacterial remains and organic matter (e.g., Fortin et al. 1993; Perret et al. 2000). In each of these environments ferrihydrite is often found in association with, and physically bound to, more crystalline Fe(III) oxides including lepidocrocite and goethite. Under these natural conditions, a different but as yet unspecified physical model may be more appropriate than the particle collection model in Figure 10. Little published information exists on the reductive biomineralization of ferrihydrite in soils, subsurface sediments, and/or natural waters upon which to base a more relevant conceptual model for the DMRB-ferrihydrite interaction and the relationships to biomineralization. This information lack stems in part from the typically low concentration of poorly crystalline Fe(III) oxides in natural materials and the attendant analytical difficulties surrounding their isolation and rigorous analysis.

Summary and Research Opportunities

The biotransformation of 2-line ferrihydrite by DMRB is a complex processes that, in spite of the work presented above, is not well understood. The primary driving force for biotransformation is the thermodynamic instability of 2-line ferrihydrite under both oxidizing and reducing conditions. Different phases may result depending on electron donor to acceptor ratio, solution conditions, coreacted ions, and other factors that define kinetic pathways and thermodynamic end states. The biomineralization process appears to be an indirect one, where biogenic Fe(II) catalyzes the transformation through its surface reaction (surface complexation, electron transfer) with the residual 2-line ferrihydrite and other cosorbed ions (e.g., PO_4^{3-}, HCO_3^-). The nature of biomineralization products produced are sensitive to the total concentration and rate of supply of Fe(II), and pH as influenced by Fe(III) oxide dissolution. Similar mineralogic products have been observed in abiotic analogue studies, where Fe(II) has been added to ferrihydrite suspensions.

This analysis concludes that a complex combination of thermodynamic and kinetic factors control whether a single, thermodynamically stable solid or a nonequilibrium phase mixture are the final products. Under certain conditions (e.g., high and low electron donor) the biomineralization products are predictable and conform to the most thermodynamically stable solid. In other cases, phase mixtures result from microenvironment or reaction path effects, or poorly resolved competitive kinetic pathways. Current knowledge is generally insufficient to predict which phase or assemblage will result under specific chemical conditions or ratios of electron donor to acceptor.

Fruitful research opportunities exist in all topical areas covered by this publication. Greater research attention is needed in DMRB biomineralization studies to the mineralogic nature of the starting Fe(III) oxide phase, its mineralogic state during the course

of bioreduction, and the solution chemical changes that accompany the biomineralization process, including chemical dynamics near the cell. Moreover, the biology of the DMRB system has also not been well studied, in particular with regard to the precise electron transfer mechanism and physiologic changes that may occur to the DMRB as the speciation and reactivity of Fe evolves.

This study has focused on laboratory studies of the DMRB transformation of synthetic 2-line ferrihydrite both without and with a number of coreacted inorganic ions. Unevaluated were the effects of bacterial remains and organic matter, which seem to be important components of natural ferrihydrites. Also unstudied where the effects of electrolyte (e.g., Cl^- versus NO_3^-) and preparation method (e.g., hydrolysis versus oxidation) on the phase transformations of 2-line ferrihydrite, but these are not expected to be significant. Surprisingly, few comparable studies exist on the biotransformation of 6-line ferrihydrite, or of poorly crystalline Fe(III) oxides in soils or subsurface environments, or in the field setting. Although it is expected that the reactions and phenomenology reported herein with synthetic Fe(III) oxides and single culture DMRB will and do occur in the environment, there may be significant differences that result from the complex nature of natural Fe(III) oxides (of both abiotic and microbiologic origin), the nature and rate of supply of electron donors, the presence of mixed bacterial populations, and the occurrence of accessory mineral phases to act as precipitation templates and adsorption repositories. Significant differences may exist in the bioreduction kinetics of poorly crystalline Fe(III) oxides from soil/geologic and aquatic environments as a result of morphologic and compositional differences. Studies on the reductive biomineralization of poorly crystalline Fe(III) oxides by DMRB in natural materials and in the field are critically needed, as are those on the reactivity and fate of these products when oxidizing conditions return.

References

Al-Borno A, Tomson MB. 1994. The temperature dependence of the solubility product constant of vivianite. Geochim Cosmochim Acta 58:5373–5378.

Ardizzone S, Formaro L. 1983. Temperature induced phase transformation of metastable $Fe(OH)_3$ in the presence of ferrous ions. Mat Chem Phys 8:125–133.

Bigham JM, Heckendorn SE, Jaynes WF, Smeck NE. 1991. Stability of iron oxides in two soils with contrasting colors. Soil Sci Soc Am J. 55:1485–1492.

Campbell AS, Schwertmann U. 1984. Iron oxide mineralogy of placic horizons. J Soil Sci 35:556–582.

Campbell AS, Schwertmann U. 1985. Evaluation of selective dissolution extractants in soil chemistry and mineralogy by differential X-ray diffraction. Clay Min 20:515–519.

Carlson L, Schwertmann U. 1981. Natural ferrihydrites in surface deposits from Finland and their association with silica. Geochim Cosmochim Acta 45:421–429.

Childs CW. 1992. Ferrihydrite: a review of structure, properties, and occurrence in relation to soils. Z Pfanzenernbhr Bndenk 155:441–448.

Chukhrov FV, Zvyagin BB, Gorshkov AI, Ermilova LP, Balashova VV. 1973. Ferrihydrite. Izvest Akad Nauk SSSR Ser Geol 4:23–33.

Cornell RM, Giovanoli R, Schindler PW. 1987. Effect of silicate species on the transformation of ferrihydrite into goethite and hematite in alkaline media. Clays Clay Miner 35:21–28.

Cornell RM, Schneider W. 1989. Formation of goethite from ferrihydrite at physiological pH under the influence of cysteine. Polyhedron 8:424–432.

Cornell RM, Schwertmann U. 1991. Iron oxides in the laboratory: preparation and characterization. VCH Weinheim, Federal Republic of Germany. 137 p.

Cornell RM, Schwertmann U. 1996. The Fe oxides: structure, properties, reactions, occurrences, and uses. VCH Weinheim, Federal Republic of Germany. 573 p.

Couling SB, Mann S. 1985. The influence of inorganic phosphate on the crystallization of magnetite (Fe_3O_4) from aqueous solution. J Chem Soc Chem Comm 1713–1715.

Dong H, Fredrickson JK, Kennedy DW, Zachara JM, Kukkadapu RK, Onstott TC. 2000. Mineral transformation associated with the microbial reduction of magnetite. Chem Geol 169:299–318.

Drissi SH, Refait PH, Abdelmoula M, Génin JMR. 1995. The preparation and thermodynamic properties of Fe(II)-Fe(III) hydroxide-carbonate (green rust 1); Pourbaix diagram of iron in carbonate-containing aqueous media. Corr Sci 37(12):2025–2041.

Dzombak DA, Morel FMM. 1990. Surface complexation modeling: hydrous ferric oxide. New York: Wiley. 393 p.

Feitknecht W, Giovanoli R, Michaelis W, Muller M. 1973. Uber die hydrolyse von eisen(III) salzlosungen. I. Die hydrolyse der losungen von eisen(III) chlorid. Helv Chim Acta 56:2847–2856.

Fischer WR. 1972. Die wirkung von zweiwertigem eisen auf losung und umwandlung von eisen(III)-hydroxiden. In: Schlichting E, Schwertmann U, editors. Pseudogley and gley. Trans Comm V and VI Int Soil Sci Soc, Weinheim: VCH, p 37–44.

Ford RG, Bertsch PM, Farley KJ. 1997. Changes in transition and heavy metal partitioning during hydrous iron oxide aging. Environ Sci Technol 31:2028–2033.

Fortin D, Leppard GG, Tessier A. 1993. Characteristics of lacustrine diagenetic iron oxyhydroxides. Geochim Cosmochim Acta 57:4391–4404.

Fox LE. 1988. The solubility of colloidal ferric hydroxide and its relevance to iron concentrations in river water. Geochim Cosmochim Acta 52:771–777.

Fox LE. 1989. A model for inorganic control of phosphate concentrations in river waters. Geochim Cosmochim Acta 53:417–428.

Fredrickson JK, Zachara JM, Kennedy DW, Li S-M, Hinman NW. 1998. Biogenic iron mineralization accompanying the dissimilatory reduction of hydrous ferric oxide by a groundwater bacterium. Geochim Cosmochim Acta 62:3239–3257.

Fredrickson JK, Zachara JM, Kukkadapu RK, Gorby YA, Smith SC, Brown CF. 2001. Biotransformation of Ni-substituted hydrous ferric oxide by an Fe(III)-reducing bacterium. Environ Sci Technol 35:703–712.

Gálvez N, Barrón V, Torrent J. 1999. Effect of phosphate on the crystallization of hematite, goethite, and lepidocrocite from ferrihydrite. Clays Clay Miner 47(3):304–311.

Garrels RM, Christ CL. 1965. Solutions, minerals, and equilibria. San Francisco: Freeman, Cooper and Company. 450 p.

Génin JMR, Bourrie G, Trolard F, Abdelmoula M, Jaffrezic A, Refait PH, Maitre V, Humbert B, Herbillon A. 1998b. Thermodynamic equilibria in aqueous suspensions of synthetic and natural Fe(II)-Fe(III) green rusts: occurrences of the mineral in hydromorphic soils. Environ Sci Technol 32:1058–1068.

Génin JMR, Refait PH, Simon L, Drissi SH. 1998a. Preparation and E_h-pH diagrams of Fe(II)-Fe(III) green rust compounds; hyperfine interaction characteristics and stoichiometry of hydroxychloride, -sulphate and -carbonate. Hyperfine Interactions 111:313–318.

Hansen HCB, Poulsen IF. 1999. Interaction of synthetic sulphate "green rust" with phosphate and the crystallization of vivianite. Clays Clay Miner 47(3):312–318.

Kostka JE, Nealson KH. 1995. Dissolution and reduction of magnetite by bacteria. Environ Sci Technol 29:2535–2540.

Kukkadapu RK, Zachara JM, Smith SC, Fredrickson JK, Liu C. 2001. Dissimilatory bacterial reduction of al-substituted goethite in subsurface sediments. Geochim Cosmochim Acta 65:2913–2924.

Lindsay W. 1979. Chemical equilibria in soils. New York: Wiley. 449 p.

Liu C, Kota S, Zachara JM, Fredrickson JK, Brinkman C. 2001a. Kinetic analysis of the bacterial reduction of goethite. Environ Sci Technol 35:2482–2490.

Liu C, Zachara JM, Gorby YA, Szecsody JE, Brown CF. 2001b. Microbial reduction of Fe(III) and sorption/precipitation of Fe(II) on *Shewanella putrefaciens* Strain CN32. Environ Sci Technol 35:1385–1393.

Lovely DR. 1991. Magnetite formation during microbial dissimilatory iron reduction. In: Frankel RB, Blakemore RP, editors. Iron biominerals. New York: Plenum Press, p 151–166.

Lovley DR, Phillips EJP. 1986. Availability of ferric iron for microbial reduction in bottom sediments of the freshwater tidal Potomac River. Appl Environ Microbiol 52:751–757.

Lovley DR, Phillips EJP. 1987. Rapid assay for microbially reducible ferric iron in aquatic sediments. Appl Environ Microbiol 53:1536–1540.

Lovley DR, Phillips EJP, Lonergan DJ. 1991. Enzymatic versus nonenzymatic mechanisms for Fe^{3+} reduction in aquatic sediments. Environ Sci Technol 25:1062–1067.

Lovley DR, Stolz JF, Nord GL, Jr, Phillips EJP. 1987. Anaerobic production of magnetite by a dissimilatory iron-reducing microorganism. Nature 330:252–254.

Manceau A, Drits VA. 1993. Local structure of ferrihydrite and feroxyhite by EXAFS spectroscopy. Clay Miner 28:165–184.

Mann S, Sparks NHC, Couling SB, Larcombe MC, Frankel RB. 1989. Crystallochemical characterization of magnetic spinels prepared from aqueous solution. J Chem Soc Faraday Trans 85:3033–3044.

McNab TK, Fox RA, Boyle AJF. 1968. Some magnetic properties of magnetite (Fe_3O_4) microcrystals. J Appl Phys 39:5703–5711.

Mortimer RJG, Coleman ML. 1997. Microbial influence on the isotopic composition of diagentic siderite. Geochim Cosmochim Acta 61:1705–1711.

Mortimer RJG, Coleman ML, Rae JE. 1997. Effect of bacteria on the elemental composition of early diagenetic siderite: implications for palaeoenvironmental interpretations. Sedimentology 44:759–765.

Murad E, Schwertmann U. 1980. The Mössbauer spectrum of ferrihydrite and its relations to those of other iron oxides. Am Mineral 65:1044–1049.

Pankhurst QA, Pollard RJ. 1992. Structural and magnetic properties of ferrihydrite. Clays Clay Miner 40:268–272.

Parmar N, Gorby YA, Beveridge TJ, Ferris FG. 2001. Formation of green rust and immobilization of nickel in response to bacterial reduction of hydrous ferric oxide. Geomicrobiology J 18:375–385.

Perret D, Gaillard J-F, Dominik J, Atteia O. 2000. The diversity of natural hydrous iron oxides. Environ Sci Technol 34:3540–3546.

Phillips EJP, Lovley DR, Roden EE. 1993. Composition of non-microbially reducible Fe^{3+} in aquatic sediments. Appl Environ Microbiol 59:2727–2729.

Postma D, Jakobsen R. 1996. Redox zonation: equilibrium constraints on the Fe(III)/SO_4-reduction interface. Geochim Cosmochim Acta 60:3169–3175.

Rancourt DG, Ping JY. 1991. Voigt-based methods for arbitrary-shape static hyperfine parameter distributions in Mössbauer spectroscopy. Nucl Instrum Meth Phys Res B58:85–87.

Reeves NJ, Mann S. 1991. Influence of inorganic and organic additives on the tailored synthesis of iron oxides. J Chem Soc Faraday Trans I 87:3875–3880.

Roden EE, Urrutia MM. 1999. Ferrous iron removal promotes microbial reduction of crystalline iron(III) oxides. Environ Sci Technol 33:1847–1853.

Roden EE, Urrutia MM, Mann CJ. 2000. Bacterial reductive dissolution of crystalline Fe(III) oxide in continuous-flow column reactors. Appl Environ Microbiol 66:1062–1065.

Roden EE, Zachara JM. 1996. Microbial reduction of crystalline iron(III) oxides: influence of oxide surface area and potential for cell growth. Environ Sci Technol 30:1618–1628.

Russell JD. 1979. Infrared spectroscopy of ferrihydrite: evidence for the presence of structural hydroxyl groups. Clay Min 14:109–114.

Schindler P, Michaelis W, Feitknecht W. 1963. Loslichkeitsprodukte von metalloxiden und-hydroxiden. 8. Mitt.: die loslichkeit gealterter eisen(III)-hydroxid-fallungen. Helv Chim Acta 46:444–451.

Schwertmann U. 1973. Use of oxalate for Fe extraction from soils. Can J Soil Sci 53:244–246.

Schwertmann U, Cornell RM. 1991. Iron oxides in the laboratory: preparation and characterization. VCH Weinheim, Federal Republic of Germany.

Schwertmann U, Fechter H. 1994. The formation of green rust and its transformation to lepidocrocite. Clay Miner 29:87–92.

Schwertmann U, Murad E. 1983. Effect of pH on the formation of goethite and hematite from ferrihydrite. Clays Clay Min 31:277–284.

Schwertmann U, Schulze DG, Murad E. 1982. Identification of ferrihydrite in soils by dissolution kinetics, differential X-ray diffraction, and Mössbauer spectroscopy. Soil Sci Soc Am J 46:869–874.

Stanjek H, Weidler PG. 1992. The effect of dry heating on the chemistry, surface area, and oxalate solubility of synthetic 2-line and 6-line ferrihydrites. Clay Miner 27:397–412.

Tessier A, Fortin D, Belzile N, DeVitre RR, Leppard GG. 1996. Metal sorption to diagenetic iron and manganese oxyhydroxides and associated organic matter: narrowing the gap between field and laboratory measurements. Geochim Cosmochim Acta 60:387–404.

Thornber MR, Nickel EH. 1976. Supergene alteration of sulphides. III. The composition of carbonates. Chem Geol 17:45–72.

Towe KM, Bradley WF. 1967. Mineralogical constitution of colloidal "hydrous ferric oxides." J Colloid Interface Sci 24:384–392.

Trolard F, Génin JMR, Abdelmoula M, Bourrie G, Humbert B, Herbillon A. 1997. Identification of a green rust mineral in a redoctomorphic soil by Mössbauer and Raman spectroscopies. Geochim Cosmochim Acta 61:1107–1111.

Urrutia MM, Roden EE, Fredrickson JK, Zachara JM. 1998. Microbial and surface chemistry controls on reduction of synthetic Fe(III) oxide minerals by the dissimilatory iron-reducing bacterium *Shewanella alga*. Geomicrobiol J 15:269–291.

Vinš J, Šubrt J, Zapletal V, Hanousek F. 1987. Preparation and properties of green rust type substances. Collection Czechoslovok Chem Commun 52:93–102.

Wang HD, White GN, Turner FT, Dixon JB. 1993. Ferrihydrite, lepidocrocite, and goethite in coatings from East Texas vertic soils. Soil Sci Soc Am J 57:1381–1386.

Whittmore DO, Langmuir D. 1975. The solubility of ferric oxyhydroxides in natural waters. Groundwater 13:360–365.

Zachara JM, Fredrickson JK, Li S-M, Kennedy DW, Smith SC, Gassman PL. 1998. Bacterial reduction of crystalline Fe(III) oxides in single-phase suspensions and subsurface materials. Am Mineral 83:1426–1443.

Zachara JM, Fredrickson JK, Smith SC, Gassman PL. 2001. Solubilization of Fe(III) oxide-bound trace metals by a dissimilatory Fe(III) reducing bacterium. Geochim Cosmochim Acta 65:75–63.